Global mountain forest cover change: patterns, drivers and implications

Xinyue He

Submitted in accordance with the requirements for the degree of Doctor of Philosophy

The University of Leeds

School of Earth and Environment

September 2023

Intellectual property

The candidate confirms that the work submitted is her own, except where work which has formed part of jointly authored publications has been included. The contribution of the candidate and the other authors to this work has been explicitly indicated below. The candidate confirms that appropriate credit has been given within the thesis where reference has been made to the work of others.

Chapter 2 consists of the following publication:

He, X., Ziegler, A.D., Elsen, P.R., Feng, Y., Baker, J.C.A., Liang, S., Holden, J., Spracklen, D.V. and Zeng, Z., 2023. Accelerating global mountain forest loss threatens biodiversity hotspots. *One Earth*, 6(3), 303–315. https://doi.org/10.1016/j.oneear.2023.02.005.

Conceptualization of the work was done by the candidate, with support from DVS, JH and ZZ. Global forest change data and DEM datasets were downloaded by YF and JCAB. The candidate analysed the data, produced the figures, and prepared the manuscript. Biodiversity analysis was generated with advice from PRE. Additional support for manuscript editing and revising was provided by ADZ. Comments on the draft were provided by all co-authors, but final editorial decisions were made by the candidate.

Chapter 3 consists of the following manuscript in preparation:

He, X., Spracklen, D.V., Holden, J., and Zeng, Z. Tropical montane forest loss dominated by increased medium-scale clearings. (*in prep.*)

The manuscript was written by the candidate with advice from supervisors (DVS, JH and ZZ), with additional (on-going) comments from co-authors during its preparation. Data analysis and processing were solely undertaken by the candidate.

Chapter 4 consists of the following publication:

He, X., Jiang, X., Spracklen, D.V., Holden, J., Liang, E., Liu, H., Xu, C., Du, J., Zhu, K., Elsen, P.R. and Zeng, Z., 2023. Global distribution and climatic controls of natural mountain treelines. *Global Change Biology*, 29, 7001–7011. http://doi.org/10.1111/gcb.16885.

Conceptualization of the work was done by the candidate, DVS, JH and ZZ. The candidate analysed the data and prepared the figures and manuscript. Scripts for processing and visualizing treelines were developed with help from XJ. In situ

treeline data for validation were provided by EL. Comments on the draft were provided by all co-authors, but final editorial decisions were made by the candidate.

Acknowledgements

Firstly, and most importantly, I would like to thank my supervisors Dom, Joe and Zhenzhong. Your support, kindness and flexibility have been invaluable, and I could not imagine a better team to guide me through my PhD experience. Thank you for gently pushing me to achieve things I never expected to be capable of.

I would like to acknowledge funding from the Southern University of Science and Technology (SUSTech) for my PhD studentship. The four-year study at Leeds and SUSTech has been a wonderful journey.

Thanks to Alan at Mae Jo University and Paul at Wildlife Conservation Society for their instructive comments and suggestions on my publications. The collaboration with them has been an amazing experience.

During my PhD I have been fortunate to be surrounded by some incredible, inspiring, and welcoming people at the University of Leeds. Thanks to everyone in the Biosphere and Atmosphere Group (BAG). I especially appreciate Jess, Ben, Callum and Ailish for providing me with the warmth of home during my stay in Leeds. I still remember the time we had a picnic and went hiking during the pandemic. It was truly memorable, considering that we had not seen each other for five months due to the lockdown and that social gatherings with no more than six people were permitted at that time.

I give a big shout-out to all members of the Earth System & Global Change (ESGC) Lab at SUSTech. I am grateful to Yu Feng and Xin Jiang who provided a great amount of coding support and technical help. Thanks to Lihong, Jie, Binbin, Yi, Shijing, Yubin, Junyu, Dashan and other members who have, in no small part, brought joy, given me confidence and provided many great memories.

Last but not least, I would like to extend my biggest thank you to my family, especially my parents for their never-ending support, motivation and so much more. Special thanks to Ruochen for all his love and support over the years. You have all given me the strength to persevere through the challenges I faced during my PhD journey.

Abstract

Mountain forests play a crucial and diverse role in the Earth system. They provide a wide range of goods and services, such as maintaining biodiversity, storing carbon and mitigating climate change. However, human activities, together with climate change, lead to significant changes in mountain forest cover. Such changes will bring about widespread impacts on resident species, regional climate, and human communities residing in both mountain regions and adjacent lowlands.

Satellite data offers the potential for assessing changes in land cover, with the advantages of global coverage, open accessibility and consistency. Using multiple satellite datasets, I show that global mountain forest loss is accelerating in the 21st century, largely driven by extensive agricultural expansion over the tropics. Much of the loss occurred in biodiversity hotspots, putting a threat to threatened species living there.

I further investigate the dynamics of tropical mountain forest loss in different patch-loss sizes. Across tropical mountains, I show that more than half of the increase in forest loss was attributed to the proliferation of intermediate and large-sized clearings (1–100 ha). Conversely, there was a declining proportion of small-scale forest loss patches (<1 ha). The observed increasing proportion of larger clearing size suggests a higher human pressure into tropical mountains.

To understand how climate and climate change impact mountain treelines, defined as the upper altitudinal limit of tree growth, I developed a novel approach to focus on the treeline that completely encircles a mountain. In total, I tracked almost 1 million kilometres of treeline across 243 mountain regions worldwide. On average, treelines moved upwards by 1.2 m/year during 2000–2010, but the shift was greatest in the tropics, with an average increase in elevation of 3.1 m/year. This upward movement of mountain treelines provides further evidence of the impacts of climate change on ecosystems around the world.

Contents

List of Figures

List of Tables

List of Abbreviations

ASTER	Advanced Spaceborne Thermal Emission and Reflection Radiometer
CLMT	Closed-loop mountain treelines
DEM	Digital Elevation Model
EO	Earth Observation
ET	Evapotranspiration
GBDT	Gradient Boosting Decision Trees
GEDI	Global Ecosystem Dynamics Investigation
GFC	Global Forest Change
GLAD	Global Land Analysis and Discovery
GMBA	Global Mountain Biodiversity Assessment
GMTED	Global Multi-resolution Terrain Elevation Data
IUCN	International Union for Conservation of Nature
LiDAR	Light Detection and Ranging
METI	Ministry of Economy, Trade, and Industry
MK	Mann-Kendall
MODIS	Moderate Resolution Imaging Spectroradiometer
NASA	National Aeronautics and Space Administration
NDVI	Normalized Difference Vegetation Index
NIR	Near-Infrared
OLS	Ordinary Least Squares
PA	Protected Areas
RSR	Range-Size Rarity
SR	Species Richness
UNEP	United Nations Environmental Programme
USGS	United States Geological Survey

WCMC	World Conservation Monitoring Centre
WDPA	World Database on Protected Areas

Chapter 1

Introduction

1.1 Background and motivation

Mountain forests, also known as montane forests, are unique ecosystems that play a vital role in maintaining ecological balance, supporting biodiversity, and providing essential ecosystem services. They are generally found at high elevations around the world, characterised by cooler temperatures, abundant moisture, and distinct plant and animal communities adapted to these challenging environments. Mountain forests cover over 9 million km^2 of the Earth's surface and represent more than one fifth of the world's forest cover area (Price et al., 2011). They play an important role in providing goods and services essential to the livelihoods of both highland and lowland communities, and across the whole Earth system through storing carbon and mitigating climate change (Macchi, 2010). Mountain forests are also indicators of climate change, and in turn, have a potential role in combating climate change (Kohler and Maselli, 2009).

However, mountain forests have experienced new pressures and are currently under threat. Human activities such as wood exploitation, agriculture expansion and grazing lead to extensive deforestation encroaching upon mountains, especially in developing counties (Price and Butt, 2000). Warming is projected to amplify over mountains according to global climate models (Zeng et al., 2015), leading to shifting of the treeline position (Qi et al., 2015; Smith et al., 2009). These changes in montane forests may have impacts on the water cycle, regional climate conditions, resident species, and human inhabitants of both mountain regions and adjacent lowlands (UNEP-WCMC, 2002). Thus, comprehensive and accurate assessments of mountain forest cover changes and their consequences are essential for promoting the sustainable development of the Earth's environment.

The mountainous areas appear to be new hotspots of forest change (Zeng et al., 2018a; Zeng et al., 2018b; Feng et al., 2021), yet the magnitude and trends of the change remain uncertain. Understanding mountain forest cover change as well as associated drivers and impacts is critical for both developing forest conservation measures and simulating future changes. The main aim of this

thesis is to build our knowledge of how montane forests are changing in the 21st century.

1.1.1 Delineation of mountains

The spatial delineation of mountain regions is more intricate than commonly assumed. Multiple delineation approaches exist, and the mountain regions differ substantially depending on the approach employed (Sayre et al., 2018). The earliest researchers used altitude as the only criterion (Messerli and Ives, 1997), but it failed to distinguish low mountain systems and categorise large areas of mid-elevation plateau (little topographic relief and few environmental gradients) as mountains.

There are three well-established methods of defining mountain ranges, i.e., the definitions by the World Conservation Monitoring Centre (WCMC; Kapos et al., 2000), the Global Mountain Biodiversity Assessment (GMBA; Körner et al., 2011) and the United States Geological Survey (USGS; Karagulle et al., 2017). Table 1.1 provides an overview of the differences in key characteristics of the three mountain definitions. The three methods define the scope of mountains quite differently, with the largest total area defined by USGS (41 million km^2), followed by WCMC (33 million km^2), and the average of two versions of GMBA being ~20 million km^2.

WCMC was developed by the United Nations Environmental Programme (UNEP; Blyth et al., 2002). In the WCMC method, Kapos et al. (2000) employed elevation, slope, and local elevation range to define mountain areas. The Digital Elevation Model (DEM) was derived from the Global 30 Arc-Second Elevation (GTOPO30) at a resolution of 30″ (~1 km), which was developed by the United States Geological Survey's EROS Data Centre in 1996. The steps were: 1) all areas >2,500 m were considered to be mountainous; 2) an effective slope criterion that can exclude mid-elevation plateau was used; 3) local elevation range (~7 km radius) was used to include low elevation and older mountains of local significance. The classified mountain ranges were further used to generate a distribution map of the world's mountain forests (Kapos et al., 2000), which was implemented by other international organisations.

GMBA was developed for mountain biodiversity and biogeography research. In the GMBA method, Körner et al. (2011) constrained mountains based on the

ruggedness of terrain only, regardless of elevation. Calculations of ruggedness were based on a 1 km DEM used by WorldClim (Hijmans et al. 2005). Ruggedness here refers to the maximum elevational difference among neighbouring grid points. Any 2.5′ pixels (~4.6 km at the equator) with the difference between the lowest and highest of the 9 points of 30″ exceeding 200 m were defined as mountainous. Based on the GMBA definition, Körner et al. (2017) provided the first version of a global inventory of the world's mountains (GMBA v1), which was subsequently used in extensive mountain-related studies (e.g., Antonelli et al., 2018; Immerzeel et al., 2020). Recently, Snethlage et al. (2022) developed the latest version of the GMBA mountain inventory (GMBA v2) at a high resolution of 7.5″. This new version has a coverage of about 18.2% of the global land area excluding Antarctica, larger than the GMBA v1 (12.3%; Snethlage et al., 2022).

In the USGS method, Karagulle et al. (2017) used slope class, relative relief, and profile to produce a characterisation of global landforms. The DEM was applied from the Global Multi-resolution Terrain Elevation Data (GMTED) 2010 at a resolution of 250 m (USGS, 2010). There are four classes of mountains: high mountains, scattered high mountains, low mountains, and scattered low mountains.

Table 1.1 *Key characteristics of WCMC, GMBA and USGS mountain definitions.*

Characteristic	WCMC	GMBA	USGS
DEM source and resolution	GTOPO30, 1 km	Hijmans et al. (2005), 1 km	GMTED, 250 m
Classification basis	Elevation, slope, and local elevation range	Ruggedness	Slope class, relative relief, and profile
Mountain classes	• >4,500 m • 3,500–4,499 m • 2,500–3,499 m • 1,500–2,499 m • 1,000–1,499 m • 300–999 m	Mountain terrain	• High mountains • Scattered high mountains • Low mountains • Scattered low mountains
Reference	Kapos et al. (2000)	Körner et al. (2011)	Karagulle et al. (2017)

1.1.2 Earth observation satellites

Satellites are human-made devices placed in space to orbit the Earth and other bodies. One of the primary purposes of satellite data is for Earth Observation (EO), providing crucial insights into Earth's surface and weather changes. Most EO satellites are situated in low Earth orbit for high-resolution data, with some in geostationary orbit for continuous coverage. There have been more than 950 EO satellites up to 2021 (Pixalytics, 2021), each varying in image resolution based on their instruments and orbital altitude.

Satellite observations, providing wall-to-wall information on the Earth's surface, serve as an important resource for global land-use change studies. Multiple land cover products or forest change datasets have been generated from satellite observations at global or regional scales. Most remote sensed forest products (Hansen et al., 2013; Feng et al., 2016; Qin et al., 2017) were derived from satellite observations using passive-optical techniques such as Landsat and MODIS (Moderate Resolution Imaging Spectroradiometer) carrying observations. While passive sensors specialise in measuring attributes such as sea surface temperature and vegetation properties, they tend to have limited spatial coverage in areas with dense cloud cover. In contrast, active sensors are adept at sensing vertical atmospheric profiles, precipitation, topography, and forest structure. One application in forest mapping involves developing a global map of forest canopy height by combining Landsat data with the Global Ecosystem Dynamics Investigation (GEDI) LiDAR (Light Detection and Ranging) observations (Potapov et al., 2021).

1.1.3 Assessments of mountain forest change

Last century, assessments of forest change were mainly conducted based on aerial photos in separate (discontinuous) years and field surveys (forest inventory). Since the 21st century, high-resolution forest change datasets have emerged, and these products have been used to assess forest change in mountains. Tree cover has been reported to increase continuously in very-high-elevation areas. An example of this can be found in the Swiss Alps, where areas situated >800 m below the current potential treeline experienced a considerable increase in forest cover percentage during 1880–2000 (Bebi et al., 2017). Similarly, in the Eastern Himalayas, forest gains were notably stronger at

elevations >3,000 m in the region from 1986 to 2021, suggesting faster forest growth at high elevations due to rising temperatures (Wang et al., 2022).

The general notion related to deforestation was that it predominately took place in lowland areas. Due to poor access, steep slopes and high elevations of mountains, forest loss in mountains was typically considered to be very limited. This idea was in line with previous work showing substantial forest loss in lowlands but only negligible loss, and even forest gain, in mountains (Curran et al., 2004; Song et al., 2018; Aide et al., 2019). However, recent studies have reported that mountain forests were converted to croplands and plantations in mainland Southeast Asia (Zeng et al., 2018a; Zeng et al., 2018b; Feng et al., 2021). Elsewhere, in a mountainous area in Zhejiang Province of China, the annual rate of forest loss has significantly increased by more than six times during 2001–2008 (Xiong et al., 2020). Following its peak magnitude in 2008, the annual forest loss rate remained stable but at a high level from 2009 to 2018 (Xiong et al., 2020).

Although there have been many local- or regional-scale studies investigating changes in mountain forest cover, these studies used different methods and datasets, making it difficult to compare or reach globally consistent conclusions. Our understanding of mountain forest change at a global scale is still lacking.

1.2 Mountain forest loss

1.2.1 Spatiotemporal pattern of forest loss and associated drivers

The spatial and temporal patterns of forest changes, i.e., forest loss and gain, have been extensively explored based on forest inventory and remote sensing forest products. However, changes in the forest area are still hotly debated. Extensive work has reported a net forest loss at a global scale. Using high-resolution satellite data, global forest loss and gain have been estimated to be 2.3 and 0.8 million km^2 during 2000–2012 (Hansen et al., 2013), and 1.81 and 0.81 million km^2 during 1990–2005 (Feng et al., 2016). According to the 2015 Global Forest Resources Assessment of the Food and Agriculture Organization of the United Nations, the global forested area fell by 3% from 41.28 million km^2 in 1990 to 39.99 million km^2 in 2015 (Keenan et al., 2015). However, a later study found an increase in global tree cover by 2.24 million km^2 from 1982 to 2016,

resulting from a net gain in the extra-tropics outweighing a net loss over the tropics (Song et al., 2018).

The drivers of forest loss have been reported to differ regionally. In boreal and temperate regions, forestry and wildfire were two main factors that have driven forest changes (Curtis et al., 2018). In Europe, there was a rising demand for forest services and products in the context of the bioeconomy, leading to a growth in forestry activities and an increase in the area of harvested forest (Ceccherini et al., 2020). As evidenced by distinct rows of planted trees, forestry activities in the United States and China showed signs of increased tree plantations (Curtis et al., 2018). Wildfire was a major cause of boreal forest change, especially in Canada and Russia (Stocks et al., 2002). Elsewhere, in eastern Australia, around 58,000 km^2 of temperate broadleaf forest was burned between September 2019 and early January 2020 by a series of mega-fires (Boer et al., 2020). High-intensity fires can spread to thousands of hectares of mountain slopes (Romme and Despain, 1989; Taylor and Skinner, 2003). For example, the Gospers Mountain fire near Sydney has ravaged over 5,100 km^2, which was the largest forest fire recorded in Australia (Boer et al., 2020). Moreover, in a future warming climate, the frequency, duration, and intensity of fires can be exacerbated, resulting in a massive forest loss (Wotton et al., 2010). Results from modelling predicted great variation in future fire-weather patterns and suggested the seasonal severity rating of fire hazard increases over much of North America under different scenarios (Dale et al., 2001).

In addition to forestry and wildfire, other disturbances such as storms and pests were also attributed to forest loss in some boreal and temperate regions (Amiro et al., 2010; Shikhov et al., 2019; Novo-Fernández et al., 2018). Mountain forests at high elevations are exposed to strong winds, especially intense storms (Greenberg and McNab, 1998). Changes in the global hydrological cycle and temperature will influence hurricane/typhoon formation, increasing the intensity and duration of individual storms as the warming of the air and ocean are sources of energy (Dale et al., 2001). Ice storms, snow avalanches and landslides may further shape montane environments and influence forest dynamics (Paolini et al., 2005; Lafon, 2004; Bebi et al., 2009). Moreover, native insects and diseases can have a large impact on forest changes. For example, the mountain pine beetle is a native insect of the pine forests of western North America, and large-scale outbreaks resulted in widespread tree mortality, further reducing forest carbon uptake and increasing emissions from the decay of dead trees (Safranyik

et al., 2010; Kurz et al., 2008). In some cases, forest insects may survive in greater numbers due to rising temperatures, especially in winter (Ogden et al., 2006; Paradis et al., 2008; Rochlin et al., 2013). It has been suggested that by the middle of the 21st century, the climate may be more suitable for pest expansion into vast areas of previously unaffected forests (Lesk et al., 2017).

Across the tropics, the main forest conversion process has been reported to be the transformation of closed, open, or fragmented forests to agricultural land (Achard et al., 2002). In Nan Province, Thailand, the annual forest loss showed a significant correlation with the global corn price, indicating agricultural expansion as a primary driver of forest loss in the region (Zeng et al., 2018a). Across Southeast Asia, many forested areas, including primary and protected forests, and lands in the process of recovering to secondary forests, have been converted to cultivated areas (Zeng et al., 2018b). In Africa, small-scale deforestation has been common, especially in the Congo Basin, and this increase in forest loss has been primarily driven by shifting agriculture (Tyukavina et al., 2018). In tropical America, the Amazon and its surrounding regions were hotspots of deforestation as a result of agricultural expansion until the early 2000s (Simon and Garagorry, 2005). Owing to the enforcement of laws, interventions in soy and beef supply chains, restrictions on access to credit, and expansion of protected areas, deforestation rates in the Brazilian Amazon decreased by 70% from 2005 to 2013 (Nepstad et al., 2014). However, after 2013, there was a renewed escalation in forest loss rates, with a significant loss of forest area driven by El Niño and the drought year of 2015/2016 (Qin et al., 2019). There was also a large loss due to deforestation-related fires in August 2019 (Barlow et al., 2020). The deforestation rate in 2020 continued to rise, reaching the peak for the decade of 2011–2020 (Silva Junior et al., 2021). The escalation in deforestation rates can be attributed to environmental setbacks, starting with a controversy over contentious modifications to the Brazilian Forest Code in 2012 (Brancalion et al., 2016).

Across mountainous regions, the contemporary trends in global mountain forest loss are uncertain. Recent studies have shown mountain forests facing increasing pressure from various forms of exploitation, such as timber harvesting and agricultural expansion, particularly in Southeast Asia (Zeng et al., 2018a; Zeng et al., 2018b; Feng et al., 2021). Contrastingly, in regions such as the Andes, evidence suggested an overall net increase in woody vegetation, with dynamics varying according to elevation (Aide et al., 2019). These different

findings result from diverse locally-sourced data and varying analytical approaches, demonstrating the need for a comprehensive global analysis using a consistent analytical framework to accurately understand the mountain forest loss pattern worldwide.

1.2.2 Dynamics in size of forest loss patches

The patterns of forest loss patch size do not remain constant as time goes by (Kalmadeen et al., 2018). Differences in forest patch sizes are associated with impacts on biodiversity, and the carbon and water cycles (Zhang et al., 2010; Liu et al., 2019). Species richness of montane forests significantly increases with increasing forest patch size (Mohandass et al., 2014). A forest patch below a specific threshold may no longer be able to sustain the original community. Forest fragmentation leads to changes in ecological functioning and species composition (Laurance et al., 2011), resulting in decreased carbon storage at forest edges (Chaplin-Kramer et al., 2015). Shifts in deforestation among different scales have the potential to alter the mechanisms and patterns of regional precipitation (Chambers and Artaxo, 2017; Khanna et al., 2017). The size of forest clearing activities is also utilised as an indicator for characterizing small-scale or large commercial and industrial-scale operations (Austin et al., 2017).

Many studies at local or regional scales have been conducted to quantify deforested clearing sizes. It was reported that over half of the increase in tropical deforestation during 2000–2012 was driven by a significant rise in medium and large clearings (>10 ha), especially in Southeast Asia and South America (Austin et al., 2017). This trend indicated the increasing dominance of industrial-scale drivers. In the Amazon, new small clearings have increased in the 21st Century, while there have been reports of a significant decrease in the number of large forest loss patches (>50 ha), leading to an observed decline in the total deforestation in the region (Rosa et al., 2012; Godar et al., 2014; Kalamandeen et al., 2018). The increased small-scale forest loss events are possibly related to anthropogenic activity rather than natural disturbances. This trend presents an alarming new challenge for forest conservation as small-scale losses are inherently more difficult to monitor and control. Similarly, in the Congo Basin, smallholder clearings have increased over time (Tyukavina et al., 2018). During 2000–2014, there was an estimated 84% of deforested areas in the region attributed to small-scale, non-mechanised forest clearings for agriculture. Across

Europe, the average patch size of deforested areas increased by 34% during 2016–2018 compared with 2004–2015 (Ceccherini et al., 2020).

There have also been some regional assessments of remaining forest patches over mountain regions. In the mountains of Chiapas, Mexico, there was a rapid decline in the mean size of forest patches from 1975 to 1990, indicating a rise in deforestation and fragmentation driven by the expanding human population and the growing demand for agriculture and timber resources (Cayuela et al., 2006). In the western United States, the remaining forest patches were reduced by 4.5% (20,000 km²) due to residential land use and transportation infrastructure in 2000. It was anticipated that the on-going expansion of residential land would lead to an additional 1.2% reduction in forest patches by 2030 (Theobald et al., 2011). In the Peruvian Andes, montane forest patches have significantly decreased from 1987 to 2007 and the mean patch size of montane forests was smaller in 2007 than in 1987 (Tovar et al., 2013). In the Western Andean Range, forest fragmentation is particularly striking (i.e., a rapid decrease in the size of alpine cloud forests) from 1991 onwards (Balthazar et al., 2015). Across the region extending from the Gulf of Bothnia to the Scandinavian Mountain Range in northern Sweden, there was a substantial and rapid loss of natural and near-natural forests from 1973 to 2014 due to intensive forest management (Svensson et al., 2019). In a tropical forest on Hainan Island, China, the large forest patches (>1 km^2) decreased from 754 km^2 to 316 km^2 in total area, and from 92 to 64 in number between 1991 and 2008, due to planting, logging, and grazing. Also, there was an increase in forest fragmentation, with the mean area of forest patches decreasing by 53% over the 17-year period (Zhang et al., 2010).

However, in a mountain watershed in Nepal, it was reported that the number of forest patches decreased continuously from 1976 to 2000 (Gautam et al., 2003). This suggests the merging of smaller patches due to forest regeneration and/or plantation establishment on degraded sites that had separated two or more forest patches (Gautam et al., 2003). These regional studies have drawn varying conclusions, leaving the dynamics of deforestation or forest patchiness in mountainous areas still unclear. A comprehensive and consistent analysis of the size of forest loss, especially across tropical mountains which are hotspots of deforestation, is needed to characterize different drivers of deforestation and better understand the changes in forest landscapes.

1.3 Mountain treelines

1.3.1 Definition of the treeline and its global pattern

The treeline definition and its global distribution have sparked heated debates among experts (Troll, 1973; Körner, 1998; Jobbágy and Jackson, 2000; Smith et al., 2003). There are multiple definitions of treelines depending on the focus of studies. It can be defined as the end of a contiguous closed forest (timberline; Smith et al. 2003), the upper limit of isolated individual trees (tree species line), or an elevation between them with groups of trees over a certain threshold (Körner and Paulsen 2004; Figure 1.1). The transition from uppermost closed montane forests to the treeless alpine vegetation is commonly characterised as treeline ecotone, a steep gradient of increasing stand fragmentation. By zooming out on remote sensing images, it becomes apparent that the entire treeline track can form a closed loop on the mountaintop (Figure 1.2).

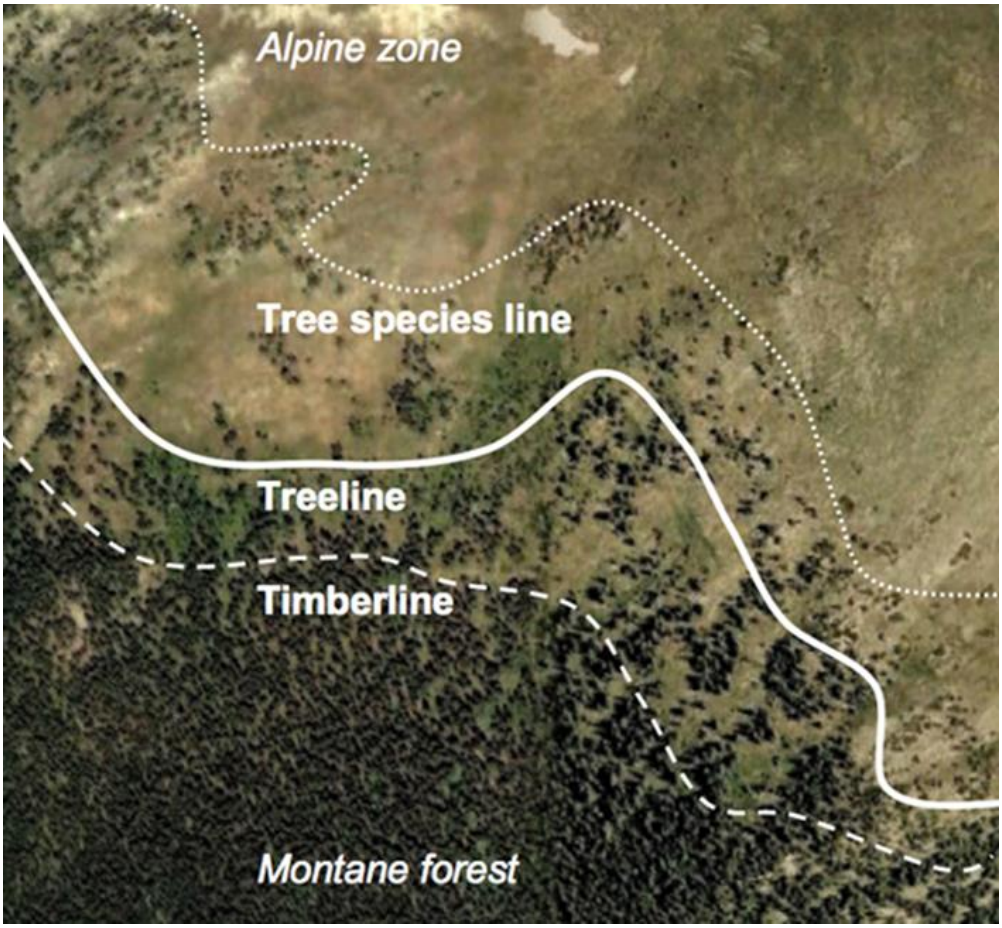

Figure 1.1 *Conceptual representation of treeline definitions. Reproduced from Berdanier (2010).*

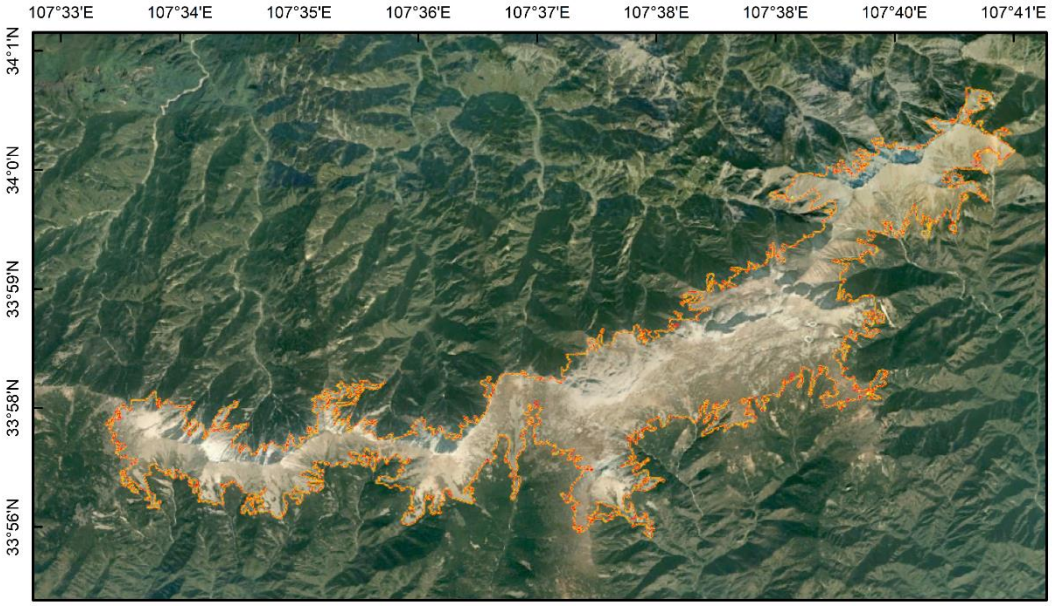

Figure 1.2 *Schematic showing an example of the treeline loop from a satellite view of a mountain in China (Qinling). The highlighted line is the track of treeline defined by tree canopy cover using the Hansen et al. (2013) definition.*

The treeline is a global phenomenon, usually found at high elevations and high latitudes, but does not apply in coastal areas or flatlands. Beyond the treeline, trees cannot tolerate harsh environmental conditions such as cold temperatures or insufficient available moisture at high altitudes (Elliott-Fisk, 2000). Other factors such as strong winds, high snowpack or lack of sunlight can also contribute to the absence of trees in a certain area.

Many studies have investigated the global latitudinal distribution of treeline elevation. The altitude of the treeline depends on both latitude and climate (Price et al., 2011). The world's highest treelines were found in the Himalayas (Miehe et al., 2007) or the Andes (Hoch and Körner, 2005; Price et al., 2011) at approximately 5,000 m. At a global scale, the relationship between the treeline elevation and latitude is not strictly correlated (Körner, 1998). A worldwide survey on treeline positions showed the highest treeline at around 30°N at ~4,000 m, rather than at the equator (Hermes, 1955). In temperate and boreal regions, the altitude of the treeline decreases with increasing latitudes (Cogbill and White, 1991; Malyshev, 1993) as a result of a decline in temperature along latitudinal gradients. Over the tropics, there is a slight decrease in treeline from the northern to the southern hemisphere (Jobbágy and Jackson, 2000). The elevation of the

treeline in the northern hemisphere has been reported higher than that at the same latitude in the southern hemisphere (Körner, 1998). Changes in environmental conditions along latitudinal and altitudinal gradients are independent, which means the rising temperature due to reducing latitude cannot be offset by the falling temperature due to increasing altitude. In continental climates, the limiting factor of a higher treeline is warm season temperature rather than annual mean or cold season temperatures (Troll, 1973). Another assessment of treeline elevations on various slope directions in the European Alps demonstrated that elevations of the treeline in a humid environment are decided by corresponding isotherms, rather than latitude and season length (Paulsen and Körner, 2001).

1.3.2 Factors determining mountain treelines

The previous understanding was that thermal limitations determine the elevation of the treeline on large scales (Körner and Paulsen, 2004; Körner, 2007; Jobbágy and Jackson, 2000; Case and Duncan, 2014; Paulsen and Körner, 2014). Globally, the treeline follows the line where the mean ground (root-zone) temperature during the growing seasonal is approximately 6.7°C, with a higher temperature of 7–8°C in the temperate and Mediterranean zones, and lower temperatures over the tropics (5–6°C) and in the subarctic and boreal regions (6–7°C) (Körner and Paulsen, 2004; Cieraad et al., 2014; Körner, 2021). Tree growth generally requires a growing season of 94 days, with the mean temperature remaining over 0.9°C (Paulsen and Körner, 2014).

Results from local studies have shown low temperature is not the only driving factor influencing the treeline. For example, on the southern Tibetan Plateau, a common sensitivity of tree growth at treeline ecotones is related to moisture variables (Lyu et al., 2019). In the Yukon Territory, Canada, excessive warming beyond a certain threshold without effective precipitation can have negative impacts on trees at the treeline (D'Arrigo et al., 2004).

1.3.3 Treeline dynamics

Abundant evidence showed that climate warming may lead to continuous advance of the treeline to greater altitudes and latitudes in the long term

(MacDonald et al., 2000; Payette et al., 2002), which may give rise to novel high-elevation vegetation patterns in a warmer future world (Kullman, 2002). Due to climate change, the structure and position of the treeline are expected to undergo significant changes (Camarero and Gutiérrez, 2004). In the Changbai Mountains, in northeast China, the treeline increased by around 80 m from 1850 to 2010, with the most intense upward shift corresponding with rapid warming since 1985 (Du et al., 2018). A global analysis of 166 sites for which treeline dynamics had been recorded from 1900 showed that 52% of these sites have advanced and only 1% have retreated (Harsch et al., 2009). Especially for those treelines that underwent substantial winter warming and that exhibited a diffuse form, they were more likely to have advanced. Similarly, a meta-analysis of 143 sites across the Northern Hemisphere found that 88.8% of the treeline sites experienced upward movement, 10.5% remained stable and 0.7% showed a downward shift during 1901–2018 (Lu et al., 2021).

However, a few studies have suggested that there was no significant upward movement of the treeline under climate warming in some areas (Cullen et al., 2001; Liang et al., 2011). It should be also noted that changes in forest dynamics may lag behind climate change because trees have a long-life span and subsequently establish resilience to the surroundings, but also climate change commonly has cumulative effects (Liu and Yin, 2013). In addition, the timing of treeline advance differs significantly between regions, which can be explained by the differences in the rate of forest response to climate or by differences in regional climate history (Lloyd and Fastie, 2003).

New evidence has shown that precipitation plays a more important role than temperature in predicting treeline shift rates across the Northern Hemisphere (Lu et al., 2021). In subarctic areas, autumn precipitation mostly determined treeline shift rates, whereas, in temperate regions, treeline shift rates were accelerated by warmer temperatures and higher autumn precipitation but negatively correlated with spring precipitation and standardised precipitation evapotranspiration index rates. There is also evidence illustrating that treeline shift rates in the Himalayas were predominantly regulated by spring precipitation (Sigdel et al., 2018). Even though recent warming trends have been observed in the central Himalayas, the ongoing arid pattern would promote downward treeline shifts if the availability of moisture falls below a crucial threshold. The relationship between temperature and growth also depends on tree age over the globe, implying that biogeographic patterns in treeline growth are influenced by local

factors (Camarero et al., 2021). Global simulations forecast longer growing seasons at treeline and faster growth rates which would be less dependent on the increasing temperature.

1.4 Impacts of mountain forest changes

1.4.1 Biodiversity impacts

Mountains are home to >85% of the world's birds, mammals, and amphibians (Rahbek et al., 2019). Montane forests play a crucial role as refuges for large numbers of rare and endangered species with limited geographical ranges (Hill et al., 2019). Mountain forest changes have great impacts on terrestrial biodiversity. Deforestation and degradation pose substantial challenges to the survival of species in specialised microenvironments (Watson et al., 2004). Furthermore, climate change is compelling many montane species to seek suitable habitats at higher elevations, yet their capacity to do so may be constrained by topographical limitations and the integrity of their habitats (Moritz et al., 2008; Colwell et al., 2008; Chen et al., 2011).

Deforestation and forest fragmentation have extensively occurred in areas with high diversity and endemism levels. For example, in South Ecuador, an area of high conservation value, the annual deforestation rate experienced a significant acceleration (Tapia-Armijos et al., 2015). By 2008, nearly half of the original forest cover had been transformed into pastures and other anthropogenic land cover types.

Across different species groups, there is significant variation in the extent and pattern of biodiversity loss (Giam, 2017). Complete tropical forest loss and degradation can result in species richness reduction ranging from less than 10% in mosquitoes to over 50% in ants and lizards (Alroy, 2017). This is possibly due to the variations in the proportion of species that rely on forests among diverse groups. In addition, deforestation-induced biodiversity loss can be doubled by the impact of anthropogenic disturbance in tropical forests (Barlow et al., 2016). In the Indian Himalaya, nearly 25% of endemic species, including 366 endemic vascular plant taxa and 35 endemic vertebrate taxa, were projected to be lost by the year 2100, given the ongoing rate of deforestation (Pandit et al., 2007).

Biodiversity hotspots

Biodiversity hotspots are biologically rich but threatened terrestrial regions, initially introduced as a concept to identify priority areas for major conservation efforts and resource allocation (Myers et al., 2000; Brooks et al., 2002; Myers, 2003). Biodiversity hotspots harbour a high concentration of species with limited ranges, yet many of their natural habitats have been cleared, putting them at risk of widespread extinction (Myers, 2003; Tracewski et al., 2016; Kobayashi et al., 2019). Biodiversity hotspots serve not only as critical regions for conservation but also as essential tools for setting priorities and informing cost-effective strategies for biodiversity conservation (Marchese, 2015).

Within biodiversity hotspots, endemic species are susceptible to land-cover changes which reduce natural habitats and increase anthropogenic interactions and disturbances (Crooks et al., 2017; Taubert et al., 2018). Deforestation is one of the primary drivers of species extinction (Brooks et al., 2002; Tracewski et al., 2016; Betts et al., 2017). In the Indo-Burma biodiversity hotspot, Bangladesh has witnessed the extinction of 31 vertebrate species over the last century (Reza and Hasan, 2019). To understand and mitigate the impact of forest change on biodiversity, researchers have combined remote-sensing datasets of changes in forest areas with biodiversity databases, providing insights into species responses at various scales (Tracewski et al., 2016; Betts et al., 2017; Hu et al., 2021).

Protected areas

Protected areas (PAs) play a critical role in forest protection. The International Union for Conservation of Nature (IUCN) defines a protected area as “a clearly defined geographical space, recognised, dedicated and managed, through legal or other effective means, to achieve the long-term conservation of nature with associated ecosystem services and cultural values” (Borrini-Feyerabend et al., 2013). Based on their management objectives, PAs are classified into six categories by the IUCN: strict nature reserve (Ia), wilderness area (Ib), national park (II), natural monument or feature (III), habitat/species management area (IV), protected landscape/seascape (V), and protected area with sustainable use of natural resources (VI).

Many studies have consistently shown that protected areas generally contributed to preventing deforestation within their boundaries (Naughton-Treves et al., 2005;

Heino et al., 2015; Yang et al., 2021). Nevertheless, forest loss rates in many protected areas remained at a high level (Yang et al., 2021). Accelerating rates of forest loss have been observed within protected areas encompassing all IUCN categories, more pronounced in the strictly protection IUCN categories (Leberger et al., 2020). Another growing concern comes from the isolation of protected areas due to forest loss and degradation in surrounding areas (Curran et al., 2004; Naughton-Treves et al., 2005).

1.4.2 Hydrological impacts

Mountain forest cover changes have significant impacts on the water cycle locally and regionally. When trees are removed, evapotranspiration is reduced, which indicates less water returning to the atmosphere. This would increase the runoff from the area. In the Amazon, for example, large-scale deforestation has led to an increase in river discharge by 20% on average (Foley et al., 2007). Meanwhile, the amount of moisture carried away by the atmosphere decreased, resulting in reduced rainfall in regions downwind (Spracklen et al., 2012). Analysis from satellite, station-based and reanalysis datasets showed recent deforestation has caused large reductions in precipitation across the tropics (Smith et al., 2023).

Evapotranspiration

Evapotranspiration (ET) includes the loss of water to the atmosphere by evaporation from soil and plant surfaces and by transpiration from plants (Tian et al., 2011). ET is controlled by the vegetation, which is closely related to local moisture conditions during the dry season (von Randow et al., 2012). The moisture regime of the region can be significantly impacted by extensive land-use changes.

In mountainous watersheds, lower ET rates can be attributed to high atmospheric humidity and low annual temperature (Wei et al., 2005). Forests are regarded as an important contributor to atmospheric moisture. ET from a forest is generally higher than that from pasture or bare land, but this rule does not apply to mountain regions. For example, in the upstream area of the Heihe River Basin with an altitude of approximately 3,000 m above sea level, ET in forested areas was far lower than that in those regions covered by grassland (Wu et al., 2015).

Results from flux tower measurements showed that evapotranspiration changes were associated with a relative decrease of about 30% of latent heat after deforestation in southwestern Amazon (Von Randow et al., 2004), while a satellite-based model simulated a smaller decline in the region (2%–27%; Zemp et al., 2017). One potential explanation for this discrepancy could be that in the latter study, large-scale data were used to calibrate the evapotranspiration model across various hydroclimatic conditions, possibly leading to an underestimation of ET changes associated with deforestation (Silvério et al., 2015). There was also evidence showing a significant positive relationship between local-scale forest cover changes and annual ET variations in subarctic China (Yao et al., 2014). The reason could be an increase in surface albedo and a reduction in the fractional vegetation cover. Moreover, the El Niño/Southern Oscillation (ENSO) could dominate the multi-decadal ET variability due to regional-scale wind speed changes.

Runoff

Forest loss impacts river flow by altering rainfall interception, transpiration, permeability of soils and soil moisture (Brown et al., 2005; Andréassian, 2004). Most of the current knowledge on annual discharge originates from paired catchment studies (Oudin et al., 2008; Andréassian, 2004; Lane and Mackay, 2001). One of the classic paired catchment studies is in Coweeta, North America, comparing the discharge regimes between deforested and forested mountain watersheds (Swank and Webster, 2014). However, annual runoff response thresholds vary among catchments, which means the change in annual runoff in a given catchment may not be detected if the percentage of forest cover change area is relatively low (Zhang et al., 2012). Normally, reductions in forest cover of less than 20% cannot be detected by measuring streamflow (Bosch and Hewlett, 1982). For example, in the snowmelt-runoff catchment of the Willow River, Canada, a significant increase in annual runoff was detected with a 30% harvesting level (Lin and Wei, 2008; Wei and Zhang, 2010). However, there was no detectable hydrological change in the Nam Pong river basin in northeast Thailand where forest cover was reduced by 53% (Wilk et al., 2001). These differences might be explained by variability in topography, vegetation, soils, climate conditions and hydrologic regime among the study watersheds (Stednick, 1996), as well as in discharge measurement quality as it is often difficult to accurately measure catchment water budgets. Also, the area of catchments is an

important factor because large catchments usually have a great ability to buffer hydrological impacts from a small degree of forest disturbances (Buttle and Metcalfe, 2000).

Rainfall

The most popular narrative is that the removal of forests decreases rainfall. There is evidence of changes in local/regional patterns of rainfall after deforestation. Many models have predicted tropical deforestation results in a decrease in rainfall over the Amazon (Werth and Avissar, 2002; Ramos da Silva et al., 2008; Nobre et al., 2009; Spracklen and Garcia-Carreras, 2015). Deforestation along the southern coast of West Africa, where the fraction of the cleared primary forest was significantly larger than the corresponding fraction for the Amazon region, resulted in a significant reduction in regional rainfall (Zheng and Eltahir, 1997).

On a larger scale, rainfall reductions have been observed over deforested regions across the tropics (Smith et al., 2023). An analysis of global hydroclimate showed that tropical deforestation greatly influenced the local and remote precipitation, but it had a weaker effect on the mid-latitude regions (Hasler et al., 2009). Due to frontal systems and the variety of air mass source regions, the impact of deforestation and mid-latitudinal rainfall changes are more difficult to estimate than those in the tropics (Pielke et al., 2007). Conversely, afforestation has led to increased local and downwind precipitation, as confirmed by a paired rain-gauge analysis in Europe (Meier et al., 2021).

1.4.3 Climate impacts

Changes in forest cover can impact climate from local/regional to global scales. Results from a land-atmosphere coupled model showed that recent tropical forest conversion increased the regional warming by 0.016°C in Southeast Asia, 0.042°C in South America and 0.047°C in Africa during the local dry season (Zeng et al., 2021). One of the biggest concerns was the local warming of up to 2°C induced by deforestation in regions where extensive forest conversion has occurred. Moreover, the climate impacts of mountain deforestation can be regulated by elevation, with the rise of local temperature weakening as elevation increases. The explanatory mechanism is related to different sensitivities of albedo and evapotranspiration changes to forest loss in the highlands and

lowlands. As elevation increases, the decrease in ET caused by deforestation diminishes significantly, while the increase in albedo remains unchanged.

Extensive land cover changes can also have remote climate impacts. Large-scale atmospheric circulations (e.g., Rossby waves, Hadley circulations) facilitate the transmission of climatic impacts to distant geographical regions through teleconnections (Werth and Avissar, 2002; Avissar and Werth, 2005; Cui et al., 2006; Bala et al., 2007; Hasler et al., 2009; Takata et al., 2009; Snyder, 2010). For example, complete deforestation in Amazon was simulated to reduce rainfall during the agricultural season in the US Midwest, Northwest, and parts of the south (Werth and Avissar, 2002; Avissar and Werth, 2005; Medvigy et al., 2013). Another model predicted that it could lead to an increase in rainfall, especially during winter, in the eastern seaboard of the US and the northeastern Atlantic, potentially extending its influence towards western Europe and impacting precipitation patterns in Europe (Gedney and Valdes, 2000).

On the global scale, the predicted average temperature could rise by 0.1–0.7 °C in the event of complete deforestation throughout the entire tropical region (Feddema et al., 2005; Findell et al., 2006; Bala et al., 2007; Lawrence and Vandecar, 2015). However, the predicted global mean precipitation remains unchanged, possibly as a consequence of the counteracting signals from local and regional impacts, as well as the dampening effect of global averaging on climate responses (Feddema et al., 2005; Avissar and Werth, 2005; Lawrence and Chase, 2010).

1.4.4 Impacts on the carbon cycle

Global forest ecosystems contain a large amount of carbon, with roughly 37% in low-latitude forests, 14% in mid-latitudes, and the remaining 49% at high latitudes (Dixon et al., 1994). As summarised by Mitchard et al. (2018), forest carbon stocks and their changes can be evaluated using multiple approaches including forest inventory plots (e.g., Feldpausch et al., 2012; Brienen et al., 2015; Sullivan et al., 2017), atmospheric inversions (e.g., Stephens et al., 2007; Peylin et al., 2013), satellites (e.g., Mitchard et al., 2012; Ryan et al., 2012; Baccini et al., 2017), and modelling (e.g., Sitch et al., 2015). Pervasive deforestation and forest degradation contribute to greenhouse gas (GHG) emissions to the atmosphere

through the combustion of forest biomass and the decomposition of the remaining plant material and soil carbon (van der Werf et al., 2009).

Tropical deforestation, currently the hotspot of global forest carbon loss (Harris et al., 2012; Zeng et al., 2018b; Harris et al., 2021), directly releases carbon stored in vegetation and soil, potentially reducing the carbon sink capacity of terrestrial ecosystems (Baccini et al., 2012; Veldkamp et al., 2020; Bonan, 2008). Numerous studies have estimated the forest carbon loss due to tropical deforestation. In Southeast Asia, upward forest loss to higher elevations and steeper slopes led to annual forest carbon loss of 0.424 Pg C yr^{-1} from 2001 to 2019 (Feng et al., 2021). Across the tropics, the gross annual carbon emissions were around 0.8 Pg C yr^{-1} during 2000–2005, from the loss of 43 million hectares of forest (Harris et al., 2012). A doubling of gross forest carbon loss driven by tropical deforestation has been further observed, from 0.97 Pg C yr^{-1} in 2001–2005 to approximately 2 Pg C yr^{-1} in 2015–2019 (Feng et al., 2022). To mitigate the negative impact on our environment, the most effective method for removing atmospheric carbon can be the restoration of natural forests in humid tropics, such as Amazonia, Borneo, or the Congo Basin (Lewis et al., 2019).

Different from tropical forests, boreal forests primarily store carbon in soil organic matter, with a very small proportion found in the active living biomass (Malhi et al., 1999). However, the increasing frequency of wildfires, driven by climate warming and drying, causes deeper burns into organic soils and releases more sequestered carbon into the atmosphere (Walker et al., 2019). Stand-replacing forest fires, which are predominantly observed in temperate and boreal forests, have led to an average of 0.188 Pg C yr^{-1} in gross emissions over the years 2001–2019 (Harris et al., 2021).

1.5 Aims and objectives

Assessment of spatiotemporal pattern of global mountain forest loss and its biodiversity impacts (Chapter 2)

In certain areas, the frontier of forest loss has encroached upon mountain regions. Yet the worldwide pattern of forest loss within the mountain regions, which are home to many of the Earth's bird, mammal, and amphibian species, remains unclear. In this research, I aim to unpack spatiotemporal patterns,

drivers, and biodiversity impacts of mountain forest loss. The specific objectives are:

- To assess forest loss patterns across global mountains and determine the proportion of areas showing signs of regrowth.
- To determine the extent of mountain forest loss within biodiversity hotspots across a range of elevation gradients.
- To estimate the fraction of mountain forest loss within mountain biodiversity hotspots in and around protected areas.
- To examine the drivers of mountain forest loss by comparing our mountain forest loss maps and statistics with other recently developed land-use maps.

Analysis of forest loss in terms of clearing sizes across tropical mountains (Chapter 3)

Tropical mountain forest loss threatens biodiversity, carbon storage and ecosystem sustainability, but a thorough and uniform assessment of the patchy nature of forest loss across tropical mountainous regions is currently absent. In this research, I will provide up-to-date and spatially explicit information on the scale of tropical mountain forest loss, as well as temporal trends associated with these patterns. The specific objectives are:

- To analyse how much forest loss was associated with clearings of different sizes.
- To uncover how the dynamics of forest loss vary across the three tropical regions.
- To determine whether the distribution of clearing sizes has changed over time.

Impacts of climate and climate change on mountain treelines (Chapter 4)

Owing to the potential interplay of human interventions that could also impact treelines, it is less well-known how climate influences mountain treelines. Previous studies have focused on individual treelines or mountain ranges. In this research, I will use satellite datasets and a novel algorithm to establish a new mountain treeline database that isolates climate impacts from other anthropogenic pressures. The specific objectives are:

- To map closed-loop treelines in mountain regions globally in 2000 based on remote sensing.
- To identify which bioclimatic factors control the position of natural mountain treelines from global to local scales.
- To explore the shifting of mountain treelines in natural systems.

1.6 Overview of methods

In this section I will outline the data and key methods used in Chapters 2–4 of this thesis. Firstly, I will examine and detail the important features and inputs of each of the datasets. Then I will summarise the core methods used to analyse the datasets. More details and limitations of the datasets will be covered in the individual analysis chapters and further discussed in Chapter 5.

1.6.1 Data

Key information on the datasets used in this thesis is listed in Table 1.2.

Table 1.2 *Summary of datasets used in this thesis.*

Dataset	Date Range	Native Resolution	Reference/link	Chapter(s) the data used in
Global Forest Change (GFC) v1.10	2000–2022, annual	30 m	Hansen et al. (2013)	Chapters 2,3,4
Driver of forest loss	2001–2015	10 km	Curtis et al. (2018)	Chapters 2,3
Global forest management data	2015	100 m	Lesiv et al. (2022)	Chapter 2
ASTER GDEM v3	2019	30 m	Tachikawa et al. (2011)	Chapters 2,4
GMBA mountain inventory v1.2	/	polygons	Körner et al. (2017)	Chapters 2,3,4
Species richness and rarity-weighted richness data v2017-3	2017	5 km	https://www.iucnredlist.org/resources/other-spatial-downloads	Chapter 2
Protected areas (WDPA)	update monthly	polygons	https://www.protectedplanet.net/en/thematic-areas/wdpa?tab=WDPA	Chapter 2
WorldClim database v2.1	1970–2000, average	1 km	Fick and Hijmans (2017)	Chapter 4
MODIS NDVI	2000–present, 16-day	463 m	https://developers.google.com/earth-engine/datasets/catalog/MODIS_MCD43A4_006_NDVI	Chapter 4

Global Forest Change (GFC) data

GFC data, developed by Hansen et al. (2013) in the Global Land Analysis and Discovery (GLAD) laboratory at the University of Maryland, provides information on forest cover change over time at 30 m spatial resolution. This dataset was

derived using Landsat time-series imagery. It provides multiple products, including tree cover for the year 2000, the year of forest loss (2001–present), and forest gain (up to 2012). We did not use the forest gain from this dataset because it was only available until 2012 and therefore its methodology will not be discussed.

In this dataset, trees are defined as all vegetation taller than 5 m in height; forest loss is defined as a stand-replacement disturbance or a change from a forest to a non-forest state. GFC tree cover data provide the percentage canopy closure of trees between 0–100%. Forest loss is updated annually, and the latest GFC (v1.10) reports global forest loss until 2022. The data can be freely accessed on the GLAD and Global Forest Watch. The GFC data have been extensively used in quantifying forest change and associated impacts from regional to global scales (Li et al., 2016; Baker and Spracklen, 2019; Hansen et al., 2019; Harris et al., 2021; Feng et al., 2021; Vancutsem et al., 2021; Feng et al., 2022; Pendrill et al., 2022; Smith et al., 2023).

Despite the broad application of the GFC dataset, there are some inconsistencies due to differences in Landsat sensor technology, improvements in global acquisition strategy, and adjustments of algorithms. This will be discussed in more detail in the discussion of uncertainties section of Chapter 5.

Drivers of forest loss

This dataset reports the dominant driver of tree cover loss at any 10 km × 10 km grid cell around the world for the period 2001–2015 at 10 km resolution (Curtis et al., 2018). Cells contain one of the five disturbance types: commodity-driven deforestation, shifting agriculture, forestry, wildfire, and urbanization. This product was generated through a decision-tree model based on visual interpretation of 4,699 training sample cells. Forest loss in a given year was determined according to the GFC data (Hansen et al., 2013). High-resolution Google Earth time-series images were used to ascertain the underlying cause of forest loss. When multiple factors contributing to forest loss were visible within a cell, the driver accounting for more than 50% of the total loss within the cell during the study period was assigned. An additional 1,565 randomly selected samples have been used to validate the model.

Curtis et al. (2018) noted that limitations may exist in the current dataset. First, time-series changes have not been evaluated in forest landscapes dominated by

shifting agriculture. Second, clearings from primary or secondary forests were not differentiated.

Global forest management data

This dataset provides spatially explicit information on forest management in 2015 over the globe at a 100 m resolution (Lesiv et al., 2022). There are six forest management classes: naturally regenerating forests without signs of management, naturally regenerating forests with signs of forest management (such as logging), planted forests (rotation >15 years), plantation forests (rotation ≤15 years), oil palm plantations, and agroforestry. Naturally regenerating forests without signs of management include three sub-types: “not disturbed” – natural forest without detectable evidence of any disturbances; “with human impact nearby” – forest within the 100 m pixel is not disturbed, but there is evidence of non-forest management related human activities (e.g., roads, houses, small agricultural fields) within 500 m in any direction; “degraded or disturbed” – forest has been disturbed by natural disturbances, (e.g., wildfire, wind throw, flooding, or insect/disease outbreaks), but there are no human activities within the 100 m pixel or nearby. Forests with signs of forest management refer to those managed by human impact within the 100 m pixel, but there is no evidence of planting. Planted forest (rotation >15 years) refers to the forest that has been planted in the 100 m pixel with a relatively long rotation time, while plantation forests (rotation ≤15 years) are those intensively managed for timber with short rotation. Oil palm plantations are those palms with very distinguishable crown shapes. Agroforestry covers some other landscapes: fruit trees, tree shelter belts and small forest patches (groups of trees in lines or patches on cropland or pastures), agroforestry or sparse trees on agricultural fields (a mixture of crops and trees, or individual trees on cropland or pastures), shifting cultivation, and trees in urban/built-up areas (buildings or infrastructure dominant in the 100 m pixel or surroundings).

The forest management map was generated based on a global reference data set of 226,322 locations. At these locations, experts and participants have visually interpreted time series of high-resolution satellite imagery to classify land cover and land use. This map has been employed to classify plantations for mapping global terrestrial habitat types and to identify areas of global significance for biodiversity conservation and climate mitigation (Jung et al., 2020; Jung et al.,

2021). It also has the potential to be applied in a wide range of biodiversity and forest studies.

ASTER GDEM

The Advanced Spaceborne Thermal Emission and Reflection Radiometer (ASTER) Global Digital Elevation Model (GDEM) is a global elevation product with a horizontal resolution of 30 m, developed jointly by the Ministry of Economy, Trade, and Industry (METI) of Japan and the United States National Aeronautics and Space Administration (NASA; Tachikawa et al., 2011). The ASTER GDEM is one of the most complete digital topographic datasets of the Earth, covering >90% of the global land (83°N–83°S). This product was generated through the combination of individual scene DEMs, both with and without cloud masks, followed by the application of various algorithms to eliminate abnormal data (Fujisada et al., 2005; Fujisada et al., 2011; Fujisada et al., 2012).

The first and second version of the ASTER GDEM was released in 2009 and 2011. The final version (v3) released in 2019 was used in the thesis. ASTER GDEM v3 represents a refinement of version 2, incorporating several hundred thousand additional scenes to enhance overall quality. It also encompasses a thorough anomaly correction program, aimed at increasing the accuracy of GDEM. ASTER GDEM v3 is available for download from NASA Earthdata (https://search.earthdata.nasa.gov/search/) and Japan Space Systems (https://www.jspacesystems.or.jp/ersdac/GDEM/E/).

GMBA mountain inventory

The Global Mountain Biodiversity Assessment (GMBA) inventory provides a series of mountain polygons over the world. The GMBA definition was developed based on a 1 km DEM applied by WorldClim (Hijmans et al., 2005). It defines the world's mountains by a ruggedness threshold, making no distinction by elevation. For a 2.5′ pixel to be defined as mountainous, the elevational amplitude between the highest and lowest of the 9 points of 30″ needs to exceed 200 m (Körner et al., 2011). The GMBA v1.2, which was used in this thesis, includes 1,048 mountain regions of the world (Körner et al., 2017). This polygon-based mountain inventory has been widely used in research related to biodiversity and land cover (Chu et al., 2023; Reader et al., 2023; Gwate et al., 2023). A new release (GMBA

v2) is now available and provides 8,616 mountain ranges globally (Snethlage et al., 2022).

Species richness and rarity-weighted richness data

The species richness data are based on the raw IUCN ranges for amphibians, birds, mammals, and reptiles. It is important to note that the rasters are specifically applicable to terrestrial areas, as marine areas are represented solely by birds and mammals.

Species richness refers to the number of species potentially occurring in each grid cell. Rarity-weighted richness, also known as range-size rarity, quantifies the aggregate significance of each grid cell for the species found within it. For a given cell, with respect to each species, rarity-weighted richness is calculated as the area of the cell divided by the species' total range area, or as 1 divided by the total number of cells overlapping the species' range. These individual values are then aggregated across all the species considered in the analysis. Therefore, the value serves as a measure of relative importance and does not have any units.

This thesis used Red List version 2017-3 species richness and rarity-weighted richness with a resolution of ~5 km, available at https://www.iucnredlist.org/resources/other-spatial-downloads.

Protected Areas (WDPA)

The World Database on Protected Areas (WDPA) stands as the most comprehensive worldwide database on protected areas, encompassing both terrestrial and marine regions. It was developed by a collaborative initiative between the United Nations Environment Programme (UNEP) and the International Union for Conservation of Nature (IUCN) and managed by the UNEP World Conservation Monitoring Centre (UNEP-WCMC) in collaboration with a wide range of governments and non-governmental organizations, academic institutions, and industry stakeholders. The WDPA is updated monthly and can be accessed through https://www.protectedplanet.net/en/thematic-areas/wdpa?tab=WDPA.

WorldClim database

WorldClim is a global database of spatially interpolated historical and future weather/climate data. Historical climate data (WorldClim v2.1), which has been used in this thesis, offers the average climate data for the years 1970–2000 at a resolution of ~1 km. The data were produced from between 9,000 and 60,000 weather stations (Fick and Hijmans, 2017). Weather station data were interpolated using thin-plate splines, incorporating various covariates such as elevation, distance to the coast, maximum and minimum land surface temperature, and cloud cover.

WorldClim v2.1 climate data include monthly climate data for minimum, mean, and maximum temperature, precipitation, solar radiation, wind speed, and water vapor pressure, as well as 19 bioclimatic variables. The bioclimatic variables that have greater biological significance, encompass annual trends, seasonality, and extreme or limiting environmental factors. This dataset has been used in many fields of research, particularly in the environmental, agricultural, and biological sciences (Bastin et al., 2019; Zhao et al., 2022; Hua et al., 2022).

MODIS combined 16-day NDVI

This product was derived from the MODIS/006/MCD43A4 surface reflectance composites. The Normalized Difference Vegetation Index (NDVI) was computed using the Near-Infrared (NIR) and Red bands of each scene, calculated as (NIR - Red) / (NIR + Red). The calculated NDVI values fall within a range of -1 to 1, with a resolution of ~463 m. The MODIS combined 16-day NDVI is available at https://developers.google.com/earth-engine/datasets/catalog/MODIS_MCD43A4_006_NDVI.

1.6.2 Overview of analytical methods

There are three main methods used to analyse the data in the research chapters. I give an overview of these methods below.

Theil-Sen estimator

Theil-Sen estimator was used to evaluate the temporal trends (i.e., slope) in both Chapter 2 and Chapter 3. It is a method that robustly fits a line to sample points in the plane (simple linear regression) by selecting the median among the slopes calculated for all lines by pairs of points (Sen, 1968). This method offers several advantages compared to Ordinary Least Squares (OLS) regression. First, Theil-Sen regression is robust and less sensitive to outliers. Second, it enables significance tests, even when residuals do not follow a normal distribution. Third, it can provide more accurate results than OLS when dealing with skewed and heteroskedastic data, or normally distributed data. The Theil-Sen estimator was recognised as “the most popular nonparametric technique for estimating a linear trend” (Wilcox, 2010). Due to its robustness for trend detection and insensitivity to outliers, Theil-Sen estimator regression has been widely used in previous research, including analyses of forest cover trends (Song et al., 2018; Alibakhshi et al., 2020; Feng et al., 2022).

Mann-Kendall test

The purpose of the Mann-Kendall (MK) test is to assess if there is a linear monotonic trend within a given time series dataset (Mann, 1945). This non-parametric test is closely linked to the concept of Kendall's correlation coefficient (Pohlert, 2023). The MK test is performed upon several assumptions regarding the provided time series data. First, the data are independence and identically distributed if a trend is absent. Second, the measurements accurately reflect the actual states of the observed variables at the respective measurement times. Third, the processes employed for sample collection, instrumental measurements, and data handling are free from bias.

The MK test offers several advantages. For example, it does not make assumptions about the data following a specific distribution, such as normal distribution. Also, it remains robust in the presence of missing data, although a reduced number of sample points can potentially affect statistical significance. Furthermore, it will not be influenced by irregular spacing between the measurement time points and by the length of the time series. Therefore, this test has been used widely in environmental, climatological, and hydrological time series analysis (Lenton, 2011; Pokhrel et al., 2011; Feng et al., 2022). In this

thesis, the MK test has been used in Chapter 2 to assess whether the annual forest loss trends are significant.

Gradient boosting decision trees

The gradient boosting decision trees (GBDT) model was used in Chapter 4 to understand the climate impact on treeline positions. GBDT model, known for its feature interpretability, is a tree-based ensemble method that combines multiple regression trees (Friedman, 2001). In this model, the negative gradient of the loss function is used as an approximation of the residuals in the iterative process (Ke et al., 2017).

The GBDT process begins with initializing a weak learner to estimate an initial constant value for loss function minimization. Subsequently, based on the datasets, it creates decision trees and conducts iterative training. Next, GBDT calculates the negative gradient (residuals) associated with the loss function for each tree. It fits a regression tree to these residuals, determining the leaf node regions for the m-th tree. To minimise the loss function, it estimates values for all leaf node regions using a linear search. These steps are repeated until the target evaluation indicator reaches an optimal state.

GBDT can provide interpretative information on the relative importance of input variables and partial dependence plots. As GBDT exhibits flexibility in handling large datasets and is particularly effective in capturing complex relationships within the data, it was used in a wide range of studies (e.g., Liu et al., 2022; Messager et al., 2021).

1.7 Thesis structure

Chapter 2 presents a detailed assessment of mountain forest cover change worldwide using multiple global datasets. Chapter 3 examines the dynamics of forest loss in terms of patch sizes across tropical mountain regions. Chapter 4 investigates how climate and climate change impact mountain treelines. Chapter 5 contains a synthesis of the main findings from the analysis, a discussion of the limitations and uncertainties in this analysis and, finally, proposals for future directions that related research could take. Supplementary materials provided in Appendix A, B and C relate to Chapters 2, 3 and 4 respectively.

References

Aide, T.M., Grau, H.R., Graesser, J., Andrade-Nuñez, M.J., Aráoz, E., Barros, A.P., Campos-Cerqueira, M., Chacon-Moreno, E., Cuesta, F., Espinoza, R. and Peralvo, M., 2019. Woody vegetation dynamics in the tropical and subtropical Andes from 2001 to 2014: satellite image interpretation and expert validation. Global Change Biology, 25, 2112–2126.

Alibakhshi, S., Naimi, B., Hovi, A., Crowther, T.W. and Rautiainen, M., 2020. Quantitative analysis of the links between forest structure and land surface albedo on a global scale. Remote Sensing of the Environment, 246, 111854.

Alroy, J., 2017. Effects of habitat disturbance on tropical forest biodiversity. Proceedings of the National Academy of Sciences, 114, 6056–6061.

Amiro, B.D., Barr, A.G., Barr, J.G., Black, T.A., Bracho, R., Brown, M., Chen, J., Clark, K.L., Davis, K.J., Desai, A.R. and Dore, S., 2010. Ecosystem carbon dioxide fluxes after disturbance in forests of North America. Journal of Geophysical Research, 115, G00K02.

Andréassian, V., 2004. Waters and forests: from historical controversy to scientific debate. Journal of Hydrology. 291, 1–27.

Antonelli, A., Kissling, W.D., Flantua, S.G., Bermúdez, M.A., Mulch, A., Muellner-Riehl, A.N., Kreft, H., Linder, H.P., Badgley, C., Fjeldså, J. and Fritz, S.A., 2018. Geological and climatic influences on mountain biodiversity. Nature Geoscience, 11, 718–725.

Avissar, R. and Werth, D., 2005. Global hydroclimatological teleconnections resulting from tropical deforestation. Journal of Hydrometeorology, 6, 134–145.

Baker, J.C.A. and Spracklen, D.V., 2019. Climate Benefits of Intact Amazon Forests and the Biophysical Consequences of Disturbance. Frontiers in Forests and Global Change, 2, 1–13.

Barlow, J., Lennox, G.D., Ferreira, J., Berenguer, E., Lees, A.C., Nally, R.M., Thomson, J.R., Ferraz, S.F.D.B., Louzada, J., Oliveira, V.H.F. and Parry, L., 2016. Anthropogenic disturbance in tropical forests can double biodiversity loss from deforestation. Nature, 535, 144–147.

Baccini, A., Goetz, S.J., Walker, W.S., Laporte, N.T., Sun, M., Sulla-Menashe, D., Hackler, J., Beck, P.S.A., Dubayah, R., Friedl, M.A. Samanta, S. and Houghton, R.A., 2012. Estimated carbon dioxide emissions from tropical deforestation improved by carbon-density maps. Nature Climate Change, 2, 182–185.

Baccini, A., Walker, W., Carvalho, L., Farina, M., Sulla-Menashe, D. and Houghton, R.A., 2017. Tropical forests are a net carbon source based on aboveground measurements of gain and loss. Science, 358, 230–234.

Bala, G., Caldeira, K., Wickett, M., Phillips, T.J., Lobell, D.B., Delire, C. and Mirin, A., 2007. Combined climate and carbon-cycle effects of large-scale deforestation. Proceedings of the National Academy of Sciences, 104, 6550–6555.

Balthazar, V., Vanacker, V., Molina, A. and Lambin, E.F., 2015. Impacts of forest cover change on ecosystem services in high Andean mountains. Ecological Indicators, 48, 63–75.

Barlow, J., Berenguer, E., Carmenta, R. and França, F., 2020. Clarifying Amazonia's burning crisis. Global Change Biology, 26, 319–321.

Bastin, J.F., Finegold, Y., Garcia, C., Mollicone, D., Rezende, M., Routh, D., Zohner, C.M. and Crowther, T.W., 2019. The global tree restoration potential. Science, 365, 76–79.

Bebi, P., Kulakowski, D. and Rixen, C., 2009. Snow avalanche disturbances in forest ecosystems—State of research and implications for management. Forest Ecology and Management, 257, 1883–1892.

Bebi, P., Seidl, R., Motta, R., Fuhr, M., Firm, D., Krumm, F., Conedera, M., Ginzler, C., Wohlgemuth, T. and Kulakowski, D., 2017. Changes of forest cover and disturbance regimes in the mountain forests of the Alps. Forest Ecology and Management, 388, 43–56.

Berdanier, A.B., 2010. Global Treeline Position. Nature Education Knowledge, 3, 11. Accessed from https://www.nature.com/scitable/knowledge/library/global-treeline-position-15897370/.

Betts, M.G., Wolf, C., Ripple, W.J., Phalan, B., Millers, K.A., Duarte, A., Butchart, S.H. and Levi, T., 2017. Global forest loss disproportionately erodes biodiversity in intact landscapes. Nature, 547, 441–444.

Blyth, S., Groombridge, B., Lysenko, I., Miles, L., Newton, A., 2002. *Mountain watch: environmental change and sustainable development in mountains*. UNEP-WCMC, Cambridge.

Boer, M.M., Resco de Dios, V. and Bradstock, R.A., 2020. Unprecedented burn area of Australian mega forest fires. Nature Climate Change, 10, 171–172.

Bonan, G.B., 2008. Forests and climate change: forcings, feedbacks, and the climate benefits of forests. Science, 320, 1444–1449.

Borrini-Feyerabend, G., Dudley, N., Jaeger, T., Lassen, B., Neema, P., Phillips, A. and Sandwith, T., 2013. Governance of protected areas: from understanding to action. *Best Practice Protected Area Guidelines Series*. IUCN.

Bosch, J.M. and Hewlett, J., 1982. A review of catchment experiments to determine the effect of vegetation changes on water yield and evapotranspiration. Journal of Hydrology, 55, 3–23.

Buttle, J. and Metcalfe, R., 2000. Boreal forest disturbance and streamflow response, northeastern Ontario. Canadian Journal of Fisheries and Aquatic Sciences, 57, 5–18.

Brancalion, P.H., Garcia, L.C., Loyola, R., Rodrigues, R.R., Pillar, V.D. and Lewinsohn, T.M., 2016. A critical analysis of the Native Vegetation Protection Law of Brazil (2012): updates and ongoing initiatives. Natureza & Conservação, 14, 1–15.

Brienen, R.J.W., Phillips, O.L., Feldpausch, T.R., Gloor, E., Baker, T.R., Lloyd, J., Lopez-Gonzalez, G., Monteagudo-Mendoza, A., Malhi, Y., Lewis, S.L., Vásquez Martinez, R. et al., 2015. Long-term decline of the Amazon carbon sink. Nature, 519, 344–348.

Brooks, T.M., Mittermeier, R.A., Mittermeier, C.G., da Fonseca, G.A., Rylands, A.B., Konstant, W.R., Flick, P., Pilgrim, J., Oldfield, S., Magin, G. and Hilton-Taylor, C., 2002. Habitat loss and extinction in the hotspots of biodiversity. Conservation Biology, 16, 909–923.

Brown, A.E., Zhang, L., McMahon, T.A., Western, A.W. and Vertessy, R.A., 2005. A review of paired catchment studies for determining changes in water yield resulting from alterations in vegetation. Journal of Hydrology, 310, 28–61.

Camarero, J.J. and Gutiérrez, E., 2004. Pace and pattern of recent treeline dynamics: response of ecotones to climatic variability in the Spanish Pyrenees. Climatic Change, 63, 181–200.

Camarero, J.J., Gazol, A., Sánchez-Salguero, R., Fajardo, A., McIntire, E.J., Gutiérrez, E., Batllori, E., Boudreau, S., Carrer, M., Diez, J. and Dufour-Tremblay, G., 2021. Global fading of the temperature–growth coupling at alpine and polar treelines. Global Change Biology, 27, 1879–1889.

Case, B.S. and Duncan, R.P., 2014. A novel framework for disentangling the scale-dependent influences of abiotic factors on alpine treeline position. Ecography, 37, 1–14.

Cayuela, L., Benayas, J.M.R. and Echeverría, C., 2006. Clearance and fragmentation of tropical montane forests in the Highlands of Chiapas, Mexico (1975–2000). Forest Ecology and Management, 226, 208–218.

Ceccherini, G., Duveiller, G., Grassi, G., Lemoine, G., Avitabile, V., Pilli, R. and Cescatti, A., 2020. Abrupt increase in harvested forest area over Europe after 2015. Nature, 583, 72–77.

Chen, I.C., Hill, J.K., Ohlemüller, R., Roy, D.B. and Thomas, C.D., 2011. Rapid range shifts of species associated with high levels of climate warming. Science, 333, 1024–1026.

Chu, D., Liu, L. and Wang, Z., 2023. Snow Cover on the Tibetan Plateau and Topographic Controls. Remote Sensing, 15, 4044.

Cieraad, E., McGlone, M.S. and Huntley, B., 2014. Southern Hemisphere temperate tree lines are not climatically depressed. Journal of Biogeography, 41, 1456–1466.

Cogbill, C.V. and White, P.S., 1991. The latitude-elevation relationship for spruce-fir forest and treeline along the Appalachian mountain chain. Vegetatio, 94, 153–175.

Colwell, R.K., Brehm, G., Cardelús, C.L., Gilman, A.C. and Longino, J.T., 2008. Global warming, elevational range shifts, and lowland biotic attrition in the wet tropics. Science, 322, 258–261.

Crooks, K.R., Burdett, C.L., Theobald, D.M., King, S.R., Di Marco, M., Rondinini, C. and Boitani, L., 2017. Quantification of habitat fragmentation reveals

extinction risk in terrestrial mammals. Proceedings of the National Academy of Sciences, 114, 7635–7640.

Cui, X., Graf, H.F., Langmann, B., Chen, W. and Huang, R., 2006. Climate impacts of anthropogenic land use changes on the Tibetan Plateau. Global Planetary Change, 54, 33–56.

Cullen, L.E., Stewart, G.H., Duncan, R.P. and Palmer, J.G., 2001. Disturbance and climate warming influences on New Zealand Nothofagus tree-line population dynamics. Journal of Ecology, 89, 1061–1071.

Curran, L.M., Trigg, S.N., McDonald, A.K., Astiani, D., Hardiono, Y.M., Siregar, P., Caniago, I. and Kasischke, E., 2004. Lowland forest loss in protected areas of Indonesian Borneo. Science, 303, 1000–1003.

Curtis, P.G., Slay, C.M., Harris, N.L., Tyukavina, A. and Hansen, M.C., 2018. Classifying drivers of global forest loss. Science, 361, 1108–1111.

D'Arrigo, R.D., Kaufmann, R.K., Davi, N., Jacoby, G.C., Laskowski, C., Myneni, R.B. and Cherubini, P., 2004. Thresholds for warming-induced growth decline at elevational tree line in the Yukon Territory, Canada. Global Biogeochemical Cycles, 18, GB3021.

Dale, V.H., Joyce, L.A., McNulty, S., Neilson, R.P., Ayres, M.P., Flannigan, M.D., Hanson, P.J., Irland, L.C., Lugo, A.E., Peterson, C.J., Simberloff, D. et al., 2001. Climate change and forest disturbances: climate change can affect forests by altering the frequency, intensity, duration, and timing of fire, drought, introduced species, insect and pathogen outbreaks, hurricanes, windstorms, ice storms, or landslides. Bioscience, 51, 723–734.

Dixon, R.K., Solomon, A.M., Brown, S., Houghton, R.A., Trexier, M.C. and Wisniewski, J., 1994. Carbon pools and flux of global forest ecosystems. Science, 263, 185–190.

Du, H., Liu, J., Li, M.H., Büntgen, U., Yang, Y., Wang, L., Wu, Z. and He, H.S., 2018. Warming-induced upward migration of the alpine treeline in the Changbai Mountains, northeast China. Global Change Biology, 24, 1256–1266.

Elliott-Fisk, D.L., 2000. The taiga and boreal forest. In *North American terrestrial vegetation*. Cambridge University Press.

Feddema, J.J., Oleson, K.W., Bonan, G.B., Mearns, L.O., Buja, L.E., Meehl, G.A. and Washington, W.M., 2005. The importance of land-cover change in simulating future climates. Science, 310, 1674–1678.

Feldpausch, T.R., Lloyd, J., Lewis, S.L., Brienen, R.J.W., Gloor, M., Monteagudo-Mendoza, A., Lopez-Gonzalez, G., Banin, L., Abu Salim, K., Affum-Baffoe, K. Alexiades, M. et al., 2012. Tree height integrated into pantropical forest biomass estimates. Biogeosciences, 9, 3381–3403.

Feng, M., Sexton, J.O., Huang, C., Anand, A., Channan, S., Song, X.P., Song, D.X., Kim, D.H., Noojipady, P. and Townshend, J.R., 2016. Earth science data records of global forest cover and change: assessment of accuracy in 1990, 2000, and 2005 epochs. Remote Sensing of Environment, 184, 73–85.

Feng, Y., Zeng, Z., Searchinger, T., Ziegler, A.D., Wu, J., Wang, D., He, X., Elsen, P., Ciais, P., Xu, R., Guo, Z., et al., 2022. Doubling of annual forest carbon loss over the tropics during the early 21st century. Nature Sustainability, 5, 444–451.

Feng, Y., Ziegler, A.D., Elsen, P.R., Liu, Y., He, X., Spracklen, D.V., Holden, J., Jiang, X., Zheng, C. and Zeng, Z., 2021. Upward expansion and acceleration of forest clearance in the mountains of Southeast Asia. Nature Sustainability, 4, 892–899.

Fick, S.E. and Hijmans, R.J., 2017. WorldClim 2: new 1-km spatial resolution climate surfaces for global land areas. International Journal of Climatology, 37, 4302–4315.

Friedman, J.H., 2001. Greedy function approximation: a gradient boosting machine. Annals of Statistics, 29, 1189–1232.

Findell, K.L., Knutson, T.R. and Milly, P.C.D., 2006. Weak simulated extratropical responses to complete tropical deforestation. Journal of Climate, 19, 2835–2850.

Foley, J.A., Asner, G.P., Costa, M.H., Coe, M.T., DeFries, R., Gibbs, H.K., Howard, E.A., Olson, S., Patz, J., Ramankutty, N. and Snyder, P., 2007. Amazonia revealed: forest degradation and loss of ecosystem goods and services in the Amazon Basin. Frontiers in Ecology and the Environment, 5, 25–32.

Fujisada, H., Bailey, G.B., Kelly, G.G., Hara, S. and Abrams, M.J., 2005. ASTER DEM performance. IEEE Transactions on Geoscience and Remote Sensing, 43, 2707–2714.

Fujisada, H., Urai, M. and Iwasaki, A., 2011. Advanced methodology for ASTER DEM generation. IEEE Transactions on Geoscience and Remote Sensing, 49, 5080–5091.

Fujisada, H., Urai, M. and Iwasaki, A., 2012. Technical methodology for ASTER global DEM. IEEE Transactions on Geoscience and Remote Sensing, 50, 3725–3736.

Gautam, A.P., Webb, E.L., Shivakoti, G.P. and Zoebisch, M.A., 2003. Land use dynamics and landscape change pattern in a mountain watershed in Nepal. Agriculture, Ecosystems & Environment, 99, 83–96.

Gedney, N. and Valdes, P.J., 2000. The effect of Amazonian deforestation on the northern hemisphere circulation and climate. Geophysical Research Letters, 27, 3053–3056.

Giam, X., 2017. Global biodiversity loss from tropical deforestation. Proceedings of the National Academy of Sciences, 114, 5775–5777.

Greenberg, C.H. and McNab, W.H., 1998. Forest disturbance in hurricane-related downbursts in the Appalachian mountains of North Carolina. Forest Ecology and Management, 104, 179–191.

Gwate, O., Canavan, K., Martin, G.D., Richardson, D.M. and Ralph Clark, V., 2023. Assessing habitat suitability for selected woody range-expanding plant species in African mountains under climate change. Transactions of the Royal Society of South Africa, 78, 1–4.

Hansen, M.C., Potapov, P. and Tyukavina, A., 2019. Comment on "Tropical forests are a net carbon source based on aboveground measurements of gain and loss". Science, 363, eaar3629.

Hansen, M.C., Potapov, P.V., Moore, R., Hancher, M., Turubanova, S.A., Tyukavina, A., Thau, D., Stehman, S.V., Goetz, S.J., Loveland, T.R., Kommareddy, A. et al., 2013. High-resolution global maps of 21st-century forest cover change. Science, 342, 850–853.

Hasler, N., Werth, D. and Avissar, R., 2009. Effects of tropical deforestation on global hydroclimate: a multimodel ensemble analysis. Journal of Climate, 22, 1124–1141.

Harris, N.L., Brown, S., Hagen, S.C., Saatchi, S.S., Petrova, S., Salas, W., Hansen, M.C., Potapov, P.V. and Lotsch, A., 2012. Baseline map of carbon emissions from deforestation in tropical regions. Science, 336, 1573–1576.

Harris, N.L., Gibbs, D.A., Baccini, A., Birdsey, R.A., de Bruin, S., Farina, M., Fatoyinbo, L., Hansen, M.C., Herold, M., Houghton, R.A., Potapov, P.V. et al., 2021. Global maps of twenty-first century forest carbon fluxes. Nature Climate Change, 11, 234–240.

Harsch, M.A., Hulme, P.E., McGlone, M.S. and Duncan, R.P., 2009. Are treelines advancing? A global meta-analysis of treeline response to climate warming. Ecology Letters, 12, 1040–1049.

Heino, M., Kummu, M., Makkonen, M., Mulligan, M., Verburg, P.H., Jalava, M. and Räsänen, T.A., 2015. Forest loss in protected areas and intact forest landscapes: a global analysis. Plos One, 10, e0138918.

Hermes, K. 1955. Die Lage der oberen Waldgrenze in den Gebirgen der Erde und ihr Abstand zur Schneegrenze. – Dissertation der Philosophischen Fakultät der Universitat du Köln.

Hill, S.L., Arnell, A., Maney, C., Butchart, S.H., Hilton-Taylor, C., Ciciarelli, C., Davis, C., Dinerstein, E., Purvis, A. and Burgess, N.D., 2019. Measuring Forest Biodiversity Status and Changes Globally. Frontiers in Forests and Global Change, 2, 70.

Hijmans, R.J., Cameron, S.E., Parra, J.L., Jones, P.G. and Jarvis, A., 2005. Very high resolution interpolated climate surfaces for global land areas. International Journal of Climatology, 25, 1965–1978.

Hoch, G. and Körner, C., 2005. Growth, demography and carbon relations of Polylepis trees at the world’s highest treeline. Functional Ecology, 19, 941–951.

Hu, X., Huang, B., Verones, F., Cavalett, O. and Cherubini, F., 2021. Overview of recent land-cover changes in biodiversity hotspots. Frontiers in Ecology and the Environment, 19, 91–97.

Hua, F., Bruijnzeel, L.A., Meli, P., Martin, P.A., Zhang, J., Nakagawa, S., Miao, X., Wang, W., McEvoy, C., Peña-Arancibia, J.L., Brancalion, P.H.S. et al., 2022. The biodiversity and ecosystem service contributions and trade-offs of forest restoration approaches. Science, 376, 839–844.

Immerzeel, W.W., Lutz, A.F., Andrade, M., Bahl, A., Biemans, H., Bolch, T., Hyde, S., Brumby, S., Davies, B.J., Elmore, A.C., Emmer, A. et al., 2020. Importance and vulnerability of the world's water towers. Nature, 577, 364–369.

Jobbágy, E.G. and Jackson, R.B., 2000. Global controls of forest line elevation in the northern and southern hemispheres. Global Ecology and Biogeography, 9, 253–268.

Jung, M., Arnell, A., de Lamo, X., García-Rangel, S., Lewis, M., Mark, J., Merow, C., Miles, L., Ondo, I., Pironon, S., Ravilious, C. et al., 2021. Areas of global importance for conserving terrestrial biodiversity, carbon and water. Nature Ecology & Evolution, 5, 1499–1509.

Jung, M., Dahal, P.R., Butchart, S.H., Donald, P.F., de Lamo, X., Lesiv, M., Kapos, V., Rondinini, C. and Visconti, P., 2020. A global map of terrestrial habitat types. Scientific Data, 7, 256.

Kapos, V., Rhind, J., Edwards, M., Price, M.F. and Ravilious, C., 2000. Developing a map of the world's mountain forests. In *Forests in sustainable mountain development: a state of knowledge report for 2000. Task Force on Forests in Sustainable Mountain Development*, 4–19. Wallingford UK: Cabi Publishing.

Karagulle, D., Frye, C., Sayre, R., Breyer, S., Aniello, P., Vaughan, R. and Wright, D., 2017. Modeling global Hammond landform regions from 250-m elevation data. Transactions in GIS, 21, 1040–1060.

Ke, G., Meng, Q., Finley, T., Wang, T., Chen, W., Ma, W., Ye, Q. and Liu, T.-Y., 2017. Lightgbm: a highly efficient gradient boosting decision tree. Advances in Neural Information Processing Systems, 30, 3146–3154.

Keenan, R.J., Reams, G.A., Achard, F., de Freitas, J.V., Grainger, A. and Lindquist, E., 2015. Dynamics of global forest area: results from the FAO Global Forest Resources Assessment 2015. Forest Ecology and Management, 352, 9–20.

Kobayashi, Y., Okada, K.I. and Mori, A.S., 2019. Reconsidering biodiversity hotspots based on the rate of historical land-use change. Biological Conservation, 233, 268–275.

Körner, C., 1998. A re-assessment of high elevation treeline positions and their explanation. Oecologia, 115, 445–459.

Körner, C., 2007. Climatic treelines: conventions, global patterns, causes. Erdkunde, 61, 316–324.

Körner, C., 2021. The cold range limit of trees. Trends in Ecology & Evolution. 36, 979–989.

Körner, C. and Paulsen, J., 2004. A world-wide study of high altitude treeline temperatures. Journal of Biogeography, 31, 713–732.

Körner, C., Jetz, W., Paulsen, J., Payne, D., Rudmann-Maurer, K. and Spehn, E.M., 2017. A global inventory of mountains for bio-geographical applications. Alpine Botany, 127, 1–15.

Körner, C., Paulsen, J. and Spehn, E.M., 2011. A definition of mountains and their bioclimatic belts for global comparisons of biodiversity data. Alpine Botany, 121, 73–78.

Kullman, L., 2002. Rapid recent range-margin rise of tree and shrub species in the Swedish Scandes. Journal of Ecology, 90, 68–77.

Kurz, W.A., Dymond, C.C., Stinson, G., Rampley, G.J., Neilson, E.T., Carroll, A.L., Ebata, T. and Safranyik, L., 2008. Mountain pine beetle and forest carbon feedback to climate change. Nature, 452, 987–990.

Lafon, C.W., 2004. Ice-storm disturbance and long-term forest dynamics in the Adirondack Mountains. Journal of Vegetation Science, 15, 267–276.

Lane, P.N. and Mackay, S.M., 2001. Streamflow response of mixed-species eucalypt forests to patch cutting and thinning treatments. Forest Ecology and Management, 143, 131–142.

Lawrence, D. and Vandecar, K., 2015. Effects of tropical deforestation on climate and agriculture. Nature Climate Change, 5, 27–36.

Lawrence, P.J. and Chase, T.N., 2010. Investigating the climate impacts of global land cover change in the community climate system model. International Journal of Climatology, 30, 2066–2087.

Leberger, R., Rosa, I.M., Guerra, C.A., Wolf, F. and Pereira, H.M., 2020. Global patterns of forest loss across IUCN categories of protected areas. Biological Conservation, 241, 108299.

Lenton, T.M., 2011. Early warning of climate tipping points. Nature Climate Change, 1, 201–209.

Lesiv, M., Schepaschenko, D., Buchhorn, M., See, L., Dürauer, M., Georgieva, I., Jung, M., Hofhansl, F., Schulze, K., Bilous, A., Blyshchyk, V. et al., 2022. Global forest management data for 2015 at a 100 m resolution. Scientific Data, 9, 199.

Lesk, C., Coffel, E., D'Amato, A.W., Dodds, K. and Horton, R., 2017. Threats to North American forests from southern pine beetle with warming winters. Nature Climate Change, 7, 713–717.

Lewis, S.L., Wheeler, C.E., Mitchard, E.T.A. and Koch, A. 2019. Restoring natural forests is the best way to remove atmospheric carbon. Nature, 568, 25–28.

Li, Y., Zhao, M., Mildrexler, D.J., Motesharrei, S., Mu, Q., Kalnay, E., Zhao, F., Li, S. and Wang, K., 2016. Potential and actual impacts of deforestation and afforestation on land surface temperature. Journal of Geophysical Research, 121, 14372–14386.

Liang, E., Wang, Y., Eckstein, D. and Luo, T., 2011. Little change in the fir tree-line position on the southeastern Tibetan Plateau after 200 years of warming. New Phytologist, 190, 760–769.

Liu, H. and Yin, Y., 2013. Response of forest distribution to past climate change: an insight into future predictions. Chinese Science Bulletin, 58, 4426–4436.

Liu, J., Coomes, D.A., Gibson, L., Hu, G., Liu, J., Luo, Y., Wu, C. and Yu, M., 2019. Forest fragmentation in China and its effect on biodiversity. Biological Reviews, 94, 1636–1657.

Lin, Y. and Wei, X., 2008. The impact of large-scale forest harvesting on hydrology in the Willow watershed of Central British Columbia. Journal of Hydrology, 359, 141–149.

Liu, Y., Ziegler, A.D., Wu, J., Liang, S., Wang, D., Xu, R., Duangnamon, D., Li, H. and Zeng, Z., 2022. Effectiveness of protected areas in preventing

forest loss in a tropical mountain region. Ecological Indicators, 136, 108697.

Lloyd, A.H. and Fastie, C.L., 2003. Recent changes in treeline forest distribution and structure in interior Alaska. Ecoscience, 10, 176–185.

Lu, X., Liang, E., Wang, Y., Babst, F. and Camarero, J.J., 2021. Mountain treelines climb slowly despite rapid climate warming. Global Ecology and Biogeography, 30, 305–315.

Lyu, L., Zhang, Q.B., Pellatt, M.G., Büntgen, U., Li, M.H. and Cherubini, P., 2019. Drought limitation on tree growth at the Northern Hemisphere's highest tree line. Dendrochronology, 53, 40–47.

MacDonald, G.M., Velichko, A.A., Kremenetski, C.V., Borisova, O.K., Goleva, A.A., Andreev, A.A., Cwynar, L.C., Riding, R.T., Forman, S.L. and Edwards, T.W., 2000. Holocene treeline history and climate change across northern Eurasia. Quaternary Research, 53, 302–311.

Malhi, Y., Baldocchi, D.D. and Jarvis, P.G., 1999. The carbon balance of tropical, temperate and boreal forests. Plant, Cell & Environment, 22, 715–740.

Malyshev, L., 1993. Levels of the upper forest boundary in northern Asia. Vegetatio, 109, 175–186.

Mann, H.B., 1945. Nonparametric tests against trend. Econometrica, 13, 245–259.

Marchese, C., 2015. Biodiversity hotspots: a shortcut for a more complicated concept. Global Ecology and Conservation, 3, 297–309.

Medvigy, D., Walko, R.L., Otte, M.J. and Avissar, R., 2013. Simulated changes in northwest U. S. climate in response to Amazon deforestation. Journal of Climate, 26, 9115–9136.

Meier, R., Schwaab, J., Seneviratne, S.I., Sprenger, M., Lewis, E. and Davin, E.L., 2021. Empirical estimate of forestation-induced precipitation changes in Europe. Nature Geosciences, 14, 473–478.

Messager, M.L., Lehner, B., Cockburn, C., Lamouroux, N., Pella, H., Snelder, T., Tockner, K., Trautmann, T., Watt, C. and Datry, T., 2021. Global prevalence of non-perennial rivers and streams. Nature, 594, 391–397.

Messerli, B. and Ives, J.D., 1997. *Mountains of the world: a global priority.* New York: Parthenon.

Miehe, G., Miehe, S., Vogel, J. and La, D., 2007. Highest treeline in the northern hemisphere found in southern Tibet. Mountain Research and Development, 27, 169–173.

Mitchard, E.T.A., 2018. The tropical forest carbon cycle and climate change. Nature, 559, 527–534.

Mitchard, E.T.A., Saatchi, S.S., Lewis, S.L., Feldpausch, T.R., Woodhouse, I.H., Sonké, B., Rowland, C. and Meir, P., 2011. Measuring biomass changes due to woody encroachment and deforestation/degradation in a forest–savanna boundary region of central Africa using multi-temporal L-band radar backscatter. Remote Sensing of Environment, 115, 2861–2873.

Mohandass, D., Hughes, A.C., Campbell, M. and Davidar, P., 2014. Effects of patch size on liana diversity and distributions in the tropical montane evergreen forests of the Nilgiri Mountains, southern India. Journal of Tropical Ecology, 30, 579–590.

Moritz, C., Patton, J.L., Conroy, C.J., Parra, J.L., White, G.C. and Beissinger, S.R., 2008. Impact of a century of climate change on small-mammal communities in Yosemite National Park, USA. Science, 322, 261–264.

Myers, N. 2003. Biodiversity hotspots revisited. Bioscience, 53, 916–917.

Myers, N., Mittermeier, R.A., Mittermeier, C.G., da Fonseca, G.A. and Kent, J., 2000. Biodiversity hotspots for conservation priorities. Nature, 403, 853–858.

Naughton-Treves, L., Holland, M.B. and Brandon, K., 2005. The role of protected areas in conserving biodiversity and sustaining local livelihoods. Annual Review of Environment and Resources, 30, 219–252.

Nepstad, D., McGrath, D., Stickler, C., Alencar, A., Azevedo, A., Swette, B., Bezerra, T., DiGiano, M., Shimada, J., Seroa da Motta, R., Armijo, E. et al., 2014. Slowing Amazon deforestation through public policy and interventions in beef and soy supply chains. Science, 344, 1118–1123.

Nobre, P., Malagutti, M., Urbano, D.F., de Almeida, R.A. and Giarolla, E. 2009. Amazon deforestation and climate change in a coupled model simulation. Journal of Climate, 22, 5686–5697.

Novo-Fernández, A., Franks, S., Wehenkel, C., López-Serrano, P.M., Molinier, M. and López-Sánchez, C.A., 2018. Landsat time series analysis for

temperate forest cover change detection in the Sierra Madre Occidental, Durango, Mexico. International Journal of Applied Earth Observation and Geoinformation, 73, 230–244.

Ogden, N.H., Maarouf, A., Barker, I.K., Bigras-Poulin, M., Lindsay, L.R., Morshed, M.G., O'callaghan, C.J., Ramay, F., Waltner-Toews, D. and Charron, D.F., 2006. Climate change and the potential for range expansion of the Lyme disease vector Ixodes scapularis in Canada. International Journal for Parasitology, 36, 63–70.

Oudin, L., Andréassian, V., Lerat, J. and Michel, C., 2008. Has land cover a significant impact on mean annual streamflow? An international assessment using 1508 catchments. Journal of Hydrology, 357, 303–316.

Pandit, M.K., Sodhi, N.S., Koh, L.P., Bhaskar, A. and Brook, B.W., 2007. Unreported yet massive deforestation driving loss of endemic biodiversity in Indian Himalaya. Biodiversity and Conservation, 16, 153–163.

Paolini, L., Villalba, R. and Ricardo Grau, H., 2005. Precipitation variability and landslide occurrence in a subtropical mountain ecosystem of NW Argentina. Dendrochronologia, 22, 175–180.

Paradis, A., Elkinton, J., Hayhoe, K. and Buonaccorsi, J., 2008. Role of winter temperature and climate change on the survival and future range expansion of the hemlock woolly adelgid (Adelges tsugae) in eastern North America. Mitigation and Adaptation Strategies for Global Change, 13, 541–554.

Paulsen, J. and Körner, C., 2001. GIS-analysis of tree-line elevation in the Swiss Alps suggests no exposure effect. Journal of Vegetation Science, 12, 817–824.

Paulsen, J. and Körner, C., 2014. A climate-based model to predict potential treeline position around the globe. Alpine Botany, 124, 1–12.

Payette, S., Eronen, M. and Jasinski, J., 2002. The circumboreal tundra-taiga interface: late Pleistocene and Holocene changes. Ambio, 15–22.

Pendrill, F., Gardner, T.A., Meyfroidt, P., Persson, U.M., Adams, J., Azevedo, T., Bastos Lima, M.G., Baumann, M., Curtis, P.G., de Sy, V., Garrett, R. et al., 2022. Disentangling the numbers behind agriculture-driven tropical deforestation. Science, 377, 1–11.

Peylin, P., Law, R.M., Gurney, K.R., Chevallier, F., Jacobson, A.R., Maki, T., Niwa, Y., Patra, P.K., Peters, W., Rayner, P.J. and Rödenbeck, C., 2013. Global atmospheric carbon budget: results from an ensemble of atmospheric CO_2 inversions. Biogeosciences, 10, 6699–6720.

Pielke, R.A., Adegoke, J., BeltraáN-Przekurat, A., Hiemstra, C.A., Lin, J., Nair, U.S., Niyogi, D. and Nobis, T.E., 2007. An overview of regional land-use and land-cover impacts on rainfall. Tellus B, 59, 587–601.

Pixalytics, 2021. How many Earth observation satellites are orbiting the planet in 2021? Accessed from https://www.pixalytics.com/eo-sats-2021/.

Pohlert, T., 2023. Non-parametric trend tests and change-point detection. https://cran.r-project.org/web/packages/trend/vignettes/trend.pdf.

Pokhrel, Y., Felfelani, F., Satoh, Y., Boulange, J., Burek, P., Gädeke, A., Gerten, D., Gosling, S.N., Grillakis, M., Gudmundsson, L. and Hanasaki, N., 2021. Global terrestrial water storage and drought severity under climate change. Nature Climate Change, 11, 226–233.

Potapov, P., Li, X., Hernandez-Serna, A., Tyukavina, A., Hansen, M.C., Kommareddy, A., Pickens, A., Turubanova, S., Tang, H., Silva, C.E., Armston, J. et al., 2021. Mapping global forest canopy height through integration of GEDI and Landsat data. Remote Sensing of Environment, 253, 112165.

Price, M.F., Gratzer, G., Duguma, L.A., Kohler, T. and Maselli, D., 2011. *Mountain forests in a changing world: realizing values, addressing challenges*. Rome: FAO/MPS and SDC.

Qin, Y., Xiao, X., Dong, J., Zhou, Y., Wang, J., Doughty, R.B., Chen, Y., Zou, Z. and Moore, B., 2017. Annual dynamics of forest areas in South America during 2007–2010 at 50-m spatial resolution. Remote Sensing of Environment, 201, 73–87.

Qin, Y., Xiao, X., Dong, J., Zhang, Y., Wu, X., Shimabukuro, Y., Arai, E., Biradar, C., Wang, J., Zou, Z., Liu, F. et al., 2019. Improved estimates of forest cover and loss in the Brazilian Amazon in 2000–2017. Nature Sustainability, 2, 764–772.

Rahbek, C., Borregaard, M.K., Colwell, R.K., Dalsgaard, B.O., Holt, B.G., Morueta-Holme, N., Nogues-Bravo, D., Whittaker, R.J. and Fjeldså, J.,

2019. Humboldt's enigma: what causes global patterns of mountain biodiversity? Science, 365, 1108–1113.

Ramos da Silva, R., Werth, D. and Avissar, R., 2008. Regional impacts of future land-cover changes on the Amazon basin wet-season climate. Journal of Climate, 21, 1153–1170.

Reader, M.O., Eppinga, M.B., de Boer, H.J., Damm, A., Petchey, O.L. and Santos, M.J., 2023. Biodiversity mediates relationships between anthropogenic drivers and ecosystem services across global mountain, island, and delta systems. Global Environmental Change, 78, 102612.

Reza, A.A. and Hasan, M.K., 2020. Forest biodiversity and deforestation in Bangladesh: the latest update. In *Forest Degradation Around the World*. IntechOpen. Accessed from https://www.intechopen.com/chapters/68528.

Rochlin, I., Ninivaggi, D.V., Hutchinson, M.L. and Farajollahi, A. 2013. Climate change and range expansion of the Asian tiger mosquito (Aedes albopictus) in Northeastern USA: implications for public health practitioners. Plos One. 8, e60874.

Romme, W.H. and Despain, D.G., 1989. Historical perspective on the Yellowstone fires of 1988. Bioscience, 39, 695–699.

Ryan, C.M., Hill, T., Woollen, E., Ghee, C., Mitchard, E.T.A., Cassells, G., Grace, J., Woodhouse, I.H. and Williams, M., 2012. Quantifying small-scale deforestation and forest degradation in African woodlands using radar imagery. Global Change Biology, 18, 243–257.

Safranyik, L., Carroll, A.L., Régnière, J., Langor, D.W., Riel, W.G., Shore, T.L., Peter, B., Cooke, B.J., Nealis, V.G. and Taylor, S.W., 2010. Potential for range expansion of mountain pine beetle into the boreal forest of North America. The Canadian Entomologist, 142, 415–442.

Sayre, R., Frye, C., Karagulle, D., Krauer, J., Breyer, S., Aniello, P., Wright, D.J., Payne, D., Adler, C., Warner, H., van Sistine, D.P. et al., 2018. A new high-resolution map of the mountains of the world and an online tool for visualizing and comparing three characterizations of global mountain distributions. Mountain Research and Development, 38, 240–249.

Sen, P.K., 1968. Estimates of the regression coefficient based on Kendall's tau. Journal of the American Statistical Association, 63, 1379–1389.

Shikhov, A.N., Perminova, E.S. and Perminov, S.I., 2019. Satellite-based analysis of the spatial patterns of fire-and storm-related forest disturbances in the Ural region, Russia. Natural Hazards, 97, 283–308.

Sigdel, S.R., Wang, Y., Camarero, J.J., Zhu, H., Liang, E. and Peñuelas, J., 2018. Moisture-mediated responsiveness of treeline shifts to global warming in the Himalayas. Global Change Biology, 24, 5549–5559.

Silva Junior, C.H., Pessôa, A.C., Carvalho, N.S., Reis, J.B., Anderson, L.O. and Aragão, L.E., 2021. The Brazilian Amazon deforestation rate in 2020 is the greatest of the decade. Nature Ecology & Evolution, 5, 144–145.

Silvério, D.V., Brando, P.M., Macedo, M.N., Beck, P.S., Bustamante, M. and Coe, M.T., 2015. Agricultural expansion dominates climate changes in southeastern Amazonia: the overlooked non-GHG forcing. Environmental Research Letters, 10, 104015.

Simon, M.F. and Garagorry, F.L., 2005. The expansion of agriculture in the Brazilian Amazon. Environmental Conservation, 32, 203–212.

Sitch, S., Friedlingstein, P., Gruber, N., Jones, S.D., Murray-Tortarolo, G., Ahlström, A., Doney, S.C., Graven, H., Heinze, C., Huntingford, C., Levis, S. et al., 2015. Recent trends and drivers of regional sources and sinks of carbon dioxide. Biogeosciences, 12, 653–679.

Smith, C., Baker, J.C.A. and Spracklen, D.V., 2023. Tropical deforestation causes large reductions in observed precipitation. Nature, 615, 270–275.

Smith, W.K., Germino, M.J., Hancock, T.E. and Johnson, D.M., 2003. Another perspective on altitudinal limits of alpine timberlines. Tree Physiology, 23, 1101–1112.

Smith, W.K., Germino, M.J., Johnson, D.M. and Reinhardt, K., 2009. The altitude of alpine treeline: a bellwether of climate change effects. The Botanical Review, 75, 163–190.

Snethlage, M.A., Geschke, J., Ranipeta, A., Jetz, W., Yoccoz, N.G., Körner, C., Spehn, E.M., Fischer, M. and Urbach, D., 2022. A hierarchical inventory of the world's mountains for global comparative mountain science. Scientific Data, 9, 149.

Snyder, P.K., 2010. The influence of tropical deforestation on the Northern Hemisphere climate by atmospheric teleconnections. Earth Interactions, 14, 1–34.

Song, X.P., Hansen, M.C., Stehman, S.V., Potapov, P.V., Tyukavina, A., Vermote, E.F. and Townshend, J.R., 2018. Global land change from 1982 to 2016. Nature, 560, 639–643.

Spracklen, D.V., Arnold, S. and Taylor, C., 2012. Observations of increased tropical rainfall preceded by air passage over forests. Nature, 489, 282–285.

Spracklen, D.V. and Garcia-Carreras, L., 2015. The impact of Amazonian deforestation on Amazon basin rainfall. Geophysical Research Letters, 42, 9546–9552.

Spracklen, D.V., Baker, J.C.A., Garcia-Carreras, L. and Marsham, J.H., 2018. The effects of tropical vegetation on rainfall. Annual Review of Environment and Resources, 43, 193–218.

Stednick, J.D. 1996. Monitoring the effects of timber harvest on annual water yield. Journal of Hydrology, 176, 79–95.

Stephens, B.B., Gurney, K.R., Tans, P.P., Sweeney, C., Peters, W., Bruhwiler, L., Ciais, P., Ramonet, M., Bousquet, P., Nakazawa, T., Aoki, S. et al., 2007. Weak northern and strong tropical land carbon uptake from vertical profiles of atmospheric CO_2. Science, 316, 1732–1735.

Stocks, B.J., Mason, J.A., Todd, J.B., Bosch, E.M., Wotton, B.M., Amiro, B.D., Flannigan, M.D., Hirsch, K.G., Logan, K.A., Martell, D.L. and Skinner, W.R., 2002. Large forest fires in Canada, 1959–1997. Journal of Geophysical Research: Atmospheres, 107, 8149.

Sullivan, M.J., Talbot, J., Lewis, S.L., Phillips, O.L., Qie, L., Begne, S.K., Chave, J., Cuni-Sanchez, A., Hubau, W., Lopez-Gonzalez, G., Miles, L. et al. 2017. Diversity and carbon storage across the tropical forest biome. Scientific Reports, 7, 39102.

Svensson, J., Andersson, J., Sandström, P., Mikusiński, G. and Jonsson, B.G., 2019. Landscape trajectory of natural boreal forest loss as an impediment to green infrastructure. Conservation Biology, 33, 152–163.

Swank, W.T. and Webster, J.R., 2014. *Long-term response of a forest watershed ecosystem: clearcutting in the southern Appalachians.* Oxford University Press.

Tachikawa, T., Hato, M., Kaku, M. and Iwasaki, A., 2011. Characteristics of ASTER GDEM version 2. In *2011 IEEE international geoscience and remote sensing symposium*, 3657–3660. IEEE.

Takata, K., Saito, K. and Yasunari, T., 2009. Changes in the Asian monsoon climate during 1700–1850 induced by preindustrial cultivation. Proceedings of the National Academy of Sciences, 106, 9586–9589.

Tapia-Armijos, M.F., Homeier, J., Espinosa, C.I., Leuschner, C. and de la Cruz, M., 2015. Deforestation and forest fragmentation in South Ecuador since the 1970s–losing a hotspot of biodiversity. Plos One, 10, e0133701.

Taubert, F., Fischer, R., Groeneveld, J., Lehmann, S., Müller, M.S., Rödig, E., Wiegand, T. and Huth, A., 2018. Global patterns of tropical forest fragmentation. Nature, 554, 519–522.

Taylor, A.H. and Skinner, C.N., 2003. Spatial patterns and controls on historical fire regimes and forest structure in the Klamath Mountains. Ecological Applications, 13, 704–719.

Theobald, D.M., Crooks, K.R. and Norman, J.B., 2011. Assessing effects of land use on landscape connectivity: loss and fragmentation of western US forests. Ecological Applications, 21, 2445–2458.

Tian, F., Zhao, C. and Feng, Z., 2011. Simulating evapotranspiration of Qinghai spruce (Picea crassifolia) forest in the Qilian Mountains, northwestern China. Journal of Arid Environments, 75, 648–655.

Tovar, C., Seijmonsbergen, A.C. and Duivenvoorden, J.F., 2013. Monitoring land use and land cover change in mountain regions: an example in the Jalca grasslands of the Peruvian Andes. Landscape and Urban Planning, 112, 40–49.

Tracewski, Ł., Butchart, S.H., Di Marco, M., Ficetola, G.F., Rondinini, C., Symes, A., Wheatley, H., Beresford, A.E. and Buchanan, G.M., 2016. Toward quantification of the impact of 21st-century deforestation on the extinction risk of terrestrial vertebrates. Conservation Biology, 30, 1070–1079.

Troll, C., 1973. The upper timberlines in different climatic zones. Arctic and Alpine Research, 5, A3–A18.

Tyukavina, A., Hansen, M.C., Potapov, P., Parker, D., Okpa, C., Stehman, S.V., Kommareddy, I. and Turubanova, S., 2018. Congo Basin forest loss dominated by increasing smallholder clearing. Science Advances, 4, eaat2993.

USGS., 2010. Global multi-resolution terrain elevation data. Retrieved from http://topotools.cr.usgs.gov/gmted_viewer/.

van der Werf, G.R., Morton, D.C., DeFries, R.S., Olivier, J.G., Kasibhatla, P.S., Jackson, R.B., Collatz, G.J. and Randerson, J.T., 2009. CO_2 emissions from forest loss. Nature Geoscience, 2, 737–738.

Vancutsem, C., Achard, F., Pekel, J.F., Vieilledent, G., Carboni, S., Simonetti, D., Gallego, J., Aragao, L.E. and Nasi, R., 2021. Long-term (1990–2019) monitoring of forest cover changes in the humid tropics. Science Advances, 7, eabe1603.

Veldkamp, E., Schmidt, M., Powers, J.S. and Corre, M.D., 2020. Deforestation and reforestation impacts on soils in the tropics. Nature Reviews Earth & Environment, 1, 590–605.

von Randow, C., Manzi, A.O., Kruijt, B., de Oliveira, P.J., Zanchi, F.B., Silva, R.D., Hodnett, M.G., Gash, J.H.C., Elbers, J.A., Waterloo, M.J., Cardoso, F.L. et al., 2004. Comparative measurements and seasonal variations in energy and carbon exchange over forest and pasture in South West Amazonia. Theoretical and Applied Climatology, 78, 5–26.

von Randow, R.C., von Randow, C., Hutjes, R.W., Tomasella, J. and Kruijt, B., 2012. Evapotranspiration of deforested areas in central and southwestern Amazonia. Theoretical and Applied Climatology, 109, 205–220.

Walker, X.J., Baltzer, J.L., Cumming, S.G., Day, N.J., Ebert, C., Goetz, S., Johnstone, J.F., Potter, S., Rogers, B.M., Schuur, E.A., Turetsky, M.R. et al., 2019. Increasing wildfires threaten historic carbon sink of boreal forest soils. Nature, 572, 520–523.

Wang, C., Wang, J., He, Z. and Feng, M., 2022. Detecting Mountain Forest Dynamics in the Eastern Himalayas. Remote Sensing, 14, 3638.

Watson, J.E., Whittaker, R.J., and Dawson, T.P., 2004. Habitat structure and proximity to forest edge affect the abundance and distribution of forest-dependent birds in tropical coastal forests of southeastern Madagascar. Biological Conservation, 120, 311–327.

Wei, X., Liu, S., Zhou, G. and Wang, C., 2005. Hydrological processes in major types of Chinese forest. Hydrological Processes: An International Journal, 19, 63–75.

Wei, X. and Zhang, M., 2010. Quantifying streamflow change caused by forest disturbance at a large spatial scale: a single watershed study. Water Resources Research, 46, W12525.

Werth, D. and Avissar, R., 2002. The local and global effects of Amazon deforestation. Journal of Geophysical Research: Atmospheres, 107, 8087.

Wilcox, R.R., 2010. *Fundamentals of modern statistical methods: substantially improving power and accuracy*. New York: Springer.

Wilk, J., Andersson, L. and Plermkamon, V., 2001. Hydrological impacts of forest conversion to agriculture in a large river basin in northeast Thailand. Hydrological Processes, 15, 2729–2748.

Wotton, B.M., Nock, C.A. and Flannigan, M.D., 2010. Forest fire occurrence and climate change in Canada. International Journal of Wildland Fire, 19, 253–271.

Wu, F., Zhan, J., Chen, J., He, C. and Zhang, Q., 2015. Water yield variation due to forestry change in the head-water area of Heihe River Basin, Northwest China. Advances in Meteorology, 2015, 1–8.

Xiong, B., Chen, R., Xia, Z., Ye, C. and Anker, Y., 2020. Large-scale deforestation of mountainous areas during the 21st Century in Zhejiang Province. Land Degradation and Development, 31, 1761–1774.

Yang, H., Viña, A., Winkler, J.A., Chung, M.G., Huang, Q., Dou, Y., McShea, W.J., Songer, M., Zhang, J. and Liu, J., 2021. A global assessment of the impact of individual protected areas on preventing forest loss. Science of the Total Environment, 777, 145995.

Yao, Y., Liang, S., Cheng, J., Lin, Y., Jia, K. and Liu, M., 2014. Impacts of deforestation and climate variability on terrestrial evapotranspiration in subarctic China. Forests, 5, 2542–2560.

Zemp, D.C., Schleussner, C.F., Barbosa, H.D.M.J. and Rammig, A., 2017. Deforestation effects on Amazon forest resilience. Geophysical Research Letters, 44, 6182–6190.

Zeng, Z., Chen, A., Ciais, P., Li, Y., Li, L.Z., Vautard, R., Zhou, L., Yang, H., Huang, M. and Piao, S., 2015. Regional air pollution brightening reverses the greenhouse gases induced warming-elevation relationship. Geophysical Research Letters, 42, 4563–4572.

Zeng, Z., Gower, D.B. and Wood, E.F., 2018a. Accelerating forest loss in Southeast Asian Massif in the 21st century: a case study in Nan Province, Thailand. Global Change Biology, 24, 4682–4695.

Zeng, Z., Estes, L., Ziegler, A.D., Chen, A., Searchinger, T., Hua, F., Guan, K., Jintrawet, A. and Wood, E.F., 2018b. Highland cropland expansion and forest loss in Southeast Asia in the twenty-first century. Nature Geoscience, 11, 556–562.

Zhang, M., Fellowes, J.R., Jiang, X., Wang, W., Chan, B.P., Ren, G. and Zhu, J., 2010. Degradation of tropical forest in Hainan, China, 1991–2008: conservation implications for Hainan Gibbon (Nomascus hainanus). Biological Conservation, 143, 1397–1404.

Zhang, M., Wei, X., Sun, P. and Liu, S., 2012. The effect of forest harvesting and climatic variability on runoff in a large watershed: the case study in the Upper Minjiang River of Yangtze River basin. Journal of Hydrology, 464, 1–11.

Zhao, J., Chen, J., Beillouin, D., Lambers, H., Yang, Y., Smith, P., Zeng, Z., Olesen, J.E. and Zang, H., 2022. Global systematic review with meta-analysis reveals yield advantage of legume-based rotations and its drivers. Nature Communications, 13, 4926.

Zheng, X. and Eltahir, E.A.B., 1997. The response to deforestation and desertification in a model of West African monsoons. Geophysical Research Letters, 24, 155–158.

Zou, L., Tian, F., Liang, T., Eklundh, L., Tong, X., Tagesson, T., Dou, Y., He, T., Liang, S. and Fensholt, R., 2023. Assessing the upper elevational limits of vegetation growth in global high-mountains. Remote Sensing of Environment, 286, 113423.

Chapter 2

Accelerating global mountain forest loss threatens biodiversity hotspots

Abstract

The frontier of forest loss has encroached into mountains in some regions. However, the global distribution of forest loss in mountain areas, which are home to >85% of the world's birds, mammals, and amphibians, is uncertain. Here we combine multiple datasets, including global forest change and selected species distributions, to examine spatiotemporal patterns, drivers and impacts of mountain forest loss. We find 78 Mha of montane forest was lost during 2001–2018 and annual loss accelerated significantly, with recent losses being 2.7-fold greater than those at the beginning of the century. Key drivers of mountain forest loss include commercial forestry, agriculture, and wildfires. Areas with the greatest forest loss overlap with important tropical biodiversity hotspots. Our results indicate that protected areas within mountain biodiversity hotspots experienced lower loss rates than their surroundings. Increasing the area of protection in mountains should be central to preserving montane forests and biodiversity in the future.

2.1 Introduction

Mountains are vital to the world's terrestrial biodiversity as they provide habitat to more than 85% of the world's bird, mammal and amphibian species (Rahbek et al., 2019). Montane forests serve as important refuges for large numbers of rare and endangered species with small geographical distributions, making them represent regions of high conservation significance (Hill et al., 2019). As many montane species have narrow ranges (Elsen et al., 2015), even relatively small reductions in forest habitat may increase their risk of extinction. Unfortunately, forest loss and degradation pose significant threats to the persistence of forest-dwelling species that rely on specific microenvironments worldwide (Watson et al., 2004). In addition, climate change is forcing many montane species to move to higher elevations in search of suitable habitats (Moritz et al., 2008; Chen et al., 2011), but their ability to do so is potentially limited by topographic constraints

and the integrity of the habitat (Colwell et al., 2008). Understanding the dynamics of mountain forest loss worldwide is therefore crucial for predicting and mitigating the potential impacts on sensitive forest species (Peters et al., 2019).

Mountain forest loss was historically limited in many areas as high elevations and steep slopes presented physical barriers to human exploitation (da Silva et al., 2014). As such, most forest exploitation occurred in more accessible lowland areas for a variety of activities including logging and agriculture (Curran et al., 2004; Soares-Filho et al., 2006; Potapov et al., 2012). However, since the turn of the 21st century, mountain forests have been increasingly exploited for timber and wood products, as well as to support emerging agricultural systems, such as boom crops and tree-based plantations, for example in Southeast Asia (Feng et al., 2021a; Zeng et al., 2018a; Zeng et al., 2018b). These activities have reshaped montane forests, potentially reducing the size and number of refuge areas, increasing the risk of extinction of forest-dwelling species (Brooks et al., 2006), and weakening the ability of forests to store carbon (Feng et al., 2021a) and regulate climate (Zeng et al., 2021). Elsewhere, such as in the Andes, there is reported evidence of an overall net gain in woody vegetation, the dynamics of which vary with elevation (Aide et al., 2019). There, mountain forest losses dominated vegetation change at lower elevations (1,000–1,499 m) from 2011 to 2014, but forest gains occurred at higher elevations above 1,500 m (Aide et al., 2019). Regional reports (Feng et al., 2021a; Zeng et al., 2018a; Zeng et al., 2018b; Brooks et al., 2006; Zeng et al., 2021; Aide et al., 2019) that are often based on a diverse array of locally derived data and varying analytical approaches, may not necessarily contribute to the determination of clear and generalised trends in mountain forest loss at a global scale, leading to difficulties in assessing the impact of forest loss over mountain regions. Thus, a wider global analysis—with a common analytical framework—conducted in the 21st century when there is evidence of the frontier of forest loss encroaching into mountains, is required to accurately understand mountain forest loss patterns, trends, drivers and impacts worldwide. This information is essential for developing effective biodiversity conservation and forest management strategies in the future.

Here, we conducted a comprehensive assessment of global mountain forest loss during the first two decades of the 21st century. We first assessed forest loss patterns across global mountains and determined the proportion of areas showing signs of regrowth. Second, we determined the extent of mountain forest loss within biodiversity hotspots across a range of elevation gradients, as

elevation regulates biophysical climate impacts (Zeng et al., 2021) and therefore potentially reshapes expected species responses to climate change (Elsen et al., 2020). Third, we estimated the fraction of mountain forest loss within mountain biodiversity hotspots in and around protected areas (PAs). We also examined the drivers of mountain forest loss by comparing our mountain forest loss maps and statistics with other recently developed land-use maps (Curtis et al., 2018). We find that annual forest loss accelerated significantly across global mountains during the first two decades of the 21st century. Unfortunately, many of the areas with the greatest mountain forest loss overlap with critical tropical biodiversity hotspots. Forestry caused the greatest mountain forest loss at the global scale. However, within biodiversity hotspots, commodity agriculture was the main driver of mountain forest loss in Southeast Asia and shifting cultivation was preeminent in tropical Africa and South America. Our results also emphasise the significance of protected areas in conserving forest-dependent biodiversity in mountains and provide a strong foundation for creating region-specific conservation recommendations aimed at preserving forests and the biodiversity they harbour.

2.2 Results

2.2.1 Patterns and drivers of mountain forest change

Mountain forests covered 1,100 million hectares (Mha) globally in 2000 (Table 2.1). Approximately 78 Mha of forest loss occurred in mountain regions between 2001 and 2018, which constitutes a relative gross loss of 7.1% worldwide since 2000 (Supplementary Table A.1). Mean annual gross loss was 4.3 Mha yr^{-1}, equivalent to 0.39% yr^{-1} (Table 2.1). We found that mountain forest loss was significantly accelerating worldwide, with a rate of 0.202 Mha yr^{-2} ($P < 0.01$). Importantly, there was a striking difference in mountain forest loss rate between periods before and after 2010. Annual forest loss in mountains increased more than 1.5-fold from <3.5 Mha yr^{-1} from 2001 to 2009 to 5.2 Mha yr^{-1} during the period 2010 to 2018. Tropical mountains experienced the most rapid acceleration, with the annual loss after 2010 being twice that before 2010. This transition was probably related to the rapid expansion of agriculture into highland areas, for example in mainland Southeast Asia (Zeng et al., 2018a; Zeng et al., 2018b), as well as increased exploitation of mountain forest products as lowland forests became depleted or were the focus of greater forest protection.

Table 2.1 *Mountain forest cover change in different regions/climates (2000 to 2018). Mountain forests in 2000 are the area of mountain forest based on the tree cover threshold of 25% in the year 2000 (Mha). Total mountain forest loss 2001–2018 is the total loss during the period (Mha). Annual relative forest loss (gross) is the mean of relative forest loss (= mountain forest loss/mountain forest cover in 2000) over the 18 years in the region (%). Mountain forest loss acceleration is the gradient in mountain forest loss with time in the region (Mha yr^{-2}), determined from the regression of annual loss (dependent variable, which is a rate in ha yr^{-1}) and year (independent) using Theil-Sen estimator, thus, the units of Mha yr^{-2}. Mountain forest gain proportion is independently estimated by forest gain divided by the total sample size in the region (%). Annual net rate of mountain forest loss is calculated by a standardised method proposed by Puyravaud (2003), by comparing forest cover in the same region in 2000 and 2018 (% per year). Asia was separated into northern and southern Asia, with a boundary of 30°N.*

Region	Mountain forest area in 2000 (Mha)	Total mountain forest loss 2001–2018 (Mha)	Annual relative mountain forest loss (%)	Mountain forest loss acceleration (10^{-2} Mha yr^{-2})	Mountain forest gain proportion (%)	Annual net rate of mountain forest loss (% yr^{-1})
Asia	560.5	39.8	0.39	12.2 (*)	27.0	0.30
Northern Asia	255.8	14.1	0.31	1.0	14.9	0.27
Southern Asia	304.7	25.7	0.47	11.4 (*)	39.9	0.29
North America [T]	220.5	18.7	0.47	1.5	15.9	0.41
South America	158.9	8.3	0.29	1.4 (*)	33.2	0.19
Africa	66.0	6.4	0.54	2.8 (*)	15.4	0.48
Europe	71.9	3.4	0.26	0.9 (*)	16.4	0.22
Australia	15.0	1.0	0.38	0.2	47.4	0.20
Oceania	7.2	0.4	0.32	0.1 (*)	46.7	0.17

Global	**1100.0**	**78.0**	**0.39**	**20.2 (*)**	**23.2**	**0.31**
Tropical	436.1	32.9	0.42	13.1 (*)	31.2	0.30
Temperate	419.9	27.9	0.37	4.6 (*)	27.3	0.28
Boreal	244.0	17.2	0.39	1.6	12.5	0.35

* indicates a significant trend at a 95% confidence interval (Mann-Kendall test).

[T] North America includes Mexico, central American countries (Belize, Costa Rica, El Salvador, Guatemala, Honduras, Nicaragua, and Panama) and nearby island countries of Cuba, Jamaica, Haiti, Dominican Republic, and Trinidad and Tobago.

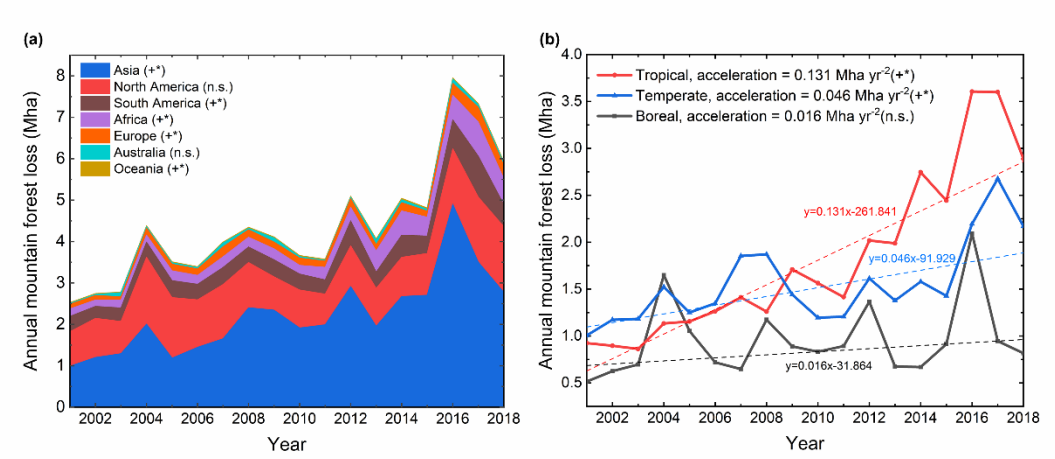

Figure 2.1 *Time series of annual mountain forest loss from 2001 to 2018. (a) Annual mountain forest loss in different continents. The total area of all seven regions for each year represents global mountain forest loss since the baseline year 2000 (i.e., the area is stacked, not superimposed). A symbol (+*) after the region shows a significant positive trend in mountain forest loss at the 95% confidence interval; (n.s.) means no significant trend in mountain forest loss. Trends are determined for the entire 2001–2018 forest loss time series. The loss areas for Oceania are comparatively small, which appear as a black line. (b) Annual mountain forest loss in tropical (24°S to 24°N), boreal (≥50°N), and temperate (residual) regions. Dashed lines are trend lines for annual mountain forest loss in tropical (red), temperate (blue), and boreal (black) regions, estimated by Theil-Sen estimator regression.*

Between 2001 and 2018, global mountain forest loss reached a prominent peak in 2016 (about 65% higher than in the previous year). This surge was mainly driven by forest loss in Asian mountains (Figure 2.1a). Compared with the 2016 peak, annual mountain forest loss decreased in 2017 and 2018, but the annual loss in these two years (mean of 6.5 Mha yr^{-1}) remained high compared with the earlier years of the 21st century. The key activities associated with mountain forest loss were commercial forestry (42%), followed by wildfires (29%), shifting cultivation (15%) and commodity agriculture (10%; Figure 2.3a). These drivers starkly contrast with the activities reported recently for global forest loss (Curtis et al., 2018). While our focus was forest loss, we note that substantial gains in mountain forests have also occurred worldwide. Using a sample-based method (Weisse and Potapov, 2021; Olofsson et al., 2014), we found that 23.2% (1,157 of 4,982 valid pixels) of the forest loss areas at some point during 2001–2018 experienced some degree of tree cover regrowth by 2019 (Supplementary Figure

A.1). For the whole period 2000–2018, the annual net rate of mountain forest loss, accounting for both forest losses and gains, was 0.31% per year (Table 2.1).

Five of seven global regions (Asia, South America, Africa, Europe, and Oceania) experienced significant acceleration in mountain forest loss during the period of observation, with North America and Australia being exceptions (Figure 2.1a; Table 2.1). Over the 18-year study period, the greatest loss of mountain forest area occurred in Asia (39.8 Mha), accounting for more than half of the global total (Table 2.1). This increase in mountain forest loss primarily occurred in southern Asia (≤30°N), where high population densities potentially have a negative effect on forest cover and integrity (Li et al., 2015; Imai et al., 2018). However, the trend in mountain forest loss in northern Asia was not significant (Table 2.1). We also find clear regional differences in the drivers of mountain forest loss and the proportion of forest gain within Asia (Table 2.1 and Supplementary Table A.1). Mountain forest loss in northern Asia (>30°N) was primarily attributed to wildfire (e.g., Russia); and this region experienced only a small proportion of forest gain (~15%). By contrast, mountain forest loss in southern Asia was driven by commercial forestry (e.g., in southern China) and commodity agriculture (e.g., in Indonesia, Vietnam and Myanmar); and ~40% of loss areas showed signs of regrowth—in part, due to the maturation of plantation trees (Supplementary Table A.1; Supplementary Figure A.1). North America had the second greatest mountain forest loss area (18.7 Mha; 24% of global mountain forest loss), with ~16% of forest gain (Table 2.1). This proportional gain was less than half that in South America (~33%) and thus the annual net rate of forest loss in North America (0.41% yr^{-1}) was more than twice that of South America (0.19% yr^{-1}; Table 2.1). Africa experienced the greatest relative forest loss of 0.54% yr^{-1} and had the smallest proportional forest gain of 15.4%. Therefore, the annual net rate of mountain forest loss in Africa was greater than that of any other region at 0.48% per year (Table 2.1).

Globally, substantial mountain forest losses occurred at elevations <1,000 m, where >70% of forest gain also occurred (Supplementary Figure A.2). From the 2000s to 2010s, there was a large increase in forest loss at low-to-moderate elevations, particularly below 1,000 m (Supplementary Figure A.3). This pattern of increased forest loss at low elevations might obscure the fact that forest loss is creeping upwards. Further, temporal patterns indicate increases in forest loss at higher elevations in Asia, South America, and particularly Africa (Supplementary Figure A.4b–e). In Asia, the peak of forest loss in 2016 was

primarily concentrated at 100–300 m, but extended up to 1,200 m, which largely followed the global pattern (Supplementary Figure A.4a, b). In North America, most mountain forest loss was concentrated in 2004 and 2005 at elevations below 1,000 m (Supplementary Figure A.4c). In South America, Africa, and Europe, mountain forest loss reached a peak in 2017 at elevations of about 250 m, 300 m, and 500 m elevation, respectively (Supplementary Figure A.4d–f). In contrast, mountain forest loss in Australia did not follow a particular trend with respect to elevation, but there were specific years (in 2003, 2007, 2009, 2013, and 2016) with significant loss (Supplementary Figure A.4g) that were linked to drought and bushfires (Bowman et al., 2016; Taylor et al., 2014; Rea et al., 2016; Wilkinson et al., 2016).

We found significant increases in mountain forest loss in tropical and temperate latitudes, but not at boreal latitudes (Figure 2.1b). Tropical montane forests, which experienced the greatest loss (32.9 Mha; 42% of global mountain forest loss), also had the fastest acceleration of loss at 0.131 Mha yr^{-2} (Figure 2.1b; Table 2.1). Around 31.2% of these losses have shown signs of regrowth, which is higher than that of temperate and boreal regions (Table 2.1). Our results show that the dominant drivers of mountain forest loss in the tropics were shifting cultivation (44%), commodity agriculture (28%), and commercial forestry (24%; Figure 2.3a). In Indonesia, the tropical country with the greatest loss of mountain forests at 3.97 Mha (relative loss of 7.1%), commodity agriculture was the dominant driver (Supplementary Table A.1). Forest loss in Laos (3.08 Mha; 16.4%) and Vietnam (2.81 Mha; 17.8%) was also substantial (Supplementary Table A.1). Parts of Laos, Vietnam, and northern Thailand (1.29 Mha; 7.9%) form a cluster in mainland Southeast Asia where agriculture-driven deforestation has moved to higher elevations in recent decades (Zeng et al., 2018b; Achard et al., 2002). The loss of forest in Myanmar (2.80 Mha; 8.8%), which was affected by both commercial forestry and commodity agriculture (Supplementary Table A.1), was likely related to its recent re-engagement with regional and global economies (Lim et al., 2017). Malaysia was ranked number 10 worldwide in mountain forest loss (2.2 Mha; 16.4%) (Supplementary Table A.1), with the most loss occurring in Peninsular Malaysia, where oil palm expansion before 2010 was an important driver (Figure 2.2a; Miyamoto et al., 2014). These Southeast Asian countries were all also in the top 10 with respect to acceleration in mountain forest loss (Supplementary Table A.1; Figure 2.2b). In those regions, the loss was primarily attributed to deforestation in mountains through permanent land-use change for

commodity production (Supplementary Table A.1), for example, rubber, oil palm, and feed corn (Curtis et al., 2018; Hurni and Fox, 2018); this process can also be validated by sample-based manual interpretation. Brazil has experienced well-publicised lowland forest loss in recent decades (Andreacci and Marenzi, 2020). Our results show that Brazil also experienced 2.26 Mha (7.6%) of mountain forest loss driven largely by shifting cultivation (Supplementary Table A.1). This result highlights the different drivers of mountain versus lowland forest loss, for which the latter is widely reported to be caused by conversion for commodity agriculture (e.g., soy) (Nepstad et al., 2006) and grazing (Neill et al., 2006). Also associated with shifting cultivation is the loss of montane forests in other South American countries (e.g., Colombia and Peru) and in Africa (e.g., Guinea and Madagascar), with a total loss of 4.99 Mha in these four countries (Supplementary Table A.1).

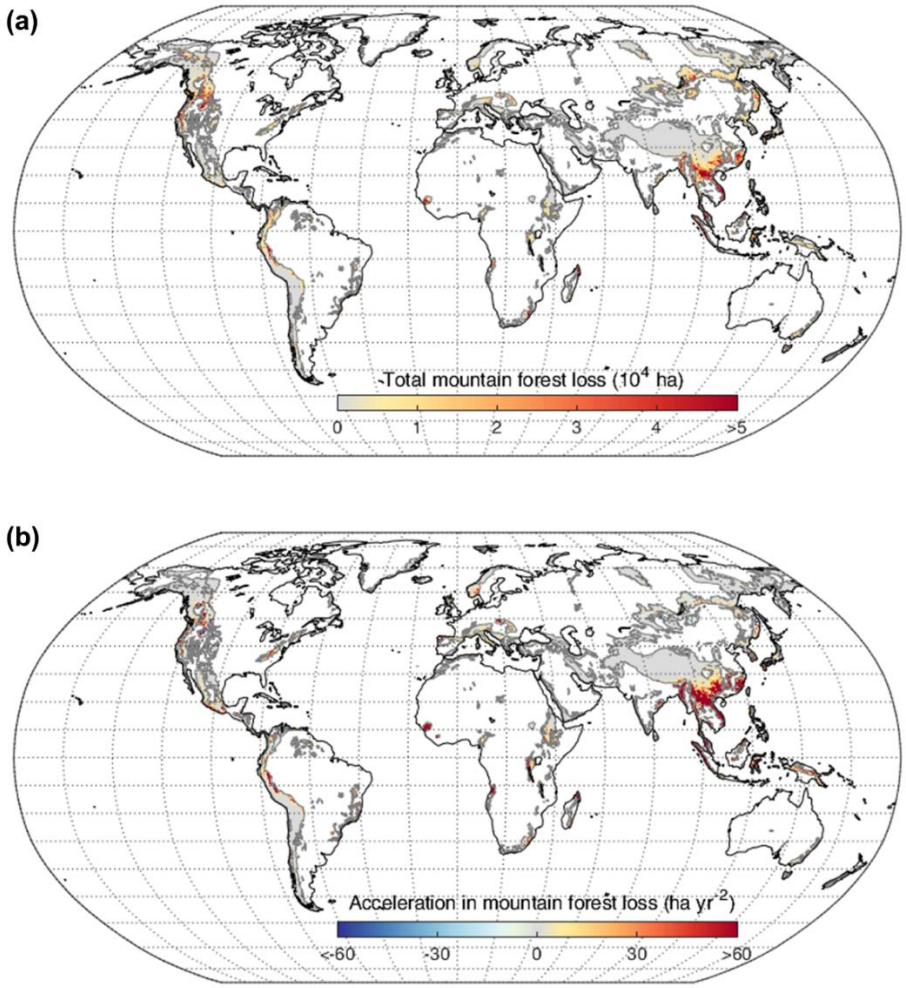

Figure 2.2 *Spatial pattern of mountain forest loss in the 21st century. (a) Total mountain forest loss area. (b) Acceleration in mountain forest loss in 0.5° cells. Mountain regions in grey show mountains with either little forest loss area or no obvious change during the period.*

Temperate montane forests had the second greatest area of losses between 2001 and 2018 (27.9 Mha; 36% of the global total). The primary cause of these losses was commercial forestry, with more than 75% of the area lost being attributed to this sector (Figure 2.3a). Despite the large area lost, temperate montane forests had the smallest annual decrease among all the forests studied, with a rate of 0.28% per year (Table 2.1). In the mountains of the United States, forest loss in the west was greater than in the east (Figure 2.2a); the leading cause was commercial forestry, followed by wildfire (Supplementary Table A.1). Most mountain forest loss in temperate China occurred in the southern mountains with a fast pace of loss (Figure 2.2b) and was primarily driven by commercial forestry (Supplementary Table A.1). Elsewhere, absolute losses of mountain forests were small in Europe, but countries like Portugal, Ireland, and the United Kingdom had substantial percentage losses relative to forest cover in 2000. Again, commercial forestry contributed to >90% of losses in these countries (Supplementary Table A.1).

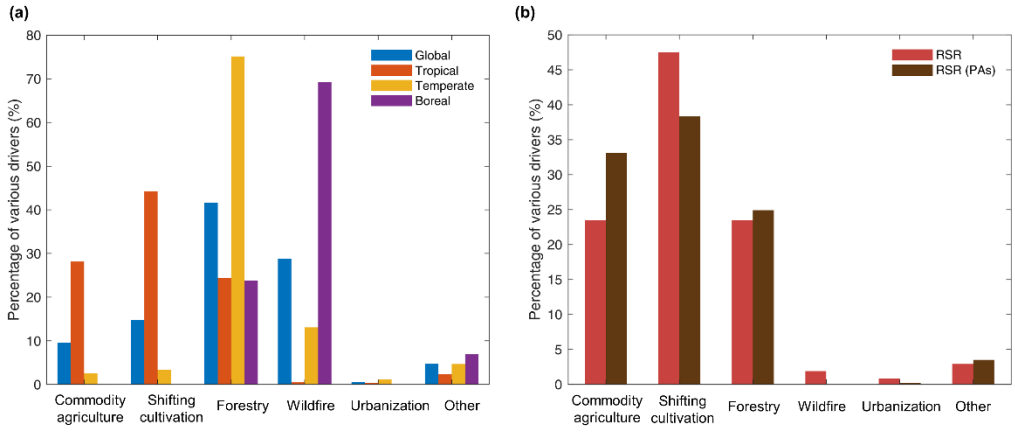

Figure 2.3 *Drivers of mountain forest loss. (a) Comparison across all mountains (global), and in tropical, temperate, and boreal regions. (b) Comparison between the biodiversity hotspots based on range-size rarity for threatened species (RSR) and inside protected areas in the hotspots (RSR (PAs)).*

Losses in boreal regions were comparatively small than at lower latitudes, but in some years montane forest losses at these high latitude locations rivalled those found in temperate areas, and were on the order of 1.6 to 2.1 Mha yr^{-1} (Figure 2.1b). The rate of acceleration in losses of boreal mountain forests was also very low (0.016 Mha yr^{-2}; Table 2.1). Russia and Canada experienced a large amount of mountain forest loss: 11.95 Mha (6.9%) and 5.57 Mha (7.4%), respectively

(Supplementary Table A.1). Wildfire (69%) was the dominant disturbance to boreal montane forests (Figure 2.3a). However, the lack of a significant trend in boreal mountain forest loss (Figure 2.1b; Table 2.1) may suggest that the reported increase in boreal wildfires (Kelly et al., 2013) only affects montane forests in particular years, and does not constitute a long-term threat. Mountain forest gain in boreal regions was the smallest observed (12.5%; Table 2.1). The annual net rate of forest loss was therefore greater than in tropical and temperate regions, at 0.35% per year (Table 2.1).

As tree plantations have expanded greatly worldwide over the last few decades (Keenan et al., 2015), their removal contributes to forest loss rates reported here. To test what proportion of tree plantation removal accounted for mountain forest loss, we separated the forest loss into naturally regenerating forests and plantations using new data on global forest management (Lesiv et al., 2022). We confirmed that nearly 70% of the global mountain forest loss occurred in naturally regenerating forests (Figure 2.4). At the regional scale, we showed naturally regenerating forests in the boreal zone accounted for the largest proportion of the loss (74%), while in the tropics, one third of mountain forest loss occurred in plantations (Figure 2.4). Crucially we found that the proportion of mountain forest loss occurring in plantations has not changed over the analysis period (Supplementary Table A.2), providing evidence that the expansion of plantation forests does not explain the large acceleration in mountain forest loss reported here. This independent analysis confirms that the majority of mountain forest loss is occurring in natural forests.

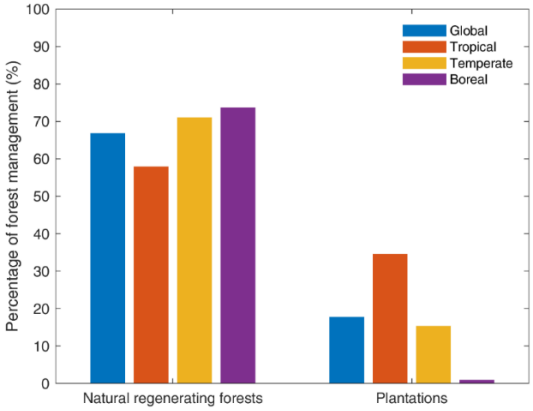

Figure 2.4 *Proportion of natural regenerating forests and plantations accounting for mountain forest loss. Naturally regenerating forests include those without any signs of management (primary forests) and with signs of management (e.g., logging, clear cuts, etc.). Plantations include planted forests, plantation forests (rotation time up to 15 years), oil palm plantations and agroforestry.*

2.2.2 Forest loss within mountain biodiversity hotspots

To map biodiversity hotspots, we focused on two species pools: one for all species of amphibians, birds, and mammals listed on the International Union for Conservation of Nature (IUCN) Red List and the second for threatened species only. We used two metrics: range-size rarity (RSR) and species richness (SR). RSR, a measure of endemicity (Reyes-Betancort et al., 2008; Williams et al., 1996), is a reliable indicator of mountain biodiversity as endemism is positively associated with elevational ranges (Noroozi et al., 2018). SR represents the total number of species present. Our mapping of mountain biodiversity hotspots shows they are primarily concentrated in tropical regions although they vary somewhat by the species pool (all or threatened) and the metric of hotspot definition (RSR versus SR; Supplementary Figures A.5, A.6). The distribution of RSR hotspots is similar for all species and threatened species, including in Sundaland, Wallacea, the Philippines, Madagascar, western Ecuador, tropical Andes, Brazil's Atlantic Forest, and Mesoamerica (Supplementary Figure A.5). By contrast, SR hotspots vary widely for all and threatened species (Supplementary Figure A.6). SR hotspots for all species have a small range probably because the most abundant species tend to inhabit the lowlands, not mountain areas, while SR hotspots for threatened species are concentrated in mountainous areas in southwestern China and Southeast Asia that contain the world's largest number of endangered species.

Total forest loss in mountain biodiversity hotspots over the 18-year study period ranged from 1.4 to 14.4 Mha (or 3.8 to 6.2%), depending on the index used. The loss of mountain forests in the hotspots for threatened species was 11.0 to 14.4 Mha (5.5 to 6.2%). Importantly, relative forest loss was greater in mountain hotspots for threatened species than for all species under the same index (Table 2.2). Further, the acceleration of forest loss in mountain biodiversity hotspots (0.005–0.064 Mha yr^{-2}) was significant ($P < 0.01$; Table 2.2) regardless of the species pool and the metric of hotspot definition. RSR hotspots, for which such areas comprise a larger proportion of the global distribution of species (Elsen et al., 2015), occur at all elevations from 0 to 3,500 m, with high RSR values located above 2,000 m (Figure 2.5). At any elevation, RSR hotspots for threatened species experienced greater relative mountain forest loss than for all species. Mountain forest loss in RSR hotspots reached the peak at about 100 m, then decayed exponentially with increasing elevation, with half occurring at about 350 m (Figure 2.5). Although the greatest RSR values were found higher than where

most forest loss occurred, substantial forest loss did occur at those elevations (i.e., approximately 2,500–3,000 m) (Figure 2.5; Supplementary Table A.3).

Within RSR hotspots for threatened species, nearly half of forest loss was associated with shifting cultivation (47%); the other two major activities were commodity agriculture (23%) and commercial forestry (23%; Figure 2.3b). The six countries with the greatest mountain forest loss within RSR (threatened) hotspots were Indonesia (1.62 Mha), Malaysia (0.95 Mha), Madagascar (0.75 Mha), Vietnam (0.71 Mha), Colombia (0.69 Mha), and Peru (0.62 Mha; Supplementary Table A.4). In the Southeast Asian countries, commodity agriculture was the main driver of mountain forest loss within the hotspots, whereas in tropical Africa and South America, shifting cultivation was preeminent (Supplementary Table A.4). In terms of relative loss of montane forests in biodiversity hotspots, more than half of the top 10 countries were in Africa: South Africa (27.71%), Zimbabwe (27.64%), Guinea (24.79%), Côte d'Ivoire (22.55%), Madagascar (15.38%), and Mozambique (12.33%); the remaining four were in Chile (34.48%), Mongolia (30.10%), Canada (14.96%), and Malaysia (13.34; Supplementary Table A.4). The four countries with the greatest acceleration in montane forest loss in biodiversity hotspots were Indonesia, Madagascar, Vietnam, and Malaysia, ranging from ~3,200 to 4,850 ha yr^{-2} (Supplementary Table A.4).

Table 2.2 *Comparison of mountain forest loss within different types of biodiversity hotspots. The proportion of forest (or loss) within protected areas (PAs) is the forest (or loss) area within PAs divided by the forest (loss) area in the corresponding hotspots. Relative forest loss inside (or outside of) PAs is the percent forest loss relative to forest cover in the baseline year 2000 inside (or outside of) PAs within hotspots.*

Hotspot Types	Forest area in 2000 (Mha)	Total forest loss 2001–2018 (Mha)	Relative forest loss 2001–2018 (%)	Forest loss acceleration (10^{-2} Mha yr^{-2})	Proportion of forest area within PA (%)	Proportion of forest loss within PA (%)	Relative forest loss inside PA (%)	Relative forest loss outside of PA (%)
RSR (all)	223.32	12.98	5.81	4.10 (*)	28.32	15.07	3.09	6.89
RSR (threatened)	177.62	11.03	6.21	3.66 (*)	29.79	16.75	3.49	7.36
SR (all)	37.49	1.43	3.81	0.48 (*)	58.98	21.95	1.42	7.26
SR (threatened)	260.15	14.41	5.54	6.40 (*)	13.14	9.02	3.80	5.80

* indicates a significant trend at a 95% confidence interval (Mann-Kendall test).

RSR: range-size rarity; SR: species richness.

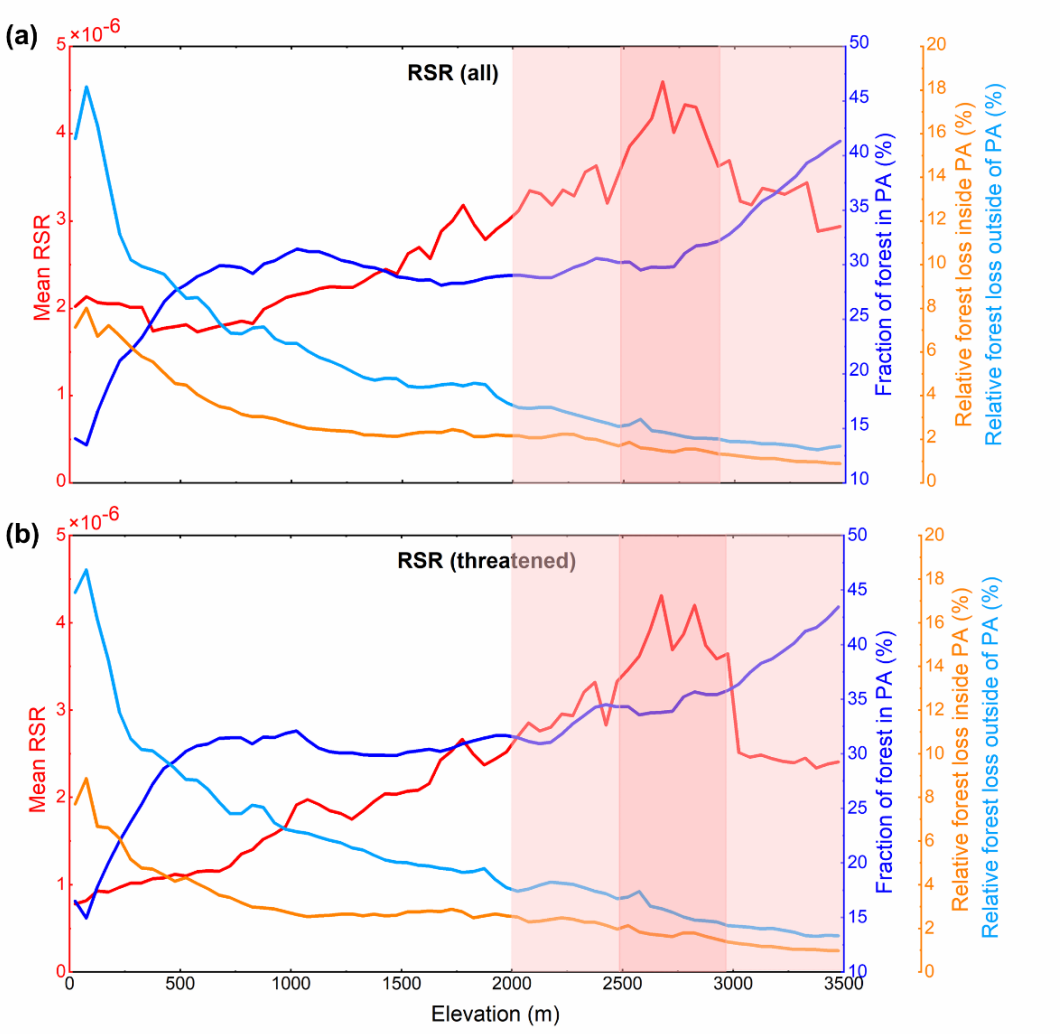

Figure 2.5 *Elevational gradients of biodiversity value, protected area (PA) coverage, and mountain forest loss inside and outside of PAs within biodiversity hotspots. Biodiversity hotspots are based on range-size rarity (RSR) for all species (a) and threatened species (b). Mean RSR (red lines) is the mean value of the biodiversity metric of RSR at each elevation bin on the pixel of 30 m. PA coverage (fraction of forest in PAs) is the ratio of mountain forests within PAs in hotspots versus mountain forests in the corresponding hotspots. Relative forest loss is the percent forest loss relative to forest cover in the baseline year 2000. Relative forest loss inside PAs and outside of PAs within hotspots are shown in orange and light blue lines, respectively. The background shading highlights the occurrence of the highest levels of biodiversity (light and dark red).*

2.2.3 Mountain forest loss in protected areas within hotspots

Protected area coverage (proportion of forest area within PAs) is the largest in the SR (all) biodiversity hotspots, with more than half of hotspot areas included

within PAs (Table 2.2). In some cases, this coverage can approach 100% in areas with very high elevations above 3,500 m (Supplementary Figure A.7). In RSR hotspots, only 30% of mountain forest within hotspots was included in PAs (Table 2.2), suggesting there is a large proportion of forest area with high rates of species endemism that is unprotected. At high elevations (>3,000 m), more than 35% of forest area within RSR hotspots is protected (Figure 2.5; Supplementary Table A.3). However, there are some countries with low PA coverage for mountainous forests in biodiversity hotspots, particularly Angola and Papua New Guinea, where PA coverage is <1% (Supplementary Table A.5).

In all types of mountain biodiversity hotspots, relative forest loss inside PAs was much less than outside (Table 2.2), suggesting that PAs within mountain biodiversity hotspots may be effective in limiting forest loss (ratio of relative forest loss inside versus outside of PAs less than 1). However, the trends depend somewhat on the metric and pool of species considered. Relative forest loss within RSR hotspots in PAs was lower than outside of PAs at all elevations, albeit less so at high elevations (Figure 2.5). In contrast, within SR hotspots, the distribution varied when all versus threatened species were considered. Relative mountain forest loss was less in PAs than outside at elevations up to 3,000 m for all species; but for threatened species, lower loss inside PAs only occurred for the elevation band ranging from 400 to 1,900 m (Supplementary Figure A.7).

In the RSR (threatened) hotspots inside PAs the dominant drivers of forest loss were shifting cultivation (38.3%), commodity agriculture (33.1%) and commercial forestry (24.9%; Figure 2.3b). The lowest relative forest loss ratio inside versus outside PAs was found in RSR hotspots where commodity agriculture was the dominant driver, while the highest ratio was observed in hotspots where shifting cultivation and commercial forestry were the main drivers (Supplementary Figure A.8). In most countries, PAs were associated with reduced forest loss relative to their surrounding areas within hotspots (Supplementary Table A.5). For example, Brunei, Chile, Canada, and New Zealand have the lowest ratios of relative forest loss inside versus outside of PAs within hotspots (Supplementary Table A.5). However, in some countries, such as Côte d'Ivoire, Haiti and Nicaragua where shifting cultivation dominates, relative forest loss inside PAs is more than twice that outside (Supplementary Table A.5). The same is true for Russia where wildfire was the main cause of mountain forest loss.

2.3 Discussion

Our global analysis renders three important findings: (1) Mountain forest loss has accelerated significantly throughout most of the first two decades of the 21st century, encroaching upon areas of known high conservation value to terrestrial biodiversity; (2) Various types of shifting cultivation emerges as the most frequent driver of mountain forest loss in the tropics, but commodity agriculture and forestry activities are also key drivers; (3) Protected areas generally have been effective in curbing mountain forest loss within their boundaries inside biodiversity hotspots, particularly where commodity agriculture is the dominant deforestation driver. However, we find great variation in these three issues throughout the world.

About three quarters of the 128 countries, we analysed experienced an acceleration of mountain forest loss (Supplementary Table A.1). Most of the countries with the greatest acceleration were within Southeast Asia. Parts of India and southern China also experienced substantial losses. These regions with large acceleration align with many of the world's most sensitive biodiversity hotspots for mammals, birds, and amphibians—thus substantial negative impacts to critical habitats have likely already occurred (Hughes, 2017; Sodhi and Brook, 2006). While we did not yet see a major upward shift in the elevation of forest loss at the global scale of analysis, this transition has been reported before in Southeast Asia (Feng et al., 2021a). Further, the history of the progression of forest loss in mountain areas suggests such a shift will likely unfold in locations with high forest pressure but limited capacity to protect forest lands from location-specific drivers, mostly related to agriculture expansion, forest product acquisition, and logging (including illegal). Increased encroachment resulting in forest loss into these sensitive areas directly increases the risk of species extinction and/or forces other species to migrate upward if possible.

Agricultural expansion is of concern worldwide with respect to forest loss (Gibbs et al., 2010). The greatest acceleration of mountain forest loss occurred in countries where shifting cultivation or commodity agriculture was dominant (Supplementary Table A.6), highlighting the importance of agricultural expansion in mountain regions. Encroachment of shifting cultivation in highland forests is problematic to address in countries where this form of agriculture contributes to food and livelihood security of rural communities (Cramb et al., 2009; van Vliet et al., 2012) and where intensification of cultivation can lead to negative

consequences for biodiversity and climate (Ziegler et al., 2012; Jakovac et al., 2015). Forest lands are often viewed as an ownerless public resource and are therefore utilised as needed by individuals for food and livelihood security (Angelsen et al., 2014). A complicating issue is that contemporary protected area boundaries are often established in areas where people have lived and exploited the forest long before governments recognised the need to conserve and manage them, with varied impacts on human welfare (Naughton-Treves et al., 2005). In cases where profit-driven commodity agriculture is the driver of mountain forest loss, intervention can be effective when the will to enforce forest protection laws is strong. An example is found in the border areas of Thailand and Laos where maize cultivation on forested lands is being phased out by the Thai government, but in Laos, the exploitation of forests for lucrative boom crops persists (Supplementary Figure A.9; Peng et al., 2005; Pongkijvorasin and Teerasuwannajak, 2019). This situation demonstrates the drastic outcome in forest loss patterns related to differing institutional efficiency and capacity to enforce existing forest conservation policies. Further, the economic situation in Laos and its geographical location in Southeast Asia makes it susceptible to external investments that drive deforestation for agriculture, timber/wood products, and energy (WWF, 2021).

We recognise the importance of promoting the regeneration of converted forests both naturally and through forestation programs. While we find that much regrowth has occurred in the locations of mountain forest loss worldwide, two issues are critical within the scope of our analysis. Firstly, reforestation with native species is preferable over the establishment of mono-specific tree plantations, which by some definitions are considered a type of forest. Secondly, initial disturbance causing forest loss may critically damage the habitat of sensitive species to the extent that they may not recover when forests reappear. Another issue is that the wellbeing of other types of organisms that contribute to biodiversity should be considered. Regarding sensitive species in biodiversity hotspots, the critical issue extends beyond simply preventing forest loss to also maintaining the integrity of forests in large enough zones to allow natural movements and sufficient space for ranging species. Protected areas should be designed with this purpose in mind.

Regionally distinctive drivers of mountain forest loss mean that efforts to curb the acceleration of mountain forest loss will require regionally appropriate interventions. In regions where shifting cultivation is a strong driver, like in Brazil,

Colombia and Peru, efforts should be made to ensure agriculture does not impact frontier (intact or primary) forests where possible. Rather, it would be better to establish new agriculture ventures where forests are already disturbed or land has been recently cleared (Dressler et al., 2021). Whereas in regions where commodity production is more prevalent (e.g., Indonesia, Vietnam, and Malaysia), increased commitment is needed urgently to halt commodity-driven forest loss and safeguard mountain forest biodiversity. Given that human population pressure has also been a major cause of biodiversity loss in PAs in the past few decades (Yang and Xu, 2003), we recommend that relevant strategies should consider balancing economic development, biodiversity conservation and sustainable livelihoods especially within and surrounding PAs.

We see examples where the existence of PAs has significantly reduced forest loss, compared with the areas surrounding them. Recent studies have also demonstrated the role of PAs worldwide in preventing forest loss (Yang et al., 2021; Feng et al., 2021b). Largely in agreement, we find that of the 78 countries with data pertaining to PAs in montane areas, about half were effective in keeping forest loss to be less than half of the loss experienced outside of PAs (Supplementary Table A.5). Unfortunately, in 12 countries the forest loss inside the PAs was greater than or equivalent to that outside. Drivers of mountain forest loss inside PAs tend to vary, with shifting cultivation, commercial forestry and commodity agriculture being important in a variety of locations. The strategic expansion and development of new PAs are thus promising avenues to improving mountain forest conservation for biodiversity now and into the future, especially in countries where PA coverage is low (Rodríguez-Rodríguez et al., 2011; Elsen et al., 2018). Many countries have only marginally effective PAs because, even in areas where forests are protected, there are destructive anthropogenic activities (e.g., logging) taking place that tax sensitive organisms. In these places, there is ample opportunity for improved PA management, and more adequate resourcing, and stricter enforcement of laws and regulations designed to protect forests.

As alluded to above, any new measures to protect mountain forests should be adapted to local conditions and contexts (Nagendra and Gokhale, 2008), and they should reconcile the need for enhanced forest protection with ensuring food production and human wellbeing (Carmenta et al., 2022). More integrated socio-ecological research is needed to improve our understanding of biodiversity and ecosystem functioning in complex and sensitive mountain ecosystems, especially

at the interface between social and natural systems. Such knowledge should boost awareness of the importance of preserving forest integrity whilst maintaining or enhancing human wellbeing, and, hopefully, help change attitudes regarding the reliance on destructive food production and energy generation systems.

In closing, our global analysis of mountain forest loss identifies an alarming acceleration in mountain forest lost worldwide over the last two decades. Important drivers have been various types of agriculture, forestry, and wildfires, with regional differences. These global results provide a foundation for further regional and local studies to examine nuanced differences more closely. Our analysis also highlights the importance of appropriately managed protected areas in preserving mountain forest biodiversity in the face of increasing human pressures for food production and a changing climate. By providing a clear understanding of the current trends and drivers of mountain forest loss, we hope that this analysis will inform and support conservation efforts aimed at preserving critical montane forest ecosystems for future generations.

2.4 Experimental Procedures

2.4.1 Data sources

Global forest change data and visual interpretation for forest gain

We used a Global Forest Change (GFC) dataset from 2000 to 2018 (version 1.6, available at https://earthenginepartners.appspot.com/science-2013-global-forest/download_v1.6.html; Hansen et al., 2013) to analyse forest loss over mountains during the 21st century. This dataset uses Landsat satellite images to detect annual forest cover loss at a 1 arc-second resolution (~30 meters at the equator), spanning latitudes from 80°N–50°S. The global dataset is divided into 10° × 10° tiles (each containing 40,000 by 40,000 pixels). Trees are defined as “all vegetation taller than 5 m in height” (Hansen et al., 2013). Forest loss is “stand-replacement disturbance” (Hansen et al., 2013), which includes both permanent loss (conversion to another land use) and temporary loss (e.g., loss from a forest fire). We first created a baseline forest cover map in 2000 from the percent tree cover layer using the criteria of Hansen et al. (2013) that forest cover comprises at least 25% tree canopy cover at the pixel scale (30 × 30 m), which

is an appropriate threshold for multispectral imagery to unambiguously identify tall woody vegetation. To investigate the degree to which our results were sensitive to the choice of threshold, we also used a tree-cover threshold of 50% to define forests for comparison (Supplementary Figure A.10). Then, we mapped forest loss for all years in the 2001 to 2018 period from the forest loss layer at the pixel level. The forest loss area is the sum of all pixel areas where forest loss occurred. To distinguish the change of pixels with latitude, we calculated the pixel area as a function of latitude: pixel area = cos(latitude) × pixel area at the equator.

To check whether there was subsequent regrowth around 2019 where the forest was lost during the study period 2001–2018, we performed an independent assessment of forest gain using a sample-based approach following recommendations from Global Forest Watch (Weisse and Potapov, 2021) and good practice guidance of Olofsson et al. (2014). We randomly sampled 5,000 pixels that experienced forest loss using random number generation, and visually interpreted forest gain using very-high-resolution imagery from Google Earth and Planet Explorer. We started with Google Earth for visual interpretation because it has a very high resolution (ranging from 15 m to even 15 cm); if there was no clear satellite image in 2019, we expanded the time range to the two years before and after, i.e., 2017–2020, but the image is at least a year after forest loss occurred. For the remaining points that have no images in Google Earth, we changed to Planet Explorer at a resolution of ~3.7 m for interpretation using daily or monthly imagery.

Drivers of forest loss

We determined the drivers of forest loss using the dataset generated by Curtis et al. (2018). This dataset shows the dominant driver of forest loss at each 10 km grid cell. There are five categories of drivers of forest loss, including commodity-driven deforestation which is defined as permanent and/or long-term clearing of trees to other land uses (e.g., commodity agriculture), shifting cultivation, forestry (a combination of logging, plantations, and other forestry operations with visible forest regrowth in subsequent years), wildfire, and urbanization. The grids that were marked as zero or minor loss in the driver dataset are categorised as “other”. We resampled data from 10 km resolution to 30 m using the nearest neighbour method, to match the scale of global forest cover change data. We then reported the proportion of each driver of mountain forest loss for each country.

Topography data

A digital elevation model and global mountain polygons were applied to quantify the topographic pattern of forest loss. We used a high-resolution (30-m) elevation dataset from the Advanced Spaceborne Thermal Emission and Reflection Radiometer (ASTER) Global Digital Elevation Model (GDEM, version 3, available at https://earthdata.nasa.gov/; NASA, 2019) to quantify the elevational gradients of mountain forest loss. The ASTER GDEM was generated by stacking the observed cloud-masked and non-cloud-masked scene DEMs, spanning latitudes from 83°N – 83°S (Fujisada et al., 2005; Fujisada et al., 2011; Fujisada et al., 2012). Each tile of data has a dimension of 3,601 × 3,601 pixels, or a 1° latitude by 1° longitude area (Li et al., 2015). As the tile size of ASTER GDEM differs slightly from that of the forest change data, we first resampled each 1° x 1° DEM tile to 4,000 × 4,000 by using the cubic convolution method and then merged it into a tile of 10° latitude by 10° longitude pixels as in the forest change dataset (i.e., 40,000 × 40,000 pixels).

We used the Global Mountain Biodiversity Assessment (GMBA) definition (version 1.2, available at www.mountainbiodiversity.org, https://ilias.unibe.ch/goto_ilias3_unibe_cat_1000515.html; Körner et al., 2017) to identify mountain regions, which adopts a ruggedness threshold indicating that the geometrical slope between the lowest and the highest point within a 2.5' pixel must exceed 200 m (Körner et al., 2011). The GMBA mountain definitions have the advantage of excluding some unstructured terrain such as large plateaus and expansive valleys or basins, while also not limiting mountains to particular elevations. Based on this definition, the world's mountainous terrain occupies about 1.64 billion ha and accounts for 12.3% of the total land area. It uses the GMBA definition along with expert delineations to provide a worldwide inventory of 1,048 distinct mountain systems as vector polygons. Mountain regions are divided into eight mega-regions (mostly continents): Asia, Africa, Europe, Australia, North America, South America, Oceania, and Greenland (Körner et al., 2017). Although mountain areas in Greenland occupy 4.3% of the total land area in the region, these mountains contain no tree cover and so are not considered here. In the analysis, we also examined forest loss in tropical (24°S to 24°N), boreal (≥50°N) and temperate (residual) regions.

Biodiversity hotspots

We identified biodiversity hotspots for amphibians, birds, and mammals (as they have been the most comprehensively assessed and thus polygon maps are available) based on two species pools: (1) all accessed species belonging to any International Union for Conservation of Nature (IUCN) Red List category; and (2) threatened species listed as CR (Critically Endangered), EN (Endangered) and VU (Vulnerable) on the IUCN Red List. Thus, the second pool is a subset of the first. Note that the dataset used a filtering process that eliminates records of Extinct (EX) and Extinct in the wild (EW) from the start. For each of the two species pools, we used existing maps of range-size rarity (RSR) and species richness (SR) based on the raw IUCN ranges (available at https://www.iucnredlist.org/resources/other-spatial-downloads). RSR within each pixel is calculated as the pixel area divided by the total distribution area of each species that occurs within this pixel and then summed across all these species to determine the aggregate importance of each pixel. SR represents the total number of species potentially occurring in each pixel (including the possibility of presence and the uncertainty of seasonal occurrence of a species). We therefore used four raster layers consisting of all combinations of the two biodiversity indicators (RSR and SR) and the two species pools (all and threatened). The resolution of these rasters is about 5 km at the equator, but we resampled them to ~30 m to match global forest change data for calculation in our analysis.

In this dataset, RSR values range from 0 to ~0.72 (for all species) and from 0 to ~0.29 (for threatened species); SR values range from 1 to 912 (for all species) and from 1 to 59 (for threatened species). For each raster, we defined biodiversity hotspots as the upper 2.5% of land cells with the highest RSR or SR values as done previously (Orme et al., 2005) and clipped it to the boundaries of the mountain range delineations. The four biodiversity hotspot criteria are referred to as: (1) RSR (all); (2) RSR (threatened); (3) SR (all); and (4) SR (threatened). In each type of biodiversity hotspot within the mountain extent, RSR values range from 0.00073 to ~0.19 (for all species) and from 0.00012 to ~0.29 (for threatened species); SR values range from 675 to 847 (for all species), and from 24 to 59 (for threatened species) respectively; these ranges were calculated based on the upper 2.5% the land area.

Protected areas

To investigate how much of the area of forest loss within biodiversity hotspots has been protected, we used polygon delineations of PAs from the World Database on Protected Areas (WDPA; available at https://www.protectedplanet.net/en/thematic-areas/wdpa?tab=WDPA). We did not include PAs represented by points, as forest loss calculations required areas. Due to the large size of the database, the data were divided into three shapefile layers. We clipped these layers to the extent of our mountain range boundaries separately and then merged them into one layer. A total of 30,515 PA polygons within the mountain range delineations were obtained. All pre-processing was performed in ArcMap 10.6.

2.4.2 Data analysis

We assessed temporal, spatial, and elevational patterns of forest loss across global mountains and within mountain biodiversity hotspots. We estimated the annual forest loss area occurring in years between 2001 and 2018, beginning from the reference year 2000. Relative forest loss is based on forest cover in the baseline year 2000, calculated as the amount of forest lost in the region relative to the amount of forest that was there (relative forest loss = forest loss area/forest cover in 2000), providing information about rates of forest loss. We evaluated the temporal trend in annual forest loss (i.e., acceleration) using a non-parametric Theil-Sen estimator regression method (Sen, 1968) due to its robustness for trend detection and insensitivity to outliers, which has been widely used in previous research, including in forest cover trend analysis (Song et al., 2018; Alibakhshi et al., 2020). We then assessed the significance of the trends using the Mann-Kendall (MK) test (Mann, 1945). To make our results more comparable among different regions or climate zones, we used a standardised annual rate of forest loss proposed by Puyravaud (2003), calculated as: $r = (1/(t_2-t_1)) \times \ln(A_2/A_1)$ where A_1 and A_2 are the forest cover at time t_1 and t_2. In our analysis, A_1 is forest cover in the baseline year 2000 (obtained by the existing tree cover layer as mentioned above) and A_2 is forest cover in 2018 (= forest cover in 2000 – forest loss 2001 to 2018 + forest gain).

To visualise mountain forest loss areas occurring at different elevations, we grouped elevation into 50 m bins within 0.5° grid cells. In mountain biodiversity

hotspots, we calculated mean RSR (and overall SR) patterns within each elevation bin to represent the potential impacts of elevation-specific forest loss on biodiversity. We then compared the amount of forest loss in mountain hotspots of all species with those associated with threatened species to reveal the differences between various species pools affected by mountain forest loss. Finally, we specifically calculated each country's mountain forest loss for the RSR biodiversity hotspot with threatened species.

To assess the elevation-specific patterns of PA protection, we calculated PA coverage (i.e., fraction of forest in PAs) as the ratio of mountain forest within PAs in hotspots versus mountain forest in the corresponding hotspots. We also compare mountain forest loss within biodiversity hotspots inside PAs and outside of PAs at different elevations. In this study, we use the ratio of relative mountain forest loss within biodiversity hotspots inside versus outside of PAs to assess forest loss in the context of PAs (i.e., when the ratio <1, PAs experienced less forest loss than unprotected areas).

2.4.3 Uncertainties and limitations

The GFC product we used, does not distinguish between natural forests and tree plantations (Hansen et al., 2009; Li and Fox, 2012). Forest loss estimates therefore include forestry activities within tree plantations. Another difficulty we encountered was distinguishing forest (tree) loss from selective logging, which tends to degrade forests rather than resulting in a transition to another type of land cover. Not only permanent forest loss poses direct threats to montane forest biodiversity, but other forms of temporary loss (including partial tree removal) and forest degradation at large spatial scales are threatening biodiversity, particularly in sensitive habitats like cloud forests, wetlands mountain patches in valleys, etc. Although forestry is an important driver of mountain forest loss as we reported, our independent analysis of forest loss and plantation loss confirms that the majority of loss occurs in natural forests, with less than 20% occurring in plantations (Figure 2.4). Thus, the forest loss estimates presented in this study are likely to be conservative.

We acknowledge that our results are based on vertebrate (amphibians, birds, and mammals) distributions only, and that a more thorough investigation of the impacts of forest loss on other taxonomic groups such as plants, fungi, protists,

and other types of wildlife (e.g., fish, insects) is needed. As the realm of most organisms (e.g., freshwater protists, fungi and other soil community members including bacteria, protozoa, nematodes, and arthropods) is largely unknown, potentially important services offered by entire mountain forest ecosystems may soon be lost, or at least degraded following forest removal (Ornetsmüller et al., 2018).

Finally, some geographic mountainous areas of known forest loss were not detected in our analysis (e.g., the islands of Timor-Leste and Dominica; Mongabay, 2020). The reason for the omission of these countries, and possibly others, is the definition of mountains following the GMBA definition (Körner et al., 2017). Although regrettable, as this paper is a global analysis, we used a standard global definition of mountains.

References

Achard, F., Eva, H.D., Stibig, H.J., Mayaux, P., Gallego, J., Richards, T. and Malingreau, J.P., 2002. Determination of Deforestation Rates of the World's Humid Tropical Forests. Science, 297, 999–1002.

Aide, T.M., Grau, H.R., Graesser, J., Andrade-Nuñez, M.J., Aráoz, E., Barros, A.P., Campos-Cerqueira, M., Chacon-Moreno, E., Cuesta, F., Espinoza, R., Peralvo, M. et al., 2019. Woody vegetation dynamics in the tropical and subtropical Andes from 2001 to 2014: satellite image interpretation and expert validation. Global Change Biology, 25, 2112–2126.

Alibakhshi, S., Naimi, B., Hovi, A., Crowther, T.W. and Rautiainen, M., 2020. Quantitative analysis of the links between forest structure and land surface albedo on a global scale. Remote Sensing of Environment, 246, 111854.

Andreacci, F. and Marenzi, R.C., 2020. Accounting for twenty-first-century annual forest loss in the Atlantic Forest of Brazil using high-resolution global maps. International Journal of Remote Sensing, 41, 4408–4420.

Angelsen, A., Jagger, P., Babigumira, R., Belcher, B., Hogarth, N.J., Bauch, S., Börner, J., Smith-Hall, C. and Wunder, S., 2014. Environmental income and rural livelihoods: a global-comparative analysis. World Development, 64, S12–S28.

Bowman, D.M.J.S., Williamson, G.J., Prior, L.D. and Murphy, B.P., 2016. The relative importance of intrinsic and extrinsic factors in the decline of obligate seeder forests. Global Ecology and Biogeography, 25, 1166–1172.

Brooks, T.M., Mittermeier, R.A., da Fonseca, G.A., Gerlach, J., Hoffmann, M., Lamoreux, J.F., Mittermeier, C.G., Pilgrim, J.D. and Rodrigues, A.S., 2006. Global biodiversity conservation priorities. Science, 313, 58–61.

Carmenta, R., Steward, A., Albuquerque, A., Carneiro, R., Vira, B. and Estrada Carmona, N., 2022. The comparative performance of land sharing, land sparing type interventions on place-based human well-being. People and Nature, 00, 1–18.

Chen, I.C., Hill, J.K., Ohlemüller, R., Roy, D.B. and Thomas, C.D., 2011. Rapid range shifts of species associated with high levels of climate warming. Science, 333, 1024–1026.

Colwell, R.K., Brehm, G., Cardelús, C.L., Gilman, A.C. and Longino, J.T., 2008. Global warming, elevational range shifts, and lowland biotic attrition in the wet tropics. Science, 322, 258–261.

Cramb, R.A., Colfer, C.J.P., Dressler, W., Laungaramsri, P., Le, Q.T., Mulyoutami, E., Peluso, N.L. and Wadley, R.L., 2009. Swidden transformations and rural livelihoods in Southeast Asia. Human Ecology, 37, 323–346.

Curran, L.M., Trigg, S.N., McDonald, A.K., Astiani, D., Hardiono, Y.M., Siregar, P., Caniago, I. and Kasischke, E., 2004. Lowland forest loss in protected areas of Indonesian Borneo. Science, 303, 1000–1003.

Curtis, P.G., Slay, C.M., Harris, N.L., Tyukavina, A. and Hansen, M.C., 2018. Classifying drivers of global forest loss. Science, 361, 1108–1111.

da Silva, F.K.G., de Faria Lopes, S., Lopez, L.C.S., de Melo, J.I.M. and Trovão, D., 2014. Patterns of species richness and conservation in the Caatinga along elevational gradients in a semiarid ecosystem. Journal of Arid Environments,110, 47–52.

Dressler, W.H., Smith, W., Kull, C.A., Carmenta, R. and Pulhin, J.M., 2021. Recalibrating burdens of blame: anti-swidden politics and green governance in the Philippine Uplands. Geoforum, 124, 348–359.

Elsen, P.R. and Tingley, M.W., 2015. Global mountain topography and the fate of montane species under climate change. Nature Climate Change, 5, 772–776.

Elsen, P.R., Monahan, W.B. and Merenlender, A.M., 2018. Global patterns of protection of elevational gradients in mountain ranges. Proceedings of the National Academy of Sciences, 115, 6004–6009.

Elsen, P.R., Monahan, W.B. and Merenlender, A.M., 2020. Topography and human pressure in mountain ranges alter expected species responses to climate change. Nature Communications, 11, 1–10.

Fujisada, H., Bailey, G.B., Kelly, G.G., Hara, S. and Abrams, M.J., 2005. ASTER DEM performance. IEEE Transactions on Geoscience and Remote Sensing, 43, 2707–2714.

Fujisada, H., Urai, M. and Iwasaki, A., 2011. Advanced methodology for ASTER DEM generation. IEEE Transactions on Geoscience and Remote Sensing, 49, 5080–5091.

Fujisada, H., Urai, M. and Iwasaki, A., 2012. Technical methodology for ASTER global DEM. IEEE Transactions on Geoscience and Remote Sensing, 50, 3725–3736.

Feng, Y., Ziegler, A.D., Elsen, P.R., Liu, Y., He, X., Spracklen, D.V., Holden, J., Jiang, X., Zheng, C. and Zeng, Z., 2021a. Upward expansion and acceleration of forest clearance in the mountains of Southeast Asia. Nature Sustainability, 4, 892–899.

Feng, Y., Wang, Y., Su, H., Pan, J., Sun, Y., Zhu, J., Fang, J. and Tang, Z., 2021b. Assessing the effectiveness of global protected areas based on the difference in differences model. Ecological Indicators, 130, 108078.

Gibbs, H.K., Ruesch, A.S., Achard, F., Clayton, M.K., Holmgren, P., Ramankutty, N. and Foley, J.A., 2010. Tropical forests were the primary sources of new agricultural land in the 1980s and 1990s. Proceedings of the National Academy of Science, 107, 16732–16737.

Hansen, M.C., Potapov, P.V., Moore, R., Hancher, M., Turubanova, S.A., Tyukavina, A., Thau, D., Stehman, S.V., Goetz, S.J., Loveland, T.R., Kommareddy, A. et al., 2013. High-resolution global maps of 21st-century forest cover change. Science, 342, 850–853.

Hansen, M.C., Stehman, S.V. and Potapov, P.V., 2010. Quantification of global gross forest cover loss. Proceedings of the National Academy of Science, 107, 8650–8655.

Hansen, M.C., Stehman, S.V., Potapov, P.V., Arunarwati, B., Stolle, F. and Pittman, K., 2009. Quantifying changes in the rates of forest clearing in Indonesia from 1990 to 2005 using remotely sensed data sets. Environmental Research Letters, 4, 034001.

Hill, S.L., Arnell, A., Maney, C., Butchart, S.H., Hilton-Taylor, C., Ciciarelli, C., Davis, C., Dinerstein, E., Purvis, A. and Burgess, N.D., 2019. Measuring Forest Biodiversity Status and Changes Globally. Frontiers in Forests and Global Change, 2, 70.

Hughes, A.C., 2017. Understanding the drivers of Southeast Asian biodiversity loss. Ecosphere, 8, e01624.

Hurni, K. and Fox, J., 2018. The expansion of tree-based boom crops in mainland Southeast Asia: 2001 to 2014. Journal of Land Use Science, 13, 198–219.

Imai, N., Furukawa, T., Tsujino, R., Kitamura, S. and Yumoto, T., 2018. Factors affecting forest area change in Southeast Asia during 1980-2010. Plos One, 13, e0199908.

Jakovac, C.C., Peña-Claros, M., Kuyper, T.W. and Bongers, F., 2015. Loss of secondary-forest resilience by land-use intensification in the Amazon. Journal of Ecology, 103, 67–77.

Keenan, R.J., Reams, G.A., Achard, F., de Freitas, J.V., Grainger, A. and Lindquist, E., 2015. Dynamics of global forest area: results from the FAO Global Forest Resources Assessment 2015. Forest Ecology and Management, 352, 9–20.

Kelly, R., Chipman, M.L., Higuera, P.E., Stefanova, I., Brubaker, L.B. and Hu, F.S., 2013. Recent burning of boreal forests exceeds fire regime limits of the past 10,000 years. Proceedings of the National Academy of Science, 110, 13055–13060.

Körner, C., Jetz, W., Paulsen, J., Payne, D., Rudmann-Maurer, K. and Spehn, E.M., 2017. A global inventory of mountains for bio-geographical applications. Alpine Botany, 127, 1–15.

Körner, C., Paulsen, J. and Spehn, E.M., 2011. A definition of mountains and their bioclimatic belts for global comparisons of biodiversity data. Alpine Botany, 121, 73.

Lesiv, M., Schepaschenko, D., Buchhorn, M., See, L., Dürauer, M., Georgieva, I., Jung, M., Hofhansl, F., Schulze, K., Bilous, A., Blyshchyk, V. et al., 2022. Global forest management data for 2015 at a 100 m resolution. Scientific Data, 9, 199.

Li, L., Liu, J., Long, H., de Jong, W. and Youn, Y.-C., 2015. Economic globalization, trade and forest transition-the case of nine Asian countries. Forest Policy and Economics, 76, 7–13.

Li, Z. and Fox, J.M., 2012. Mapping rubber tree growth in mainland Southeast Asia using time-series MODIS 250 m NDVI and statistical data. Applied Geography, 32, 420–432.

Lim, C.L., Prescott, G.W., de Alban, J.D.T., Ziegler, A.D. and Webb, E.L., 2017. Untangling the proximate causes and underlying drivers of deforestation and forest degradation in Myanmar. Biological Conservation, 31, 1362–1372.

Mann, H.B., 1945. Nonparametric tests against trend. Econometrica, 13, 245–259.

Miyamoto, M., Parid, M.M., Aini, Z.N. and Michinaka, T., 2014. Proximate and underlying causes of forest cover change in Peninsular Malaysia. Forest Policy and Economics, 44, 18–25.

Mongabay, 2020. Deforestation statistics for [Timor-Leste & Dominica]. Accessed from rainforests.mongabay.com.

Moritz, C., Patton, J.L., Conroy, C.J., Parra, J.L., White, G.C. and Beissinger, S.R., 2008. Impact of a century of climate change on small-mammal communities in Yosemite National Park, USA. Science, 322, 261–264.

Nagendra, H. and Gokhale, Y., 2008. Management regimes, property rights, and forest biodiversity in Nepal and India. Environmental Management, 41, 719–733.

NASA/METI/AIST/Japan Spacesystems and U.S./Japan ASTER Science Team, 2019. ASTER Global Digital Elevation Model V003 [Data set]. NASA EOSDIS Land Processes DAAC. Accessed from https://doi.org/10.5067/ASTER/ASTGTM.003.

Naughton-Treves, L., Holland, M.B. and Brandon, K., 2005. The role of protected areas in conserving biodiversity and sustaining local livelihoods. Annual Review of Environment and Resources, 30, 219–252.

Nepstad, D.C., Stickler, C.M. and Almeida, O.T., 2006. Globalization of the Amazon soy and beef industries: opportunities for conservation. Conservation Biology, 20, 1595–1603.

Neill, C., Piccolo, M.C., Cerri, C.C., Steudler, P.A. and Melillo, J.M., 2006. Soil solution nitrogen losses during clearing of lowland Amazon forest for pasture. Plant Soil, 281, 233–245.

Noroozi, J., Talebi, A., Doostmohammadi, M., Rumpf, S.B., Linder, H.P. and Schneeweiss, G.M., 2018. Hotspots within a global biodiversity hotspot-

areas of endemism are associated with high mountain ranges. Scientific Reports, 8, 1–10.

Olofsson, P., Foody, G.M., Herold, M., Stehman, S.V., Woodcock, C.E. and Wulder, M.A., 2014. Good practices for estimating area and assessing accuracy of land change. Remote Sensing of Environment, 148, 42–57.

Orme, C.D.L., Davies, R.G., Burgess, M., Eigenbrod, F., Pickup, N., Olson, V.A., Webster, A.J., Ding, T.S., Rasmussen, P.C., Ridgely, R.S. and Stattersfield, A.J., 2005. Global hotspots of species richness are not congruent with endemism or threat. Nature, 436, 1016–1019.

Ornetsmüller, C., Castella, J.-C. and Verburg, P.H., 2018. A multiscale gaming approach to understand farmer's decision making in the boom of maize cultivation in Laos. Ecology and Society, 23, 35.

Peters, M.K., Hemp, A., Appelhans, T., Becker, J.N., Behler, C., Classen, A., Detsch, F., Ensslin, A., Ferger, S.W., Frederiksen, S.B. and Gebert, F., 2019. Climate–land-use interactions shape tropical mountain biodiversity and ecosystem functions. Nature, 568, 88–92.

Peng, W.Y., Zhang, K.L., Chen, Y. and Yang, Q.K., 2005. Research on soil quality change after returning farmland to forest on the loess sloping croplands. Journal of Natural Resources, 20, 272–278.

Pongkijvorasin, S. and Teerasuwannajak, K.T., 2019. A study of farmer's decision and incentive scheme to reduce highland maize farming in Thailand. Int. J. Agric. Sustainability, 17, 257–270.

Potapov, P.V., Turubanova, S.A., Hansen, M.C., Adusei, B., Broich, M., Altstatt, A., Mane, L. and Justice, C.O., 2012. Quantifying forest cover loss in Democratic Republic of the Congo, 2000–2010, with Landsat ETM+ data. Remote Sensing of Environment, 122, 106–116.

Puyravaud, J.P., 2003. Standardizing the calculation of the annual rate of deforestation. Forest Ecology and Management, 177, 593–596.

Rahbek, C., Borregaard, M.K., Colwell, R.K., Dalsgaard, B.O., Holt, B.G., Morueta-Holme, N., Nogues-Bravo, D., Whittaker, R.J. and Fjeldså, J., 2019. Humboldt's enigma: what causes global patterns of mountain biodiversity? Science, 365, 1108–1113.

Rea, G., Paton-Walsh, C., Turquety, S., Cope, M. and Griffith, D., 2016. Impact of the New South Wales fires during October 2013 on regional air quality in eastern Australia. Atmospheric Environment, 131, 150–163.

Reyes-Betancort, J.A., Guerra, A.S., Guma, I.R., Humphries, C.J. and Carine, M.A., 2008. Diversity, rarity and the evolution and conservation of the Canary Islands endemic flora. In *Anales del Jardín Botánico de Madrid*. 25–45. Consejo Superior de Investigaciones Científicas.

Rodríguez-Rodríguez, D., Bomhard, B., Butchart, S.H. and Foster, M.N., 2011. Progress towards international targets for protected area coverage in mountains: a multi-scale assessment. Biological Conservation, 144, 2978–2983.

Sen, P.K., 1968. Estimates of the regression coefficient based on Kendall's tau. Journal of the American Statistical Association, 63, 1379–1389.

Soares-Filho, B.S., Nepstad, D.C., Curran, L.M., Cerqueira, G.C., Garcia, R.A., Ramos, C.A., Voll, E., McDonald, A., Lefebvre, P. and Schlesinger, P., 2006. Modelling conservation in the Amazon basin. Nature, 440, 520–523.

Sodhi, N.S. and Brook, B.W., 2006. *Southeast Asian biodiversity in crisis.* Cambridge University Press.

Song, X.P., Hansen, M.C., Stehman, S.V., Potapov, P.V., Tyukavina, A., Vermote, E.F. and Townshend, J.R., 2018. Global land change from 1982 to 2016. Nature, 560, 639–643.

Taylor, C., McCarthy, M.A. and Lindenmayer, D.B., 2014. Nonlinear effects of stand age on fire severity. Conservation Letters, 7, 355–370.

van Vliet, N., Mertz, O., Heinimann, A., Langanke, T., Pascual, U., Schmook, B., Adams, C., Schmidt-Vogt, D., Messerli, P., Leisz, S., Castella, J.C. et al., 2012. Trends, drivers and impacts of changes in swidden cultivation in tropical forest-agriculture frontiers: a global assessment. Global Environmental Change, 22, 418–429.

Watson, J.E., Whittaker, R.J. and Dawson, T.P., 2004. Habitat structure and proximity to forest edge affect the abundance and distribution of forest-dependent birds in tropical coastal forests of southeastern Madagascar. Biological Conservation, 120, 311–327.

Weisse, M. and Potapov, P., 2021. Assessing trends in tree cover loss over 20 years of data. Global Forest Watch. Accessed from https://www.globalforestwatch.org/blog/data-and-research/tree-cover-loss-satellite-data-trend-analysis/.

Williams, P., Gibbons, D., Margules, C., Rebelo, A., Humphries, C. and Pressey, R., 1996. A comparison of richness hotspots, rarity hotspots, and complementary areas for conserving diversity of British birds. Conservation Biology, 10, 155–174.

Wilkinson, C., Eriksen, C. and Penman, T., 2016. Into the firing line: civilian ingress during the 2013 “Red October” bushfires, Australia. Natural Hazards, 80, 521–538.

WWF., 2021. Deforestation fronts. World Wildlife Foundation. Accessed from https://wwf.panda.org/discover/our_focus/forests_practice/deforestation_fronts_/fact_sheets/.

Yang, H, Viña, A., Winkler, J. A., Chung, M. G., Huang, Q., Dou, Y., McShea, W. J., Songer, M. Zhang, J. and Liu, J., 2021. A global assessment of the impact of individual protected areas on preventing forest loss. Science of the Total Environment, 777, 145995.

Yang, X. and Xu, M., 2003. Biodiversity conservation in Changbai Mountain Biosphere Reserve, northeastern China: status, problem, and strategy. Biodiversity and Conservation, 12, 883–903.

Zeng, Z., Gower, D.B. and Wood, E.F., 2018a. Accelerating forest loss in Southeast Asian Massif in the 21st century: a case study in Nan Province, Thailand. Global Change Biology, 24, 4682–4695.

Zeng, Z., Estes, L., Ziegler, A.D., Chen, A., Searchinger, T., Hua, F., Guan, K., Jintrawet, A. and Wood, E.F., 2018b. Highland cropland expansion and forest loss in Southeast Asia in the twenty-first century. Nature Geosciences, 11, 556–562.

Zeng, Z., Wang, D., Yang, L., Wu, J., Ziegler, A.D., Liu, M., Ciais, P., Searchinger, T.D., Yang, Z.L., Chen, D., Chen, A. et al., 2021. Deforestation-induced warming over tropical mountain regions regulated by elevation. Nature Geosciences, 14, 23–29.

Ziegler, A.D., Phelps, J., Yuen, J.Q., Webb, E.L., Lawrence, D., Fox, J.M., Bruun, T.B., Leisz, S.J., Ryan, C.M., Dressler, W., Mertz, O. et al., 2012. Carbon

outcomes of major land-cover transitions in SE Asia: great uncertainties and REDD+ policy implications. Global Change Biology, 18, 3087–3099.

Chapter 3

Tropical montane forest loss dominated by increased medium-scale clearings

Abstract

Tropical forest loss continues across mountain regions at alarming rates, threatening biodiversity, carbon storage and ecosystem sustainability. To improve our understanding of the dynamics of tropical mountain forest loss, we examined trends in forest loss patch size during the first two decades of the 21st century. As tropical mountain forest loss increased from 0.9 Mha yr^{-1} in 2001 to approximately 2.5 Mha yr^{-1} in 2021, more than 50% of this increase was attributed to the proliferation of intermediate-sized clearings (1–10 ha). Conversely, there was a declining proportion of small-scale forest loss patches (<1 ha) across all continents over time. Throughout the study period, 78% of tropical mountain forest loss associated with very large clearings (>100 ha) occurred in Southeast Asia, primarily driven by commodity agriculture. This emerging prominence of large-scale drivers of forest loss suggests the growing need for policy interventions that target agricultural commodity producers. By providing up-to-date and spatially explicit information on the scale of tropical mountain forest loss, and temporal trends associated with these patterns, this study contributes valuable information for understanding potential drivers and designing effective interventions to slow or reverse forest loss.

3.1 Introduction

Tropical montane forests play a crucial role in global ecosystem services, including carbon sequestration, climate mitigation, biodiversity conservation, and regulation of the water cycle (Bruijnzeel et al., 2011; Spracklen and Righelato, 2014; Zeng et al., 2021). However, increasing rates of forest cover loss resulting from land-use changes across tropical mountains threaten the provision of these essential services (Zeng et al., 2021; Feng et al., 2022; Smith et al., 2023; He et al., 2023). The spatial pattern of forest loss could amplify the negative effects on tropical ecosystems. For example, evidence shows that the formation of new forest edges due to the increase in deforested patch size will result in higher tree

mortality and frequency of wildfires (Broadbent et al., 2008). Therefore, spatially explicit information on the scale of forest loss in mountainous areas, along with an understanding of how these patterns have changed over time, is of great importance for developing effective strategies to preserve tropical montane forests and to maintain related ecosystem services.

The dynamics of forest loss are not static over time (Kalmadeen et al., 2018). Forest fragmentation alters ecological functioning and species composition (Laurance et al., 2011), reducing the amount of carbon stored at forest edges (Chaplin-Kramer et al., 2015). A shift from small-scale to large-scale deforestation could modify the mechanisms and patterns of regional precipitation (Chambers and Artaxo, 2017; Khanna et al., 2017). The size of a forest clearing activity is often used as a proxy for characterizing small-scale activities or large commercial and industrial-scale operations (Austin et al., 2017). Distinguishing between small- and large-scale clearings may therefore be helpful in understanding changing mountain forest landscapes (Malhi et al., 2014).

Extensive studies have been conducted in tropical forests to quantify deforested size or forest fragmentation (Austin et al., 2017; Hansen et al., 2020). In lowland areas, for example, significant declining rates of large-scale deforestation were observed in the Amazon, while a pervasive rise of small clearings occurred over time (Rosa et al., 2012; Godar et al., 2014; Kalamandeen et al., 2018). Similarly, in the Congo Basin, small-scale forest clearings for agriculture have increased over time (Tyukavina et al., 2018). Across tropical mountain regions, despite some local or regional assessments of remaining forest patches (Cayuela et al., 2006; Canale et al., 2012), a comprehensive and consistent analysis of the size of forest loss in tropical mountainous regions still lacking.

Here, we used a time series of forest loss to quantify this loss in terms of clearing sizes between 2001 and 2021 across tropical mountains. The objectives of this work are to analyse how much forest loss was associated with clearings of different sizes and to determine whether the distribution of clearing sizes has changed over time. This study provides critical insights into shifts in potential drivers of forest conversion and helps conservation policy debate where there is a desire to maintain larger and contiguous patches of forest cover.

3.2 Methods

We used the Global Forest Change (GFC) data (Hansen et al., 2013) to investigate how mountain forest loss patch sizes varied in the tropics (24°S–24°N) in the 21st century. Forest loss was defined by Hansen et al. (2013) as a stand-replacement disturbance or the complete removal of tree cover canopy at a pixel scale of 30 m based on Landsat imagery. In the GFC dataset, only the first occurrence of a forest loss event in each pixel has been reported. This means that forest loss was only detected when it happened for the first time, and each pixel was marked only once to indicate the time of the initial forest loss in that area.

Our study relies on the GFC v1.9 dataset, which covers the period from 2001 to 2021 for analysis. The GFC used different algorithms for detecting forest cover loss in two periods (2001–2010 and 2011–2019). This change in detection methodology, as well as variations in satellite data sources (Landsat 7 and Landsat 8), may result in inconsistencies in the data during the two periods. While previous studies have used sample-based approaches to corroborate findings consistent with GFC mapping (Feng et al., 2022), in this study we calculated three-year moving averages of annual forest loss for time-series analysis, following recommendations from prior research (Tyukavina et al., 2018; Kleinschroth et al., 2019; Weisse and Potapov, 2021).

Mountain extent in the tropics was mapped by a series of mountain polygons developed by the Global Mountain Biodiversity Assessment (GMBA) inventory (version 1.2; Körner et al., 2017). GMBA defines a 2.5′ pixel to be mountainous if the difference between the highest and lowest points of 30″ within the pixel exceeds 200 m. According to this definition, there are 304 mountain regions in the tropics (Supplementary Figure B.1), occupying 8.76 million km^2 (14%) of tropical land surface. The remaining 86% of the tropical land surface was treated as lowland.

We defined the forest loss patch as a contiguous area (eight-neighbour rule) of forest that was cleared within a year. We used annual forest loss maps to determine the area of forest loss each year during 2001–2021 and the size distribution of forest loss patches in that year. Forest loss patches were classified into four categories: small (<1 ha), intermediate (1–10 ha), large (10–100 ha), and very large (>100 ha). We used the Theil-Sen estimator to identify trends in the size of forest loss patches over time. To visualise the spatial distribution of

sizes of forest loss patches, we aggregated the annual data to 5 × 5 km grids over our study area.

Further, we determined the drivers of forest loss using the dataset generated by Curtis et al. (2018). This dataset shows the dominant driver of forest loss at each 10 km grid for 2001–2015. There are five categories of drivers of forest loss: commodity-driven deforestation, shifting agriculture, forestry, wildfire, and urbanization. The data were created using decision-tree models trained by high-resolution Google Earth imagery. We resampled the data from 10 km resolution to 30 m using the nearest-neighbour method to match the scale of the GFC data.

3.3 Results

From 2001 to 2021, there was a reduction in the proportion of tropical mountain forest loss associated with small clearings (<1 ha), from approximately 50% in 2001 to 30% in 2021 (Figure 3.1a). Conversely, over the same period, there were increases in the proportion of tropical mountain forest loss associated with intermediate (1–10 ha) and large clearings (10–100 ha), with intermediate clearings increasing from 40% to 50% and large patches increasing from 10% to >15%. These results suggest that the increase in tropical mountain forest loss during the period was driven by the increases in the area cleared in patches of 1–100 ha (Figure 3.1e).

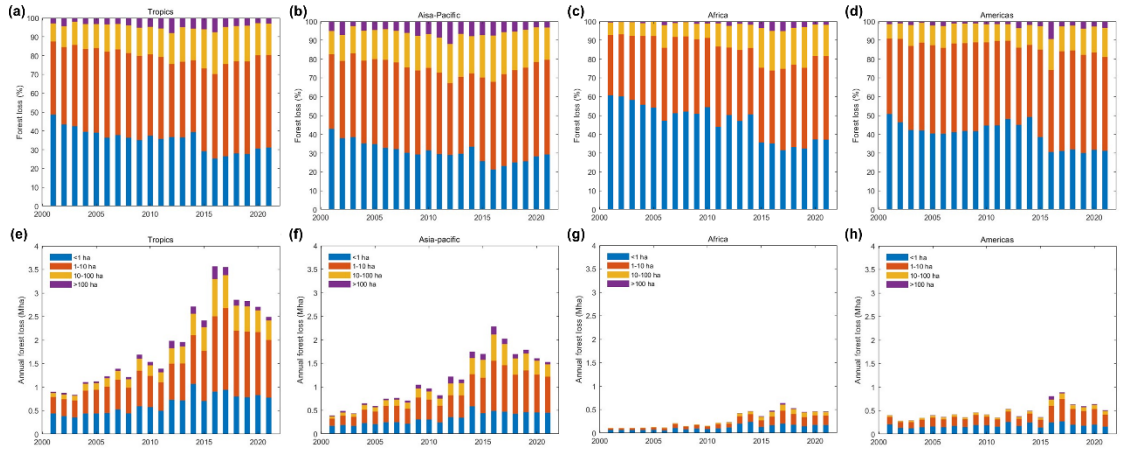

Figure 3.1 *Percentage (a–d) and area (e–h) of forest loss patches of different sizes across tropical mountains from 2001 to 2021 in the tropics (a, e), Asia-Pacific (b, f), Africa (c, g) and Americas (d, h).*

The Asia-Pacific experienced a rapid increase in the rate of mountain forest loss. On average, about 0.44 million hectares of mountain forest were lost annually in the Asia-Pacific region during 2001–2003. This annual loss increased to an average of 1.64 million hectares between 2018 and 2021 (Figure 3.1f). This rapid increase in the rate of forest loss was driven principally by intermediate and large clearings, which comprised 52% of forest loss in 2001 and 67% in 2021. The proportion of very large-scale (>100 ha) forest loss is greater in the Asia-Pacific region than in the other regions. Over the study period, 78% of very large forest loss patches (>100 ha) across all tropical mountains as a whole, occurred in the Asia-Pacific region.

Africa had the highest proportion of small-scale forest loss, reaching 60% at the beginning of the 21st century, but the proportion of small clearings decreased to ~40% in 2021 (Figure 3.1c). Similarly, the Americas witnessed a 20% decline in the proportion of small clearings over the two decades, decreasing from 50% in 2001 to 30% in 2021 (Figure 3.1d). Compared to the Asia-Pacific, stronger increases in the proportion of intermediate and large clearings have been found in Africa (23%) and the Americas (18%).

Over tropical Asian mountains, the increase in forest loss patches was primarily caused by forestry and commodity agriculture, while in Africa and the Americas, shifting agriculture played a key role (Figure 3.2). Notably, while shifting agriculture declined a bit in the area of small (<1 ha) forest loss patches in the Americas, it led to an increase in intermediate and large patch sizes (Figure 3.2c). Meanwhile, in the Americas, fires contributed more to mountain forest loss compared to Asia and Africa.

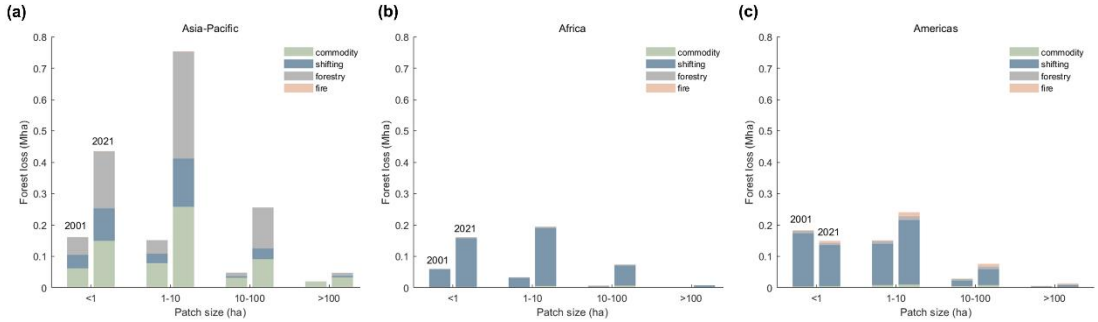

Figure 3.2 *Regional forest loss and its drivers across tropical mountains in 2001 and 2021.*

Between 2001 and 2021, the mean forest loss patch size was 0.64 ha. We showed that a majority (87%) of forest loss patches were below 1 ha, but in area terms, patches below 1 ha only accounted for 33% of total forest loss across our study period. Africa has the highest proportion of small forest loss patches (<1 ha) to the total number in the region, accounting for more than 90%, because small-scale agriculture continues to be the dominant form of forest loss across the continent (Figure 3.2b). In Asia-Pacific and Africa, the area of small forest loss patches showed a gradual increase from 2001 to 2014, followed by a slight decrease thereafter (Supplementary Figure B.2b, c). Conversely, in the Americas, the occurrence of small forest loss events remained relatively stable during the two decades of the 21st century (Supplementary Figure B.2d). There were pronounced increases in intermediate forest loss events (1–10 ha) in 2016 or 2017 across all continents, with a minor decline in subsequent years (Supplementary Figure B.2).

We also found increases in forest loss area of all size categories from the 2000s to the 2010s (Supplementary Figure B. 3). Specially, although larger forest loss patches accounted for a relatively small percentage of the total forest loss area, the number of very large (>100) ha patches increased by more than a factor of 2 between 2001–2010 and 2011–2020. There were also increases in forest loss patches of intermediate and large size (1–10 ha and 10–100 ha) by more than one-fold, while the number of small forest loss patches (<1 ha) increased by ~44% between the two study periods.

Spatially, the mean forest loss patch size on the Malay Peninsula was the greatest; other areas with relatively high value in the mean forest loss patch size included Indonesia, Laos, and Vietnam in Asia-Pacific, Brazil, Bolivia, and Peru in the Americas, as well as Guyana in Africa (Figure 3.3a). Considerable changes were also observed in the geographical pattern of forest loss patch size between 2001 and 2021. The trend in mean forest loss patch size was greatest in mainland Southeast Asia and western Africa (Figure 3.3b). Despite the larger average patch size in marine Southeast Asia, there was a decreasing trend in mean forest loss patch size in the region (Figure 3.3a, b). The distribution of median forest loss patch size was similar to that of mean forest loss patch size, but the maximum forest loss patch size had a different pattern, which showed that Southeast Asian mountains had the greatest absolute maximum forest loss patch size and the highest trend in maximum patch size (Figure 3.3).

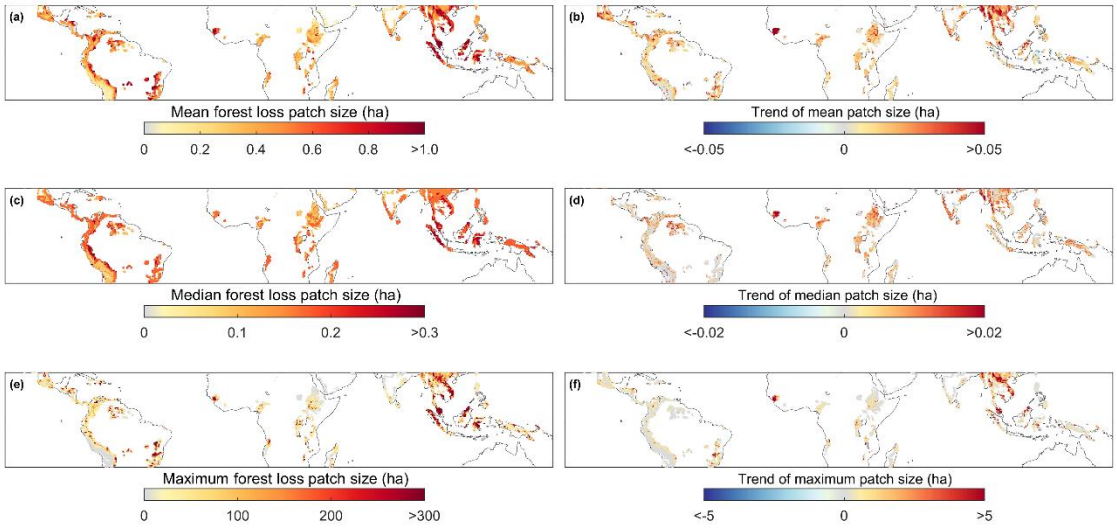

Figure 3.3 *Spatial pattern of forest loss patches across tropical mountains during the period 2001–2021.*

Our analysis also demonstrates distinct patterns between mountainous and lowland regions in the tropics. In lowland areas, the proportion of lowland forest loss with different patch size classes was roughly constant throughout the study period (Figure 3.4). Overall, it looks like the dynamics of forest loss in the mountains are starting to look more like the lowlands – in the mountains, 50% of forest loss was due to patches greater than 1 ha in 2001, increasing to 70% in 2021 and roughly matching the fraction in the lowlands (~70%; Figure 3.4). This suggests higher land-use pressures encroaching into the mountains over the tropics, as reported in some previous studies (Zeng et al., 2018a; Feng et al., 2021; Feng et al., 2022).

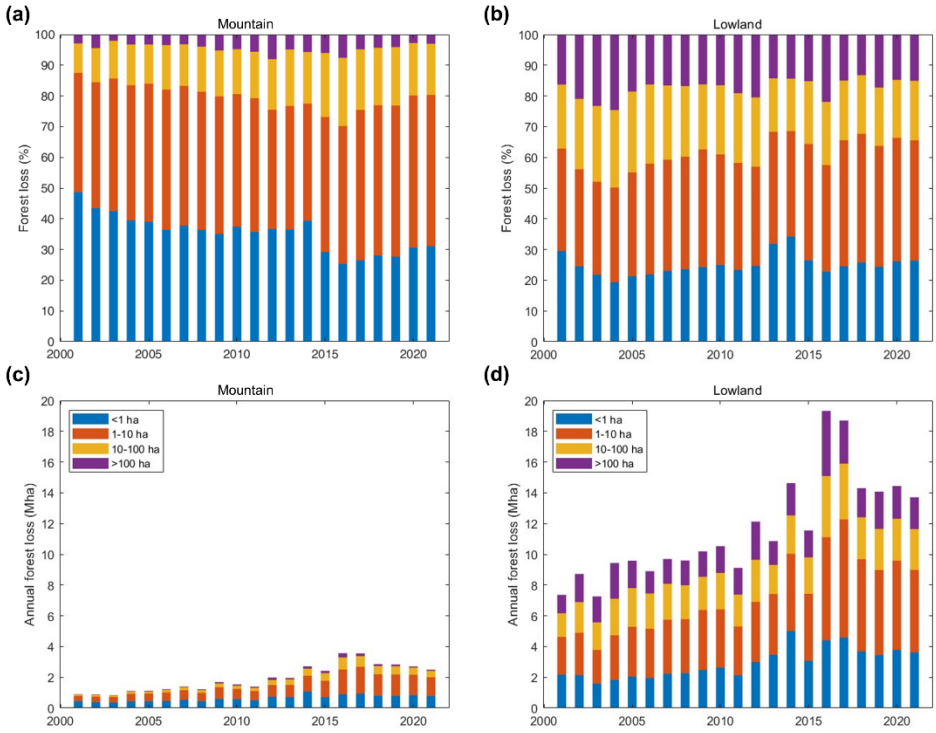

Figure 3.4 *Comparison of forest loss patches of different sizes between mountains (a, c) and lowlands (b, d) over the tropics.*

3.4 Discussion

Artefacts related to enhanced detention capabilities in the GFC data are likely to increase the detection of small clearings. However, we have still observed a decrease in the proportion of small forest loss patches (<1 ha) across all continents. This further confirms the trends of decreasing small-scale deforestation and increasing large-scale clearings over tropical mountain regions, contrasting with previous research that indicated an increase in small-scale deforestation in the lowland Amazon in recent years (Kalamandeen et al., 2018).

In this analysis, we used the eight-neighbour rule to delineate contiguous areas indicating forest loss patches. To investigate the influence of choosing four versus eight adjacent pixels (Supplementary Figure B.4), we randomly sampled sizeable patches (comprising over 100 pixels each) from three continents. This aimed to evaluate the extent to which identified large patches authentically represent substantial blocks of deforestation, or simply several adjacent smaller patches. Our assessment, based on Google Earth images (Supplementary Figure B.5),

demonstrated that the eight-neighbour rule effectively captures the true conditions of forest loss patches in most cases, although in very few isolated cases, the four adjacent pixel method seems to represent separate deforested patches. To ensure the consistency of the study, we retained the eight-pixel method for calculations.

While the widely-reported recent increase in forest loss in Southeast Asian mountains (Zeng et al., 2018b; Feng et al., 2022; He et al., 2023) was clearly observed in our analysis, we also highlight the growth of larger forest loss patches there. These very large (>100 ha) forest loss events were attributed to large-scale commercial agriculture. The expansion of commodity agriculture is generally driven by various factors, including crop productivity, available land, governance structure, land tenure, access to labour, markets, as well as local land-use policies (Deininger and Byerlee, 2012). There are multiple lines of evidence showing that countries with lower to middle income levels are more likely to experience significant increases in large-scale deforestation (Tilman et al., 2011; Deininger and Byerlee, 2012; Laurance et al., 2014; Austin et al., 2017).

The observed growing number of large tropical clearings could amplify local temperature changes related to forest loss (Zeng et al., 2021). In the largest deforested patches of tropical rainforests, maximum temperatures significantly surpass those expected from the random draws, with some areas even exceeding 10°C (Zeppetello et al., 2020). There was also evidence showing that in Maritime Southeast Asia, forest loss over larger areas appears to induce more substantial warming than equivalent fractional forest loss in smaller regions (Crompton et al., 2021). What is more concerning is that this warming could extend beyond the location of forest removal, affecting undisturbed locations up to 6 km away (Crompton et al., 2021). The combined impacts of deforestation and climate change on tropical temperatures will pose a unique challenge to public health and economic security in the long term.

The majority of tropical deforestation occurs in landscapes where agriculture is the dominant driver of tree cover loss (Pendrill et al., 2022). Expansion of medium- to large-scale agriculture at the expense of forest loss into mountains requires extra attention and concern. Previous studies have also emphasised the importance of addressing large-scale agriculture as the primary driver of forest loss (Laurance et al., 2014). Meanwhile, efforts to eliminate deforestation from supply chains are needed (Lambin et al., 2018), especially those impacting forests in Southeast Asia. Moratoriums on sourcing commodities from recently

deforested land (for example, Brazil's Amazon Soy Moratorium) have contributed to reduced rates of deforestation (Heilmayr et al., 2020). Forest protection needs to involve and benefit local communities through a range of approaches including community forest management (Klooster and Masera, 2000; Pagdee et al., 2006; Salam et al., 2006). Protected areas can also help reduce deforestation rates (Spracklen et al., 2015; Wolf et al., 2021), including in tropical mountain regions (He et al., 2023). Increasing the amount of forest owned and managed by Indigenous Peoples, which can be as effective as protected areas at reducing deforestation (Sze et al., 2022), is also crucial.

References

Austin, K.G., González-Roglich, M., Schaffer-Smith, D., Schwantes, A.M. and Swenson, J.J., 2017. Trends in size of tropical deforestation events signal increasing dominance of industrial-scale drivers. Environmental Research Letters, 12, 054009.

Broadbent, E.N., Asner, G.P., Keller, M., Knapp, D.E., Oliveira, P.J. and Silva, J.N., 2008. Forest fragmentation and edge effects from deforestation and selective logging in the Brazilian Amazon. Biological Conservation, 141, 1745–1757.

Bruijnzeel, L.A., Mulligan, M. and Scatena, F.N., 2011. Hydrometeorology of tropical montane cloud forests: emerging patterns. Hydrological Processes, 25, 465–498.

Canale, G.R., Peres, C.A., Guidorizzi, C.E., Gatto, C.A.F. and Kierulff, M.C.M., 2012. Pervasive defaunation of forest remnants in a tropical biodiversity hotspot. Plos One, 7, e41671.

Cayuela, L., Benayas, J.M.R. and Echeverría, C., 2006. Clearance and fragmentation of tropical montane forests in the Highlands of Chiapas, Mexico (1975–2000). Forest Ecology and Management, 226, 208–218.

Chambers, J.Q. and Artaxo, P., 2017. Deforestation size influences rainfall. Nature Climate Change, 7, 175–176.

Chaplin-Kramer, R., Ramler, I., Sharp, R., Haddad, N.M., Gerber, J.S., West, P.C., Mandle, L., Engstrom, P., Baccini, A., Sim, S. and Mueller, C., 2015. Degradation in carbon stocks near tropical forest edges. Nature Communications, 6, 10158.

Crompton, O., Corrêa, D., Duncan, J. and Thompson, S., 2021. Deforestation-induced surface warming is influenced by the fragmentation and spatial extent of forest loss in Maritime Southeast Asia. Environmental Research Letters, 16, 114018.

Curtis, P.G., Slay, C.M., Harris, N.L., Tyukavina, A., and Hansen, M.C., 2018. Classifying drivers of global forest loss. Science, 361, 1108–1111.

Deininger, K. and Byerlee, D., 2012. The rise of large farms in land abundant countries: do they have a future? World Development, 40, 701–714.

Feng, Y., Ziegler, A.D., Elsen, P.R., Liu, Y., He, X., Spracklen, D.V., Holden, J., Jiang, X., Zheng, C. and Zeng, Z., 2021. Upward expansion and acceleration of forest clearance in the mountains of Southeast Asia. Nature Sustainability, 4, 892–899.

Feng, Y., Zeng, Z., Searchinger, T., Ziegler, A.D., Wu, J., Wang, D., He, X., Elsen, P., Ciais, P., Xu, R., Guo, Z., et al., 2022. Doubling of annual forest carbon loss over the tropics during the early 21st century. Nature Sustainability, 5, 444–451.

Godar, J., Gardner, T.A., Tizado, E.J. and Pacheco, P., 2014. Actor-specific contributions to the deforestation slowdown in the Brazilian Amazon. Proceedings of the National Academy of Sciences, 111, 15591–15596.

Hansen, M.C., Potapov, P.V., Moore, R., Hancher, M., Turubanova, S.A., Tyukavina, A., Thau, D., Stehman, S.V., Goetz, S.J., Loveland, T.R., Kommareddy, A. et al., 2013. High-resolution global maps of 21st-century forest cover change. Science, 342, 850–853.

Hansen, M.C., Wang, L., Song, X.P., Tyukavina, A., Turubanova, S., Potapov, P.V. and Stehman, S.V., 2020. The fate of tropical forest fragments. Science Advances, 6, eaax8574.

Heilmayr, R., Rausch, L.L., Munger, J. and Gibbs, H.K., 2020. Brazil's Amazon soy moratorium reduced deforestation. Nature Food, 1, 801–810.

He, X., Ziegler, A.D., Elsen, P.R., Feng, Y., Baker, J.C.A., Liang, S., Holden, J., Spracklen, D.V. and Zeng, Z., 2023. Accelerating global mountain forest loss threatens biodiversity hotspots. One Earth, 6, 303–315.

Lambin, E.F., Gibbs, H.K., Heilmayr, R., Carlson, K.M., Fleck, L.C., Garrett, R.D., le Polain de Waroux, Y., McDermott, C.L., McLaughlin, D., Newton, P., Nolte, C. et al., 2018. The role of supply-chain initiatives in reducing deforestation. Nature Climate Change, 8, 109–116.

Laurance, W.F., Camargo, J.L., Luizão, R.C., Laurance, S.G., Pimm, S.L., Bruna, E.M., Stouffer, P.C., Williamson, G.B., Benítez-Malvido, J., Vasconcelos, H.L., van Houtan, K.S. et al., 2011. The fate of Amazonian forest fragments: a 32-year investigation. Biological Conservation, 144, 56–67.

Laurance, W.F., Sayer, J. and Cassman, K.G., 2014. Agricultural expansion and its impacts on tropical nature. Trends in Ecology & Evolution, 29, 107–116.

Kalamandeen, M., Gloor, E., Mitchard, E.T.A., Quincey, D., Ziv, G., Spracklen, D.V., Spracklen, B., Adami, M., Aragão, L.E. and Galbraith, D., 2018. Pervasive rise of small-scale deforestation in Amazonia. Scientific Reports, 8, 1600.

Khanna, J., Medvigy, D., Fueglistaler, S. and Walko, R., 2017. Regional dry-season climate changes due to three decades of Amazonian deforestation. Nature Climate Change, 7, 200–204.

Kleinschroth, F., Laporte, N., Laurance, W.F., Goetz, S.J. and Ghazoul, J., 2019. Road expansion and persistence in forests of the Congo Basin. Nature Sustainability, 2, 628–634.

Klooster, D. and Masera, O., 2000. Community forest management in Mexico: carbon mitigation and biodiversity conservation through rural development. Global Environmental Change, 10, 259–272.

Körner, C., Jetz, W., Paulsen, J., Payne, D., Rudmann-Maurer, K. and Spehn, E.M., 2017. A global inventory of mountains for bio-geographical applications. Alpine Botany, 127, 1–15.

Malhi, Y., Gardner, T.A., Goldsmith, G.R., Silman, M.R. and Zelazowski, P., 2014. Tropical forests in the Anthropocene. Annual Review of Environment and Resources, 39, 125–159.

Pagdee, A., Kim, Y.S. and Daugherty, P.J., 2006. What makes community forest management successful: a meta-study from community forests throughout the world. Society and Natural resources, 19, 33–52.

Pendrill, F., Gardner, T.A., Meyfroidt, P., Persson, U.M., Adams, J., Azevedo, T., Bastos Lima, M.G., Baumann, M., Curtis, P.G., de Sy, V., Garrett, R. et al., 2022. Disentangling the numbers behind agriculture-driven tropical deforestation. Science, 377, eabm9267.

Rosa, I.M., Souza Jr, C. and Ewers, R.M., 2012. Changes in size of deforested patches in the Brazilian Amazon. Conservation Biology, 26, 932–937.

Smith, C., Baker, J.C.A. and Spracklen, D.V., 2023. Tropical deforestation causes large reductions in observed precipitation. Nature, 615, 270–275.

Salam, M.A., Noguchi, T. and Pothitan, R., 2006. Community forest management in Thailand: current situation and dynamics in the context of sustainable development. New Forests, 31, 273–291.

Spracklen, B.D., Kalamandeen, M., Galbraith, D., Gloor, E. and Spracklen, D.V., 2015. A global analysis of deforestation in moist tropical forest protected areas. Plos One, 10, e0143886.

Spracklen, D.V. and Righelato, R., 2014. Tropical montane forests are a larger than expected global carbon store. Biogeosciences, 11, 2741–2754.

Sze, J.S., Carrasco, L.R., Childs, D. and Edwards, D.P., 2022. Reduced deforestation and degradation in Indigenous Lands pan-tropically. Nature Sustainability, 5, 123–130.

Tilman, D., Balzer, C., Hill, J. and Befort, B.L., 2011. Global food demand and the sustainable intensification of agriculture. Proceedings of the National Academy of Sciences, 108, 20260–20264.

Tyukavina, A., Hansen, M.C., Potapov, P., Parker, D., Okpa, C., Stehman, S.V., Kommareddy, I. and Turubanova, S., 2018. Congo Basin forest loss dominated by increasing smallholder clearing. Science Advances, 4, eaat2993.

Weisse, M. and Potapov, P., 2021. Assessing trends in tree cover loss over 20 years of data. Global Forest Watch. https://www.globalforestwatch.org/blog/data-andresearch/tree-cover-loss-satellite-data-trend-analysis/.

Wolf, C., Levi, T., Ripple, W.J., Zárrate-Charry, D.A. and Betts, M.G., 2021. A forest loss report card for the world's protected areas. Nature Ecology & Evolution, 5, 520–529.

Zeng, Z., Gower, D.B. and Wood, E.F., 2018a. Accelerating forest loss in Southeast Asian Massif in the 21st century: a case study in Nan Province, Thailand. Global Change Biology, 24, 4682–4695.

Zeng, Z., Estes, L., Ziegler, A.D., Chen, A., Searchinger, T., Hua, F., Guan, K., Jintrawet, A. and Wood, E.F., 2018b. Highland cropland expansion and forest loss in Southeast Asia in the twenty-first century. Nature Geoscience, 11, 556–562.

Zeng, Z., Wang, D., Yang, L., Wu, J., Ziegler, A.D., Liu, M., Ciais, P., Searchinger, T.D., Yang, Z.L., Chen, D., Chen, A. et al., 2021. Deforestation-induced warming over tropical mountain regions regulated by elevation. Nature Geosciences, 14, 23–29.

Zeppetello, L.R.V., Parsons, L.A., Spector, J.T., Naylor, R.L., Battisti, D.S., Masuda, Y.J. and Wolff, N.H., 2020. Large scale tropical deforestation drives extreme warming. Environmental Research Letters, 15, 084012.

Chapter 4

Global distribution and climatic controls of natural mountain treelines

Abstract

Mountain treelines are thought to be sensitive to climate change. However, how climate impacts mountain treelines is not yet fully understood as treelines may also be affected by other human activities. Here we focus on “closed-loop” mountain treelines (CLMT) that completely encircle a mountain and are less likely to have been influenced by human land-use change. We detect a total length of ~916,425 km of CLMT across 243 mountain ranges globally and reveal a bimodal latitudinal distribution of treeline elevations with higher treeline elevations occurring at greater distances from the coast. Spatially, we find that temperature is the main climatic driver of treeline elevation in boreal and tropical regions, whereas precipitation drives CLMT position in temperate zones. Temporally, we show that 70% of CLMT have moved upwards, with a mean shift rate of 1.2 m/year over the first decade of the 21st century. CLMT are shifting fastest in the tropics (mean of 3 m/year), but with greater variability. Our work provides a new mountain treeline database that isolates climate impacts from other anthropogenic pressures, and has important implications for biodiversity, natural resources, and ecosystem adaptation in a changing climate.

4.1 Introduction

The mountain treeline is the upper altitudinal limit of tree growth toward the top of mountains, a transitional zone from forests to treeless alpine vegetation (Körner and Paulsen, 2004). Treeline ecotones play important environmental roles, including as habitats for endemic species and by contributing to water supply (Grace, 1989). Mountain treelines are important indicators of the impact of climate change on upland ecosystems (Verrall and Pickering, 2020; Lu et al., 2021) as they are strongly associated with growing season lengths and minimum daily temperatures (Paulsen and Körner, 2014). Consequently, as a response to global warming, mountain treelines are expected to shift upward as high elevations become more favourable for tree establishment under a changing

climate (Holtmeier and Broll, 2005; Du et al., 2018). Furthermore, treeline shifts give rise to novel high-elevation vegetation patterns and could redefine habitable areas for forest-dependent species in a warmer future world (Bolton et al., 2018; Mohapatra et al., 2019). However, the treelines in many mountain regions have been heavily altered by land-use change and land-use management (Gehrig-Fasel et al., 2007; Ameztegui et al., 2016). Such land-use driven treelines are generally lower than the elevation of the local theoretical climatic treelines, making it difficult to isolate potential influences of climate on treeline position and obscuring the impact of climate change on treeline shifts. Therefore, accurate and reproducible detection of natural mountain treelines and their shifts are of great importance to understanding global climate change and the associated response of vegetation dynamics in alpine areas in natural systems.

Previous studies reporting local treeline sites have mainly relied on field investigation (Wardle and Coleman, 1992; Liang et al., 2014; Elliott et al., 2015; Sigdel et al., 2018). While such studies have enhanced our understanding of treeline patterns, a key limitation of field-based studies is sparse geographic coverage. Remote sensing can overcome such a limitation by providing globally consistent coverage, but the determination of treeline positions only through visually interpreting satellite imagery (Paulsen and Körner, 2014; Irl et al., 2016; Karger et al., 2019) is time-consuming and labour-intensive at large spatial scales. Recently, regional attempts to combine remote sensing data with automated image processing techniques have emerged (Wei et al., 2020; Xu et al., 2020; Wang et al., 2022; Birre et al., 2023), but inconsistent analytical approaches and treeline definitions complicate regional comparisons and make it difficult to generalise global patterns. Early assessment at the global scale suggested that low temperatures limited tree growth at treelines (Körner and Paulsen, 2004), but there is also regional evidence that tree growth at the treeline does not increase under global warming due to moisture limitations (Liang et al., 2014; Lyu et al., 2019; Camarero et al., 2021). A generalizable pattern of the climatic limiting factors of global treelines is still lacking.

The aforementioned challenges and limitations associated with delineating treelines and determining climatic influences on treeline positions have hindered our understanding of the global impact of climate on treelines in natural systems. To address this issue, we focused on “closed-loop” mountain treelines (CLMT)—treelines with a continuous band of tree cover around a mountain. Such systems are less likely to have been influenced by land-use change. By focusing on this

subset of treelines, we are better able to exclude treelines that may be impacted by topographic constraints or anthropogenic land use in order to isolate the effects of climate on mountain treelines in natural systems. An advance over previous studies that only provide a handful of data points for each treeline is a complete depiction of the treeline at 30 m resolution. Our approach allows us to calculate the treeline elevation around the entire treeline, providing unprecedented detail on the variability of treeline elevation at the local scale. More importantly, using CLMT as a proxy for natural treelines with little influence from land-use change allows us to make a new and more robust assessment of how natural treelines are responding to changes in climate.

Here, we map closed-loop treelines in mountain regions globally in 2000 based on remote sensing, via integrating a high-resolution tree cover map (Hansen et al., 2013) with a digital elevation model at the same spatial resolution (Tachikawa et al., 2011). For this purpose, we develop a novel automatic detection algorithm that can produce consistent characterisations of CLMT across space. Our detection of mountain treeline is based on tree cover data that consider trees as any vegetation taller than 5 m (Hansen et al., 2013), using a 5% tree cover threshold to delineate forested and non-forested areas. The algorithm starts from the highest elevation point for each mountain range and generates a forest boundary map from which we extract the closed-loop treelines. To further ensure that our CLMT are natural treelines that are not impacted by anthropogenic disturbances, we conduct a manual inspection of high-resolution imagery to remove treelines with any indication of anthropogenic land use and restrict our analysis to regions where the human footprint is low (Mu et al., 2022). To understand which bioclimatic factors control the position of natural mountain treelines from global to local scales, we use the gradient boosting decision trees (GBDT) model (Friedman, 2001) to calculate the feature importance of each temperature or precipitation variable. Further, we map the new natural treeline positions in 2010 using the same algorithm above and the amount of tree cover in 2010 (Hansen et al., 2013) to explore the shifting of mountain treelines in natural systems.

4.2 Methods

4.2.1 Tree canopy cover data

We used a high-resolution remote sensing global map of tree canopy cover for the year 2000 (Hansen et al., 2013) to delineate forested and non-forested areas. The dataset was produced at a 30 m resolution based on multiple types of forest sample data and spectral curves of Landsat time series using a decision tree method (Hansen et al., 2013). To test which tree cover threshold is suitable for treeline mapping, we undertook a sensitivity analysis with different thresholds in mountains, finding there is little difference among different thresholds from 0 to 10% (examples refer to Supplementary Figures C.1–C.3). Thus, we took the mean value of 0 to 10%, namely 5%, as the tree cover threshold, and define the treeline to be the transition zone above which tree cover is ≤5% and below which tree cover is >5%. We then binary-classified the tree canopy cover data using the threshold, assigning a value of 1 for the alpine land zone (the area above the treeline) with tree cover ≤5% (non-forested area), and 0 for pixels with greater than 5% tree cover (forested area).

4.2.2 Topography data

We combined global mountain polygons with a high-resolution digital elevation model to restrict the search area of mountain treelines. Mountain boundaries were collected from the Global Mountain Biodiversity Assessment (GMBA) inventory (version 1.2; Körner et al., 2017). The GMBA inventory delineated global mountains into discrete regions (polygons) based on topographic ruggedness metrics and expert delineation (Körner et al., 2017). The elevation information in mountains was provided by the Advanced Spaceborne Thermal Emission and Reflection Radiometer Global Digital Elevation Model (version 3; Tachikawa et al., 2011) at a spatial resolution of 30 m.

4.2.3 Iterative mountain treeline extraction algorithm

We developed an algorithm to automatically detect CLMT (Supplementary Figure C.4). We first determined the coordinates of the highest peak within each mountain region. The algorithm starts at this peak point if it is within the alpine

area that is non-forested, then expands outward (i.e., downslope), and determines all other pixels of the image that are connected to the point and equivalent (marked as “1”). The eight-neighbourhood region of the pixel $I(x, y)$ is expressed as:

$$R8 = \{(x + i, y + j); i, j \in (-1,1)\} \quad (1)$$

where i, j are integers. In the collection of the eight neighbourhood pixels, if $I(x, y) = I(x + i, y + j)$, there are connected relationships. The connected domain generated by this method is the connected alpine area. Because the algorithm determines the starting search point, we marked only one connected domain (namely the treeline zone) after one iteration.

To accelerate the efficiency of the algorithm, we set search blocks to determine the full altitudinal range of treelines within mountain ranges (Supplementary Figure C.4). Specifically, the first round of the search takes the highest point of the mountain as the centre and the buffer zone with a side length of R as the search area for the treeline. After testing, the square area with 8,000 rows/ranks (side length R about 240 km) covered most alpine areas of mountains. For some of the mountaintops larger than this range, we expanded the side length to ~720 km to ensure that all CLMT of the world’s mountaintops were covered.

There may be multiple treelines within a mountain range because a mountain may have multiple peaks. To account for this, we next searched for the second highest starting point (i.e., the highest point of the unsearched part) and repeated the process until the selected highest point was covered by forests (tree cover >5%).

After each iteration, the loops that were determined to be “open” were removed. Focusing only on closed treeline loops generated from the algorithm, we then visually inspected all loops using Google Earth (with spatial resolution ranging from 15 m to ~15 cm) to further exclude treelines with apparent signs of anthropogenic disturbances, such as roads, buildings, or croplands and removed the part of water bodies (i.e., pixels that were determined to be water). Last, we filled all the holes in the closed-loop polygons using the “imfill” function and extracted the edges of the binary images using the “bwperim” function in Matlab R2019a to obtain the CLMT positions.

To validate the robustness of the elevational distribution of CLMT derived from satellite images, at the pixel level, we used an independent validation dataset by manual interpretation using Google Earth’s high-resolution images. We randomly

produced 100 validation samples at a spatial resolution of 30 m. On a larger scale, we validated our CLMT database by comparison with in situ measures (n = 62; Supplementary Table C.1). For each treeline site, we corresponded it to the closest treeline loop detected in this study and compared its elevation with the range of the corresponding treeline loop.

4.2.4 Climate data

Considering the effect of climatic lag effects on treelines (Harsch et al., 2009), we used the climate data from WorldClim (version 2.1; Fick and Hijmans, 2017), which provided the average for the years 1970–2000 at a resolution of 30 seconds (~1 km^2), to understand which climate variables are important in controlling treeline elevations. We used bioclimatic variables, which were derived from monthly temperature and precipitation. A total of eight temperature variables and eight precipitation variables were included, representing annual trends, seasonality, and extreme or limiting environmental factors. They are annual mean temperature (annual T), temperature seasonality (T seasonality; calculated as the standard deviation of the monthly mean temperatures, then multiply by 100), the maximum temperature of the warmest month (maximum T), the minimum temperature of the coldest month (minimum T), mean temperature of the wettest quarter (wet season T), mean temperature of the driest quarter (dry season T), mean temperature of the warmest quarter (warm season T), mean temperature of the coldest quarter (cold season T), annual precipitation (annual P), precipitation of the wettest month (maximum P), precipitation of the driest month (minimum P), precipitation seasonality (P seasonality; calculated as the coefficient of variation, which is the ratio of the standard deviation to the mean), precipitation of the wettest quarter (wet season P), precipitation of the driest quarter (dry season P), precipitation of the warmest quarter (warm season P), and precipitation of the coldest quarter (cold season P). A ‘quarter’ here refers to any consecutive three months. For example, the coldest quarter consists of the three months that are colder than any other set of three consecutive months. For each pixel determined to be on a CLMT, we extracted the values of all 16 climate variables.

4.2.5 Gradient boosting decision trees (GBDT) model

We applied a GBDT method to model the treeline elevation as a function of climate factors. The GBDT model is a type of tree model with good interpretability for feature values (Friedman, 2001), which assembles and iterates over multiple regression trees, with the values of the negative gradient of the loss function in the model as an approximation of the residuals of the lifting tree algorithm in the regression problem (Ke et al., 2017). It is flexible in handling large amounts of data and often performs well in dealing with complex relationships in data (Ke et al., 2017). The GBDT initialises a weak learner, estimating a constant value of the loss of function minimization, and then creates decision trees according to the datasets and performs iterative training on them. Next, it calculates the negative gradient for loss of function (residuals) corresponding to each tree, fits a regression tree to the residuals to obtain the leaf node region of the m-th tree, and minimises loss of function by estimating the values of all leaf node regions using a linear search. Last, GBDT repeats the above steps until the target evaluation indicator is optimal. Using this model, we calculated the feature importance of each variable and determined the dependent correlations for each factor after the model was built. The GBDT analysis was undertaken in Python 3.7 with the “sklearn.ensemble” module.

We carried out the GBDT analyses at global and local scales, as well as separately for different climatic belts (i.e., boreal, temperate, and tropical regions). At the global and regional scales, we considered each treeline loop as a sample, namely, using the mean of treeline elevation in each loop for the analysis. A total of 1,690 samples (treeline loops) were used for the global model. At the local scale, we regarded one treeline pixel as a sample. Hence, in each treeline loop, the repeated GBDT model represents the local effect of climate factors on treeline positions.

4.2.6 Mountain treeline shift rate

We mapped the new treeline positions in 2010 based on the global 2010 tree cover data (Hansen et al., 2013; Potapov et al., 2015), which is an update of the 2000 tree cover product. Using this dataset, we re-ran the algorithm around treelines to detect the new closed-loop treelines in 2010. Starting from the highest elevation point we detected before, we expanded the rectangular area of the

original treeline around by 10 km as the search area. Then we manually checked the results from the 1,690 treeline loops to (i) exclude treelines without closed loops; (ii) isolate examples of “broken treeline loops” and restrict them to corresponding areas in 2000 and 2010 (Supplementary Figure C.5); and (iii) remove outliers (>95th percentile of both increasing and decreasing rates) to avoid the inclusion of any special cases with extremely steep changes. This filtering resulted in 1,110 treeline loops in 2010 (65.7% of all treelines initially assessed) being available for analysis of the treeline change. The main reason for the reduction in number of treeline loops between 2000 and 2010 is that some of the closed-loop treelines detected in 2000 did not form closed loops in 2010. We then calculated the mean elevation of closed-loop treelines in 2010 and the corresponding treelines in 2000 and used the difference to represent the treeline change over the 10-year period. The treeline shift rate (m/year) at each treeline loop was calculated as follows:

$$shift\ rate = \frac{\text{mean elevation 2010} - \text{mean elevation 2000}}{\text{10 years}} \quad (2)$$

4.3 Results

4.3.1 A map of global closed-loop mountain treelines

We detected 27,468,662 closed-loop mountain treeline positions (pixels at 30 m resolution) across 243 mountain ranges globally. The total length of the closed-loop treelines we detected is ~916,425 km. Those treeline pixels form 1,690 treeline loops covering all continents except Antarctica, ranging from 64°N (Khrebet Polyarnyy, Russia) to 46°S (Princess Mountains, New Zealand), with mean elevations spanning from 489 ±283 m on Khrebet Chayatyn (Russia) to 4,528 ±104 m on Ruwenzori (Uganda, Kenya). The average length of these closed-loop treelines is 542 km, and the average alpine land area above them is 142 km^2. To visualise global patterns of the elevation of CLMT, we calculated the mean elevation for each treeline loop and plotted their locations using the mean latitude and longitude of treeline pixels at 30 m resolution in each loop (Figure 4.1a). The CLMT derived from satellite tree cover data are consistent with fine resolution remote sensing images available on Google Earth (Figure 4.1b–g). At the pixel level, the CLMT showed good agreement with manually interpreted data at 30 m resolution (R^2 = 0.96; Supplementary Figure C.6). On a larger scale, the validity of our CLMT database was further supported by corroboration against in

situ measures from previous studies (n = 62 measurements; Supplementary Table C.1), which fall within the elevation range of CLMT loops (R^2 = 0.98; Supplementary Figure C.7).

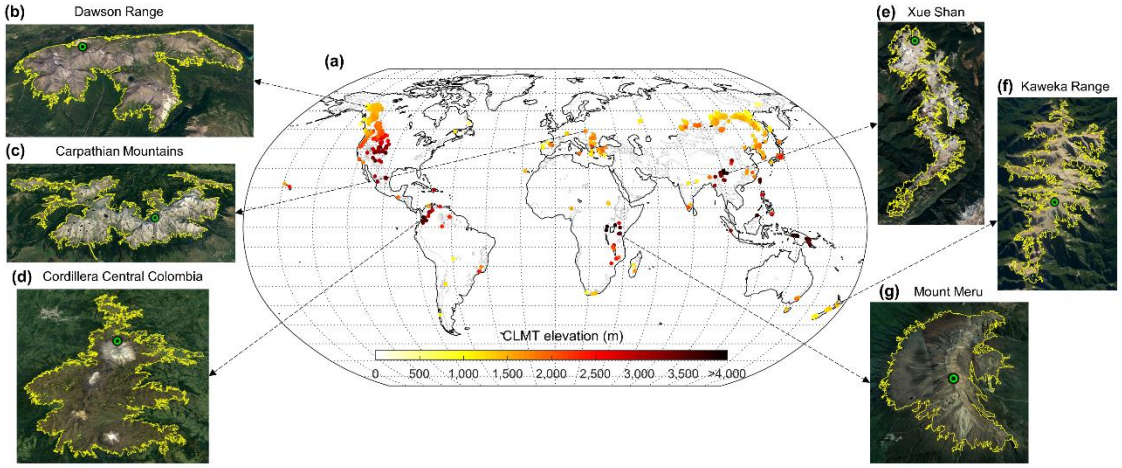

Figure 4.1 *Global distribution of closed-loop mountain treeline (CLMT) elevation. To improve readability, plot (a) is based on the mean value of each closed-loop mountain treeline (at each 30-m pixel). Grey boundaries indicate mountain regions defined by GMBA inventory data. (b)–(g) show examples of CLMT extraction results superimposed with Google Earth images. The yellow line represents the position of the treeline, and the green circle shows the highest elevation point that formed the starting point of each search by the treeline algorithm.*

We found a bimodal pattern for the closed-loop mountain treeline elevation along latitude, with peaks at the equator and ~25°N (Figure 4.2a). Between 0° and 10°, the elevation of CLMT is symmetrical in the northern and southern hemispheres, but beyond this range, treeline elevations in the northern hemisphere are higher than those in the southern hemisphere at equivalent latitudes (Figure 4.2a), which is attributed to the oceanic influence on a smaller southern landmass (Cieraad et al., 2014). Our global CLMT distribution is consistent with previous global assessments, though there are some differences. In the tropics, the elevation of CLMT reaches up to 3,500 m (Figure 4.2), a lower elevation than in a recent global assessment by Testolin et al. (2020) that reported tropical treelines higher than 4,000 m. This discrepancy may be due to our strict definition of trees, >5 m in height, as well as the exclusion of some unilateral and non-closed treelines in high mountains. At low latitudes (especially at 0–20°N), there is a large variation in the range of CLMT elevation (Figure 4.2a). Among different continents, South

America has a large CLMT elevation range variation. At 50°N–60°N and 20°N–30°N, many mountains in Asia and North America have similar treeline elevations, whereas there is a rather different behaviour at 30°N–50°N where treelines in North America are higher than those in Europe and Asia (Figure 4.2a). To help understand what causes this behaviour, we calculated the distance to the coast for each treeline. We found lower treelines in coastal mountains at the same latitude (Figure 4.2a) as has been suggested in the literature (Irl et al., 2016), which can be largely attributed to the thermo-dynamic effect of large high-elevation landmasses (Karger et al., 2019). At 40°N–60°N, mountains close to the coast have lower treelines than their latitude might suggest (i.e., fall below the fitted curve; Figure 4.2a). Similarly, along with longitude decreasing from 150°W to 100°W, treeline elevations in North America increase due to an increase in the distance to the coast (Figure 4.2b).

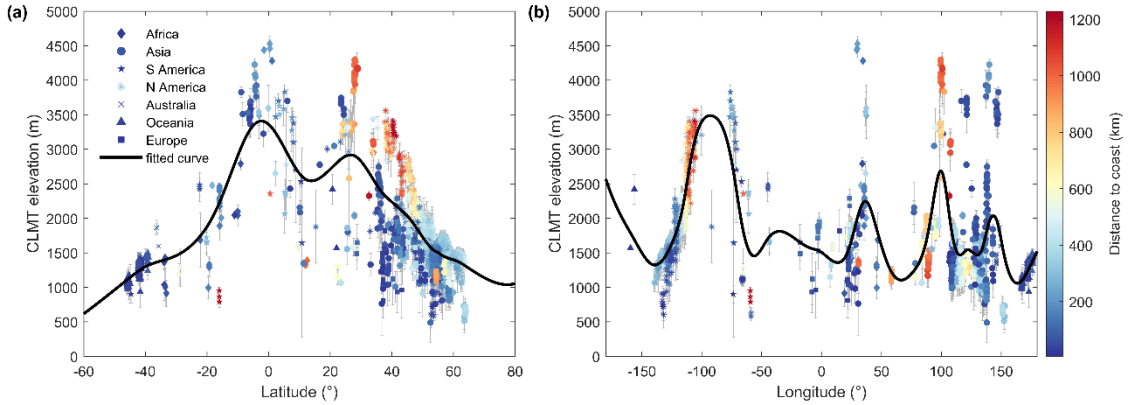

Figure 4.2 *Global latitudinal (a) and longitudinal (b) variation of closed-loop mountain treeline (CLMT) elevation.* Different symbols represent different regions and colours represent the distance to the coast. The data points show the mean elevation of all of the pixels in the CLMT. The error bar is the elevation range of the corresponding treeline loop.

4.3.2 Climatic determinants of closed-loop mountain treelines

We found that T seasonality, cold season P, and warm season T predict nearly 60% of the spatial distribution of CLMT globally (Figure 4.3a). We then assessed how the three leading factors modulated the elevation of CLMT spatially. The results showed the abrupt transition of CLMT elevation occurring at the T seasonality threshold of ~9°C, but attenuated transitions in areas where T seasonality exceeded 10°C (Supplementary Figure C.8a). Similarly, there is a CLMT elevation gradient that is spatially driven by cold season P, with abrupt

transitions occurring at the thresholds of 320 mm and 450 mm along the gradient of cold season P (Supplementary Figure C.8b). By contrast, we did not find such a dramatic transition of CLMT elevation along the warm season T gradient (Supplementary Figure C.8c).

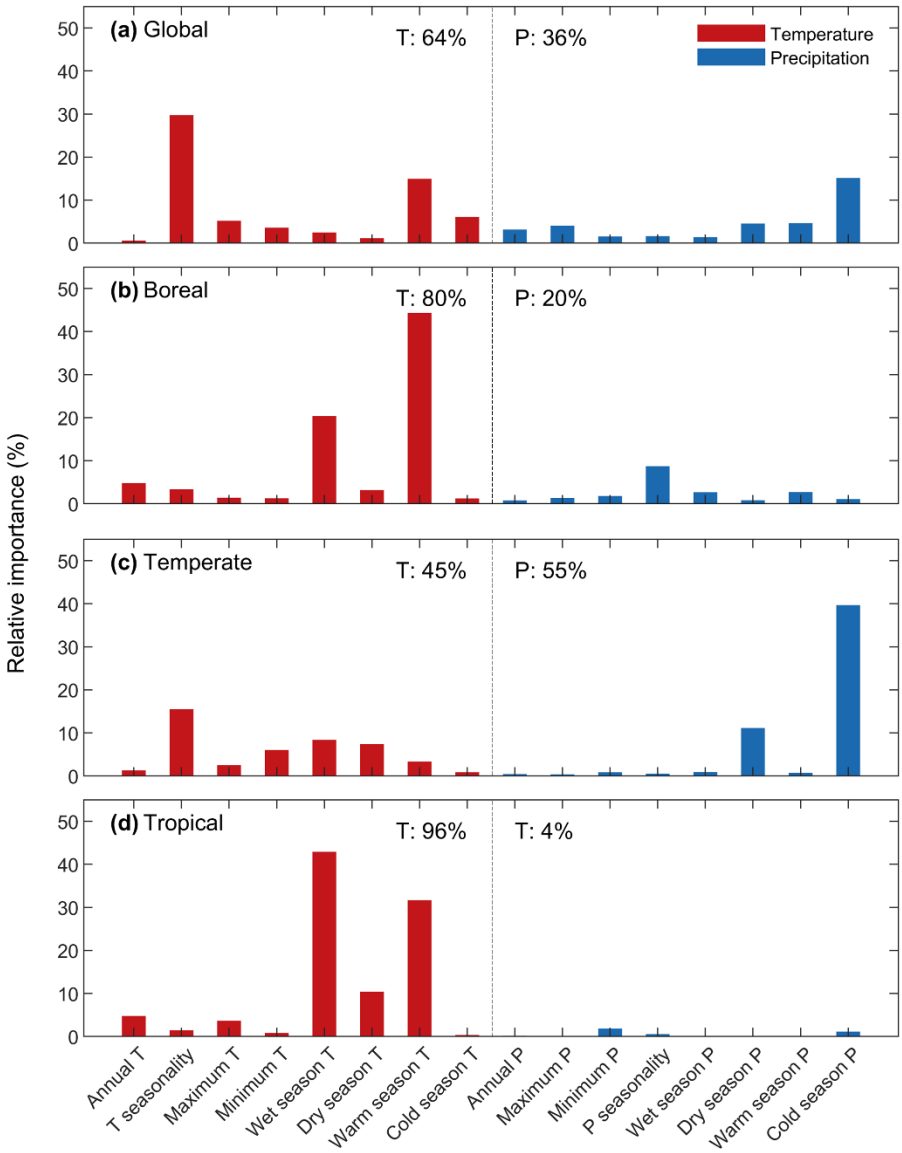

Figure 4.3 *Climate drivers controlling the variability in treeline elevation for the globe (a), boreal (≥50°N, b), temperate (23.5° – 50°N/S, c) and tropical (23.5°N – 23.5°S, d) regions.*

Collectively, temperature-related factors (64%) are more important than precipitation-related factors for limiting CLMT elevations on a global scale (Figure 4.3a). In different latitudinal belts, temperature-related factors are most important

in boreal and tropical regions, especially the temperature of the warmest and the wettest quarters, respectively, while precipitation dominates the CLMT elevation in temperate regions (Figure 4.3b–d). We found that T seasonality is the most important individual factor (30%) at the global scale, whereas its importance is lower than 10% for boreal and tropical regions (Figure 4.3). These patterns may be because thermal limitation to growth at treelines during the summer is most critical in the cold boreal regions, while in the tropics where the temperature is high throughout the year, the temperature of the wettest season plays a key role in limiting tree growth at treelines. Our results confirm the importance of temperature during the warm part of the year in the boreal zone (Jobbágy and Jackson, 2000), but suggest that precipitation is more important than temperature in temperate regions. It agrees with the climatic sensitivity of tree growth in the Norther Hemisphere (Gao et al., 2022). Especially under dry environmental conditions, moisture availability is crucial to limiting tree growth in the treeline ecotone (Liang et al., 2014; Ren et al., 2018).

Our study provides vastly more data points for each treeline compared to previous global assessments (Jobbágy and Jackson, 2000; Körner and Paulsen, 2004), allowing us to explore for the first time what controls treeline position at a local scale. We found that temperature remains the dominant explanation for the altitudinal variation of 76% of the treeline within a single treeline loop with similar climatic conditions (Supplementary Figure C.9).

4.3.3 Shifts in closed-loop mountain treelines

Between 2000 and 2010, mountain treelines have shifted upwards at 777 out of the 1,110 treeline loops (70%) and downward at 333 treeline loops (Figure 4.4a). The mean global treeline shift rate was an upward shift of 1.2 m/year, which is consistent with case studies of treeline change, with rates >1 m/year reported in the literature (Supplementary Table C.2). A synthesis of treeline shift rates reported in the literature suggests the rate was 0.67 m/year before 1970 compared to 4.36 m/year after 1970 and 6.16 m/year after 2000 (Supplementary Figure C.10; Supplementary Table C.2). This provides evidence that the rate of change in treeline elevation is accelerating, possibly due to recent rapid climate change (Bolton et al., 2018). Treeline shift rates in the tropics (mean of 3.1 m/year) were higher than those in boreal and temperate regions (Figure 4.4b). The faster changes in the topics could be related to hydrothermal conditions: in

the tropics, higher temperatures and more abundant precipitation bring a longer growing season, which naturally favours the growth of seedlings and young trees. By contrast, there is a slight downward shift in temperate regions (an average of -0.5 m/year), where the position of the treeline is dominated by precipitation (Figure 4.3c). This could be due to decreasing precipitation in some mountain areas of the temperate zone, for example in northern China (Piao et al., 2010).

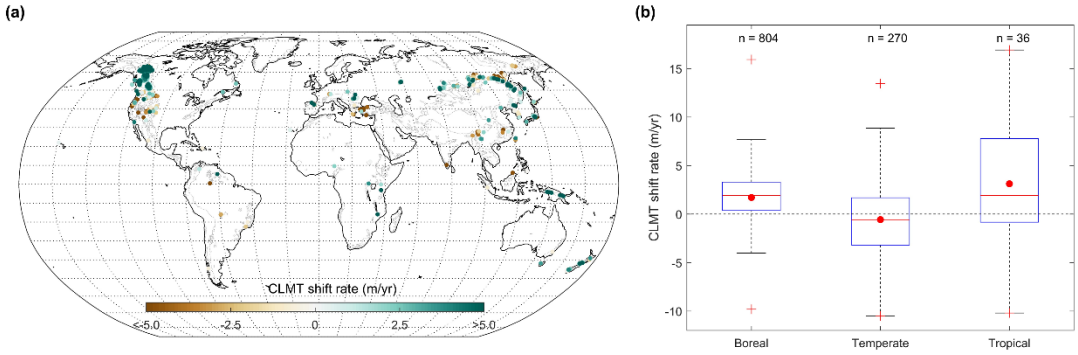

Figure 4.4 *Closed-loop mountain treeline (CLMT) shift rate during 2000–2010. (a) Spatial pattern of CLMT shift rate. (b) Box-plot showing CLMT shift rate in boreal (≥50°N), temperate (23.5°–50°N/S) and tropical (23.5°N–23.5°S) regions (central line: median; red dot: mean; box: 25th and 75th percentiles, respectively; error bar: maximum and minimum whisker values; +: maximum and minimum values). The black dashed line is the zero line. Numbers of the studied CLMT are shown above the boxes.*

Although the tropical CLMT have the fastest shift rates, their variability is the largest, ranging from -10.2 to 16.9 m/year (Figure 4.4b). In the tropics, treeline shift rates greater than 10 m/year in the mountains of Malawi, Papua New Guinea, and Indonesia may reflect a more extreme trend in these tropical systems. In other regions, there are also some treelines that have shifted much more than expected (>10 m/year; Figure 4.4b): in boreal regions, these expectations are mainly in Russia and Canada; in temperate regions, they are geographically concentrated in East Asia (North Korea, Japan, and China). On the contrary, there are also cases of treelines receding at a high rate, possibly driven by fire in some areas, either through the physical destruction of trees that acts to lower the existing treelines, or through the destruction of seedlings established upslope that acts to prevent treeline advances (Kim and Lee, 2015).

For example, treelines have significantly receded in the western USA where climate and vegetation are favourable for fire (Seven Devils Mountains, Swan Range, etc.; Figure 4.4a).

In addition, independent analysis for the changes in annual maximum Normalized Difference Vegetation Index (NDVI) at CLMT that we identified for the year 2000 shows the NDVI has significantly increased by 3.3% by 2020, at a rate of 0.0012 per year ($P < 0.01$; Supplementary Figure C.11a). There are significant positive trends in NDVI at treeline zones in boreal, temperate, and tropical regions during 2000–2020 ($P < 0.01$), and tropical areas have the highest rate, approaching 0.0016 per year (Supplementary Figure C.11b). The increase in NDVI occurred at most treeline zones (~90%; Supplementary Figure C.11c). This greening at the treeline may also be conducive to upward movement of the treeline in the future.

4.4 Discussion

4.4.1 Comparison of treeline datasets before and after considering human footprint

Although we have examined CLMT by manual interpretation to remove anthropogenic treelines, we further conduct a stricter assessment of human pressures to check whether our results would still be impacted by human activity. We used a global Human Footprint dataset (Mu et al., 2022) and found 83% of our CLMT in the wilderness (Human Footprint < 1) or in highly intact areas (Human Footprint < 4). We then removed those treelines with human footprint values ≥ 4, re-ran the analysis with the higher human footprint values excluded, and updated all the results above (Supplementary Figures C.12–C.14). By comparing these new results with those using the whole dataset, we found a similar pattern along latitude and longitude gradients (Figure 4.2 and Supplementary Figure C.12). The results regarding climate dominants (Figure 4.3 and Supplementary Figure C.13) and treeline shift rates (Figure 4.4 and Supplementary Figure C.14) were also consistent using either approach. Thus, the additional criterion to further focus our analysis on treelines with no human disturbance does not alter our overall results or conclusions, and further confirms that our CLMT product can well represent the change and pattern of climatic treelines.

4.4.2 Implications of treeline shifts for carbon, biodiversity, and hydrology

Changing treeline position can affect the carbon cycle, biodiversity, and hydrological processes in mountain environments. Mountain treelines moving upward to higher elevations increase woody biomass at and above the treeline, accumulating carbon and increasing their ability to act as carbon sinks (Lopatin et al., 2006; Tarnocai et al., 2009). However, such increases may be offset by increases in soil respiration, leading to a net loss of ecosystem carbon (Wilmking et al., 2006; Hartley et al., 2012). The ascent of mountain treelines also substantially influences biodiversity patterns at high elevations, with enhanced habitat loss of endemic alpine species within a narrow range of mountains (Wang et al., 2022) and potential expansion of habitat for forest-dependent species whose upper range limits coincide with the treeline ecotones (Elsen et al., 2017). For alpine species isolated at the top of mountains, upward treeline shifts could increase the risk of extinction, where there is not enough room for the alpine zone to move upward under future climate change (Dirnböck et al., 2011). In Siberia, for example, we show many treelines have shifted upwards (Figure 4.4b), inevitably reducing the area of the tundra, which is rich in floristic and species diversity and supports indigenous land use types. The expansion of Siberian forests has been predicted to continue, thus causing huge losses of tundra in the future (Kruse and Herzschuh, 2022). While we focused here on treeline shifts in areas with minimal human impacts, treeline ascent in areas with pronounced human disturbance will further hinder species' ability to track vegetation changes and likely lead to more pronounced population declines (Feeley and Silman, 2010; Elsen et al., 2020). There are many instances with high high-elevation pressure especially from burning, grazing, and wood harvesting (Bader et al., 2008; Jiménez-García et al., 2021). The combined impact of shifting treelines and human disturbances may also affect local livelihoods and act as a double-blow for sensitive alpine species. In addition, tree expansions into the formerly treeless area may alter the downstream water supply. Recent advances of the treeline have decreased the area of alpine tundra, thereby affecting its critical role as a reservoir of freshwater resources and in water release (Barredo et al., 2020).

4.4.3 Uncertainties and caveats

To isolate the impacts of climate on treelines, our analysis identifies CLMT that completely encircle a mountain. However, focusing on this kind of treeline could omit some climate-related treelines as climatic treelines may not be in a closed loop shape in some cases. We acknowledge that our CLMT database does not include all climatic treelines, but is a subset of climatic treelines that specifically form a closed loop, because these enable us to analyse climatic determinants with greater confidence. We also note that tree cover can increase in various ways, either through new or existing trees growing above the 5 m height threshold, or existing trees having increased canopy cover. However, our analysis is based on the definition of treeline according to remotely sensed tree cover, and we used this definition to assess treeline position at two time periods and assess change. While our analysis period is short and errors will exist at a pixel scale, our global detection of a shifting treeline provides an early indication of climate-induced changes that need to be carefully monitored in the future. To reduce uncertainties and further advance our understanding of treeline dynamics, future studies require more high-resolution remote sensing products for a longer period and more field data in alpine treeline zones for cross-validation.

4.5 Conclusion

Our study develops a novel remote sensing-based algorithm to map closed-loop treelines across global mountain regions, isolating the effects of climate on treeline position. Our approach provides a globally consistent way of detecting and monitoring closed-loop treelines around mountains, which are more likely to reflect natural systems with minimal impact of land-use change. Focusing on these closed-loop treelines as a proxy for natural treelines allows us to isolate the impacts of climate and climate change on the elevation distribution and change of treelines. We found the temperature was the dominant control on natural treelines both at a global and local scale. Our results indicated an upward migration of treelines over the period 2000 to 2010 in boreal and tropical regions but a slight downward shift in temperate zones. Our new findings and the global closed-loop mountain treeline database produced in this study also provide a useful tool for biodiversity and carbon assessments, ecological modelling, and analyses of the adaptation of species to future climate change.

References

Ameztegui, A., Coll, L., Brotons, L. and Ninot, J.M., 2016. Land-use legacies rather than climate change are driving the recent upward shift of the mountain tree line in the Pyrenees. Global Ecology and Biogeography, 25, 263–273.

Bader, M.Y., Rietkerk, M. and Bregt, A.K., 2008. A simple spatial model exploring positive feedbacks at tropical alpine treelines. Arctic, Antarctic, and Alpine Research, 40, 269–278.

Barredo, J. I., Mauri, A. and Caudullo, G., 2020. Alpine tundra contraction under future warming scenarios in Europe. Atmosphere, 11, 698.

Birre, D., Feuillet, T., Lagalis, R., Milian, J., Alexandre, F., Sheeren, D., Serrano-Notivoli, R., Vignal, M. and Bader, M.Y., 2023. A new method for quantifying treeline-ecotone change based on multiple spatial pattern dimensions. Landscape Ecology, 38, 779–796.

Bolton, D.K., Coops, N.C., Hermosilla, T., Wulder, M.A. and White, J.C., 2018. Evidence of vegetation greening at alpine treeline ecotones: three decades of Landsat spectral trends informed by lidar-derived vertical structure. Environmental Research Letters, 13, 084022.

Camarero, J.J., Gazol, A., Sánchez-Salguero, R., Fajardo, A., McIntire, E.J.B., Gutiérrez, E., Batllori E., Boudreau, S., Carrer, M., Diez, J., Dufour-Tremblay, G. et al., 2021. Global fading of the temperature-growth coupling at alpine and polar treelines. Global Change Biology, 27, 1879–1889.

Cieraad, E., McGlone, M. S. and Huntley, B., 2014. Southern Hemisphere temperate tree lines are not climatically depressed. Journal of Biogeography, 41, 1456–1466.

Dirnböck, T., Essl, F. and Rabitsch, W., 2011. Disproportional risk for habitat loss of high-altitude endemic species under climate change. Global Change Biology, 17, 990–996.

Du, H., Liu, J., Li, M.-H., Büntgen, U., Yang, Y., Wang, L., Wu, Z. and He, H.S., 2018. Warming-induced upward migration of the alpine treeline in the Changbai Mountains, northeast China. Global Change Biology, 24, 1256–1266.

Elliott, G.P. and Cowell, C.M., 2015. Slope aspect mediates fine-scale tree establishment patterns at upper treeline during wet and dry periods of the 20th century. Arctic, Antarctic, and Alpine Research, 47, 681–692.

Elsen, P.R., Tingley, M.W., Kalyanaraman, R., Ramesh, K. and Wilcove, D.S., 2017. The role of competition, ecotones, and temperature in the elevational distribution of Himalayan birds. Ecology, 98, 337–348.

Elsen, P.R., Monahan, W.B. and Merenlender, A.M., 2020. Topography and human pressure in mountain ranges alter expected species responses to climate change. Nature Communications, 11, 1–10.

Feeley, K.J. and Silman, M.R., 2010. Land-use and climate change effects on population size and extinction risk of Andean plants. Global Change Biology, 16, 3215–3222.

Fick, S.E. and Hijmans, R.J., 2017. WorldClim 2: new 1-km spatial resolution climate surfaces for global land areas. International Journal of Climatology, 37, 4302–4315.

Friedman, J.H., 2001. Greedy function approximation: a gradient boosting machine. Annals of Statistics, 29, 1189–1232.

Gao, S., Liang, E., Liu, R., Babst, F., Camarero, J.J., Fu, Y.H., Piao, S., Rossi, S., Shen, M., Wang, T. and Peñuelas, J., 2022. An earlier start of the thermal growing season enhances tree growth in cold humid areas but not in dry areas. Nature Ecology & Evolution, 6, 397–404.

Gehrig-Fasel, J., Guisan, A. and Zimmermann, N.E., 2007. Tree line shifts in the Swiss Alps: climate change or land abandonment? Journal of Vegetation Science, 18, 571–582.

Grace, J., 1989. Tree lines. Philosophical Transactions of the Royal Society of London, 324, 233–245.

Hansen, M.C., Potapov, P.V., Moore, R., Hancher, M., Turubanova, S.A., Tyukavina, A., Thau, D., Stehman, S.V., Goetz, S.J., Loveland, T.R., Kommareddy, A., et al., 2013. High-resolution global maps of 21st-century forest cover change. Science, 342, 850–853.

Harsch, M.A., Hulme, P.E., McGlone, M.S. and Duncan, R.P., 2009. Are treelines advancing? A global meta-analysis of treeline response to climate warming. Ecology Letters, 12, 1040–1049.

Hartley, I.P., Garnett, M.H., Sommerkorn, M., Hopkins, D.W., Fletcher, B.J., Sloan, V. L., Phoenix, G.K. and Wookey, P.A., 2012. A potential loss of carbon associated with greater plant growth in the European Arctic. Nature Climate Change, 2, 875–879.

Holtmeier, F. and Broll, G., 2005. Sensitivity and response of northern hemisphere altitudinal and polar treelines to environmental change at landscape and local scales. Global Ecology Biogeography, 14, 395–410.

Hope, G., 2009. Environmental change and fire in the Owen Stanley Ranges, Papua New Guinea. Quaternary Science Reviews, 28, 2261–2276.

Irl, S.D., Anthelme, F., Harter, D.E., Jentsch, A., Lotter, E., Steinbauer, M.J. and Beierkuhnlein, C., 2016. Patterns of island treeline elevation—a global perspective. Ecography, 39, 427–436.

Jiménez-García, D., Li, X., Lira-Noriega, A. and Peterson, A.T., 2021. Upward shifts in elevational limits of forest and grassland for Mexican volcanoes over three decades. Biotropica, 53, 798–807.

Jobbágy, E.G. and Jackson, R.B., 2000. Global controls of forest line elevation in the northern and southern hemispheres. Global Ecology Biogeography, 9, 253–268.

Karger, D.N., Kessler, M., Conrad, O., Weigelt, P., Kreft, H., König, C. and Zimmermann, N.E., 2019. Why tree lines are lower on islands—Climatic and biogeographic effects hold the answer. Global Ecology Biogeography, 28, 839–850.

Ke, G., Meng, Q., Finley, T., Wang, T., Chen, W., Ma, W., Ye, Q. and Liu, T.-Y., 2017. Lightgbm: a highly efficient gradient boosting decision tree. Advances in Neural Information Processing Systems, 30, 3146–3154.

Kim, J.W. and Lee, J.S., 2015. Dynamics of alpine treelines: positive feedbacks and global, regional and local controls. Journal of Ecology and Environment, 38, 1–14.

Körner, C. and Paulsen, J., 2004. A world-wide study of high altitude treeline temperatures. Journal of Biogeography, 31, 713–732.

Körner, C., Jetz, W., Paulsen, J., Payne, D., Rudmann-Maurer, K. and Spehn, E.M., 2017. A global inventory of mountains for bio-geographical applications. Alpine Botany, 127, 1–15.

Kruse, S. and Herzschuh, U., 2022. Regional opportunities for tundra conservation in the next 1000 years. eLife, 11, e75163.

Liang, E., Dawadi, B., Pederson, N. and Eckstein, D., 2014. Is the growth of birch at the upper timberline in the Himalayas limited by moisture or by temperature? Ecology, 95, 2453–2465.

Lyu, L., Zhang, Q.B., Pellatt, M.G., Büntgen, U., Li, M.H. and Cherubini, P., 2019. Drought limitation on tree growth at the Northern Hemisphere's highest tree line. Dendrochronologia, 53, 40–47.

Lopatin, E., Kolström, T. and Spiecker, H., 2006. Determination of forest growth trends in Komi Republic (northwestern Russia): combination of tree-ring analysis and remote sensing data. Boreal Environment Research, 11, 341–353.

Lu, X., Liang, E., Wang, Y., Babst, F. and Camarero, J.J., 2021. Mountain treelines climb slowly despite rapid climate warming. Global Ecology and Biogeography, 30, 305–315.

Mohapatra, J., Singh, C.P., Tripathi, O.P. and Pandya, H.A., 2019. Remote sensing of alpine treeline ecotone dynamics and phenology in Arunachal Pradesh Himalaya. International Journal of Remote Sensing, 40, 7986–8009.

Mu, H., Li, X., Wen, Y., Huang, J., Du, P., Su, W., Miao, S. and Geng, M., 2022. A global record of annual terrestrial Human Footprint dataset from 2000 to 2018. Scientific Data, 9, 176.

Paulsen, J. and Körner, C., 2014. A climate-based model to predict potential treeline position around the globe. Alpine Botany, 124, 1–12.

Potapov, P., Turubanova, S., Tyukavina, A., Krylov, A., McCarty, J., Radeloff, V. and Hansen, M., 2015. Eastern Europe's forest cover dynamics from 1985 to 2012 quantified from the full Landsat archive. Remote Sensing of Environment, 159, 28–43.

Piao, S., Ciais, P., Huang, Y., Shen, Z., Peng, S., Li, J., Zhou, L., Liu, H., Ma, Y., Ding, Y., Friedlingstein, P. et al., 2010. The impacts of climate change on water resources and agriculture in China. Nature, 467, 43–51.

Ren, P., Rossi, S., Camarero, J.J., Ellison, A.M., Liang, E. and Peñuelas, J., 2018. Critical temperature and precipitation thresholds for the onset of

xylogenesis of Juniperus przewalskii in a semi-arid area of the north-eastern Tibetan Plateau. Annals of Botany, 121, 617–624.

Sigdel, S.R., Wang, Y., Camarero, J.J., Zhu, H., Liang, E. and Peñuelas, J., 2018. Moisture-mediated responsiveness of treeline shifts to global warming in the Himalayas. Global Change Biology, 24, 5549–5559.

Tachikawa, T., Hato, M., Kaku, M. and Iwasaki, A., 2011. Characteristics of ASTER GDEM version 2. In *2011 IEEE international geoscience and remote sensing symposium*, 3657–3660. IEEE.

Tarnocai, C., Canadell, J.G., Schuur, E.A.G., Kuhry, P., Mazhitova, G. and Zimov, S., 2009. Soil organic carbon pools in the northern circumpolar permafrost region. Global Biogeochemical Cycles, 23, GB2023.

Testolin, R., Attorre, F. and Jiménez-Alfaro, B., 2020. Global distribution and bioclimatic characterization of alpine biomes. Ecography, 43, 779–788.

Verrall, B. and Pickering, C.M., 2020. Alpine vegetation in the context of climate change: a global review of past research and future directions. Science of the Total Environment, 748, 141344.

Wang, X., Wang, T., Xu, J., Shen, Z., Yang, Y., Chen, A., Wang, S., Liang, E. and Piao, S., 2022. Enhanced habitat loss of the Himalayan endemic flora driven by warming-forced upslope tree expansion. Nature Ecology & Evolution, 6, 890–899.

Wardle, P. and Coleman, M., 1992. Evidence for rising upper limits of four native New Zealand forest trees. New Zealand Journal of Botany, 30, 303–314.

Wei, C., Karger, D.N. and Wilson, A.M., 2020. Spatial detection of alpine treeline ecotones in the Western United States. Remote Sensing of Environment, 240, 111672.

Wilmking, M., Harden, J. and Tape, K., 2006. Effect of tree line advance on carbon storage in NW Alaska. Journal of Geophysical Research, 111, 1–10.

Xu, D., Geng, Q., Jin, C., Xu, Z. and Xu, X., 2020. Tree line identification and dynamics under climate change in Wuyishan National Park based on Landsat images. Remote Sensing, 12, 2890.

Chapter 5

Conclusion

5.1 Summary of results

The overall aim of this thesis was to understand how montane forests have changed in the 21st century. The paper presented in Chapter 2 was, at the time of publication, the first study to investigate the patterns and drivers of forest loss across global mountain regions using multiple global datasets. This work showed that more than 7% of mountain forests worldwide were lost between 2001 and 2018, with rates of loss almost doubling after 2010. The acceleration of mountain forest loss was largely driven by various forms of agriculture in the tropics (Figure 5.1). This informed the research direction of Chapter 3, which analysed the dynamics of forest loss in tropical mountains. I showed that the proportion of tropical mountain forest loss associated with larger clearings has significantly increased (Figure 5.1). This trend further underscores that the expansion of medium- to large-scale agriculture at the expense of tropical mountain forests requires attention and concern. Chapter 4 presents published research which provides a global picture of upward shifting treelines in response to rising global temperatures (Figure 5.1). This research developed a new mountain treeline database across global mountain regions to demonstrate how climate and climate change impact treelines. From this, I found that treelines are moving upwards fastest in regions where temperature is the dominant control of treeline position, while in temperate regions where rainfall is more important, treelines are not changing so fast.

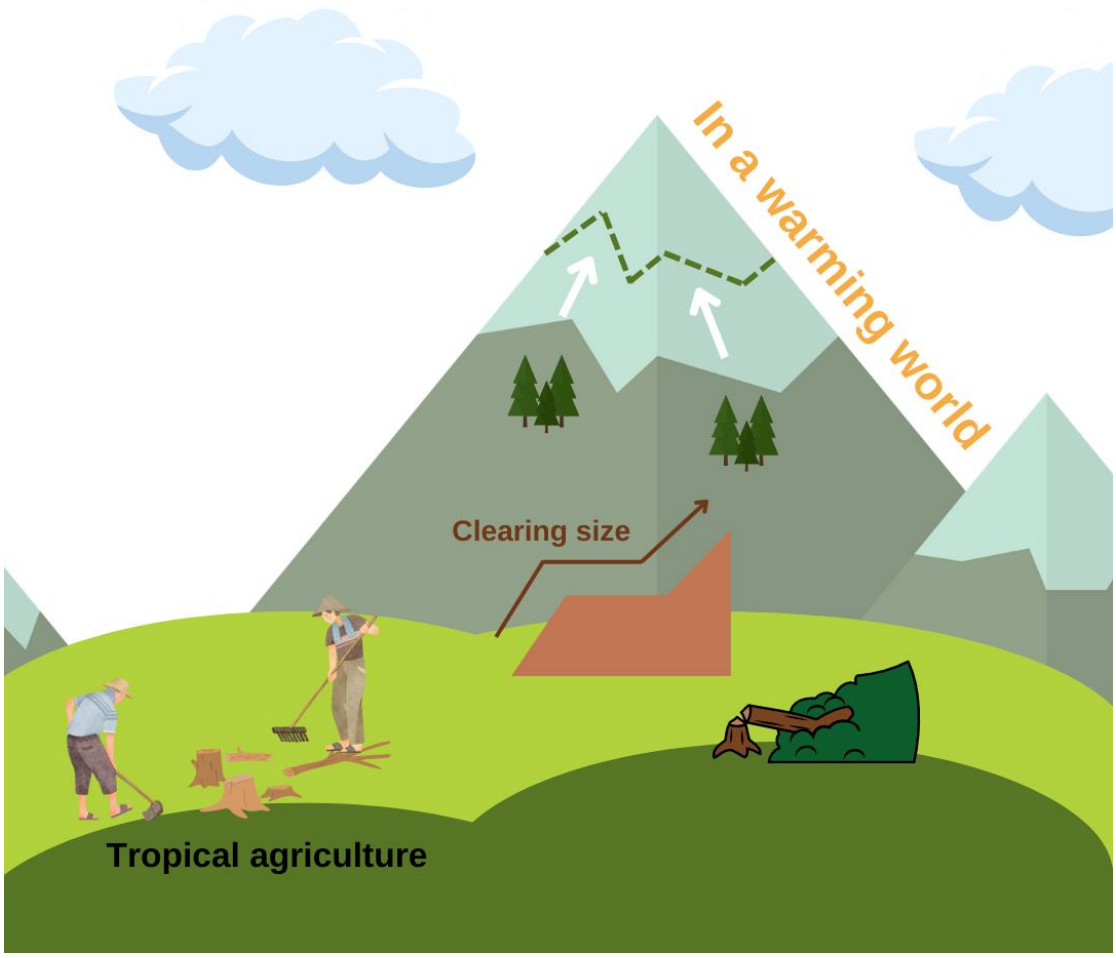

Figure 5.1 *Schematic highlighting the main findings of this thesis. Due to human activities, montane forests at low elevations are being lost at an alarming rate and the proportion of loss in larger clearing sizes is increasing; due to climate change, mountain treelines are shifting upwards.*

Key findings

- **Global mountain forests are disappearing at an accelerating rate**

The global assessment of mountain forest loss reveals that over 78 million hectares (>7%) of mountain forests have been lost since 2000. This loss has been accelerating, with the annual rate doubling from the 2000s to the 2010s, resulting in approximately 5.2 million hectares of mountain forests being lost per year. Regionally, the amount of mountain forest loss varies, with tropical mountain forests experiencing the most loss, comprising 42% of the global total, and the fastest acceleration rate. The expansion of farming into highland areas has been a significant cause of this accelerated loss in the tropics.

Notably, much of these losses occurred in tropical biodiversity hotspots, putting increasing pressure on endangered species. The finding raises significant concerns for biodiversity conservation, as more than 85% of the world's species entirely or partially rely on mountain forests. In alignment with prior research findings (Spracklen et al., 2015), this research has also demonstrated that protected areas have varying success at reducing deforestation.

- **Increasing proportion in larger deforested patches in tropical mountains**

Chapter 3 focuses on the dynamics of mountain forest loss over the tropics, building upon the forest loss hotspots highlighted in Chapter 2. It shows that >50% of the surge in tropical mountain forest loss can be attributed to the widespread clearing of medium to large-size areas. In contrast, there has been a decrease in the proportion of small-scale forest loss patches across all continents. This is the opposite to what has been seen in the lowland Amazon where small-scale deforestation increased in recent years (Kalamandeen et al., 2018).

Additionally, the dynamics of forest loss in mountains are starting to look more like those in lowlands. While tropical lowland forest loss continues to accelerate, the size distribution of clearings remains relatively constant. In contrast, tropical mountains are experiencing a trend of expanding clearing sizes, suggesting an intensified anthropogenic pressure on tropical montane forest ecosystems.

- **Upward movement of mountain treelines in response to climate change**

My analysis of treeline dynamics shows that, between 2000 and 2010, approximately 70% of global treelines experienced an uphill shift. On average, these mountain treelines ascended at a rate of 1.2 m per year, which aligns with findings from some previous local studies (Figure 5.2). A synthesis of treeline shift rates underscores that the rate of change in treeline elevation has accelerated over time, with faster rates in recent years compared to the past century. Tropical regions experienced the faster shift rate with an average of 3.1 m per year, albeit with the greatest variability.

Additional NDVI analysis also detected greening trends at the treeline, which will be conducive to continued upward movement of the treeline in the future. The upward shift of the treeline suggests an increasing number of trees in alpine regions, resulting in greater carbon removal from the atmosphere and potential habitat expansion for specific forest species. However, this shift may also reduce tundra areas, which poses a threat to alpine species and has the potential to affect water supply for dependent regions.

This research extensively tracked nearly one million kilometres of treeline in 243 mountain regions worldwide, completely encircling the upper slopes of mountains and being less susceptible to the impacts of land use changes. This globally consistent approach provides an exemplar for future treeline-related studies (Qiu et al., 2023). The global identification of shifting treelines offers further evidence of the impact of climate change on upland ecosystems.

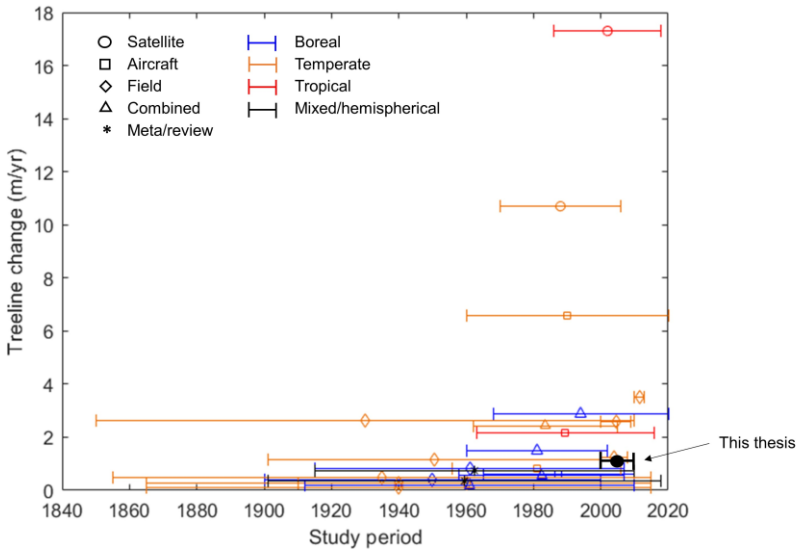

Figure 5.2 *Treeline shift rates reported in previous studies versus this thesis.*

Overall, the findings reported in the thesis improve our understanding of forest cover change across mountain regions and represent a first step in identifying impacts and potential areas of interest for policy. In addition to new insights into biodiversity conservation that were discussed in Chapter 2, our results also have important implications for global water and carbon cycles (refer to section 5.3). The section below provides a discussion of some of the larger sources of uncertainties and limitations in the thesis. Finally, a further discussion is also

provided below on future work that could be undertaken to build on what is reported here.

5.2 Discussion of uncertainties

5.2.1 Observational uncertainty and limitations

Remote sensing observations obtained from satellite instruments inherently carry errors, and these errors are accompanied by associated uncertainties. The Global Forest Change (GFC) data (Hansen et al., 2013) have been widely used in this thesis to estimate changes in mountain forest loss over time. However, the GFC product was created using different satellite sensors and algorithms during the study period (Wernick et al., 2021; Palahí et al., 2021). Firstly, sensor technology has improved with the advent of Landsat 8. From 2001 to 2012, the data relied on Landsat 7, which employed a 'whiskbroom' sensor. In 2013, Landsat 8 was launched with a new 'pushbroom' sensor, which extended the dwell time for each observation, resulting in an improvement in land cover change detection. Secondly, the number of viable observations has fluctuated throughout the years. In the early 2000s, there were around 150,000 observations, while this number has recently exceeded 250,000 each year. Also, there was a significant drop in 2012 when the number of observations fell to <100,000, due to the gap between the decommissioning of Landsat 5 and the use of Landsat 8. Thirdly, algorithm modifications have been introduced after 2012. The dataset relied on a single algorithm run between 2001 and 2012, while in the following years, models were made iteratively. These temporal inconsistencies could potentially create a limitation for time-series analysis. Feng et al. (2022) used a stratified random-sample approach (Olofsson et al., 2014), which is the most robust method for analysing forest loss area trends in the GFC dataset, to reveal a notable similarity between forest loss estimates obtained from this sample-based approach and those derived from GFC mapping. Both approaches consistently indicate an upward trend in forest loss in the first two decades of the 21st century (Feng et al., 2022).

While the GFC dataset offers reliable indicators for large-scale forest change, it is likely to underestimate small clearings (<2 ha) even though these are much larger than its minimum mapping unit (0.09 ha), as noted by Milodowski et al. (2017). In addition, forest gain in the GFC dataset was only available for the years

2001 to 2012. To address this issue, in Chapter 2 I performed an independent assessment of the GFC product using random-sample reference data. I randomly sampled 5,000 forest loss pixels and visually interpreted forest change using Landsat imagery to determine forest regrowth. The results showed that around 23% of forest loss pixels have experienced some degree of tree cover regrowth in recent years.

The dataset of forest loss drivers developed by Curtis et al. (2018) has a relatively coarse resolution (~10 km), compared to other land cover products. This product could only determine the dominant forest loss driver within a grid cell, potentially causing other drivers to be ignored when multiple factors are at play. For example, according to the Curtis map, shifting agriculture is the sole driver of deforestation covering extensive regions in Africa, as well as Central and South America, but some of these areas are home to various productive commodities that are not consumed locally (Hoang et al., 2021). Another uncertainty comes from the difficulty of separating commodity agriculture from shifting agriculture due to the similar spatial patterns between commodity-driven deforestation and shifting agriculture in tropical Africa, as noted by Curtis et al. (2018). Additionally, the dataset only provides a static map over 2001–2015, rather than annual forest loss drivers, obscuring some of the land use dynamics in forest landscapes.

5.2.2 Analytical uncertainty and limitations

Alongside uncertainty from satellite observations, analytical uncertainty also exists throughout the thesis. Forest conversion at scales smaller than a 30 m Landsat pixel (e.g., small-scale fallow-based swidden agriculture) has occurred in some tropical mountain areas (Zeng et al., 2018; Fox et al., 2014) that I could not detect, possibly causing an underestimation of mountain forest loss. Another uncertainty relates to the inability to quantify the impact of fragmentation and edge effects of forest loss, which can alter microclimates and thus regulate the growth and structure of nearby trees (Brinck et al., 2017). This could be a potential threat to species migration and reproduction on the landscape. Additionally, forest degradation which has been shown to be important (e.g., Lapola et al., 2023) is likely to be missed in this thesis. New satellite radar methods provide a unique opportunity to detect forest degradation and small forest disturbances (Aquino et al., 2022; Carstairs et al., 2022a), with potential applicability in hilly terrain (Carstairs et al., 2022b). Furthermore, there is a need

for field measurements of mountain forests expanding on the current network of (largely lowland) forest plots (Blundo et al., 2021).

In Chapter 4, I used the GFC data, which characterises trees as vegetation exceeding 5 m in height, with a 5% tree cover threshold to define the treeline in the main analysis. I attempted to add robustness by conducting sensitivity analysis and found little differences between 0 and 10% tree cover thresholds (refer to Supplementary Figures C.1–C.3). Still, it is important to note that there may be some uncertainties when compared to other studies, as they may employ different treeline definitions. Also, due to the availability of the data, I estimated treeline dynamics over a relatively short period (10 years). Noting that the study period may not be long enough for capturing treeline changes given their slow growth, the global detection of treeline shifts at least provides an early indication of climate-induced changes, and, as commented by Qiu et al. (2023), complements previous studies on the response of natural treelines in a warming world (Camarero et al., 2021; Korner and Paulsen, 2004).

5.2.3 Impacts of landslides on mountain deforestation

In mountainous areas, landslides may contribute to forest loss. Slope gradients and soil properties are typically linked to landslides. The susceptibility to landslides tends to be greatest in areas featuring slope gradients between 10 and 30 degrees, coupled with deep soils that exhibit an increasing proportion of clay with depth (García-Ruiz et al., 2017). Landslides have become an increasing hazard to humans and infrastructure in densely populated mountains, especially in the tropics (Restrepo et al., 2009), and extensive landslide episodes in protected tropical mountains have previously been treated as a major ecological disaster (Restrepo and Alvarez, 2006).

Landslides cause vegetation loss (Ren et al., 2012), due to considerable changes in environmental conditions induced by landslides, including increased photoactive radiation (Myster and Fernandez, 1995) and instability of soils (Walker and Shiels, 2008). Additionally, the loss of the organic soil layer leads to a long-term reduction in soil nutrient content after a slide event (Wilcke et al., 2003). These modified conditions have far-reaching effects on tree characteristics such as growth, establishment and mortality throughout the process of forest succession (Dislich and Huth, 2012).

Aside from landslides, other climate-induced hazards including hurricanes, droughts, and intense rainstorms might increase damage to montane forests (Foster, 2001; Feng et al., 2018). Future climate warming also has the potential to induce alterations in landslides. The anticipated rise in surface temperature could result in more intense and frequent rainfall events, particularly in the mid-latitude and wet tropical regions (IPCC, 2014). There is evidence that changes in heavy precipitation will increase the occurrence of landslides (Guzzetti et al., 2008; Crozier, 2010; Ren et al., 2012; Seneviratne et al., 2012; Gariano et al., 2017).

Due to changes in soil hydrology and reduced soil strength, deforestation, in turn, has the potential to trigger widespread landslides in mountainous regions (García-Ruiz et al., 2010; Caviezel et al., 2014; García-Ruiz et al., 2016; García-Ruiz et al., 2017; Laimer, 2017; Lehmann et al., 2019; Depicker et al., 2021). Consequently, this phenomenon could lead to modifications in runoff generation (Lana-Renault et al., 2010, Lana-Renault et al., 2011) and fluvial dynamics (Sanjuán et al., 2016). Future studies should delve into the implications of climate-induced geo-hydrological hazards. It is also needed to determine what role landslides have in total mountain forest loss globally and in the tropics in future research.

5.3 Implications for water and carbon cycles

While this thesis did not delve deeply into the analysis of water and carbon impacts, my findings carry substantial implications for water and carbon cycles. The loss of mountain forests poses a significant threat to the carbon cycle, as it releases the carbon stored in vegetation and soil to the atmosphere and indirectly decreases the carbon sink capacity of terrestrial ecosystems (Bonan, 2008; Baccini et al., 2012; Veldkamp et al., 2020). The observed acceleration of loss and the increase in the size of loss patches in mountain forests raise concerns, as these forests in certain regions contain similar carbon stocks compared to lowland forests (Spracklen and Righelato, 2014; Cuni-Sanchez et al., 2021). This could result in the redistribution and depletion of tropical forest carbon in the near future (Feng et al., 2021), potentially transforming tropical forests from a carbon-neutral contributor (Mitchard et al., 2018) to a net carbon source (Baccini et al., 2017; Harris et al., 2021) in the global carbon budget. Conversely, the upward migration of the treeline suggests that more trees can absorb carbon from the

atmosphere at higher altitudes than before and so this may need to be accounted for in global carbon models.

The discoveries of changing mountain forest cover in this study also hold significance for multiple components of the water cycle. Deforestation generally drives a reduction in evapotranspiration, but the sensitivity of evapotranspiration to forest loss may weaken with increasing elevation, as pointed out by Zeng et al. (2021). This means a smaller evapotranspiration reduction from deforestation at higher elevations. The increasing mountain forest loss could potentially give rise to distinct hydrological patterns driven by deforestation in mountain regions compared to lowlands. In contrast to deforestation, greening can impact the terrestrial water cycle by increasing land evapotranspiration and precipitation, as well as decreasing soil moisture in dry regions (Zeng et al., 2017). The findings of treeline shifts and NDVI change provide a useful basis for further hydrological studies to understand the impacts of mountain greening.

5.4 Future research directions

Mountain forest loss versus gain

While this thesis highlights forest loss occurring at lower elevations and forest gain (treeline shift) at higher elevations in mountain areas, it would be interesting to understand whether forest loss could be offset by forest gain along an elevation gradient. The diversity of forest species and structure contributes to distinct patterns of forest carbon stock across different elevations (Haq et al., 2022). Further work could involve comparing carbon emissions resulting from forest loss with the carbon sink due to vegetation greening in mountain ecosystems.

Influence on carbon sequestration by forest management

The intensively managed fraction of the world's forests has increased to fulfill humanity's demands for food, wood, fibre, and ecosystem services (Noormets et al., 2015). Forest management holds the potential to enhance the terrestrial carbon pool (Jandl et al., 2007). However, the net impact on carbon balance depends on the end uses of forestry products. If forest products are short lived (such as pulp and paper), the carbon is rapidly released back to the atmosphere. Only if the products have a long lifetime (like construction, furniture) does this

lead to a longer-term store of carbon. As pointed out by Lewis et al. (2019), restoring natural forests is a better way to store carbon compared to plantations. Future research could explore the extent to which mountain forest management can enhance carbon sequestration levels, carrying significant implications for improved forest management strategies in response to climate change and the provision of ecosystem services.

Hydrological impacts of mountain forest cover change

Prior studies have assessed the impacts of mountain greening on evapotranspiration, but these efforts have been largely limited to case studies (Xu et al., 2018; Yang et al., 2021). Further work could conduct a wider analysis of interactions between mountain greening (treeline shift) and precipitation, and especially how any such interactions might vary across spatial scales. The impacts of mountain greening on precipitation could be evaluated by a modified WRF model (Qin et al., 2023), for example, which performs an accurate simulation of daily precipitation.

Additionally, it would be interesting to understand how mountain forest loss impacts water quality. Forest disturbance and harvest will alter soil carbon and nutrient cycles (Chen and Li, 2003; James and Harrison, 2016), thus affecting water quality. Especially if the primary forests were altered, soil carbon and nutrient storage would be greatly affected (Chen and Li, 2003). It could be possible to use the Intact Forest Landscape (IFL) data (Potapov et al., 2017) that are available freely online to separate primary/intact forest components in forest landscapes.

5.5 Summary of key advances

Using multiple global datasets, my research has yielded significant insights into the changing environment of mountain forests. Firstly, it became evident that mountain forest loss has surged worldwide since 2000. A substantial proportion of this loss has taken place within areas with high biodiversity, potentially posing a threat to threatened species residing there. Secondly, the depletion of tropical mountain forests has largely been attributed to median and large-scale clearings, indicating an escalating human pressure on mountainous regions. Lastly, my findings reveal an upward shift in mountain treelines in response to the warming

climate. This shift presents unique challenges for fragile ecosystems at high altitudes.

Moreover, this study has developed a globally consistent approach for identifying and tracking closed-loop treelines in mountains, offering a valuable tool for carbon assessments, ecological modelling, and the analysis of species adaptation to changing environments. This research sparks interest in algorithm advancements for global treeline mapping through a combination of diverse data sources, including multi-source remote sensing and ground-based datasets. Additionally, it encourages broader investigations into the far-reaching impacts of climate change on upland ecosystems and how these ecosystems adapt to a changing climate.

References

Aquino, C., Mitchard, E.T.A., McNicol, I.M., Carstairs, H., Burt, A., Puma Vilca, B.L., Obiang Ebanéga, M., Modinga Dikongo, A., Dassi, C., Mayta, S. and Tamayo, M., 2022. Reliably mapping low-intensity forest disturbance using satellite radar data. Frontiers in Forests and Global Change, 5, 1018762.

Baccini, A.G.S.J., Goetz, S.J., Walker, W.S., Laporte, N.T., Sun, M., Sulla-Menashe, D., Hackler, J., Beck, P.S.A., Dubayah, R., Friedl, M.A. and Samanta, S., 2012. Estimated carbon dioxide emissions from tropical deforestation improved by carbon-density maps. Nature Climate Change, 2, 182–185.

Blundo, C., Carilla, J., Grau, R., Malizia, A., Malizia, L., Osinaga-Acosta, O., Bird, M., Bradford, M., Catchpole, D., Ford, A. and Graham, A., 2021. Taking the pulse of Earth's tropical forests using networks of highly distributed plots. Biological Conservation, 260, 108849.

Bonan, G.B., 2008. Forests and climate change: forcings, feedbacks, and the climate benefits of forests. Science, 320, 1444–1449.

Brinck, K. Fischer, R., Groeneveld, J., Lehmann, S., de Paula, M.D., Pütz, S., Sexton, J.O., Song, D. and Huth, A., 2017. High resolution analysis of tropical forest fragmentation and its impact on the global carbon cycle. Nature Communications, 8, 14855.

Camarero, J., Gazol, A., Sanchez-Salguero, R., Fajardo, A., McIntire, E., Gutierrez, E., Batllori, E., Boudreau, S., Carrer, M., Diez, J., Dufour-Tremblay, G. et al., 2021. Global fading of the temperature-growth coupling at alpine and polar treelines. Global Change Biology, 27, 1879–1889.

Carstairs, H., Mitchard, E.T.A., McNicol, I., Aquino, C., Chezeaux, E., Ebanega, M.O., Dikongo, A.M. and Disney, M., 2022a. Sentinel-1 shadows used to quantify canopy loss from selective logging in Gabon. Remote Sensing, 14, 4233.

Carstairs, H., Mitchard, E.T.A., McNicol, I., Aquino, C., Burt, A., Ebanega, M.O., Dikongo, A.M., Bueso-Bello, J.L. and Disney, M., 2022b. An effective method for InSAR mapping of tropical forest degradation in hilly areas. Remote Sensing, 14, 452.

Caviezel, C., Hunziker, M., Schaffner, M. and Kuhn, N.J., 2014. Soil–vegetation interaction on slopes with bush encroachment in the central Alps–adapting slope stability measurements to shifting process domains. Earth Surface Processes and Landforms, 39, 509–521.Chen, X. and Li, B.L., 2003. Change in soil carbon and nutrient storage after human disturbance of a primary Korean pine forest in Northeast China. Forest Ecology and Management, 186, 197–206.

Crozier, M.J., 2010. Deciphering the effect of climate change on landslide activity: A review. Geomorphology, 124, 260–267.

Cuni-Sanchez, A., Sullivan, M.J., Platts, P.J., Lewis, S.L., Marchant, R., Imani, G., Hubau, W., Abiem, I., Adhikari, H., Albrecht, T., Altman, J. et al., 2021. High aboveground carbon stock of African tropical montane forests. Nature, 596, 536–542.

Depicker, A., Govers, G., Jacobs, L., Campforts, B., Uwihirwe, J. and Dewitte, O., 2021. Interactions between deforestation, landscape rejuvenation, and shallow landslides in the North Tanganyika–Kivu rift region, Africa. Earth Surface Dynamics, 9, 445–462.

Dislich, C. and Huth, A., 2012. Modelling the impact of shallow landslides on forest structure in tropical montane forests. Ecological Modelling, 239, 40-53. Modelling the impact of shallow landslides on forest structure in tropical montane forests. Ecological Modelling, 239, 40–53.

Feng, Y., Negron-Juarez, R.I., Patricola, C.M., Collins, W.D., Uriarte, M., Hall, J.S., Clinton, N. and Chambers, J.Q., 2018. Rapid remote sensing assessment of impacts from Hurricane Maria on forests of Puerto Rico. PeerJ Preprints, 6, e26597v1.

Feng, Y., Zeng, Z., Searchinger, T.D., Ziegler, A.D., Wu, J., Wang, D., He, X., Elsen, P.R., Ciais, P., Xu, R., Guo, Z. et al., 2022. Doubling of annual forest carbon loss over the tropics during the early twenty-first century. Nature Sustainability, 5, 444–451.

Foster, P., 2001. The potential negative impacts of global climate change on tropical montane cloud forests. Earth-Science Reviews, 55, 73–106.

Fox, J., Castella, J.C. and Ziegler, A.D., 2014. Swidden, rubber and carbon: can REDD+ work for people and the environment in montane mainland Southeast Asia? Global Environmental Change, 29, 318–326.

García-Ruiz, J.M., Beguería, S., Alatorre, L.C. and Puigdefábregas, J., 2010. Land cover changes and shallow landsliding in the flysch sector of the Spanish Pyrenees. Geomorphology, 124, 250–259.

García-Ruiz, J.M., Beguería, S., Arnáez, J., Sanjuán, Y., Lana-Renault, N., Gómez-Villar, A., Álvarez-Martínez, J. and Coba-Pérez, P., 2017. Deforestation induces shallow landsliding in the montane and subalpine belts of the Urbión Mountains, Iberian Range, Northern Spain. Geomorphology, 296, 31–44.

García-Ruiz, J.M., Sanjuán, Y., Gil-Romera, G., González-Sampériz, P., Beguería, S., Arnáez, J., Coba-Pérez, P., Gómez-Villar, A., Álvarez-Martínez, J., Lana-Renault, N. and Pérez-Cardiel, E., 2016. Mid and late Holocene forest fires and deforestation in the subalpine belt of the Iberian range, northern Spain. Journal of Mountain Science, 13, 1760–1772.

Gariano, S.L., Rianna, G., Petrucci, O. and Guzzetti, F., 2017. Assessing future changes in the occurrence of rainfall-induced landslides at a regional scale. Science of the total environment, 596, 417–426.

Guzzetti, F., Peruccacci, S., Rossi, M. and Stark, C.P., 2008. The rainfall intensity–duration control of shallow landslides and debris flows: An update. Landslides, 5, 3–17.

Hansen, M.C., Potapov, P.V., Moore, R., Hancher, M., Turubanova, S.A., Tyukavina, A., Thau, D., Stehman, S.V., Goetz, S.J., Loveland, T.R., Kommareddy, A., et al., 2013. High-resolution global maps of 21st-century forest cover change. Science, 342, 850–853.

Haq, S.M., Rashid, I., Calixto, E.S., Ali, A., Kumar, M., Srivastava, G., Bussmann, R.W. and Khuroo, A.A., 2022. Unravelling patterns of forest carbon stock along a wide elevational gradient in the Himalaya: implications for climate change mitigation. Forest Ecology and Management, 521, 120442.

Hoang, N.T. and Kanemoto, K., 2021. Mapping the deforestation footprint of nations reveals growing threat to tropical forests. Nature Ecology & Evolution, 5, 845–853.

IPCC, 2014. Intergovernmental Panel on Climate Change Climate Change 2014: Synthesis Report. Contribution of Working Groups I, II and III to the Fifth Assessment Report of the Intergovernmental Panel on Climate Change,

Geneva, Switzerland. James, J. and Harrison, R., 2016. The effect of harvest on forest soil carbon: a meta-analysis. Forests, 7, 308.

Jandl, R., Vesterdal, L., Olsson, M., Bens, O., Badeck, F. and Roc, J., 2007. Carbon sequestration and forest management. CAB Reviews: Perspectives in Agriculture, Veterinary Science, Nutrition and Natural Resources, 2, 1–16.

Kalamandeen, M., Gloor, E., Mitchard, E.T.A., Quincey, D., Ziv, G., Spracklen, D.V., Spracklen, B., Adami, M., Aragão, L.E. and Galbraith, D., 2018. Pervasive rise of small-scale deforestation in Amazonia. Scientific Reports, 8, 1600.

Korner, C. and Paulsen, J., 2004. A world-wide study of high altitude treeline temperatures. Journal of Biogeography, 31, 713–732.

Laimer, H.J., 2017. Anthropogenically induced landslides–A challenge for railway infrastructure in mountainous regions. Engineering Geology, 222, 92–101.

Lana-Renault, N., Alvera, B. and Ruiz, J.G., 2010. The snowmelt period in a Mediterranean high mountain catchment: runoff and sediment transport. Cuadernos de investigación geográfica, 36, 99–108.

Lana-Renault, N., Alvera, B. and García-Ruiz, J.M., 2011. Runoff and sediment transport during the snowmelt period in a Mediterranean high-mountain catchment. Arctic, Antarctic, and Alpine Research, 43, 213–222.

Lapola, D.M., Pinho, P., Barlow, J., Aragão, L.E., Berenguer, E., Carmenta, R., Liddy, H.M., Seixas, H., Silva, C.V., Silva-Junior, C.H., Alencar, A.A. et al., 2023. The drivers and impacts of Amazon forest degradation. Science, 379, eabp8622.

Lehmann, P., von Ruette, J. and Or, D., 2019. Deforestation effects on rainfall-induced shallow landslides: Remote sensing and physically-based modelling. Water Resources Research, 55, 9962–9976.

Lewis, S.L., Wheeler, C.E., Mitchard, E.T.A. and Koch, A., 2019. Restoring natural forests is the best way to remove atmospheric carbon. Nature, 568, 25–28.

Milodowski, D.T., Mitchard, E.T.A. and Williams, M., 2017. Forest loss maps from regional satellite monitoring systematically underestimate deforestation in

two rapidly changing parts of the Amazon. Environmental Research Letters, 12, 094003.

Myster, R.W. and Fernandez, D.S., 1995. Spatial gradients and patch structure on two Puerto Rican landslides. Biotropica, 149–159.

Noormets, A., Epron, D., Domec, J.C., McNulty, S.G., Fox, T., Sun, G. and King, J.S., 2015. Effects of forest management on productivity and carbon sequestration: a review and hypothesis. Forest Ecology and Management, 355, 124–140.

Olofsson, P., Foody, G.M., Herold, M., Stehman, S.V., Woodcock, C.E. and Wulder, M.A., 2014. Good practices for estimating area and assessing accuracy of land change. Remote Sensing of Environment, 148, 42–57.

Palahí, M., Valbuena, R., Senf, C., Acil, N., Pugh, T.A., Sadler, J., Seidl, R., Potapov, P., Gardiner, B., Hetemäki, L., Chirici, G. et al., 2021. Concerns about reported harvests in European forests. Nature, 592, E15–E17.

Potapov, P., Hansen, M.C., Laestadius, L., Turubanova, S., Yaroshenko, A., Thies, C., Smith, W., Zhuravleva, I., Komarova, A., Minnemeyer, S. and Esipova, E., 2017. The last frontiers of wilderness: tracking loss of intact forest landscapes from 2000 to 2013. Science Advances, 3, e1600821.

Qin, Y., Wang, D., Cao, Y.E., Cai, X., Liang, S., Beck, H.E. and Zeng, Z., 2023. Sub-grid representation of vegetation cover in land surface schemes improves the modelling of how climate responds to deforestation. Geophysical Research Letters, 50, e2023GL104164.

Qiu, J., Feng, S. and Yuan, W., 2023. Upward-moving mountain treelines: an indicator of changing-climate impact. Global Change Biology, in press.

Ren, D., Leslie, L.M. and Duan, Q., 2012. Landslides caused deforestation. In *Deforestation around the World*, 95, 123.

Restrepo, C. and Alvarez, N., 2006. Landslides and Their Contribution to Land-cover Change in the Mountains of Mexico and Central America. Biotropica, 38, 446–457.

Restrepo, C., Walker, L.R., Shiels, A.B., Bussmann, R., Claessens, L., Fisch, S., Lozano, P., Negi, G., Paolini, L., Poveda, G. and Ramos-Scharrón, C., 2009. Landsliding and its multiscale influence on mountainscapes. BioScience, 59, 685–698.

Sanjuán, Y., Gómez-Villar, A., Nadal-Romero, E., Álvarez-Martínez, J., Arnáez, J., Serrano-Muela, M.P., Rubiales, J.M., González-Sampériz, P. and García-Ruiz, J.M., 2016. Linking land cover changes in the sub-alpine and montane belts to changes in a torrential river. Land Degradation & Development, 27, 179–189.

Seneviratne, S., Nicholls, N., Easterling, D., Goodess, C., Kanae, S., Kossin, J., Luo, Y., Marengo, J., McInnes, K., Rahimi, M., Reichstein, M., et al., 2012. Changes in climate extremes and their impacts on the natural physical environment. In *Managing the Risks of Extreme Events and Disasters to Advance Climate Change Adaptation*. Cambridge University Press, Cambridge, UK, and New York, NY, USA, 109–230.

Spracklen, D.V. and Righelato, R., 2014. Tropical montane forests are a larger than expected global carbon store. Biogeosciences, 11, 2741–2754.

Spracklen, B.D., Kalamandeen, M., Galbraith, D., Gloor, E. and Spracklen, D.V., 2015. A global analysis of deforestation in moist tropical forest protected areas. Plos One, 10, e0143886.

Veldkamp, E., Schmidt, M., Powers, J.S. and Corre, M.D., 2020. Deforestation and reforestation impacts on soils in the tropics. Nature Reviews Earth & Environment, 1, 590–605.

Walker, L.R. and Shiels, A.B., 2008. Post-disturbance erosion impacts carbon fluxes and plant succession on recent tropical landslides. Plant and Soil, 313, 205–216.

Wernick, I.K., Ciais, P., Fridman, J., Högberg, P., Korhonen, K.T., Nordin, A. and Kauppi, P.E., 2021. Quantifying forest change in the European Union. Nature, 592, E13–E14.

Wilcke, W., Valladarez, H., Stoyan, R., Yasin, S., Valarezo, C. and Zech, W., 2003. Soil properties on a chronosequence of landslides in montane rain forest, Ecuador. Catena, 53, 79–95.

Xu, S., Yu, Z., Yang, C., Ji, X. and Zhang, K., 2018. Trends in evapotranspiration and their responses to climate change and vegetation greening over the upper reaches of the Yellow River Basin. Agricultural and Forest Meteorology, 263, 118–129.

Yang, L., Feng, Q., Adamowski, J.F., Alizadeh, M.R., Yin, Z., Wen, X. and Zhu, M., 2021. The role of climate change and vegetation greening on the

variation of terrestrial evapotranspiration in northwest China's Qilian Mountains. Science of the Total Environment, 759, 143532.

Zeng, Z., Gower, D.B. and Wood, E.F., 2018. Accelerating forest loss in Southeast Asian Massif in the 21st century: a case study in Nan Province, Thailand. Global Change Biology, 24, 4682–4695.

Zeng, Z., Wang, D., Yang, L., Wu, J., Ziegler, A.D., Liu, M., Ciais, P., Searchinger, T.D., Yang, Z.L., Chen, D., Chen, A. et al., 2021. Deforestation-induced warming over tropical mountain regions regulated by elevation. Nature Geosciences, 14, 23–29.

Zeppetello, L.R.V., Parsons, L.A., Spector, J.T., Naylor, R.L., Battisti, D.S., Masuda, Y.J. and Wolff, N.H., 2020. Large scale tropical deforestation drives extreme warming. Environmental Research Letters, 15, 084012.

Appendix A

Supplementary materials for Chapter 2

Tables

Supplementary Table A.1 *Summary of mountain forest loss between 2001 and 2018 for countries (ranking by the total area of mountain forest loss). Relative forest loss is the percent forest loss relative to forest cover in the baseline year 2000. Acceleration is estimated using Theil–Sen regression of the time series of annual mountain forest loss per country. Drivers of mountain forest loss are obtained from the results by Curtis et al. (2018). The numbers underlined represent the primary drivers of forest loss in mountains in the corresponding country (>50%), but if no driver exceeds 50% the top two drivers are marked. In total, 128 countries have detectable values in the analysis. Countries not listed below either do not have mountain regions following the GMBA methods or have no detectable forest or forest loss.*

Country	Mountain Forest area in 2000 (ha)	Total mountain forest loss 2001–2018 (ha)	Relative mountain forest loss 2001–2018 (%)	Mountain forest loss acceleration (ha yr^{-2})	Drivers (%)					
					C	S	F	W	U	O
Russia	172797952	11945881	6.91	10983.39	0	0.01	15.73	76.65	0	7.61
United States	92871993	10746091	11.57	3350.86	2.56	0.32	54.20	37.70	1.83	3.39
China	133757975	7311963	5.47	26854.04	1.27	1.40	91.44	0.58	0.42	4.88
Canada	75112314	5574072	7.42	8503.62	0.36	0	57.10	36.82	0.26	5.46
Indonesia	55910968	3974427	7.11	13319.18	60.63	29.42	6.68	0	0.48	2.78
Laos	18759266	3076750	16.40	18657.98	35.51	13.75	50.29	0	0	0.44
Vietnam	15759321	2812125	17.84	17375.41	54.74	13.97	29.88	0	1.03	0.38
Myanmar	31850647	2799669	8.79	17427.21	38.53	17.12	43.14	0	0.10	1.10

Brazil	29877836	2255924	7.55	5066.74	9.74	52.89	35.29	0.23	0.13	1.72
Malaysia	13666976	2243921	16.42	7146.80	79.92	3.91	15.39	0	0.16	0.62
Chile	19257111	1622955	8.43	3162.96	7.29	6.43	82.03	0.53	0.17	3.55
Colombia	30519639	1602598	5.25	1229.22	2.57	90.66	3.39	0.01	0.94	2.44
Peru	26927950	1458218	5.42	4012.08	3.09	91.23	0.82	0.04	0	4.81
India	24130828	1401833	5.81	7170.90	0.94	4.31	90.44	0.01	0.51	3.79
Thailand	16329759	1285731	7.87	5360.63	23.55	16.80	58.30	0	0.07	1.27
South Africa	4561442	1195584	26.21	1771.20	0.57	12.66	83.78	0.32	0.23	2.44
Australia	15014332	1026849	6.84	1700.90	0.49	0.06	66.00	28.50	0.78	4.17
Guinea	4222773	973141	23.05	9302.98	14.15	84.97	0.04	0.33	0.02	0.49
Madagascar	6474059	963600	14.88	5238.25	0.60	96.66	0.67	0	0	2.06
Mexico	35176265	927668	2.64	2693.49	2.22	66.78	0.26	15.56	1.14	14.03
Spain	6628150	607198	9.16	2995.61	0	0	92.41	3.61	0	3.97
Ethiopia	14613024	548790	3.76	1707.57	1.56	84.58	0.87	0.01	0.07	12.91
D.R. Congo	8137828	547455	6.73	2826.90	0	98.59	0	0	0.15	1.26
Venezuela	20914386	539442	2.58	141.78	1.48	91.06	1.32	0.07	0.25	5.81
Mongolia	3637132	525159	14.44	-1387.80	0	1.52	2.79	89.43	0.07	6.19

Bolivia	15226635	522864	3.43	1173.44	13.59	80.56	0	0.14	0	5.71
Honduras	3411027	485110	14.22	1162.22	5.53	91.16	0.70	2.33	0.09	0.20
Angola	4698860	483186	10.28	2248.22	0	99.14	0.03	0	0	0.84
Papua New Guinea	18876554	471626	2.50	2066.27	0.99	74.56	6.89	7.17	2.27	8.12
Philippines	8185745	456755	5.58	1684.28	38.32	48.22	9.91	0	0.77	2.78
Japan	16941719	374170	2.21	619.01	0	0.06	93.01	0.07	0.07	6.79
Norway	8603580	363133	4.22	1025.10	0	0	91.18	0.06	0	8.76
New Zealand	5071648	352177	6.94	444.09	1.41	0	83.45	6.62	3.31	5.21
Cambodia	2662245	343162	12.89	1393.21	85.85	5.16	7.51	0	0	1.49
Portugal	666346	337907	50.71	1460.48	0	0.28	96.89	2.81	0	0.03
Tanzania	4877968	335685	6.88	1356.19	0.45	91.37	3.84	0	0.09	4.25
Ecuador	10115833	304685	3.01	323.34	0.11	89.85	3.68	0	0.94	5.41
Romania	5570343	292583	5.25	225.66	0	0	96.97	0.09	0	2.93
Austria	3631368	240358	6.62	45.95	0	0	98.98	0	0	1.02
Nicaragua	1792416	235099	13.12	119.21	0.18	97.90	0	1.51	0	0.41
Italy	8409608	234280	2.79	880.60	0	0.11	79.44	1.67	0	18.77

Turkey	6429027	218055	3.39	721.49	0	0.54	81.53	0.53	1.22	16.18
North Korea	5271217	216129	4.10	-26.23	0	17.75	76.59	1.18	0	4.47
France	5924319	212698	3.59	428.96	0	0.03	92.31	0.85	0	6.81
Slovakia	2381987	207062	8.69	744.35	0	0	98.58	0.44	0	0.98
South Korea	4589497	203922	4.44	793.51	0	0.22	92.94	0.02	4.31	2.50
Algeria	1345040	197708	14.70	681.32	6.74	66.89	16.92	0	4.84	4.61
United Kingdom	1071274	177800	16.60	371.50	0	0	96.13	1.86	0	2.01
Guatemala	1581466	169226	10.70	385.35	0	82.10	6.43	11.21	0	0.27
Ukraine	1815939	156817	8.64	255.45	0	0	99.68	0.16	0	0.16
Zimbabwe	613690	152063	24.78	477.50	0	26.34	72.83	0	0	0.83
Dominican Republic	1464403	147069	10.04	164.49	15.17	77.80	5.16	0	1.57	0.31
Panama	3269837	146837	4.49	129.69	1.85	95.21	0.11	0.33	0	2.50
Argentina	5707062	141562	2.48	356.28	49.44	21.43	9.25	1.79	0	18.09
Cameroon	5914318	132648	2.24	510.26	0.93	89.99	0.07	0	0	9.01
Costa Rica	2848866	131409	4.61	-98.75	0	93.12	2.14	1.24	1.60	1.90

Malawi	941654	131282	13.94	613.10	0	89.91	8.37	0	0	1.72
Nigeria	2724535	114873	4.22	335.36	0	91.98	0.09	0	0	7.93
Mozambique	714700	103173	14.44	373.61	0	93.36	6.51	0	0	0.14
Eswatini	356339	100894	28.31	33.25	3.82	8.31	86.88	0	0	0.99
Bangladesh	585624	95608	16.33	767.64	0	4.53	95.05	0	0	0.42
Greece	2444633	92176	3.77	-13.38	0	0	62.95	22.85	0.08	14.11
Côte d'Ivoire	545452	88683	16.26	568.72	0.62	99.28	0	0	0	0.10
Uganda	1357201	70755	5.21	308.05	2.21	90.01	0.08	0	3.36	4.34
Rwanda	822691	58812	7.15	318.27	1.32	73.83	6.14	0	8.18	10.52
Sri Lanka	1742414	55156	3.17	258.33	1.93	3.38	75.71	0.11	17.05	1.81
Bulgaria	2457191	53405	2.17	59.16	0	0	90.47	0.84	0	8.70
Nepal	5579768	51624	0.93	25.07	4.19	3.37	37.60	1.28	4.24	49.32
Haiti	716488	50956	7.11	115.11	0	90.72	0.51	0	1.46	7.32
Kenya	629375	48992	7.78	53.07	11.24	68.45	10.67	0	0	9.64
Slovenia	1061155	40031	3.77	168.06	0	0	96.46	0.98	0	2.55
Burundi	704374	36534	5.19	166.83	0.81	81.13	0.18	0	1.37	16.52
Morocco	668605	35435	5.30	19.85	7.12	61.76	15.54	0	0.16	15.41

Poland	818735	32732	4.00	30.30	0	0	95.18	0	0	4.82
Germany	882464	30192	3.42	-33.05	0	0	99.63	0	0	0.37
Guyana	3301059	29413	0.89	110.73	0	87.27	0	0	0	12.73
Bosnia and Herzegovina	2405504	29284	1.22	47.49	0	0	67.02	2.55	0	30.44
Bhutan	2975354	27271	0.92	97.97	44.67	5.68	13.46	8.49	0	27.70
Switzerland	1446116	25418	1.76	50.35	0	0	70.58	0	0	29.42
Croatia	1049740	22566	2.15	18.57	0	0	67.71	5.61	0	26.68
Montenegro	653242	18017	2.76	66.37	0	0	72.28	4.30	0	23.42
Sweden	949963	17286	1.82	19.27	0	0	83.75	1.02	0	15.23
Czech Republic	190268	16048	8.43	65.30	0	0	100	0	0	0
Syria	70423	15420	21.90	77.61	0	13.53	80.58	1.02	0	4.87
Belize	416467	15208	3.65	-12.73	3.44	92.76	0	0	0	3.79
Cuba	405623	15025	3.70	-11.63	0	95.25	3.73	0	0	1.02
Kazakhstan	2648629	13955	0.53	-54.36	0	4.39	30.28	12.59	0.45	52.30
Zambia	154254	13361	8.66	66.05	0	100	0	0	0	0

South Sudan	655918	13032	1.99	22.64	0	76.96	0	0	0	23.04
Serbia	1282921	12758	0.99	44.46	0	0	57.66	1.26	0	41.08
Jamaica	200491	12699	6.33	9.11	0	99.62	0	0	0	0.38
Ireland	52377	12041	22.99	-4.55	0	0	97.85	0	0	2.15
Pakistan	1209034	10654	0.88	-70.32	0	0	51.05	3.40	0	45.55
Georgia	2961132	9786	0.33	-27.27	0	0.42	41.36	1.88	0	56.33
Tunisia	108203	9689	8.95	22.28	0	48.90	34.57	0	0	16.53
Albania	206912	9159	4.43	-7.22	0	0	71.59	12.77	0	15.63
Macedonia	282673	8815	3.12	-4.57	0	0	86.10	0	0	13.90
Hungary	192834	8783	4.55	6.71	0	0	98.51	1.28	0	0.21
Azerbaijan	1163678	7143	0.61	-38.37	0	8.00	39.30	0	0	52.71
Kosovo	223359	6190	2.77	14.17	0	0.93	92.19	0.02	0	6.86
Lebanon	68017	5146	7.57	12.78	0	0	44.49	0	36.79	18.72
Cyprus	122380	4267	3.49	8.02	0	35.80	43.63	2.50	0	18.07
Mali	29789	4167	13.99	38.34	0	97.24	0	0	0	2.76
Iran	1903342	4013	0.21	-15.61	0	0	2.77	0	0	97.23
Brunei	149210	3850	2.58	15.66	14.85	19.98	57.68	0	0	7.48

Kyrgyzstan	719670	3641	0.51	-18.58	0	9.15	0.47	0	0	90.38
El Salvador	64296	3335	5.19	-5.58	0	99.46	0.54	0	0	0
Armenia	356705	2296	0.64	-8.17	0	0.08	40.49	0	0	59.43
Sierra Leone	23265	2266	9.74	14.38	65.93	34.07	0	0	0	0
Sudan	45686	2016	4.41	-5.61	0	47.46	0	0	0	52.54
Afghanistan	285944	1914	0.67	-15.19	0	0	36.95	3.09	0	59.97
Trinidad and Tobago	80088	1681	2.10	-0.93	0	83.56	0	0	0	16.44
Suriname	916823	963	0.11	0.17	0	14.97	0	0	0	85.03
Lesotho	14057	650	4.63	1.33	0	0.21	1.30	0	0	98.50
Tajikistan	70487	442	0.63	-2.09	0	0	0	0	0	100
Uzbekistan	74848	386	0.52	-0.50	0	4.34	0	0	0	95.66
Liechtenstein	10273	97	0.94	-0.06	0	0	75.81	0	0	24.19
Andorra	19823	87	0.44	0.08	0	0	23.39	0	0	76.61
Turkmenistan	4062	85	2.09	-0.10	0	0	0	0	0	100
French Guiana	29130	74	0.25	-0.09	0	37.32	0	0	0	62.68
Israel	1488	43	2.91	0.07	0	0	0	0	9.87	90.13

Yemen	124	32	25.77	-0.04	0	0	0	0	0	100
Northern Cyprus	223	13	5.74	0.07	0	0	0	0	0	100
Finland	2337	8	0.33	0	0	0	0	0	0	100
San Marino	958	8	0.78	-0.01	0	0	0	0	0	100
Namibia	70	7	10.21	-0.01	0	0	0	0	0	100
Iraq	519	5	1.04	0	0	0	0	0	0	100
Monaco	3	0	6.82	0	0	0	66.67	0	0	33.33
all mountains	**1101832954**	**78122650**	**7.09**	**201473.60**	**9.56**	**14.75**	**41.64**	**28.76**	**0.53**	**4.75**

C: Commodity agriculture; S: Shifting cultivation; F: Forestry; W: Wildfire; U: Urbanization; O: Other. “Other” are the grids that were marked as zero or minor loss by Curtis et al. (2018) at a resolution of ~10 km.

Supplementary Table A.2 *Proportion of mountain forest loss in naturally regenerating forests and plantations by year.*

Year	Naturally regenerating forests (%)	Plantations (%)
2001	64.10	18.61
2002	65.32	16.18
2003	68.83	14.71
2004	63.17	11.87
2005	61.59	14.48
2006	62.24	18.53
2007	66.32	17.85
2008	68.31	15.50
2009	61.49	18.77
2010	60.05	18.62
2011	57.78	18.88
2012	62.11	15.95
2013	64.14	18.05
2014	61.65	22.51
2015	71.55	19.49
2016	77.29	16.20
2017	73.41	21.89
2018	75.47	20.91

Supplementary Table A.3 *Elevational patterns of biodiversity values and mountain forest loss in RSR biodiversity hotspots.*

Hotspots	Elevation range (m)	RSR range ($\times 10^{-6}$)	Total forest loss 2001–2018 (Mha)	Relative forest loss 2001–2018 (%)	Proportion of forest area within PA (%)	Proportion of forest loss within PA (%)	Relative forest loss within PA (%)	Relative forest loss outside of PA (%)
RSR (all)	0–350	1.74–2.13	4.38	11.64	19.93	11.07	6.47	12.93
	350–2,000	1.73–3.00	7.15	5.45	29.46	16.45	2.93	6.21
	2,000–2,500	2.79–3.85	1.09	3.16	29.66	21.66	2.04	3.11
	2,500–3,000	3.22–4.59	0.24	2.00	31.03	22.72	1.46	2.24
	3,000–3,500	2.88–3.38	0.12	1.55	39.54	27.87	1.09	1.85
RSR (threatened)	0–350	0.78–1.07	3.85	11.70	21.59	10.88	5.89	13.29
	350–2,000	1.07–2.53	5.95	5.76	30.71	17.06	3.09	6.66
	2,000–2,500	2.37–3.46	0.91	3.53	32.71	22.52	2.29	3.82
	2,500–3,000	2.51–4.31	0.21	2.32	34.78	24.72	1.65	2.68
	3,000–3,500	2.24–2.49	0.11	1.59	41.54	29.78	1.14	1.91

Supplementary Table A.4 *Summary of mountain forest loss in RSR (threatened) biodiversity hotspots from 2000 to 2018 for countries (ranking by the total area of forest loss). Here we specifically calculated each country's statistics in the RSR (threatened) hotspots because we particularly focus on threatened species with narrow range, facing a high risk of extinction. Relative forest loss is the percent forest loss relative to forest cover in the baseline year 2000. Acceleration is estimated using Theil–Sen regression of the time series of annual mountain forest loss per country. Drivers are obtained from the results by Curtis et al. (2018). The numbers underlined represent the primary drivers of forest loss in mountains in the corresponding country (>50%), but if no driver exceeds 50% the top two drivers are marked. In total, 84 countries have detectable values. Countries not listed below either are not in the biodiversity hotspot criteria or have no detectable forest or forest loss.*

Country	Forest area in 2000 (ha)	Total forest loss 2001–2018 (ha)	Relative forest loss 2001–2018 (%)	Forest loss acceleration (ha yr^{-2})	Drivers (%)					
					C	S	F	W	U	O
Indonesia	22905665	1617314	7.06	4849.38	60.52	31.45	4.43	0	0.77	2.82
Malaysia	7127183	950964	13.34	3196.33	78.76	7.21	12.83	0	0.15	1.05
Madagascar	4905203	754346	15.38	4253.05	0.68	98.41	0.39	0	0	0.51
Vietnam	5831585	709553	12.17	4144.16	61.75	16.66	19.44	0	1.32	0.83
Colombia	17708975	690113	3.90	217.29	0.39	90.46	3.73	0.02	1.81	3.60
Peru	13027091	620724	4.76	1309.72	0.83	93.27	0.29	0.10	0	5.52
China	12419292	431670	3.48	1451.36	5.21	1.43	86.09	0.19	0.66	6.42
Philippines	7712977	420163	5.45	1473.84	39.25	49.40	8.19	0	0.67	2.50

Brazil	5871398	367851	6.27	1062.36	1.17	63.34	32.70	0.01	0.29	2.48
Chile	1030526	355354	34.48	353.28	1.73	1.15	96.74	0	0.11	0.27
D.R. Congo	3871003	320365	8.28	1855.68	0	98.84	0	0	0.24	0.92
South Africa	1155818	320316	27.71	380.94	1.16	17.19	80.47	0.05	0.34	0.79
Mexico	9545377	300330	3.15	1006.03	1.47	75.25	0.58	13.47	0.95	8.29
Laos	3462507	299514	8.65	1856.30	36.15	27.69	34.88	0	0	1.28
Ecuador	9331215	272172	2.92	259.02	0.12	90.03	3.43	0	1.03	5.39
India	5355761	236904	4.42	1141.75	1.98	1.69	91.35	0	1.11	3.88
Australia	3639937	232947	6.40	574.80	0.73	0.22	63.16	32.12	0.55	3.21
Venezuela	4483051	147792	3.30	82.62	0	94.62	0	0.27	0.53	4.59
Zimbabwe	492824	136194	27.64	404.10	0	24.07	75.70	0	0	0.22
Thailand	2862147	135350	4.73	506.93	31.51	20.84	44.78	0	0	2.87
Dominican Republic	1339935	129982	9.70	167.75	16.98	76.30	5.09	0	1.41	0.22
United States	1418700	125836	8.87	679.40	10.59	1.19	49.96	27.52	5.97	4.77
Tanzania	1744167	120348	6.90	378.47	0.93	88.43	6.52	0	0	4.12
Guinea	457656	113465	24.79	1107.99	5.50	92.02	0.20	2.24	0	0.05

Guatemala	1190299	112248	9.43	270.18	0	75.64	8.47	15.48	0	0.41
Honduras	880017	97088	11.03	285.07	19.91	75.29	0.58	3.26	0.26	0.70
Costa Rica	2289535	91415	3.99	-50.61	0	91.81	1.85	1.40	2.30	2.63
Myanmar	1613542	66917	4.15	267.38	43.01	29.55	23.72	0	0	3.72
Papua New Guinea	3074803	66516	2.16	247.49	5.17	58.48	19.64	8.98	0.20	7.53
Panama	2208172	66466	3.01	99.34	0	96.11	0.22	0	0	3.67
Ethiopia	1093271	64467	5.90	229.39	0	85.42	2.58	0	0.29	11.71
Bolivia	2505084	63136	2.52	150.23	6.64	81.32	0	0	0	12.04
Japan	1841570	61922	3.36	153.04	0	0	95.71	0.41	0	3.88
Cameroon	2765262	55875	2.02	218.87	2.16	90.31	0.13	0	0	7.40
Mozambique	332070	40936	12.33	134.85	0	86.11	13.60	0	0	0.30
Angola	465189	40617	8.73	190.91	0	99.13	0.27	0	0	0.60
Haiti	508699	38798	7.63	85.44	0	93.82	0	0	1.45	4.73
Sri Lanka	1288684	35919	2.79	146.94	0.19	0.61	73.96	0	23.67	1.57
Cambodia	902999	30365	3.36	191.73	68.49	13.06	13.16	0	0	5.29
Canada	198711	29720	14.96	18.19	0	0	98.30	0.63	0	1.07

Rwanda	374899	28763	7.67	169.88	1.95	78.80	1.05	0	13.43	4.78
Spain	519847	26955	5.19	146.59	0	0	88.38	5.96	0	5.66
New Zealand	832838	25715	3.09	24.85	4.40	0	52.49	11.71	21.11	10.29
Côte d'Ivoire	104802	23633	22.55	186.45	0	100	0	0	0	0
Uganda	401392	21583	5.38	84.08	0.03	91.74	0	0	4.89	3.34
Nigeria	432662	16900	3.91	42.87	0	96.24	0	0	0	3.76
Cuba	356060	13841	3.89	-9.69	0	95.58	3.75	0	0	0.68
Malawi	244418	12256	5.01	7.09	0	87.61	6.57	0	0	5.82
Jamaica	194070	11612	5.98	-0.73	0	99.59	0	0	0	0.41
Kenya	290461	11415	3.93	38.10	11.47	43.62	26.16	0	0	18.76
Belize	346904	11408	3.29	-22.78	1.02	96.09	0	0	0	2.89
Burundi	113757	9460	8.32	57.53	0	93.89	0	0	5.20	0.90
Italy	254342	7747	3.05	22.28	0	0	91.79	0	0	8.21
Nicaragua	84088	4807	5.72	18.42	5.07	94.79	0	0	0	0.14
Bhutan	511175	3929	0.77	14.94	49.30	0	14.30	5.65	0	30.75
France	69357	3835	5.53	-1.79	0	0	96.69	0.03	0	3.28
Russia	158977	3425	2.15	-0.01	0	5.95	75.16	6.06	0	12.83

Argentina	809797	3140	0.39	8.29	0.14	31.43	0	2.56	0	65.87
South Korea	53334	3123	5.86	6.04	0	0	47.09	0	50.46	2.45
Trinidad and Tobago	74998	1558	2.08	-0.49	0	85.12	0	0	0	14.88
Portugal	13707	1538	11.22	-0.51	0	0	94.48	0	0	5.52
El Salvador	43156	1367	3.17	-0.63	0	98.69	1.31	0	0	0
Greece	12522	1334	10.65	2.54	0	0	66.88	0	0	33.12
Croatia	14688	1295	8.82	0.46	0	0	39.15	52.30	0	8.55
Algeria	18258	1269	6.95	4.39	0	89.96	4.29	0	5.68	0.07
Turkey	13181	1189	9.02	-0.44	0	0	94.36	0	0	5.64
Nepal	88648	759	0.86	-1.09	8.36	0	62.90	0	0	28.74
Guyana	84857	507	0.60	2.75	0	76.81	0	0	0	23.19
Georgia	149621	408	0.27	0.18	0	0	8.05	0	0	91.95
Brunei	49804	391	0.79	2.15	70.14	0.41	20.32	0	0	9.13
Montenegro	16986	308	1.82	0.45	0	0	25.79	0	0	74.21
Austria	1273	114	8.99	-0.26	0	0	100	0	0	0
Zambia	4663	96	2.07	0.54	0	99.63	0	0	0	0.37

Albania	2956	81	2.73	-0.08	0	0	53.83	0	0	46.17
Kazakhstan	10404	78	0.75	-0.13	0	0	0	0	0	100
North Korea	3038	49	1.60	-0.16	0	0	60.65	0	0	39.35
Israel	1266	41	3.20	0.06	0	0	0	0	10.54	89.46
Armenia	2535	33	1.29	-0.03	0	0	0	0	0	100
Kyrgyzstan	231	24	10.55	-0.07	0	68.41	0	0	0	31.59
Mongolia	23	7	30.10	-0.05	0	0	0	0	0	100
Iran	1957	6	0.33	-0.03	0	0	0	0	0	100
Lebanon	671	5	0.71	0	0	0	0	0	0	100
Uzbekistan	329	2	0.54	0	0	0	0	0	0	100
Morocco	8	1	8.70	0	0	0	0	0	0	100
all	**177620863**	**11027982**	**6.21**	**36630.09**	**23.45**	**47.44**	**23.49**	**1.88**	**0.82**	**2.92**

C: Commodity agriculture; S: Shifting cultivation; F: Forestry; W: Wildfire; U: Urbanization; O: Other. “Other” are the grids that were marked as zero or minor loss by Curtis et al. (2018) at a resolution of ~10 km.

Supplementary Table A.5 *Summary of forest protection in mountain biodiversity hotspots (based on rarity-size rarity for threatened species) for countries (ranking by relative forest loss inside protected areas (PAs)). Relative forest loss is the percent forest loss relative to forest cover in the baseline year 2000. The ratio of relative forest loss inside versus outside of PAs greater than 1 was marked as an asterisk (*) after the number. Drivers are obtained from the results by Curtis et al. (2018). The numbers underlined represent the primary drivers of forest loss in mountains in the corresponding country (>50%), but if no driver exceeds 50% the top two drivers are marked. In total, 78 countries have detectable values. Countries not listed below either are not to the extent of PAs.*

Country	Fraction of forest area in PAs (%)	Fraction of forest loss in PAs (%)	Relative forest loss inside PAs (%)	Relative forest loss outside of PAs (%)	Ratio of relative forest loss inside versus outside of PAs	Drivers (%)					
						C	S	F	W	U	O
Zimbabwe	23.62	23.90	27.96	27.54	1.02 *	0	29.03	<u>70.95</u>	0	0	0.02
Côte d'Ivoire	48.78	58.24	26.93	18.38	1.46 *	0	<u>100</u>	0	0	0	0
Guinea	4.47	4.41	24.46	24.81	0.99	1.24	<u>98.76</u>	0	0	0	0
Haiti	7.96	19.15	18.36	6.70	2.74 *	0	<u>99.95</u>	0	0	0	0.05
South Africa	35.89	23.75	18.34	32.96	0.56	3.46	<u>47.59</u>	<u>47.38</u>	0.21	0	1.36
Greece	6.73	7.76	12.28	10.54	1.17 *	0	0	32.98	0	0	<u>67.02</u>
Honduras	53.77	52.85	10.84	11.25	0.96	36.33	<u>61.67</u>	0.38	0.21	0.50	0.91
Madagascar	54.54	37.76	10.65	21.06	0.51	1.29	<u>97.14</u>	0.83	0	0	0.74
Kyrgyzstan	99.85	99.76	10.54	16.67	0.63	0	<u>68.33</u>	0	0	0	31.67

Morocco	51.30	60.00	10.17	7.14	1.42 *	0	0	0	0	0	100
Portugal	57.62	47.28	9.21	13.96	0.66	0	0	99.94	0	0	0.06
Nicaragua	31.58	49.64	8.99	4.21	2.14 *	10.21	89.79	0	0	0	0
United States	15.39	15.18	8.75	8.89	0.98	16.38	0.20	14.66	60.01	6.35	2.40
Croatia	94.02	93.22	8.74	9.99	0.87	0	0	36.65	56.10	0	7.25
Mozambique	22.96	16.14	8.67	13.42	0.65	0	54.13	44.04	0	0	1.83
Dominican Republic	42.52	35.70	8.14	10.85	0.75	43.91	55.61	0.33	0	0	0.15
Guatemala	23.29	18.25	7.39	10.05	0.74	0	58.28	35.46	6.23	0	0.03
Angola	0.25	0.19	6.75	8.74	0.77	0	80.65	0	0	0	19.35
Spain	73.74	80.35	5.65	3.88	1.46 *	0	0	87.67	7.10	0	5.23
Vietnam	27.14	12.35	5.54	14.64	0.38	56.82	16.38	25.73	0	0	1.07
Ethiopia	57.24	52.90	5.45	6.50	0.84	0	91.74	1.24	0	0	7.02
D.R. Congo	25.50	16.18	5.25	9.31	0.56	0	97.22	0	0	0.07	2.71
Malawi	92.40	81.00	4.40	12.54	0.35	0	89.71	3.54	0	0	6.75
Australia	45.44	31.11	4.38	8.08	0.54	0.16	0.01	33.50	61.42	0.29	4.62
South Korea	39.11	28.31	4.24	6.89	0.61	0	0	69.60	0	30.31	0.09

Algeria	26.42	15.26	4.01	8.00	0.50	0	84.58	14.99	0	0	0.43
Tanzania	45.53	24.50	3.71	9.56	0.39	0.31	74.98	16.19	0	0	8.52
Uganda	44.72	29.26	3.52	6.88	0.51	0.05	90.39	0	0	9.40	0.15
France	69.28	43.36	3.46	10.19	0.34	0	0	96.74	0	0	3.26
Laos	30.72	11.86	3.34	11.00	0.30	30.18	44.82	22.04	0	0	2.96
Kenya	75.61	63.55	3.30	5.87	0.56	16.29	44.77	27.40	0	0	11.54
Philippines	17.80	10.56	3.23	5.93	0.55	20.40	68.78	6.67	0	1.64	2.52
Cambodia	98.63	91.69	3.13	20.37	0.15	68.19	12.66	13.59	0	0	5.55
Venezuela	80.69	75.05	3.07	4.26	0.72	0	94.51	0	0.32	0.70	4.47
Nigeria	29.00	22.42	3.02	4.27	0.71	0	92.88	0	0	0	7.12
Cuba	31.23	23.13	2.88	4.35	0.66	0	99.57	0	0	0	0.43
Russia	66.60	84.46	2.73	1.00	2.72 *	0	3.68	82.87	4.85	0	8.61
Indonesia	25.40	9.57	2.66	8.56	0.31	41.99	45.11	4.32	0	0.60	7.98
Belize	91.50	69.81	2.51	11.68	0.21	0.81	95.26	0	0	0	3.93
Burundi	44.99	12.05	2.23	13.29	0.17	0	100	0	0	0	0
El Salvador	22.28	15.33	2.18	3.45	0.63	0	91.45	8.55	0	0	0
Jamaica	30.73	10.79	2.10	7.71	0.27	0	99.62	0	0	0	0.38

Italy	46.64	32.04	2.09	3.88	0.54	0	0	94.71	0	0	5.29
Japan	27.06	16.82	2.09	3.83	0.55	0	0	95.24	1.12	0	3.64
Zambia	100.00	100.00	2.07	\	\	0	99.63	0	0	0	0.37
Colombia	20.52	10.78	2.05	4.37	0.47	0.77	82.95	3.69	0	4.27	8.33
Brazil	45.26	13.36	1.85	9.92	0.19	0.80	70.87	17.59	0.08	0.17	10.50
Bolivia	58.08	39.75	1.72	3.62	0.48	0.23	84.10	0	0	0	15.67
Myanmar	20.68	8.58	1.72	4.78	0.36	6.33	12.71	71.95	0	0	9.01
Chile	3.97	0.19	1.66	35.84	0.05	0	0.51	56.38	0	40.61	2.50
Malaysia	25.00	3.08	1.64	17.24	0.10	65.51	21.58	7.60	0	0.06	5.25
Mexico	16.80	8.16	1.53	3.47	0.44	4.11	46.06	0.51	26.82	0.18	22.32
Albania	38.98	20.69	1.45	3.55	0.41	0	0	0	0	0	100
Panama	53.86	24.50	1.37	4.93	0.28	0.01	90.05	0	0	0	9.94
Armenia	76.41	77.89	1.32	1.21	1.09 *	0	0	0	0	0	100
Thailand	70.86	18.51	1.24	13.23	0.09	12.86	38.64	39.74	0	0	8.76
Rwanda	35.51	5.39	1.17	11.26	0.10	0	82.62	0	0	10.75	6.64
Sri Lanka	17.32	7.08	1.14	3.13	0.36	0.90	2.17	74.70	0	14.33	7.91
Canada	29.42	2.07	1.05	20.75	0.05	0	0	78.10	4.58	0	17.32

China	10.51	3.05	1.01	3.77	0.27	45.32	4.21	29.57	3.40	0	17.51
Peru	25.94	5.16	0.95	6.10	0.16	1.67	76.28	0	0	0	22.05
Nepal	73.95	71.90	0.83	0.92	0.90	7.36	0	56.93	0	0	35.71
India	12.93	2.32	0.79	4.96	0.16	14.96	0.79	68.37	0	0	15.87
New Zealand	76.85	17.36	0.70	11.02	0.06	6.43	0	12.58	47.88	0.56	32.56
Ecuador	24.40	5.58	0.67	3.64	0.18	0	77.91	0.26	0	0	21.83
Costa Rica	36.92	5.85	0.63	5.96	0.11	0	78.90	0.78	0	4.74	15.58
Montenegro	51.08	16.07	0.57	3.12	0.18	0	0	0.23	0	0	99.77
Uzbekistan	99.46	100.00	0.55	\	\	0	0	0	0	0	100
Cameroon	16.17	4.02	0.50	2.31	0.22	0	76.39	0	0	0	23.61
Papua New Guinea	0.53	0.12	0.49	2.17	0.23	0	86.04	1.58	0	0	12.39
Bhutan	60.26	36.90	0.47	1.22	0.39	43.26	0.01	8.48	0	0	48.26
Kazakhstan	81.59	48.89	0.45	2.08	0.22	0	0	0	0	0	100
Argentina	68.75	64.58	0.36	0.44	0.83	0.01	36.06	0	0.69	0	63.24
Iran	3.73	3.23	0.28	0.33	0.86	0	0	0	0	0	100
Guyana	1.35	0.58	0.26	0.60	0.42	0	0	0	0	0	100

Trinidad and Tobago	14.61	1.57	0.22	2.39	0.09	0	44.64	0	0	0	55.36
Georgia	15.96	12.75	0.22	0.28	0.77	0	0	0	0	0	100
Brunei	80.29	7.00	0.07	3.71	0.02	42.07	5.18	10.36	0	0	42.39

\ means forest and forest loss within hotspots are all within the extent of PA, so there is no value outside of PA.

C: Commodity agriculture; S: Shifting cultivation; F: Forestry; W: Wildfire; U: Urbanization; O: Other. “Other” are the grids that were marked as zero or minor loss by Curtis et al. (2018) at a resolution of ~10 km.

Supplementary Table A.6 *Mean relative acceleration of forest loss from 2001 to 2018 in countries with different drivers where those drivers contribute less than 25% or more than 75% of the forest loss. For example, the average relative acceleration is a factor of 5.41 in countries where commodity agriculture and shifting cultivation are the dominant drivers (i.e., the sum of the proportion of loss driven by commodity agriculture and shifting cultivation is >75%). Relative acceleration (units: % yr^{-1}) was calculated as acceleration divided by mean forest loss multiplied by 100%.*

Drivers	<25%	>75%
Commodity agriculture	2.77	6.52
Shifting cultivation	2.16	5.01
Forestry	3.37	3.00
Wildfire	3.29	-1.55
Commodity agriculture + Shifting cultivation	1.40	5.41

Figures

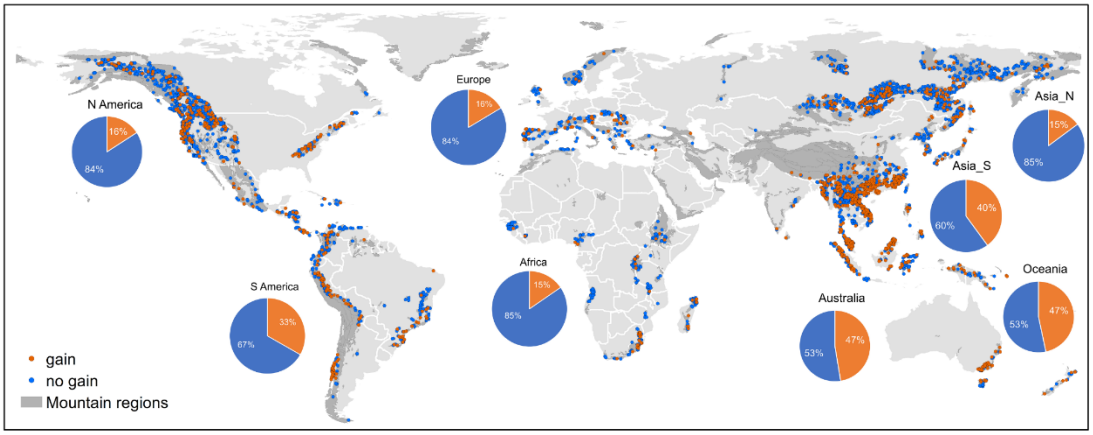

Supplementary Figure A.1 *Location of forest gain/no gain in 2019 in 5,000 randomly-sampled pixels where forest was lost between 2001 and 2018 in mountain regions. The information on forest gain or not around 2019 (i.e., 2017–2021) is visually interpreted from very-high-resolution satellite imagery from Google Earth or Planet. The pie chart next to the continent shows the proportion of forest gain (orange) in the region. As there is a big difference in climate and drivers of forest loss between north and south Asia, we divided Asia into two parts, bounded by 30°N.*

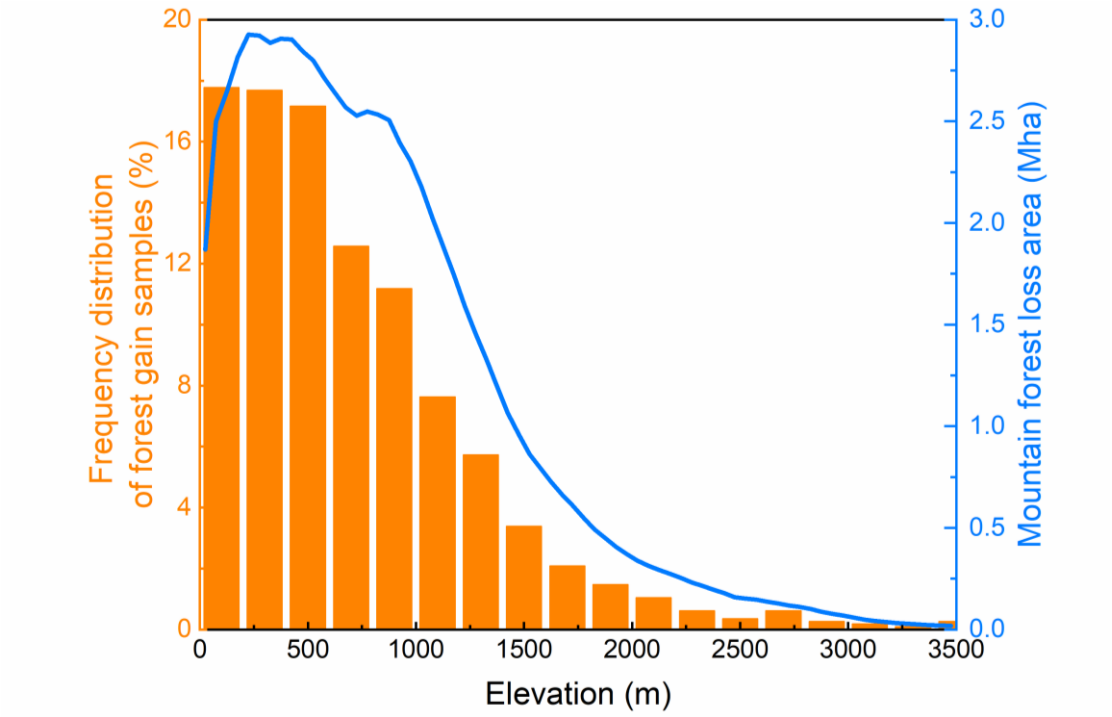

Supplementary Figure A.2 *Elevational patterns of forest loss area and forest gain frequency distribution in mountain ranges. The histogram is based on the frequency of the elevation of 1,157 gain pixels in 5,000 samples (the cumulative value equals 100%).*

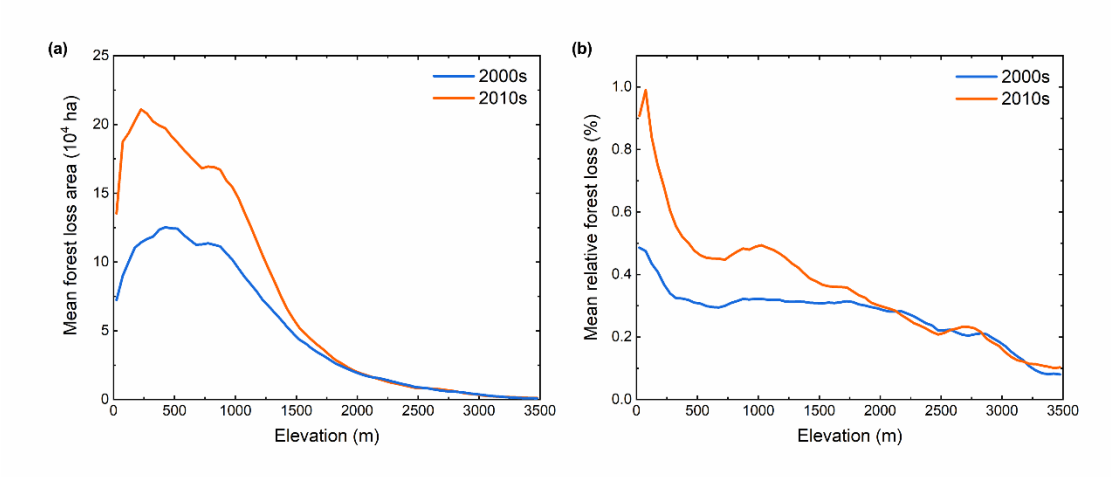

Supplementary Figure A.3 *Elevational distributions of mean annual forest loss across mountain regions in the 2000s (2001–2009) and 2010s (2010–2018). (a) Absolute forest loss area. (b) Relative forest loss. Relative forest loss is calculated based on forest cover in the baseline year 2000 within that elevation bin.*

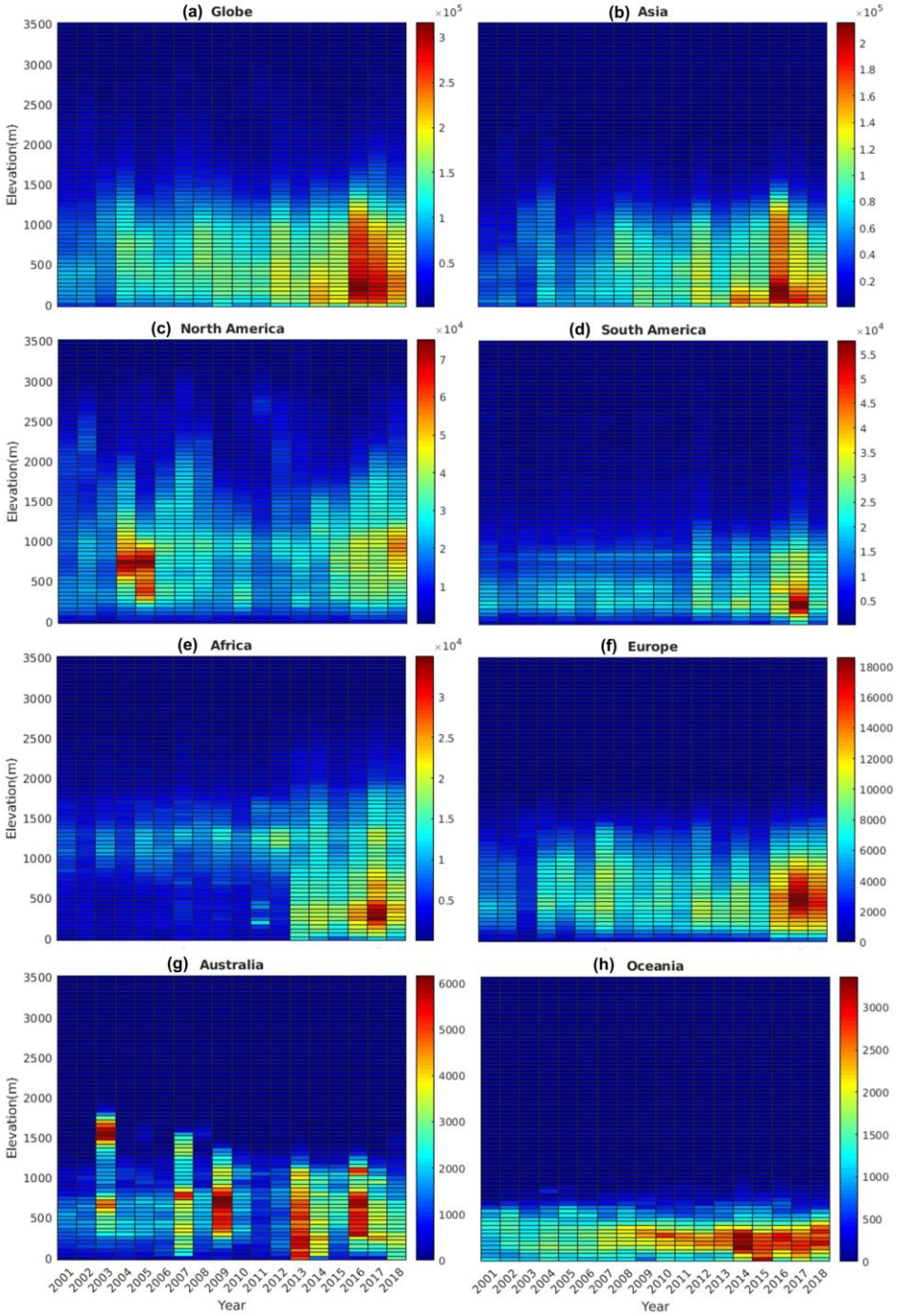

Supplementary Figure A.4 *Temporal patterns in the elevation of annual mountain forest loss during 2001–2018 on (a) worldwide and (b–h) continental scales. Colour bars represent the area of forest loss (unit: hectare). Forest loss area for elevations above the highest value of the y-axis is included in the top bin of elevation for each graph. Note that scales of colour bars on the right differ among panels to optimise data visibility.*

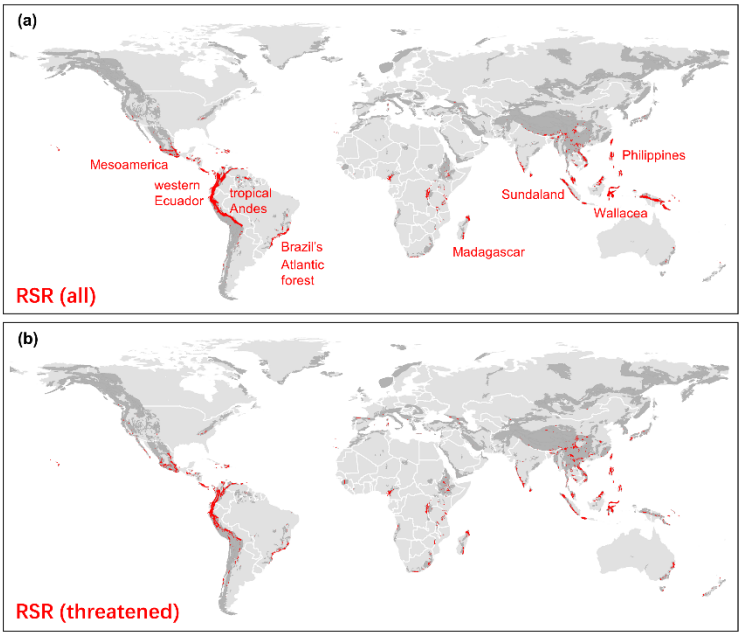

Supplementary Figure A.5 *The distributions of range-size rarity (RSR) hotspots based on (a) all species and (b) threatened species. For each species pool, hotspots shown are determined as the upper 2.5% of the total grid area, i.e., the cells with the highest RSR values. Dark grey shading shows mountain areas outside of hotspots with lower RSR. Our mapping hotspots align closely with the 25 hotspots proposed by Myers et al. (2000), which identified hotspots based on species endemism and degree of threat for both plants and vertebrates.*

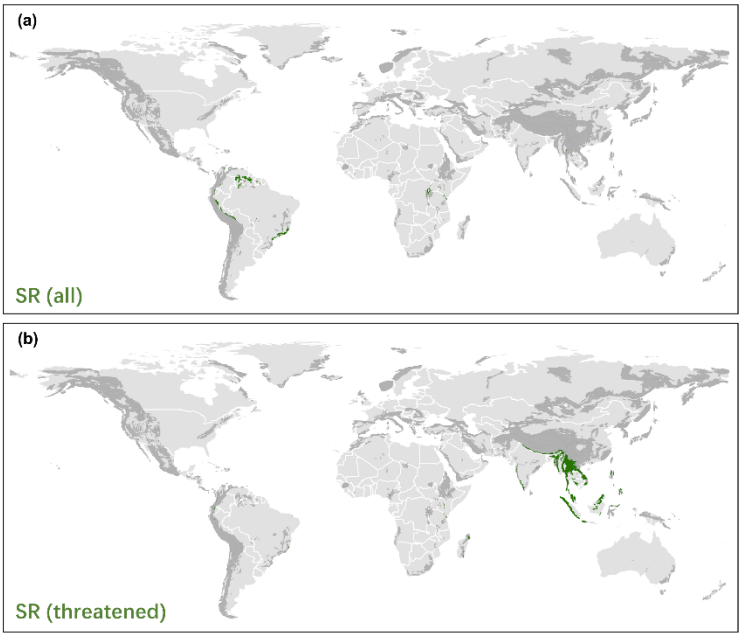

Supplementary Figure A.6 *The distributions of species richness (SR) hotspots based on (a) all species and (b) threatened species.*

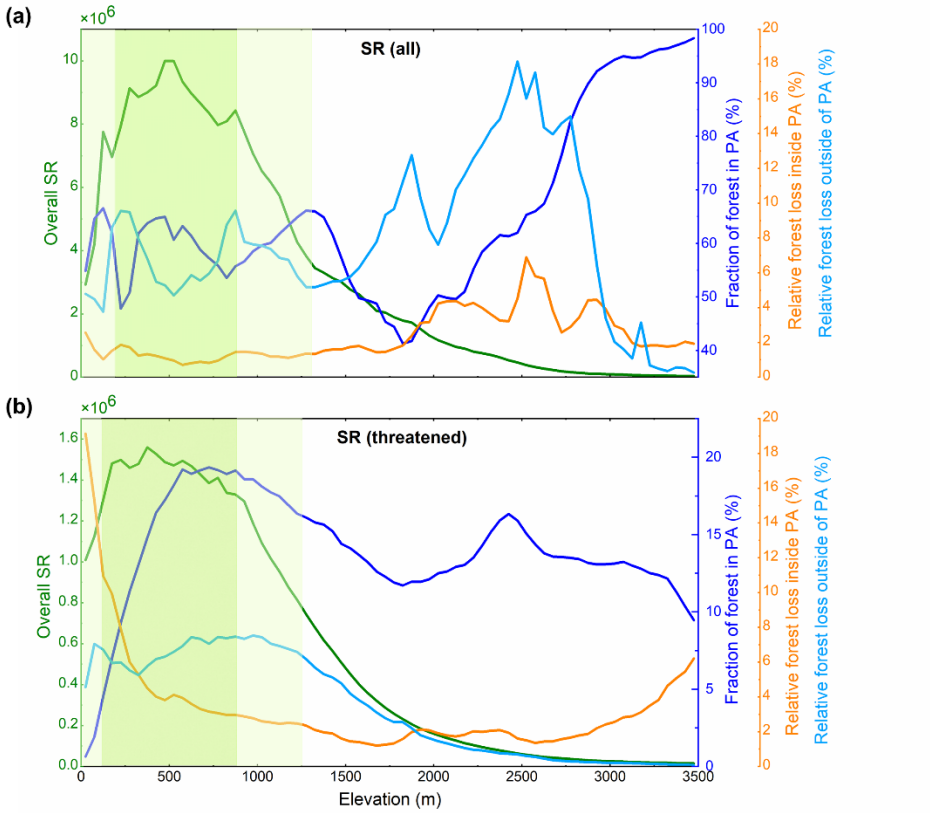

Supplementary Figure A.7 *Elevational gradients of species richness (SR), protected area (PA) coverage, and mountain forest loss inside and outside of PA within biodiversity hotspots. Note that y-axis scales in (a) and (b) differ between panels to optimise data visibility. Different from the RSR metric, the highest SR values are located in low-elevation mountainous areas, particularly in the range of about 250 to 850 m for all species (a), and 150 to 850 m for threatened species (b).*

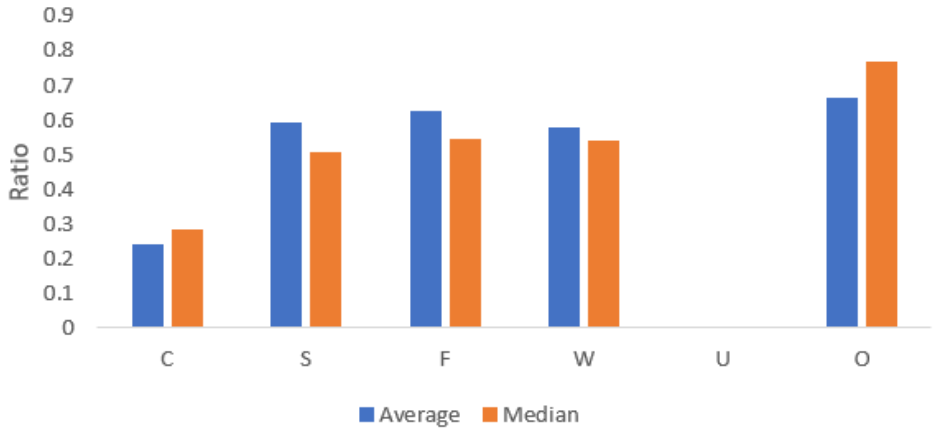

Supplementary Figure A.8 *Relationship between protected area (PA) effectiveness (ratio of relative forest loss inside PA versus outside of PA) and driver of mountain forest loss within range-size rarity hotspots for threatened species. The ratio with a lower number indicates the PA is more effective. Drivers are obtained from the results by Curtis et al. (2018). C: Commodity-driven deforestation; S: Shifting cultivation; F: Forestry; W: Wildfire; U: Urbanization; O: Others. Others are the grids that were marked as zero or minor loss by Curtis et al. (2018) at a resolution of ~10 km.*

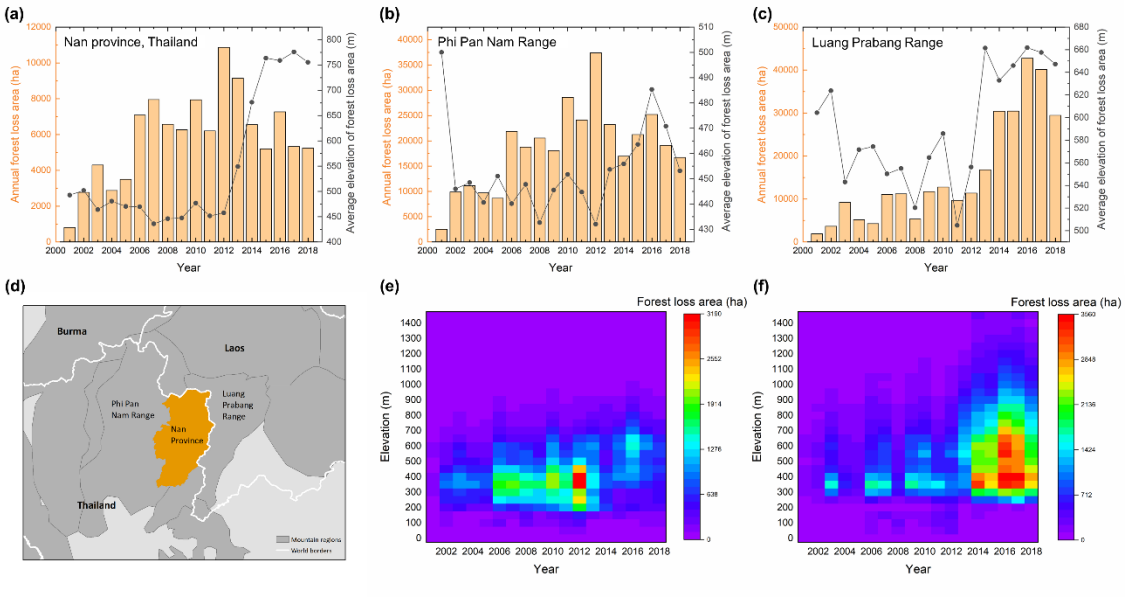

Supplementary Figure A.9 *An example of within-region differences in mountain forest loss. (a) Time series of annual forest loss area and average elevation of forest area in Nan Province, Thailand. (b, c) Time series of annual forest loss area and average elevation of forest area in two nearby mountains, Phi Pan Nam Range (Thailand) and Luang Prabang Range (Laos), respectively. (d) Location of Nan Province and its surrounding mountain regions. Mountain forest loss trends in elevation-year space during 2001–2018 in (e) Phi Pan Nam Range and (f) Luang Prabang Range.*

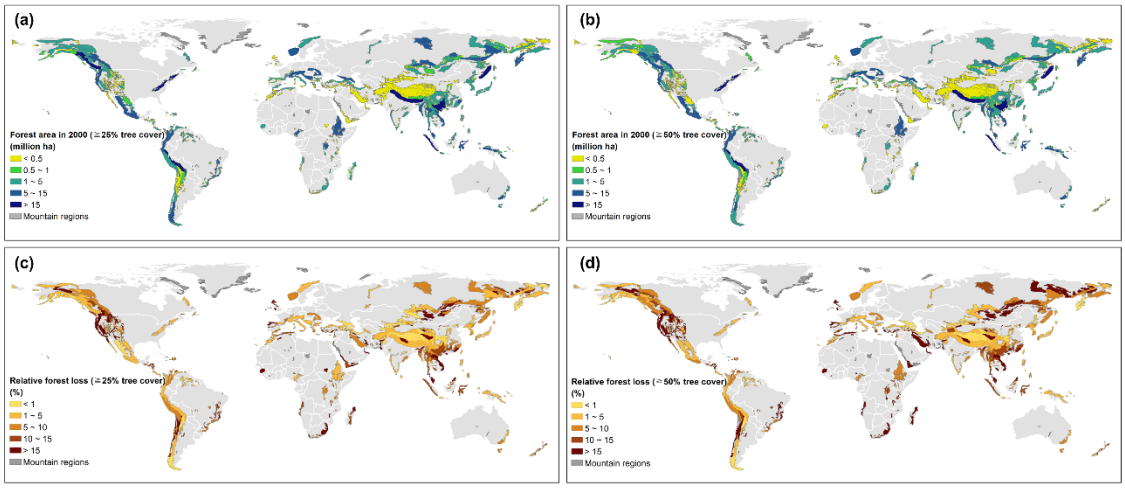

Supplementary Figure A.10 *Spatial patterns of mountain forest area and relative mountain forest loss using tree cover thresholds of 25% and 50% for each mountain range. (a, b) Mountain forest area in 2000 for the 25% and 50% thresholds. (c, d) Relative mountain forest loss occurred between 2001 and 2018 for the two thresholds. Mountain regions in dark grey show mountain forest area (top panels) or relative mountain forest loss (bottom panels) equals zero.*

References

Curtis, P.G., Slay, C.M., Harris, N.L., Tyukavina, A. and Hansen, M.C., 2018. Classifying drivers of global forest loss. Science, 361, 1108–1111.

Myers, N., Mittermeier, R.A., Mittermeier, C.G., da Fonseca, G.A. and Kent, J., 2000. Biodiversity hotspots for conservation priorities. Nature, 403, 853–858.

Appendix B

Supplementary materials for Chapter 3

Figures

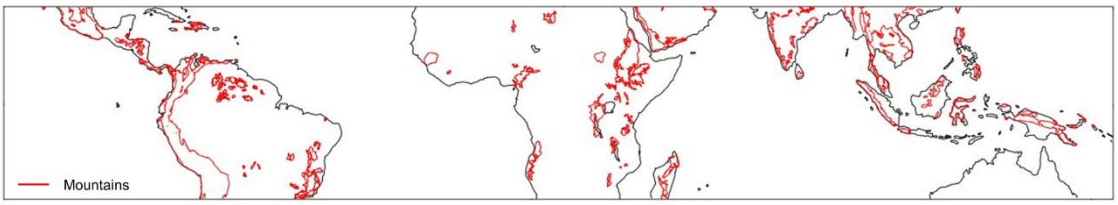

Supplementary Figure B.1 *Mountain extent in the tropics. Red boundaries indicate mountain regions defined by Global Mountain Biodiversity Assessment (GMBA) inventory data.*

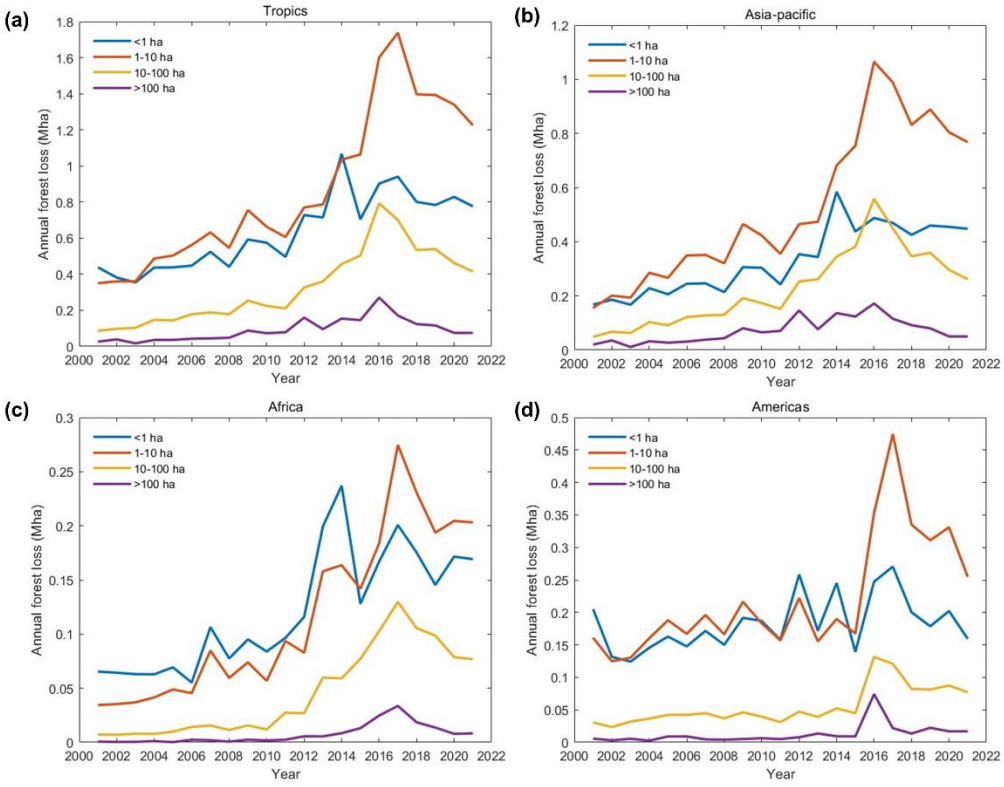

Supplementary Figure B.2 *Time series of mountain forest loss area of different patch sizes for the tropics (a) and by region (b–d).*

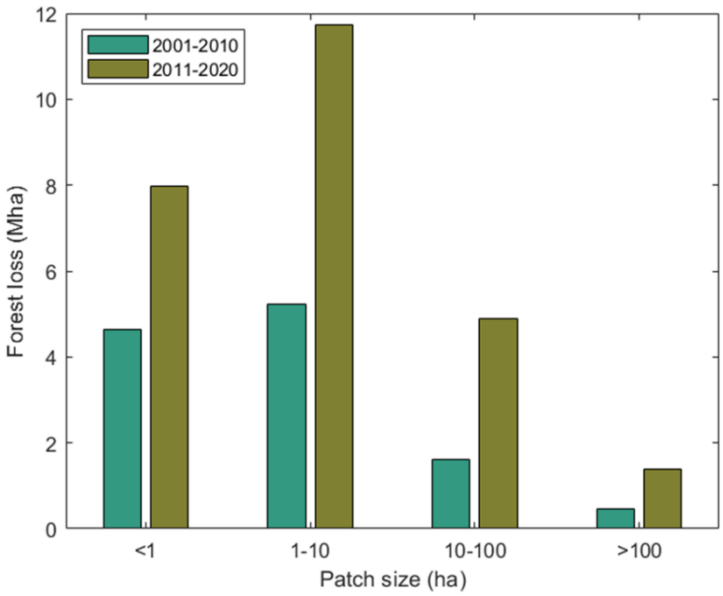

Supplementary Figure B.3 *Change in forest loss area (Mha) of different size categories between 2001–2010 and 2011–2020 across tropical mountains.*

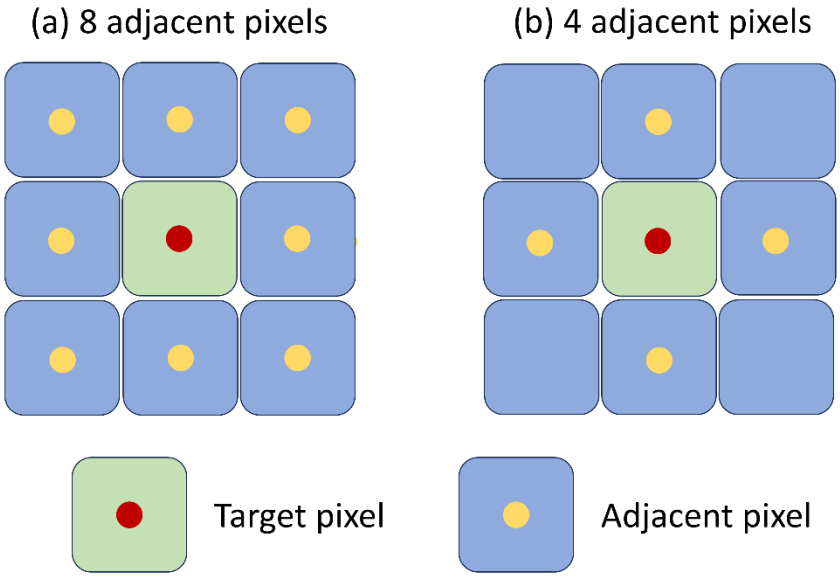

Supplementary Figure B.4 *Neighbour sampling of (a) eight or (b) four adjacent pixels.*

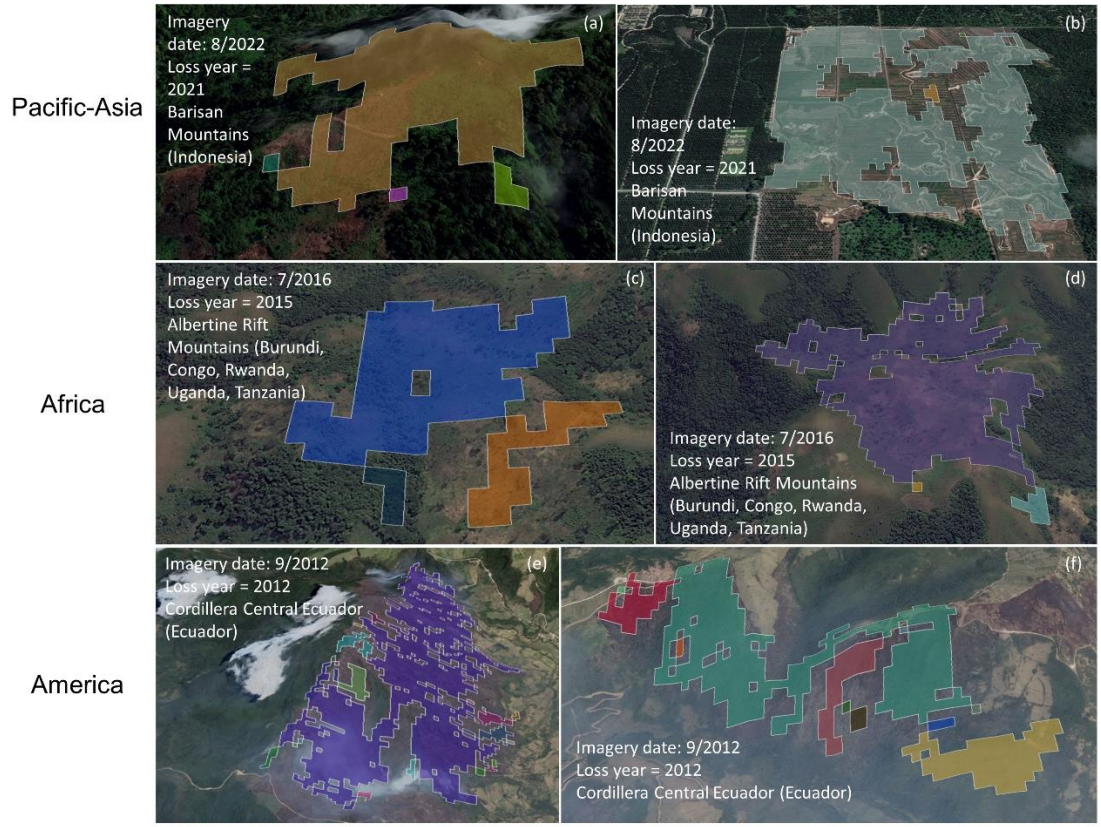

Supplementary Figure B.5 *Examples of visual interpretation of forest loss patches using Google Earth images for different continents. The utilization of different colours signifies potential variations when employing four adjacent pixels, indicating that they might be distinct patches under such conditions.*

Appendix C

Supplementary materials for Chapter 4

Tables

Supplementary Table C.1 *List of in situ measured treeline sites from literature.*

Number	Latitude	Longitude	Elevation (m)	Reference
1	53.10	-120.10	2,300	Jobbágy and Jackson (2000)
2	48.90	-113.80	2,100	Jobbágy and Jackson (2000)
3	43.60	-110.90	3,300	Jobbágy and Jackson (2000)
4	48.80	-121.70	1,600	Jobbágy and Jackson (2000)
5	47.80	-123.50	1,550	Jobbágy and Jackson (2000)
6	46.90	-121.70	2,000	Jobbágy and Jackson (2000)
7	45.30	-121.70	2,200	Jobbágy and Jackson (2000)
8	41.30	-122.10	2,600	Jobbágy and Jackson (2000)
9	49.30	20.00	1,730	Jobbágy and Jackson (2000)
10	56.00	114.00	1,550	Jobbágy and Jackson (2000)
11	54.00	108.00	1,500	Jobbágy and Jackson (2000)
12	49.00	138.00	1,100	Jobbágy and Jackson (2000)
13	36.00	138.30	2,500	Jobbágy and Jackson (2000)
14	-42.10	171.60	1,200	Jobbágy and Jackson (2000)
15	-42.10	172.10	1,250	Jobbágy and Jackson (2000)
16	-5.67	145.02	3,800	Körner and Paulsen (2004)
17	-3.08	37.33	3,800	Körner and Paulsen (2004)
18	-36.43	148.33	2,000	Körner and Paulsen (2004)
19	-36.43	148.33	2,000	Körner and Paulsen (2004)
20	-39.17	175.85	1,350	Körner and Paulsen (2004)

21	-42.33	172.08	1,220	Körner and Paulsen (2004)
22	53.25	-132.48	888	Irl et al. (2016)
23	49.66	-125.76	1,717	Irl et al. (2016)
24	43.64	142.86	1,533	Irl et al. (2016)
25	37.77	14.97	2,187	Irl et al. (2016)
26	35.35	138.72	2,750	Irl et al. (2016)
27	28.73	-17.90	2,195	Irl et al. (2016)
28	23.47	120.96	3,721	Irl et al. (2016)
29	20.70	-156.28	2,706	Irl et al. (2016)
30	16.59	120.91	2,760	Irl et al. (2016)
31	6.98	125.27	2,293	Irl et al. (2016)
32	6.07	116.56	3,922	Irl et al. (2016)
33	-1.69	101.26	3,323	Irl et al. (2016)
34	-4.03	137.12	4,061	Irl et al. (2016)
35	-41.88	146.04	1,252	Irl et al. (2016)
36	-44.66	-73.70	1,022	Irl et al. (2016)
37	48.91	-113.65	1,996	Lu et al. (2021)
38	48.91	-113.65	1,983	Lu et al. (2021)
39	48.91	-113.65	1,981	Lu et al. (2021)
40	48.91	-113.65	1,980	Lu et al. (2021)
41	48.91	-113.65	2,000	Lu et al. (2021)
42	33.95	107.61	3,100	Lu et al. (2021)
43	33.95	107.61	3,100	Lu et al. (2021)
44	33.95	107.61	3,200	Lu et al. (2021)
45	33.95	107.61	3,200	Lu et al. (2021)
46	41.99	127.99	2,194	Lu et al. (2021)
47	41.30	-106.30	3,349	Lu et al. (2021)

48	41.30	-106.30	3,304	Lu et al. (2021)
49	44.30	-107.00	3,090	Lu et al. (2021)
50	44.30	-107.00	2,889	Lu et al. (2021)
51	54.53	58.85	1,330	Lu et al. (2021)
52	40.84	-110.32	3,415	Lu et al. (2021)
53	40.85	-110.49	3,354	Lu et al. (2021)
54	40.85	-110.49	3,430	Lu et al. (2021)
55	40.85	-110.51	3,384	Lu et al. (2021)
56	40.85	-110.51	3,354	Lu et al. (2021)
57	33.95	107.61	3,400	Lu et al. (2021)
58	33.95	107.61	3,400	Lu et al. (2021)
59	33.95	107.61	3,400	Lu et al. (2021)
60	33.95	107.61	2,850	Lu et al. (2021)
61	33.95	107.61	2,850	Lu et al. (2021)
62	33.95	107.61	2,850	Lu et al. (2021)

Supplementary Table C.2 *List of treeline changes from literature.*

Number	Mean treeline shift rate (m/yr)	Method	Study period	Region	Reference
1	0.11	Field	1865–2015	Temperate	Sigdel et al. (2018)
2	10.7	Satellite	1970–2006	Temperate	Singh et al. (2012)
3	0.74	Meta /review	1915–2010	Mixed /hemispherical	Cudlín et al. (2017)
4	2.88	Combined	1968–2020	Boreal	Cazzolla Gatti et al. (2019)
5	0.28	Field	1865–2015	Temperate	Sigdel et al. (2020)
6	0.354	Meta /review	1901–2018	Mixed /hemispherical	Lu et al. (2021)
7	6.6	Aircraft	1960–2020	Temperate	Zindros et al. (2020)
8	0.5	Field	1855–2015	Temperate	Du et al. (2018)
9	2.61	Field	1850–2010	Temperate	Gaire et al. (2014)
10	0.8	Field	1915–2007	Boreal	Kullman (2010)
11	2.6 (3.5)	Field	2000–2009 (2010–2013)	Temperate	Leonelli et al. (2016)
12	1.15 (1.25)	Field	1901–2000	Temperate	Leonelli et al. (2011)

			(2000–2008)		
13	0.6	Aircraft	1965–2010	Boreal	Hagedorn et al. (2014)
14	0.8	Aircraft	1956–2006	Temperate	Ameztegui et al. (2016)
15	0.29	Field	1910–2010	Temperate	Liang et al. (2016)
16	2.435	Combined	1962–2005	Temperate	Beckage et al. (2008)
17	1.5	Combined	1960–2002	Boreal	Kharuk et al. (2010)
18	0.4	Field	1900–2000	Boreal	Kirdyanov et al. (2012)
19	17.3	Satellite	1986–2018	Tropical	Jiménez-García et al. (2021)
20	2.17	Aircraft	1963–2016	Tropical	Morley et al. (2020)
21	0.55	Combined	1958–2007	Boreal	Mathisen et al. (2014)
22	0.2	Combined	1912–2010	Boreal	Van Bogaert et al. (2021)

Figures

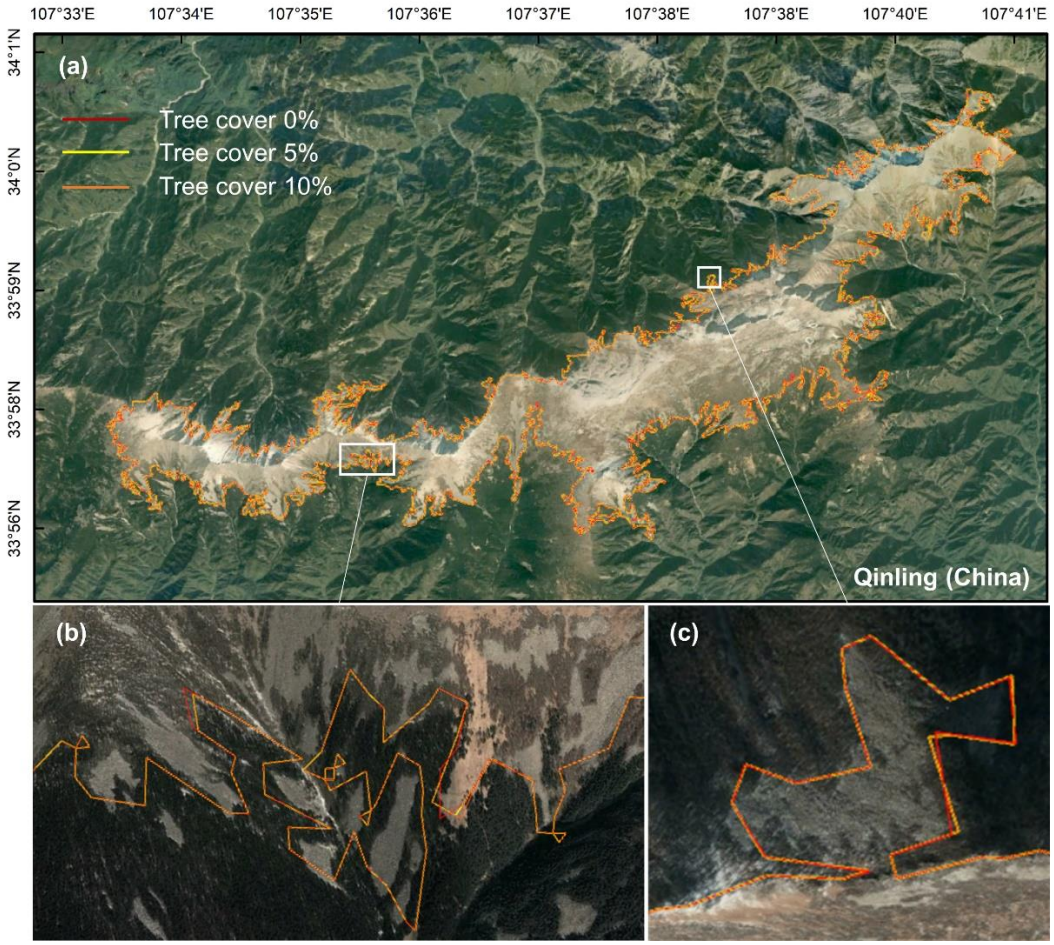

Supplementary Figure C.1 *An example in Asia illustrating the difference in tree cover thresholds (0%, 5%, and 10%) to map the alpine treeline. (b) and (c) are enlargements of the indicated frame. The background images are from Google Earth.*

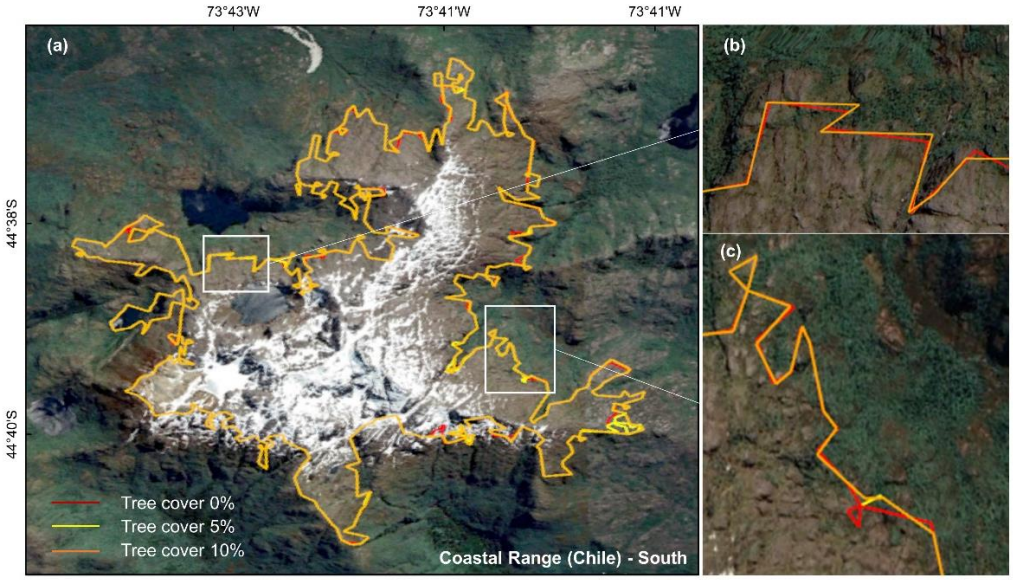

Supplementary Figure C.2 *Same as Supplementary Figure C.1, but with another example in South America.*

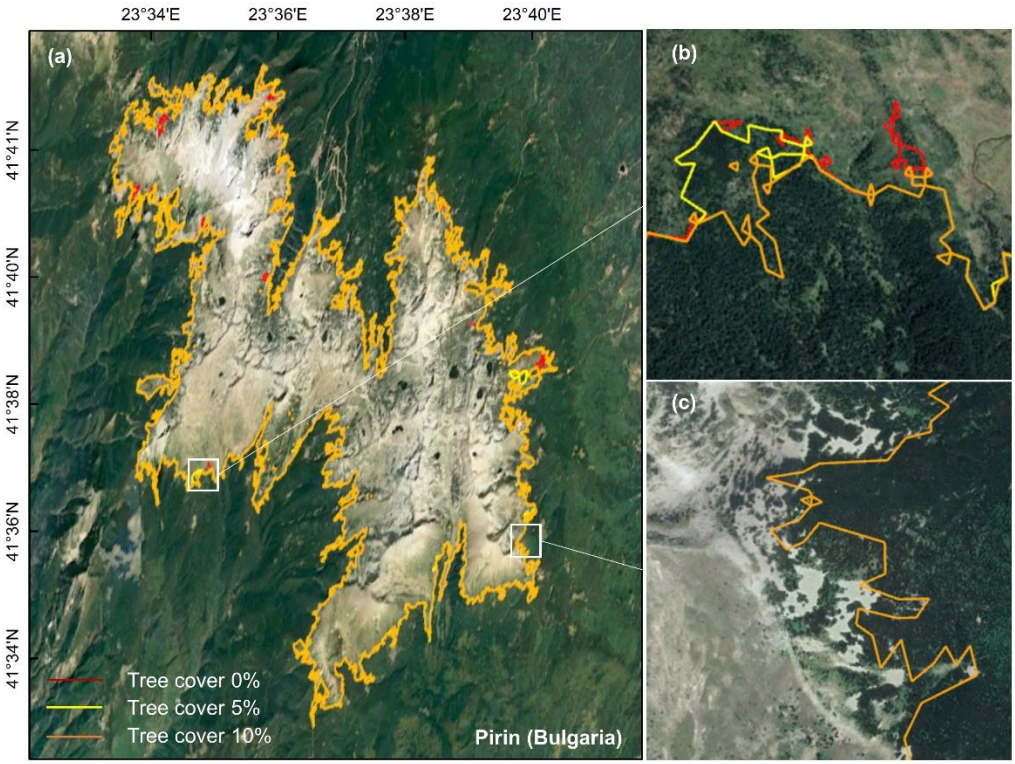

Supplementary Figure C.3 *Same as Supplementary Figure C.1, but with another example in Europe.*

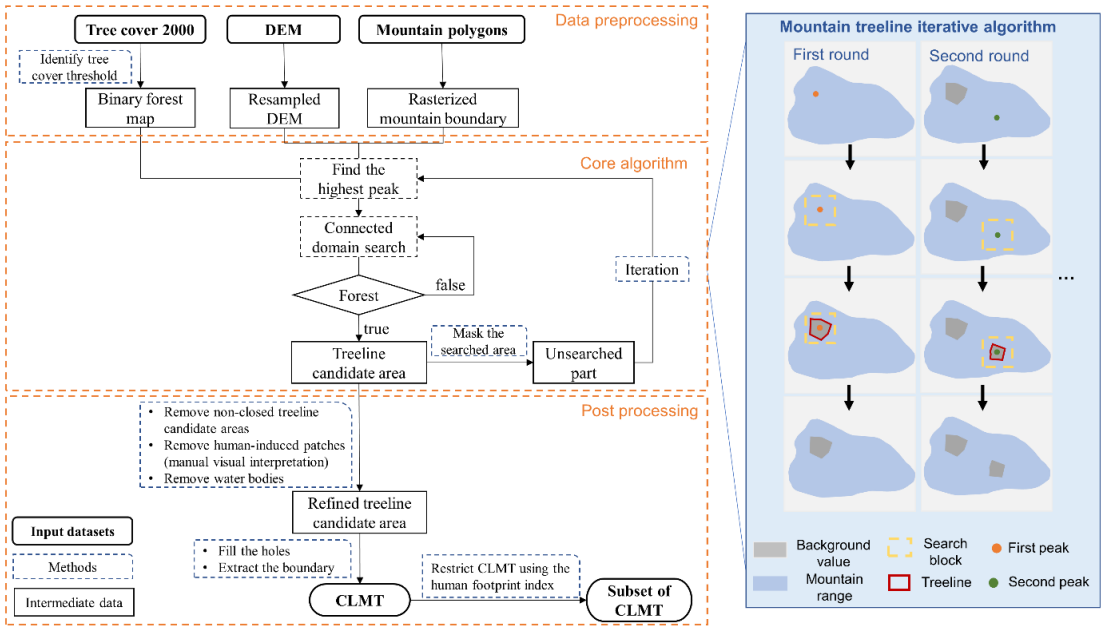

Supplementary Figure C.4 *A schematic diagram of the full procedure for delineating the closed-loop mountain treeline (CLMT). The orange dashed box indicates the processing procedure. The blue subplot illustrates how the mountain treeline iterative algorithm works.*

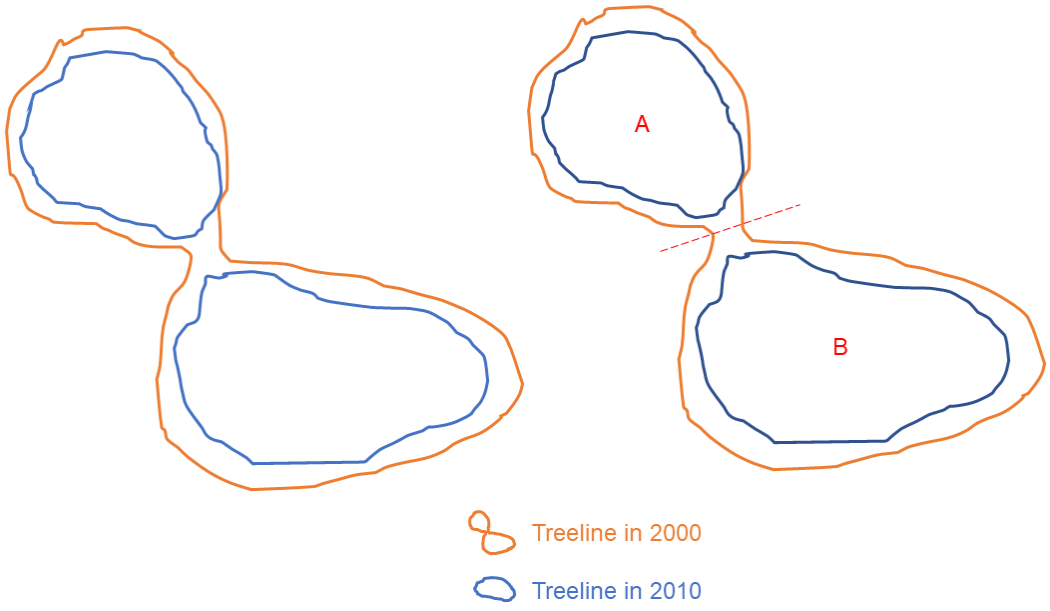

Supplementary Figure C.5 *Sketch map showing the process of "broken treeline loops". We split the treeline in 2000 into two corresponding parts according to the 2010 treeline and then calculate the treeline shift rate of parts A and B, respectively.*

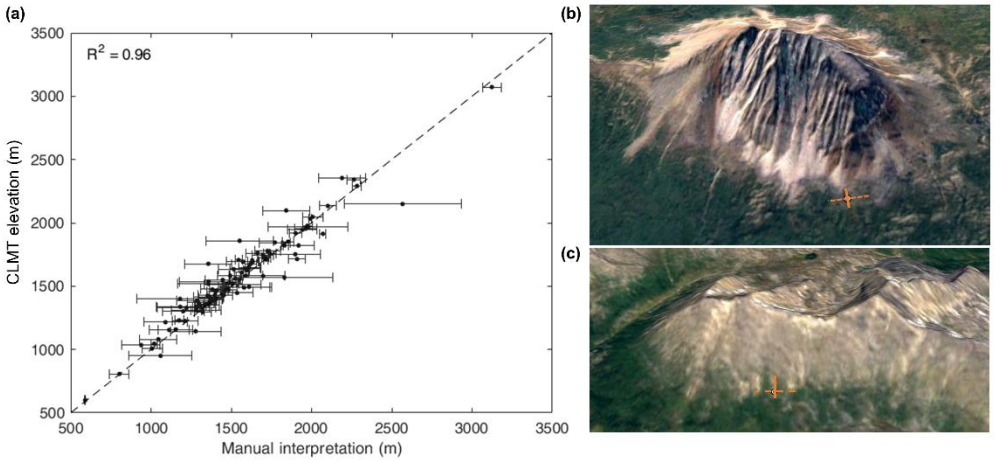

Supplementary Figure C.6 *Validation of CLMT at the pixel level using manual interpretation from Google Earth high-resolution images. (a) The relationship of CLMT elevation detected by our study with manually interpreted treelines, with the 1:1 line (dashed). The error bar shows the upper and lower elevations of the interpreted treelines in Google Earth. The black dot shows the mean elevational range of these treelines. (b, c) Representative examples of Google Earth imagery around the treeline pixel. The ends of the solid orange line represent the upper and lower points through manual interpretation.*

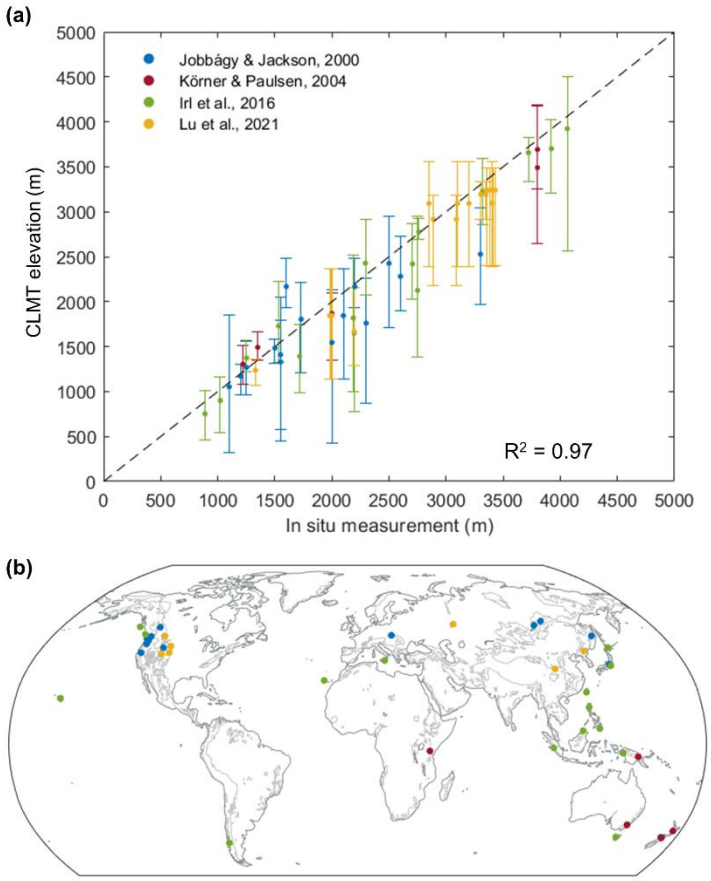

Supplementary Figure C.7 *Validation of CLMT loops using in situ measurements. (a) The relationship of CLMT with in situ measurements, with the 1:1 line (dashed). The dot and error bar in the y-axis represent the mean and range of elevation in the same lap of the CLMT identified in this study. (b) Spatial distribution of in situ measured treeline sites over mountain ranges (n = 62). Detailed information is available in Supplementary Table C.1.*

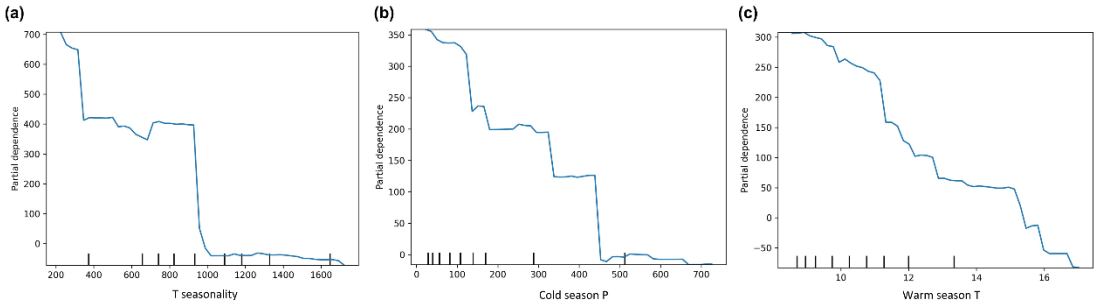

Supplementary Figure C.8 *Partial dependence of the three most important factors to the spatial pattern of CLMT. (a) Temperature seasonality (standard deviation ×100). (b) Cold season precipitation. (c) Warm season temperature. Thick bars at the bottom of each graph represent each decile of the factor.*

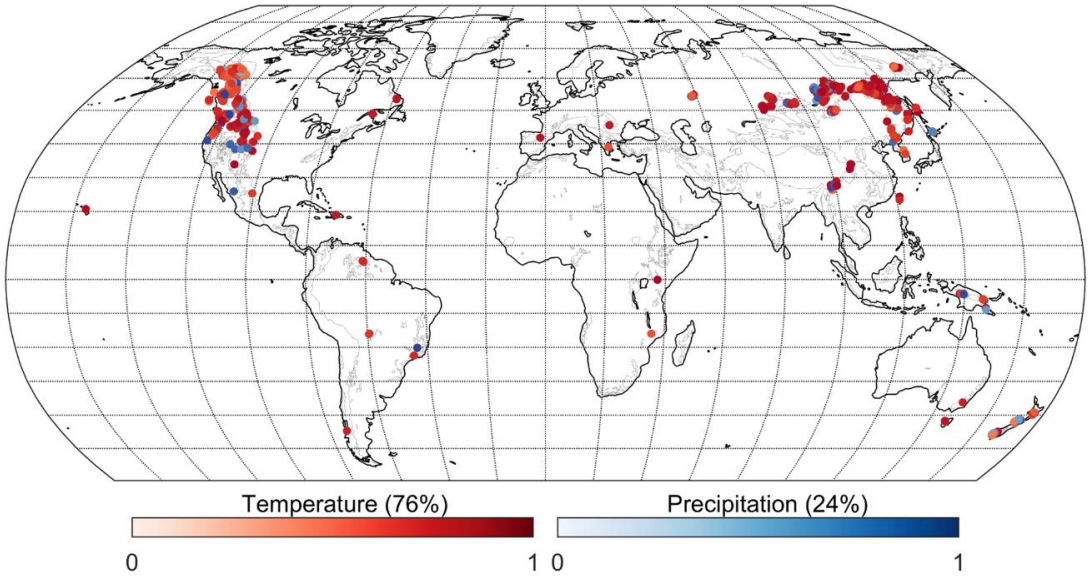

Supplementary Figure C.9 *Climate drivers controlling the variability in CLMT elevation at the local scale. The 16 variables are separated into temperature and precipitation categories. The importance of each climate variable was calculated for each CLMT loop. We add up the importance according to the two categories and mark the most important category within each CLMT loop.*

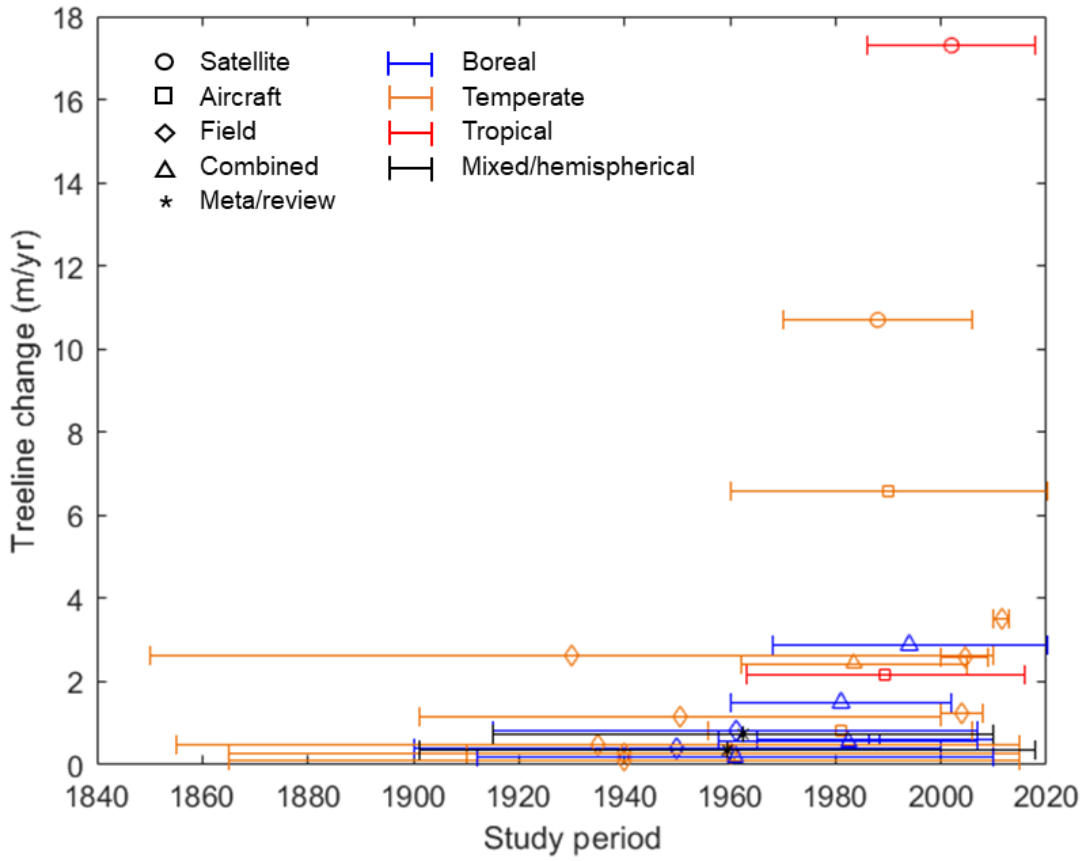

Supplementary Figure C.10 *Treeline changes from literature. The treeline change on the y-axis is the mean treeline shift rate (m/year). The middle of the period is represented by a point, with an error bar spanning the years of the study. Different symbols show methods (satellite, aircraft, fieldwork, etc.) and different colour symbols show boreal, temperate, and tropical regions. Combined means the study contains any two of satellites, aircraft, and fieldwork. Mixed means the study covers two or more climate regions (e.g., a study including boreal and temperate regions). Detailed information is available in Supplementary Table C.2.*

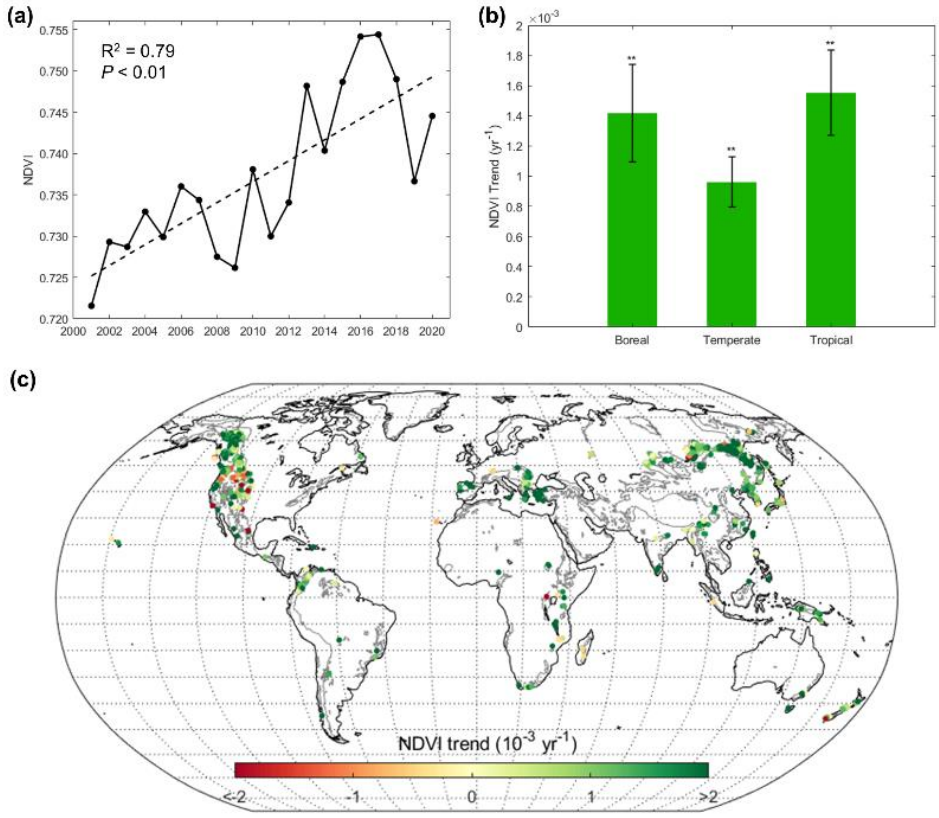

Supplementary Figure C.11 *Trends in the annual maximum Normalized Difference Vegetation Index (NDVI) at CLMT during 2001–2020. (a) Inter-annual variability of annual maximum NDVI at CLMT between 2001 and 2020 globally. (b) NDVI trend in boreal, temperate, and tropical regions. The error bars indicate the standard error of the linear trend. **Statistically significant trend at the level of P < 0.01. (c) Spatial pattern of NDVI trend in each treeline loop.*

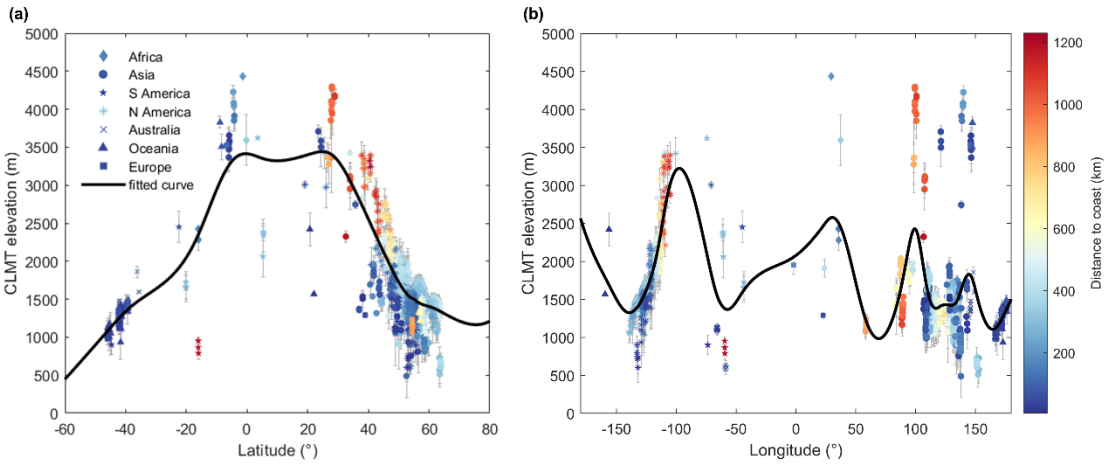

Supplementary Figure C.12 *Global latitudinal and longitudinal variation of the elevation of CLMT with low human footprint.*

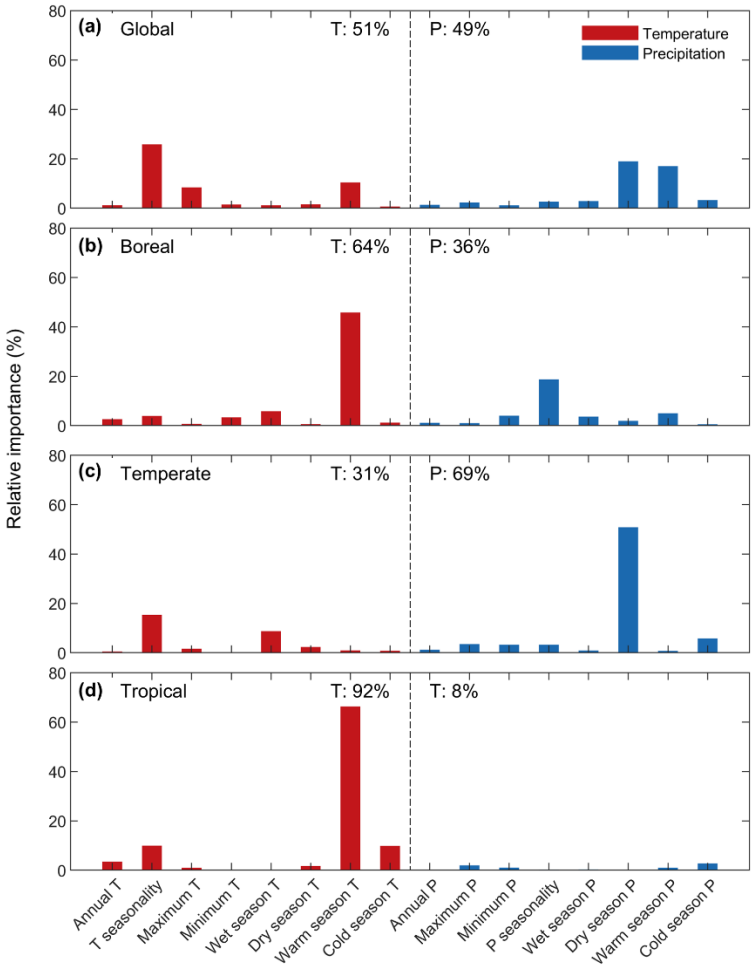

Supplementary Figure C.13 *Climate drivers controlling the variability in the elevation of CLMT with low human footprint.*

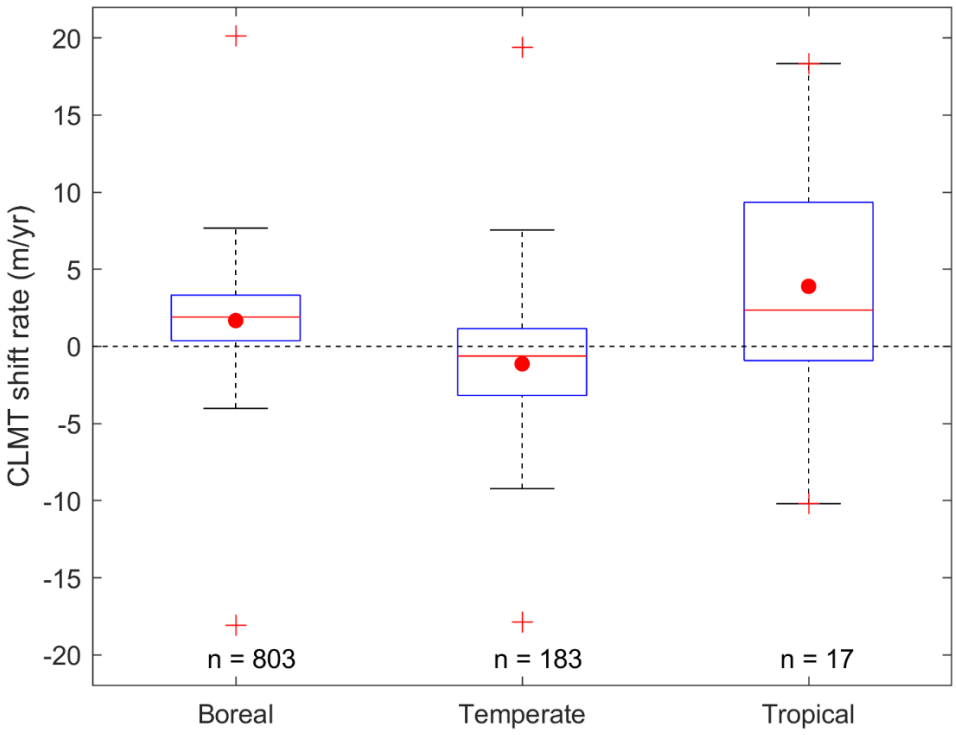

Supplementary Figure C.14 *Shift rate of CLMT with low human footprint.*

References

Ameztegui, A., Coll, L., Brotons, L. and Ninot, J.M., 2016. Past human use drives upward tree line shift in the Pyrenees. Global Ecology and Biogeography, 25, 263–273.

Beckage, B., Osborne, B., Gavin, D. G., Pucko, C., Siccama, T. and Perkins, T., 2008. A rapid upward shift of a forest ecotone during 40 years of warming in the Green Mountains of Vermont. Proceedings of the National Academy of Sciences, 105, 4197–4202.

Cazzolla Gatti, R., Callaghan, T., Velichevskaya, A., Dudko, A., Fabbio, L., Battipaglia, G. and Liang, J., 2019. Accelerating upward treeline shift in the Altai Mountains under last-century climate change. Scientific Reports, 9, 1–13.

Cudlin, P., Klopčič, M., Tognetti, R., Máliand, F., Alados, C.L., Bebi, P., Grunewald, K., Zhiyanski, M., Andonowski, V., La Porta, N., Bratanova-Doncheva, S. et al., 2017. Drivers of treeline shift in different European mountains. Climate Research, 73, 135–150.

Du, H., Liu, J., Li, M.H., Büntgen, U., Yang, Y., Wang, L., Wu, Z. and He, H.S., 2018. Warming-induced upward migration of the alpine treeline in the Changbai Mountains, northeast China. Global Change Biology, 24, 1256–1266.

Gaire, N.P., Koirala, M., Bhuju, D.R. and Borgaonkar, H.P., 2014. Treeline dynamics with climate change at the central Nepal Himalaya. Climate of the Past, 10, 1277–1290.

Hagedorn, F., Shiyatov, S.G., Mazepa, V.S., Devi, N.M., Grigor'ev, A.A., Bartysh, A.A., Fomin, V.V., Kapralov, D.S., Terent'ev, M., Bugman, H., Rigling, A. et al., 2014. Treeline advances along the Urals mountain range—driven by improved winter conditions? Global Change Biology, 20, 3530–3543.

Irl, S.D., Anthelme, F., Harter, D.E., Jentsch, A., Lotter, E., Steinbauer, M.J. and Beierkuhnlein, C., 2016. Patterns of island treeline elevation—a global perspective. Ecography, 39, 427–436.

Jiménez-García, D., Li, X., Lira-Noriega, A. and Peterson, A.T., 2021. Upward shifts in elevational limits of forest and grassland for Mexican volcanoes over three decades. Biotropica, 53, 798–807.

Jobbágy, E.G. and Jackson, R.B., 2000. Global controls of forest line elevation in the northern and southern hemispheres. Global Ecology Biogeography, 9, 253–268.

Kharuk, V.I., Ranson, K.J., Im, S.T. and Vdovin, A.S., 2010. Spatial distribution and temporal dynamics of high-elevation forest stands in southern Siberia. Global Ecology and Biogeography, 19, 822–830.

Kirdyanov, A.V., Hagedorn, F., Knorre, A.A., Fedotova, E.V., Vaganov, E.A., Naurzbaev, M.M., Moiseev, P.A. and Rigling, A., 2012. 20th century tree-line advance and vegetation changes along an altitudinal transect in the Putorana Mountains, northern Siberia. Boreas, 41, 56–67.

Körner, C. and Paulsen, J., 2004. A world-wide study of high altitude treeline temperatures. Journal of Biogeography, 31, 713–732.

Kullman, L., 2010. One century of treeline change and stability—experiences from the Swedish Scandes. Landscape Online, 17, 1–31.

Leonelli, G., Pelfini, M., Morra di Cella, U. and Garavaglia, V., 2011. Climate warming and the recent treeline shift in the European Alps: the role of geomorphological factors in high-altitude sites. Ambio, 40, 264–273.

Leonelli, G., Masseroli, A. and Pelfini, M., 2016. The influence of topographic variables on treeline trees under different environmental conditions. Physical Geography, 37, 56–72.

Liang, E., Wang, Y., Piao, S., Lu, X., Camarero, J.J., Zhu, H., Zhu, L., Ellison, A.M., Ciais, P. and Peñuelas, J., 2016. Species interactions slow warming-induced upward shifts of treelines on the Tibetan Plateau. Proceedings of the National Academy of Sciences, 113, 4380–4385.

Lu, X., Liang, E., Wang, Y., Babst, F. and Camarero, J.J., 2021. Mountain treelines climb slowly despite rapid climate warming. Global Ecology and Biogeography, 30, 305–315.

Morley, P.J., Donoghue, D.N.M., Chen, J.-C. and Jump, A.S., 2020. Montane forest expansion at high elevations drives rapid reduction in non-forest area, despite no change in mean forest elevation. Journal of Biogeography, 47, 2405–2416.

Mathisen, I.E., Mikheeva, A., Tutubalina, O.V., Aune, S. and Hofgaard, A., 2014. Fifty years of tree line change in the Khibiny Mountains, Russia:

advantages of combined remote sensing and dendroecological approaches. Applied Vegetation Science, 17, 6–16.

Sigdel, S.R., Wang, Y., Camarero, J.J., Zhu, H., Liang, E. and Peñuelas, J., 2018. Moisture-mediated responsiveness of treeline shifts to global warming in the Himalayas. Global Change Biology, 24, 5549–5559.

Sigdel, S.R., Liang, E., Wang, Y., Dawadi, B. and Camarero, J.J., 2020. Tree-to-tree interactions slow down Himalayan treeline shifts as inferred from tree spatial patterns. Journal of Biogeography, 47, 1816–1826.

Singh, C.P., Panigrahy, S., Thapliyal, A., Kimothi, M.M., Soni, P. and Parihar, J.S., 2012. Monitoring the alpine treeline shift in parts of the Indian Himalayas using remote sensing. Current Science, 102, 559–562.

van Bogaert, R., Haneca, K., Hoogesteger, J., Jonasson, C., de Dapper, M. and Callaghan. T.V., 2011. A century of tree line changes in sub-Arctic Sweden shows local and regional variability and only a minor influence of 20th century climate warming. Journal of Biogeography, 38, 907–921.

Zindros A., Radoglou K., Milios E. and Kitikidou K., 2020. Tree line shift in the Olympus Mountain (Greece) and climate change. Forests, 11, 985.